PLASMA GAS CLEANING PROCESSES FOR THE CONVERSION OF MODEL TAR FROM BIOMASS GASIFICATION

A THESIS
SUBMITTED TO THE UNIVERSITY OF LIVERPOOL

BY

Shiyun Liu

IN PARTIAL FULFILLMENT OF THE REQUIREMENTS
FOR THE DEGREE OF
DOCTOR OF PHILOSOPHY

SEPTEMBER 2017

DEPARTMENT OF ELECTRICAL ENGINEERING AND ELECTRONICS,
THE UNIVERSITY OF LIVERPOOL

ACKNOWLEDGEMENTS

ABSTRACT

Biomass has been highlighted as a key renewable feedstock to respond to the vital societal need for a step change in the sustainability of energy production required to combat climate change. Biomass gasification represents a major sustainable route to produce a higher value syngas from a renewable and CO_2-neutral source. However, one of the major challenges in the gasification process is the contamination of the product syngas with tar, particulate matter and other pollutants. Tar is a complex mixture of condensable hydrocarbons. The formation of tar causes major process and syngas end-use problems, resulting in high operational cost and even plant shut-down. Therefore, efficient removal of tars from product gas is crucial in the biomass gasification processes. Compared to the conventional approaches (e.g. physical/mechanical, thermal cracking and catalytic conversion technologies), non-thermal plasma has been considered as a promising alternative for biomass tar conversion. In this study, plasma-catalytic steam reforming of model tar from biomass gasification is carried out in the gliding arc discharge (GAD) reactor and the coaxial dielectric barrier discharge (DBD) reactor to gain a better understanding on the plasma processing of tar conversion and help to design the effective plasma system for biomass tar removal. This work will contribute to promote the utilisation of biomass in the global energy consumption.

In the plasma steam reforming of biomass tar, an AC GAD reactor has been developed for the conversion of toluene as a tar model compound using nitrogen as a carrier gas. The presence of steam in the plasma reaction produces OH radicals, which opens a new reaction route for the conversion of toluene through a stepwise oxidation of toluene and intermediates, resulting in a significant enhancement in both the conversion of toluene and the energy efficiency of the plasma process. The effects of steam-to-carbon (S/C) molar ratio, toluene feed rate and specific energy input (SEI) on the performance of the plasma steam reforming of toluene have been investigated. The optimal S/C molar ratio was found to be between 2 and 3 for high toluene conversion and energy efficiency. The maximum toluene conversion of 51.8% was achieved at an optimal S/C molar ratio of 2, a toluene feed flow rate of 4.8

ml/h and a SEI of 0.3 kWh/m^3, while the energy efficiency of the plasma process reached a maximum (~46.3 g/kWh) at a toluene feed flow rate of 9.6 ml/h and a SEI of 0.19 kWh/m^3. H_2, CO and C_2H_2 were identified as the major gas products with a maximum syngas yield of 73.9% (34.9% for H_2 and 39% for CO). Optical emission spectroscopy has been used to understand the role of steam on the formation of reactive species in the plasma conversion of toluene. The possible reaction pathways in the plasma conversion of toluene have also been proposed by combined means of the analysis of gas and liquid samples and OES diagnostics.

In the combined (CO_2 and steam) reforming of biomass tar, the effectiveness of applying an atmosphere pressure GAD reactor to remove toluene as the tar model compound in the gas stream of N_2 containing CO_2 and steam with different contents has been investigated. Experimental results show that in the absence of steam, the conversion of toluene peaks (59.9%) in the N_2 stream containing 3% CO_2, 16.1 g/Nm^3 toluene at an SEI of 0.25 kWh/m^3, and subsequently monotonically decreases to 56.2% when the concentration of CO_2 is further increased to 12%. H_2 and C_2H_2 are identified as the major gas products in the pure N_2 stream and their corresponding yield is 9.7% and 14.5%; whereas the primary products are syngas in the presence of CO_2. The highest yield of syngas is 58.3% (27.5 % for H_2 and 30.8 % for CO) at a CO_2 concentration of 3%. Adding steam into the feed containing CO_2/N_2 gas mixture and toluene firstly enhances the conversion of toluene due to the high reactivity of OH radicals generated from the dissociation of H_2O. Further increasing the S/C_T molar ratio (C_T stands for the carbon in toluene) leads to a decline in the conversion of toluene because of the electronegative property of H_2O and the quench of the electronically excited nitrogen species by H_2O and its derivatives. The optimum S/C_T molar ratio is 1.0 for the high toluene conversion and energy efficiency. In the liquid by-products, more N-containing substituent mixtures are detected in the toluene conversion using pure N_2 discharge; while more oxidised polycyclic aromatics are detected in the humid CO_2/N_2 environment due to the co-effect of strong oxidation of oxygen-derived radicals and electron impact reactions.

In plasma-catalytic conversion of biomass tar, steam reforming of toluene over the Ni/γ-Al$_2$O$_3$ catalysts in a coaxial DBD reactor is firstly investigated. The effect of nickel loadings (5-20 wt. %) of the Ni/γ-Al$_2$O$_3$ catalysts on the plasma-catalytic gas cleaning process is evaluated in terms of toluene conversion, gas yield, by-products formation and energy efficiency of the plasma-catalytic process. Compared to the plasma reaction without a catalyst, the combination of DBD with the Ni catalysts significantly enhances the toluene conversion, hydrogen yield and energy efficiency of the plasma process, whilst significantly reduces the production of organic by-products. Increasing Ni loading of the catalyst improves the performance of the plasma-catalytic processing of toluene, with the highest toluene conversion of 52 % and energy efficiency of 2.6 g/kWh when placing the 20 wt.% Ni/γ-Al$_2$O$_3$ catalyst in the plasma. The possible reaction pathways in the plasma-catalytic process were proposed through the combined analysis of both gas and liquid products.

In the plasma steam reforming of tar mixture (toluene and naphthalene) in the GAD reactor, the effect of the processing parameters including S/C molar ratio, initial naphthalene concentration and discharge power is firstly investigated in the absence of a catalyst. The results indicate that the highest toluene conversion (79.2%) and naphthalene conversion (63.2%) is obtained at the S/C molar ratio of 1.5 and 1.0, respectively, when keeping other processing parameters constant (C$_7$H$_8$ content: 16.5 g/Nm^3; C$_{10}$H$_8$ content: 1.1 g/Nm^3; discharge power: 60 W; total flow rate: 3.5 L/min). The energy efficiency for toluene conversion and naphthalene conversion reaches the highest value (48.1 g/kWh for toluene conversion and 2.2 g/kWh for naphthalene conversion) at the same condition. Increasing the initial naphthalene concentration decreases the conversion of both toluene and naphthalene and the energy efficiency for toluene conversion, but increases the energy efficiency for naphthalene due to the increase in the amount of converted naphthalene. Increasing the discharge power increases the conversion of toluene and naphthalene and the yield of gas products (e.g. CO, CO$_2$, H$_2$ and C$_2$H$_2$). The energy efficiency for toluene and naphthalene conversion is slightly changed by the discharge power, with the highest energy efficiency of 48.6 g/kWh for toluene conversion and of 2.2 g/kWh for naphthalene conversion at a discharge power of 60 W.

The feasibility of plasma-catalytic steam reforming of toluene and naphthalene mixture in the GAD reactor is studied using different catalysts (15 wt.% Ni/γ-Al$_2$O$_3$ (15Ni) , 7.5 wt.% Ni + 7.5 wt.% Co/γ-Al$_2$O$_3$ (7.5Ni7.5Co) and 15 wt.% Co/γ-Al$_2$O$_3$ (15Co)). The 7.5Ni7.5Co catalyst exhibits the highest plasma-catalytic activity for steam reforming of toluene and naphthalene mixture, compared to the 15Ni and 15Co catalysts. This can be ascribed to the easy reducibility of the 7.5Ni7.5Co catalyst and the synergy between Ni and Co in the Ni-Co alloy formed during the reduction process of the calcined 7.5Ni7.5Co catalyst. The highest conversion of toluene (93.7%) and of naphthalene (82.2%) is achieved when the 7.5Ni7.5Co catalyst is integrated with the GAD plasma system at a toluene content of 16.0 g/Nm^3, a naphthalene content of 1.1 g/Nm^3, a discharge power of 86 W, a total flow rate of 3.5 L/min and an S/C molar ratio of 1.5. These highest conversion is enhanced by 7.6% and 11.8% compared to that in the plasma-only process. The highest energy efficiency for the conversion of toluene and naphthalene, the highest yield of gas products (e.g. H$_2$, CO, C$_2$H$_2$ and CH$_4$) and the lowest amount of carbon deposition on the spent catalyst are obtained for the plasma steam reforming of tar mixture over the 7.5Ni7.5Co catalyst under the same condition. The highest energy efficiency for the conversion of toluene and naphthalene is 37.0 g/kWh and 2.2 g/kWh, respectively.

TABLE OF CONTENTS

List of Figures

List of Tables

List of Abbreviation

AC	Alternating current
DBD	Dielectric barrier discharge
DC	Direct current
FENETRe	Fast Equilibrium to Non-equilibrium
F-T	Fischer-Tropsch
FID	Flame ionisation detector
GAD	Gliding arc discharge
GC	Gas chromatography
GC-MS	Gas chromatography - mass spectrometry
IEO	International Energy Outlook
IPC	In plasma catalysis
IPCC	Intergovernmental Panel on Climate Change
LHV	Low heating value
MW	Microwave
MFC	Mass flow controller
NTP	Non-thermal plasma
OES	Optical emission spectroscopy
PAH	Polycyclic aromatic hydrocarbon
PPC	Post plasma catalysis
RF	Radiofrequency
SEI	Specific energy input
SS	Stainless steel
TCD	Thermal conductivity detector
TEM	Transmission electron microscopy
TGA	Thermo-gravimetric analysis
TPR	Temperature-programmed reduction
VOCs	Volatile organic compounds
XRD	X-ray diffraction
DCM	Dichloromethane
TEA	Techno-economic analysis

CHAPTER ONE   INTRODUCTION

1.1 Background

1.1.1 Utilisation of biomass energy

The global energy demand is steadily increasing due to the fast growth in the world population, rapid urbanisation and industrialisation as well as the increasing improvement in the living standards and economies of society. The International Energy Outlook 2013 (IEO2013) has projected that world energy consumption will grow by 56% in 2040 (based on that in 2010) and almost 80% of world primary energy will be supplied by the fossil fuels by 2040 [1]. However, the utilisation of fossil fuel has released a large amount of greenhouse gases (mainly CO_2) into atmosphere, which has caused a long term and irreversible damage to the environment, leading to global warming and climate change. Intergovernmental Panel on Climate Change (IPCC) has reported that the global annual anthropogenic greenhouse gas emissions were increased by 81.5% from 1970 to 2010 and energy-related CO_2 emissions accounted for 85.5% of the total anthropogenic carbon emissions in 2010 [2]. The finite reserve of fossil fuels and their limited distribution in few countries would cause the uncertainty of their prices and consequently the worldwide energy crisis. All of these factors necessitate a switch from conventional fossil fuels to renewable and alternative energy sources, such as hydropower energy, solar energy, wind power, biomass energy, etc. It is reported that the renewable share of world energy use would increase from 11% in 2010 to 15% in 2040, which is the fastest growing source of world energy [1]. Biomass utilisation has an advantage over other renewable energy sources (e.g. hydropower energy, solar energy and wind power), as the latter ones are strongly dependent on the location and climate and suffer from the intermittent power generation issue. In addition, biomass energy is more easily available with low price and has lower impact on the environment compared to fossil fuels, which makes it viable and promising as a sustainable energy source. It was among the top four energy sources in term of world final energy consumption in 2011 [3]. Biomass contributed around 14% of the world's energy in 1991, which was the equivalent of

approximately 25 million barrels of oil per day [4]. In the remote and rural areas of some developing countries in the world, biomass has a share up to 90% of the total energy supply [5]; whilst it also plays an important role on the energy consumption in certain industrialised countries. The UK government has set a target to obtain 15% of overall energy requirements (electricity, heat and transport) from renewables by 2020, helping to achieve the emissions cutting at 34% by 2020 and no less than 80% by 2050 [6]. Among all the renewable energies, biomass accounted for 3% of the total UK energy supply in 2007 [7] and this could reach up to 12% by 2050 according to the Royal Commission on Environmental Pollution [8].

Biomass mainly comprises five organic elements (including C, H, O, N and S) and other inorganic elements (such as Al, Si, K, Ca, Na, etc.). The compositions and their corresponding contents depend on the source of biomass. Biomass can be available from agricultural and forestry residues, biological material by-products, wood as well as the organic parts of municipal and sludge wastes. Renewable Energy Directive of EU has defined biomass as "the biodegradable fraction of products, waste and residues of biological origin from agriculture (including vegetal and animal substances), forestry and related industrials (including fisheries and the aquaculture), as well as the biodegradable fraction of industrial and municipal wastes" [9].

Biomass can be converted into various useful energy such as heat, solid, liquid and gaseous fuels by four main routes (e.g. direct combustion, physical, biochemical and thermochemical conversions), as shown in Figure 1.1 [10]. In the biochemical process, biomass can be converted into liquid and gaseous products via aerobic and anaerobic fermentation with the aid of the activities of microorganisms; while in the thermochemical process, biomass can be converted by torrefaction, direct liquefaction, pyrolysis and gasification. Thermochemical conversion of biomass is better than biochemical conversion due to the large variety of feedstock and fast conversion rate [11]. Among all of the thermochemical process for biomass conversion, biomass gasification has been considered as a promising way to convert biomass into combustible gas (producer gas) using gasifying agent, such as air, steam, oxygen, CO_2, etc. Table 1.1 shows the main gas composition in the

producer gas from biogas gasification in an atmospheric bubbling fluidized bed gasifier using different gasifiying agents [12].
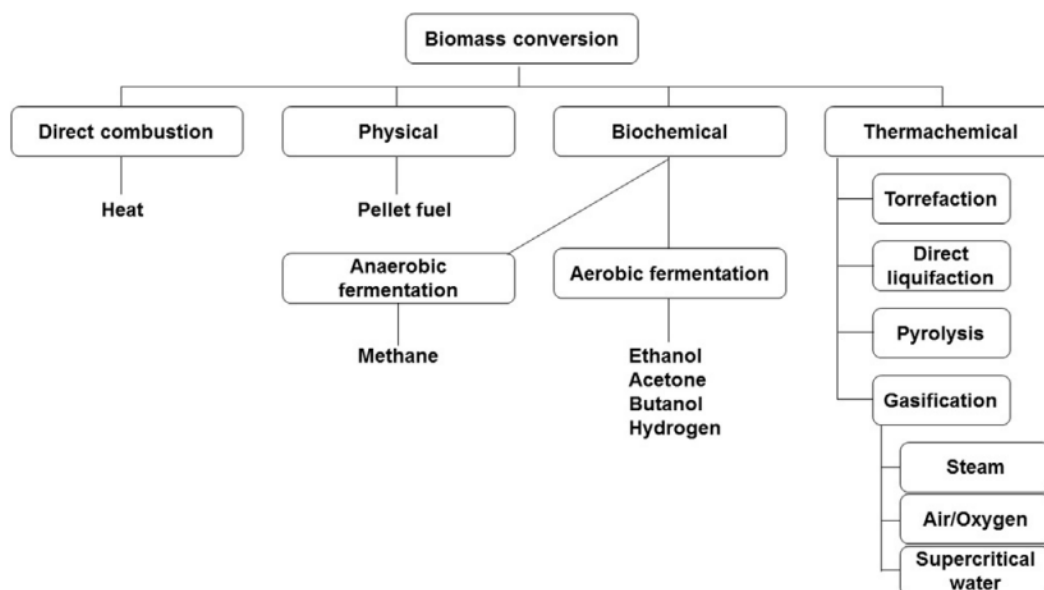
Figure 1.1 Four possible routes for biomass energy conversion [10].

Syngas (H_2 and CO) is the main composition in the producer gas. Figure 1.2 shows the main application of the produced syngas [13]. Most of the syngas can be directly used for power generation in fuel cells, gas turbines and/or engines. It can also be used for the generation of value-added fuels and chemicals via Fischer-Tropsch (F-T) and methanol synthesis processes. In the F-T process, syngas is converted into liquid hydrocarbon through chemical reactions on heterogeneous catalysts at relatively low temperature (e.g. 150 – 300 °C). The generated liquid hydrocarbons can be further refined to various fuels – from crudes and diesel to kerosene. Methanol can be synthesised through CO or CO_2 hydrogenation. As a liquid fuel, methanol is easy to store and transport; it also can be converted into a variety of useful fuels and chemicals commonly used in industrial and commercial applications. Hydrogen in the syngas can be separated and used in refinery hydrotreating, fuel cells and fertiliser industry through ammonia synthesis. In this regard, biomass gasification has attracted the most attention in the field of both industry and scientific researches.

Table 1.1 Major gas products composition in the producer gas from biomass gasification [12].

Gasifying agent	Temperature range (°C)	Gas product (vol.%)						
		H_2	CO	CO_2	CH_4	$C_{2's}$	N_2	H_2O
Air	780-830	5-16	10-22	9-19	2-6	0-3	42-62	11-34
Steam	750-780	38-56	17-32	13-17	7-12	2	0	52-60
Steam + O_2	785-830	14-32	43-52	14-36	6-8	3-4	0	38-61
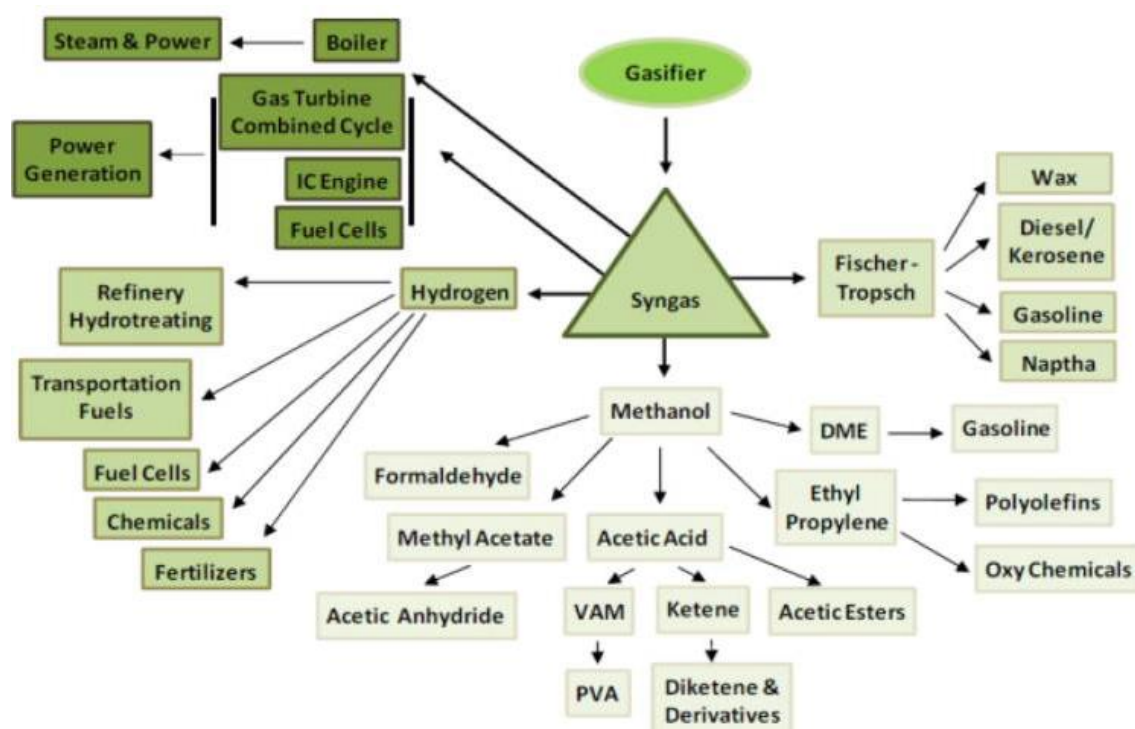
Figure 1.2 Main applications of the producer gas from the gasification process [13].

Biomass gasification is an intricate process, involving the heating and drying of biomass, followed by pyrolysis, partial combustion of intermediates, and finally gasification (reduction) of the resulting products, as shown in Figure 1.3 [10]. Depending on its sources and nature, the moisture content in the biomass generally varies from 5% to 35%. High amount of moisture in biomass will cause energy loss and degrade the quality of the final products. The optimal moisture content should- be less than 15% for gasification. In the step of heating and drying, the moisture in the biomass is evaporated. Due to the low temperature

(around 200 ^oC), the biomass will not experience any thermal decomposition. In the pyrolysis step, the dry biomass will be decomposed into gases with small molecules and volatiles with different molecular weights as well as solid residues containing carbon, known as char. Part of the volatiles will condense to liquid after cooled down to room temperature, which is called tar. The pyrolysis products will be partially or completely oxidised in the partial combustion (or oxidation) step. Only the char and the H_2 are considered to participate in the partial combustion reaction. The combustion product is a mixture of CO, CO_2 and H_2O if only O_2 is used. This oxidation process will generate the heat energy with peak temperature varying from 1100 to 1500 ^oC, which will be used for the endothermic reactions in the drying, pyrolysis and final gasification steps. In the gasification step, all the products in the preceding steps will be involved in a series of high temperature chemical reactions to generate the combustible products, including CO, H_2 and CH_4. The main reactions in the whole gasification process are shown in Table 1.2 [5, 14].
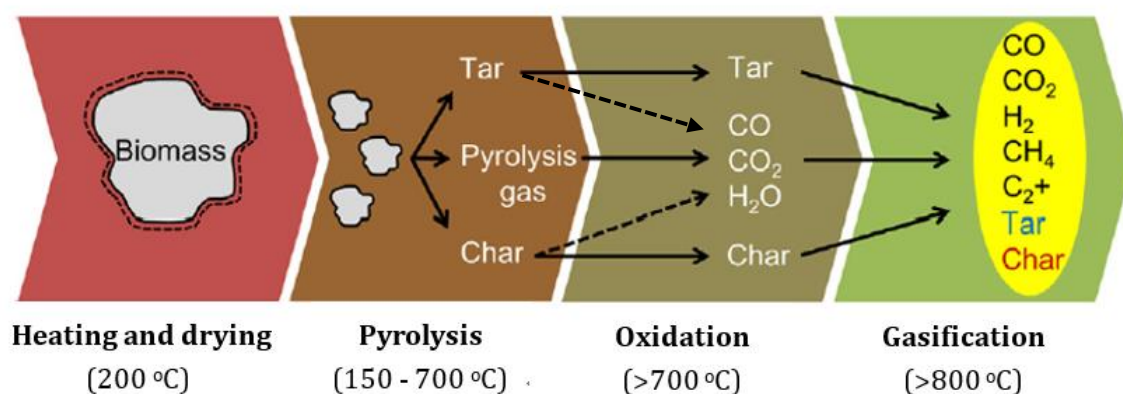
Figure 1.3 Main steps during biomass gasification [10].

In addition to the producer gas, char, other useful chemicals and unwanted byproducts including particulate matter, condensable hydrocarbons (also named tar), alkali metals and some trace gases (H_2S, HCl, HCN, NH_3, NO_x, etc.) will also be generated in the gasification process [15], which have serious problems for the further producer gas utilisation. Table 1.3 shows the main contaminants and their potential problems in the producer gas [12].

Table 1.2 Details of the main four steps during biomass gasification [5, 10, 14].

Step	Temperature	Main reactions
Heating and drying	From the start to a temperature around 200 ºC	Moist feedstock + Heat → Dry feedstock + H_2O (g)
Pyrolysis	150 to 900 ºC	Dry feedstock + Heat → H_2 + CO + CO_2 + CH_4 + H_2O + Char + Tar
Partial combustion (or oxidation)	over 700 ºC	Char combustion: $C + O_2 \rightarrow CO_2 \quad \Delta H = -394\,kJ/mol$ Partial oxidation: $C + \frac{1}{2}O_2 \rightarrow CO \quad \Delta H = -111\,kJ/mol$ H_2 combustion: $H_2 + \frac{1}{2}O_2 \rightarrow H_2O \quad \Delta H = -242\,kJ/mol$
Gasification (or reduction)	over 800 ºC	Boudouard reaction: $C + CO_2 \rightarrow CO \quad \Delta H = 172\,kJ/mol$ Char reforming: $C + H_2O \rightarrow CO + H_2 \quad \Delta H = 131\,kJ/mol$ Water gas shift reaction: $CO + H_2O \rightarrow CO_2 + H_2 \quad \Delta H = -41\,kJ/mol$ Methanation: $C + 2H_2 \rightarrow CH_4 \quad \Delta H = -75\,kJ/mol$

Table 1.3 Contaminant presence in the producer gas and their corresponding problems [12].

Contaminants	Presence	Potential problems
Particulates	Derive from ash, char, condensing compounds and bed material for the fluidized bed reactor.	Cause erosion of metallic components and environmental pollution.
Alkali metals	Exist in vapour phase, specially sodium and potassium.	Cause high-temperature corrosion of metal due to the stripping off of their protective oxide layer.
Fuel-bond nitrogen	Forming NO_x during combustion.	NO_x pollution.
Sulfur and chlorine	Usually sulfur and chlorine contents of biomass and waste are not considered to be a problem.	Could cause dangerous pollutants and acid corrosion of metals.
Tar	Bituminous oil constituted by a complex mixture of oxygenated hydrocarbons existing in vapour phase, which is difficult to remove by simple condensation.	Clog filters and valves and produce metallic corrosion.

1.1.2 Tar issues in biomass gasification

1.1.2.1 Definition and classification of tar

Tar formation is one of the major problems during the gasification process. Tar is a complex mixture of condensable hydrocarbons, including single to multiple ring aromatic compounds as well as other oxygen-containing hydrocarbons and complex polycyclic aromatic hydrocarbons [12]. Different definitions of tar have been reported and one widely accepted definition is "all organic molecules with molecular weights greater than that of benzene" [16]. After the moisture is evaporated in the early stage of biomass gasification, the organic matter will be volatilised. The volatilised materials will either be further decomposed, or undergo the reactions of dehydration, condensation and polymerisation, resulting in the formation of different tar molecules. Figure 1.4 shows the formation scheme of tar as a function of process temperature [10, 17]. Clearly, the organic compounds become more stable by increasing the temperature.
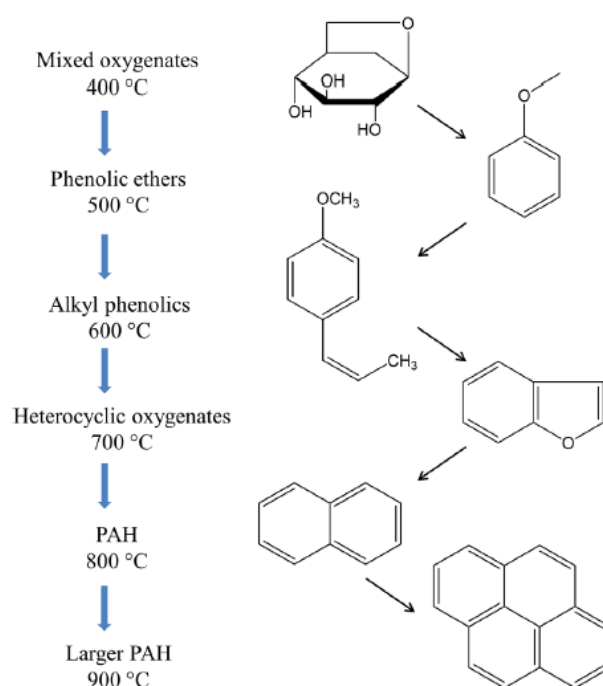
Figure 1.4 Tar formation scheme as a function of process temperature [10, 17].

Based on the complexity of the molecules (or its appearance), tar can be classified into primary, secondary and tertiary tars, as shown in Table 1.4 [10, 18]. Table 1.5 shows the

classification of tar based on the gas chromatography-mass spectrometry (GC-MS) analysis [17, 18]. The relationship between these two classifications is shown in Figure 1.5 [19].

Table 1.4 Tar classification based on its appearance [10, 18].

Tar class	Property	Representative examples
Primary	Low molecular weight oxygenated hydrocarbons	Levoglucosan, furfural and hydroxyacetaldehyde
Secondary	Phenolic and olefin compounds	Phenol, cresol and xylene
Tertiary	Complex aromatic compounds	benzene, naphthalene, pyrene and toluene

Table 1.5 Tar classification based on GC-MS analysis [17, 18].

Tar class	Class name	Property	Representative compounds
1	GC-undetectable	Very heavy tars, cannot be detected by GC	Determined by subtracting the GC-detectable tar fraction from the total gravimetric tar
2	Heterocyclic aromatics	Tars containing hetero atoms; highly water soluble compounds	Pyridine, quinolone, isoquinoline
3	Light aromatic (1 ring)	Usually light hydrocarbons with single ring; do not pose a problem regarding solubility and condensability	Toluene, ethyl benzene, xylenes, styrene, phenol, cresols
4	Light PAH compounds (2-3 rings)	2 and 3 rings compounds; condense at low temperature even at very low concentration	Indene, naphthalene, biphenyl, methylnapthene, acenaphthalene, fluorine, phenanthrene, anthracene, benzophenone
5	Heavy PAH compounds (4-7 rings)	Large than 3-ring, these components condense at high-temperature at low concentrations	Pyrene, chrysene, perylene, coronene, fluoranthene
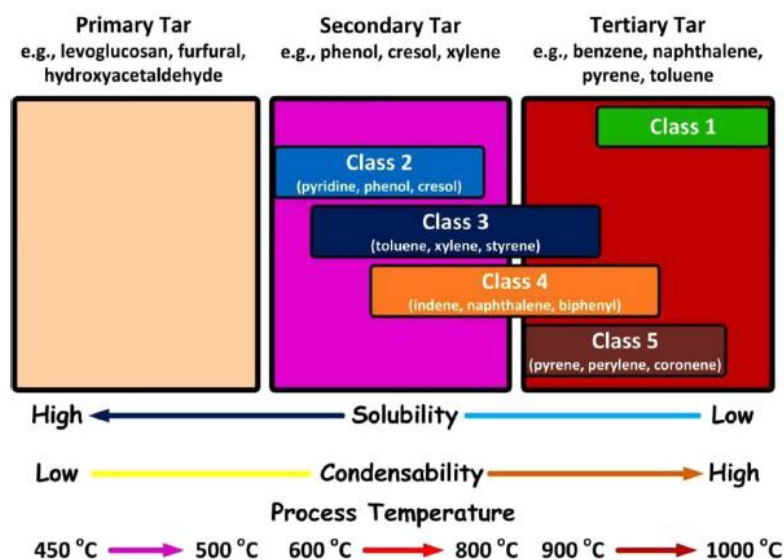
Figure 1.5 Two typical classifications of biomass tar [19].

The amount and composition of biomass tar is dependent on the types of biomass feed stock, gasifiers, gasifying agents and operating conditions (e.g. temperature and pressure) [10]. It is reported that lignin has higher tar yields and produces more stable components in the tar compared to cellulose and hemicellulose. Increasing the temperature will decrease the tar formation. In addition, more class 1 and class 2 tars are decomposed and more class 3 and class 5 tars are formed with the increase in the temperature. Adding steam and/or oxygen into the gasification system will reduce the tar yield to a large extent [10]. The commonly used gasifiers can be divided into three categories: (1) fixed-bed gasifiers, (2) fluidised-bed gasifiers and (3) entrained flow gasifiers [15, 20]. The fixed-bed gasifiers can be further divided into updraft (countercurrent), downdraft (concurrent) and crossdraft gasifiers according to the place where the gasifying agent is introduced into the reactor; while the fluidised-bed gasifiers can be further divided into bubbling fluidised-bed, circulating fluidised-bed and dual fluidised bed gasifiers [20]. Compared to the updraft gasifiers, the tar content in the producer gas from the downdraft gasifier is much lower, as the tar produced in the downdraft gasifier are thermally cracked in the oxidation zone at approximately 1300 ℃ before exiting from the bottom of reactor; while in the updraft gasifiers, the tar produced in the pyrolysis zone only passes though the drying zone at a relatively low temperature and cannot be thermally cracked, leading to a higher tar yield [20,

21]. The tar content in the producer gas from the fluidised-bed gasifier is higher compared to that from the downdraft gasifier due to the lower oxidation temperature (< 900 $^{\circ}$C) in the fluidised-bed gasifier. However, compared to the updraft gasifier, the tar content in the producer gas from the fluidised-bed gasifier is lower as it has enough board for tars to be converted [20, 21]. The fixed-bed gasifiers have extensive applications in the small scale installation (10 – 10000 kW) as they are have simple constructions, while the fluidised-bed gasifiers are suitable for intermediate units within the range of 5-100 MW due to the capability of treating high throughputs and easy scaling up. For the entrained flow gasifiers, they are used for the large capacity units (e.g. above 50 MW). Almost no tar will be generated from the entrained flow gasifiers; however, their utilisation in the biomass gasification is very limited, as a fuel particle size of 100 – 400 µm is required in this type gasifier, which is very difficult to achieve [15]. Table 1.6 shows the comparison of tar concentration in different biomass gasifiers [20].

Table 1.6 Comparison of tar produced in different biomass gasifier systems [20].

Gasifier type	Fixed-bed gasifier			Fluidised-bed gasifier			Entrained flow gasifier
	Downdraft	Updraft	Crossdraft	Bubbling	Circulating	Dual	
Tar range (g/Nm^3)	0.01-5	30-150	0.01-1	3.7-62	4-20	0.2-2	0.01-4

1.1.2.2 Tar elimination technologies

The formation of tar during the gasification process will cause the problems of (1) plugging and fouling of pipes and downstream equipment; (2) clogging of gas cleaning filters; (3) formation of solid coke, tar aerosols and polymerisation into more complex structures; (4) deactivation of the catalysts used for reforming and cleaning and (5) contaminating water in the wet clean-up processes [10, 21]. It is also harmful to our health due to its carcinogenic character [10]. In addition, most downstream applications of producer gas have strict allowable tar levels. Table 1.7 shows the acceptable limit of tar content for different downstream applications [3]. For example, the tar tolerance for the fuel cells, gas

turbines, internal combustion engines and compressors are < 1 g/Nm^3, $0.05 \sim 5$ g/Nm^3, $<$ 100 g/Nm^3 and < 500 g/Nm^3, respectively. When the tar is used for direct combustion (e.g. in a boiler), there is no limit on tar content provided the tar would not be cooled down below its dew point at the outlet of the gasifier and the inlet of the burner (e.g. bolier). However, measures still should be taken to ensure that the flue gas from the combustion is in accordance with the local emission standards [3]. Therefore, the produced tar in the biomass gasification process must be removed and controlled to an acceptable level based on the individual application.

Figure 1.7 Acceptable range of tar for various downstream applications [3].

Constitutes	Fuel cells	Gas turbines	Internal combustion engines	Compressors	Direct combustion (i.e. boiler)
Tar (g/Nm^3)	< 1	$0.05 \sim 5$	< 100	< 500	No limit

Great efforts have been devoted to tar removal from the producer gas. Fundamentally, tar removal technologies can be divided into two catalogues according to the location where tar is removed: primary tar reduction and secondary tar reduction [3, 12, 20]. In the primary measures, the tar is degraded inside the gasifier by selecting the appropriate gasifier designs, optimum operating parameters (e.g. temperature, pressure, gasifying agents, residence time, etc.), as well as the proper additives and catalysts [3, 20]. The primary tar reduction methods are also called self-modification methods [3]. Some primary methods can reduce the tar content significantly, but suffer from the limitations in the biomass feedstock flexibility and scaling up, the production of waste stream, a decline in the cold gas efficiency, the complicated gasifier constructions and/or a narrow operating window [12]. Tar cannot be completely removed only with the primary methods without using the secondary measures [12]. The secondary measures aim to remove and/or crack the tar in the downstream of gasifier and to clean the producer gas from the gasifier. In the secondary measures, tars can be removed by physical/mechanical, thermal cracking and catalytic tar elimination processes as well as some emerging approaches (e.g. plasma technology).

(1) Physical/mechanical methods

The physical/mechanical methods are divided into dry gas cleaning and wet gas cleaning [3, 12]. Dry gas cleaning is used at a temperature above 500 ^{o}C (before gas cooling) and partly below 200 ^{o}C (after gas cooling). Cyclones, rotating particle separators and various filters are used in the dry gas cleaning process to remove tars. Wet gas cleaning employs the electrostatic precipitators, wet scrubbers, solvent extraction and wet cyclones to remove tar after gas cooling where the temperature is typically 20 - 60 ^{o}C. In the wet gas cleaning process, a huge amount of waste water is produced in the gas cooling system, which incurs the cost for waste water treatment. Table 1.8 shows a summary of the tar reduction using a variety of physical/mechanical methods [22]. Clearly, the tar reduction can be high in the physical/mechanical methods, especially using the sand bed filter (e.g. 50-97%). However, the physical/mechanical methods only remove the tars in the producer gas, while the energy in the tars is lost, as they contain a large amount of energy which can be transferred to the fuel gas (e.g. CO, H_2 and CH_4) [22, 23].

Table 1.8 Tar reduction in various physical/mechanical methods [22].

	Temperature (^{o}C)	Tar reduction (%)
Sand bed filter	10-20	50-97
Wash tower	50-60	10-25
Venturi scrubber	-	50-90
Wet electrostatic precipitator	40-50	0-60
Fabric filter	130	0-50
Rotational particle separator	130	30-70
Fixed bed tar adsorber	80	50

(2) Thermal cracking

Thermal cracking is decomposition of the heavy aromatic tar species to lighter and less problematic smaller molecules (e.g. CH_4, CO and H_2) at relatively higher temperatures from

1000 to 1300 °C with the residence time < 1-12 s [21]. The high temperature for the thermal cracking can be obtained by (1) using the high temperature gasifiers, (2) using heat exchangers to heat the gas stream, (3) adding air or O_2 in the downstream of the gasifier and/or (4) applying the energy efficient radio frequency [20]. Table 1.9 shows the tar content after the thermal cracking at different temperatures [22]. Thermal cracking is only effective at relatively high temperatures, thus it is considered to be energy intensive and expensive. Due to the high temperature, the thermal cracking equipment must be made up of heat-resisting materials (e.g. high temperature tolerable expensive alloys) and the system should contain a highly controllable complex heating system and an intensive cooling system for gas products to be used in the downstream applications. High temperature thermal cracking also increases the soot production and the ash will melt at this severe temperature condition [24]. In addition, the biomass-derived tars are very refractory and hard to be cracked by thermal treatment alone [22], which cannot meet the stringent requirements (e.g. in gas turbines and/or internal combustion engines).

Table 1.9 Tar content in the gas after thermal cracking at different temperatures [22].

Temperature in reactor (°C)	1200	1250	1290	1290
Gas producer	Pyrolysis	Pyrolysis	Pyrolysis	Updraft
Light tar in condenser determined with GC/MS (mg/kg dry feed stock)	607	21	1	7
Light tar in aerosol filter determined with GC/MS (mg/kg dry feed stock)	250	n.d	5	10
Light tar in soot determined with GC/MS (mg/kg dry feed stock)	n.d	n.d	n.d	15
PAH in condensate sum of 27 components (mg/kg dry feed stock)	19	0.021	0.033	0.07

(3) Catalytic reforming of tar

The catalytic tar removal methods are more effective and have been regarded as one of the most promising approaches for the large scale application because of the fast reaction

rate and reliability as well as the ability to convert tars into value-added gases (e.g. CO and H_2) in the presence or absence of H_2O [25]. The research on catalytic tar conversion involves two methods: one approach involves incorporating or mixing catalyst with the biomass feedstock. In this case, the biomass tar can be converted inside the gasifier, therefore it is called catalytic gasification or pyrolysis (also called in situ). This method is one of the primary methods used for tar reduction, where the tar is removed in the gasifier itself. The other approach uses a separated reactor located at the downstream of the gasifier and converts tar outside the gasifier. This approach is one of the secondary methods used for tar reduction, where the tar is removed outside the gasifier [26]. Although the latter one could provide a better performance of tar conversion, it is either costly or complex for those small and medium scale systems [26]. Among hot gas conditioning systems, catalytic cracking and steam reforming of high molecular weight hydrocarbons offer several advantages, such as thermal integration and high tar conversion. The catalytic cracking tar can occur at a low temperature range of $500 - 900\ ^{\circ}C$ with the aid of catalysts, as the decomposing activation energies are reduced in the presence of catalysts [20]. This relatively low temperature eliminates the operating complexities and high costs related to the high temperature processes.

The steam reforming of tar is the most attractive technique for tar removal as it can remove tar with high efficiency and convert the biomass tar into useful gases, i.e., CO, H_2 and CH_4 simultaneously. In the presence of excess steam, the produced CO could further react with steam to produce more hydrogen. As H_2O, CO_2, H_2 and CO are the main gas components in the producer gas from biomass gasification, dry reforming and other reactions should also be considered in the steam reforming process. Figure 1.6 shows the different mechanisms of catalytic steam and dry reforming of tar inspired from the literatures with metal catalysts (Ni, Co, etc.) based on ceramic supports (Al_2O_3, SiO_2, etc.) [13]. Numerous reactions occur simultaneously and the product distribution from the tar reforming is dependent on the competition among these reactions. These reactions can be lumped into one overall reaction, as shown in Figure 1.7 [16].
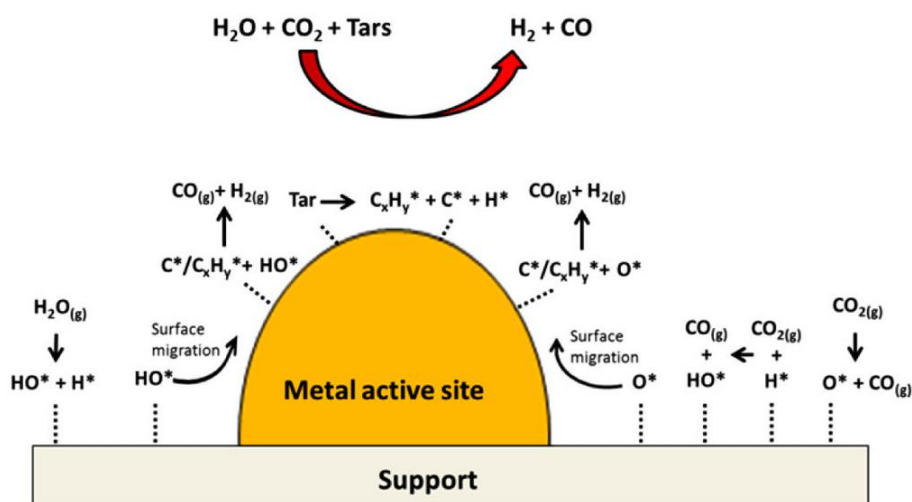
Figure 1.6 General scheme of catalytic reforming of tar [13].
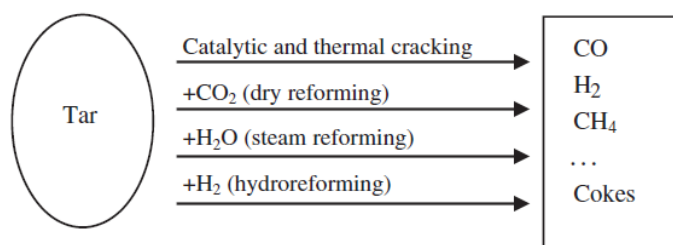
Figure 1.7 One lump model for tar conversion [16].

The catalysts for the catalytic tar reforming should be selected based on the following criteria: (1) the catalysts should be effective in removing tar; (2) the catalysts should have the capability of reforming of methane and providing a suitable syngas ratio for the intended process if the desired product is syngas; (3) the catalysts should be resistant to deactivation due to carbon deposition and sintering and can be easily regenerated; (4) the catalysts should have high strength and can be available with low price [22]. The catalyst developed so far can be classified into six groups, they are (1) nickel-based catalysts (supported on Al_2O_3, olivine, ZrO_2, TiO_2, CeO_2, MgO, etc.), (2) non-nickel transition metal catalysts (Rh, Ru, Pd, Pt, Co, Fe, Zn, Cu, etc.), (3) alkali catalysts (Li, Na, K, etc.), (4) natural catalysts (dolomite, olivine, shell, etc.), (5) zeolite catalysts (Y-zeolite, ZSM-5, etc.) and (6) carbon (active carbon and char)-supported catalysts [10]. The advantages and disadvantages of each type catalyst used for tar removal are summarised in Table 1.10.

Table 1.10 Advantages and disadvantages of various catalysts for tar removal [27].

Catalyst	Advantage	Disadvantage
Calcined Rocks	1. Inexpensive and abundant; 2. Attain high tar conversion ~95% with dolomite; 3. Often used as guard beds for expensive catalysts most popular for tar elimination.	Fragile materials and quickly eroded from fluidized beds.
Olivine	1. Inexpensive; 2. High attrition resistance	Lower catalytic activity than dolomite.
Clay Minerals	1. Low cost and abundant; 2. Fewer disposal problems	1. Rapid deactivation by coke; 2. Do not support the high temperatures (>800 ^{o}C) needed for tar elimination
Iron ores	Inexpensive and abundant	1. Rapidly deactivated in the absence of H_2; 2. Poor catalytic activity than dolomite.
Activated Alumina	High tar conversion comparable to that of dolomite.	Rapid deactivation by coke.
Alkali-metal-based	1. Natural production in the gasifier; 2. Reduce ash-handing problems.	1. Particle agglomeration at high temperatures; 2. Lower catalytic activity than dolomite.
Transition-metal-based	1. Able to attain complete tar elimination at ~900 ^{o}C; 2. Increases the yield of syngas (H_2 and CO); 3. Higher tar reforming activity.	1. Rapid deactivation because of sulphur and high tar content in the feed; 2. Relatively expensive; 3. Relatively easier regenerated.
Char	1. Cheap and abundant; 2. Sustainable (natural production inside the gasifier); 3. High tar conversion compared to dolomite; 4. Neutral or weak base properties.	1. Consumption because of gasification reactions; 2. Its properties are not stable and fixed, depending on biomass types and process conditions.

Nickel-based catalysts are used extensively for biomass tar conversion because of their high destruction activity, along with the added actively for methane reforming and water gas shift, which is beneficial to produce more syngas and adjust the syngas composition. Table 1.11 lists some representative Ni-based catalysts for steam reforming of tar model compounds (benzene, toluene and naphthalene). Simell et al. studied the effectiveness of Ni/Al_2O_3 and several other catalysts including dolomite, active alumina, silica-alumina and silica carbide for tar decomposition [28, 29]. They found that the supported nickel catalyst almost completely decomposed the tar compound at the temperatures of 900 ^oC. Nevertheless, Corrella and his group also indicated that the nickel-based catalyst can only survive when the concentration of tar in the inlet gas is less than 2 g/Nm^3 [30]. The nickel-based catalysts are easily sintered, active component lost, carbon deposit and phase transformed; which are responsible for its deactivation. Carbon formation on the catalyst surface (carbon deposition) and high sulphur content (poisoning with sulfur) in the feed gas are regarded as the main reasons responsible for the deactivation of Ni-based catalysts. Coke deposition is one of the most serious issue in catalytic reforming of hydrocarbons, especially for aromatic hydrocarbons. Catalyst regeneration by coke removal such as combustion would be necessary. However, the process of catalyst regeneration often causes aggregation and structural changes in the metal particles and leading to a poor activity and a short catalyst life [31]. Therefore, these factors would inhibit the extensive applications of Ni-based catalysts.

As the non-nickel transition metal catalysts, noble metal catalysts such as Ru, Rh and Pt have very high catalytic activity with high sulphur resistance and long-term stability in the process of tar elimination [32, 33]. Tomishige and his co-workers studied the steam reforming of tar over noble metal catalysts supported on CeO_2/SiO_2 and compared their catalytic activity with Ni-based catalysts [34]. They found that the supported Rh-metal catalyst had better performance than the commercial nickel catalysts. They also reported that among the noble metals, Rh was significantly more active than others with a selectivity order of Rh>Pt>Pd>Ru=Ni. Although noble metal-based catalysts have high catalytic activity,

long-term stability and high carbon deposition resistance, their high cost is the main problem for the large-scale applications in tar elimination.

Natural minerals such as dolomite, olivine and shells could be used as catalysts directly or with some pre-treatment, like calcination or modification by the addition of some metals [35]. These natural catalysts exhibit considerable activity for the reforming of tar with low price and high abundance. Virginie et al [36] indicated that the conversion of toluene and the yield of H_2 were improved by a factor of 3 when using Fe/olivine as the catalyst compared to using olivine alone in the reforming process. However, the main problem of these catalysts is their low mechanical strength, which is not suitable to be used in fluidised bed reactor [35]. Zeolites have been widely used in heterogeneous catalysis due to their well-defined pore structure, extremely high surface area and surface acidity. The modification of zeolites with dispersed metals can obtain catalysts for hydrogenation and ring breaking of aromatic hydrocarbons [37]. In the case of the catalytic cracking of tar component, Duo et al evaluated the activity of five kinds of catalysts including Y-zeolite, NiMo catalyst, silica, alumina and lime [38]. They found that Y-zeolite and NiMo catalysts were the most effective catalysts, which removed almost 100% tar at 550 ^{o}C and no deactivation was observed over 10 h. However, the main disadvantages of these catalysts are the rapid deactivation resulted from coke formation.

Recently, some researchers revealed that the activated carbons and char derived from biomass and coal have great potential to be used as catalyst supports and/or catalysts for the conversion of hydrocarbons and tar cracking [39-41]. Bhandari et al reported that bio-char, activated carbon and acidic surface activated carbon had good performance for tar reduction with removal efficiencies of 69-92 % [40]. Min et al also evaluated the catalytic activity of char and char-supported catalysts in steam reforming of tar [42]. They found that the char-supported iron/nickel catalysts exhibited much higher activity than char itself in the process of tar reduction. The attractiveness of bio-chars as catalysts originates from low cost and natural production inside the gasifier. It should be mentioned that the char-supported catalysts can be simply gasified to recover energy of char without the need of frequent regeneration after deactivation. However, char would be consumed by steam or CO_2 in the

producer gas and its properties are not stable and fixed, mainly depending on the types of biomass feedstock and process conditions. From the above statement, it is clear that the development of novel catalysts with high activity, long-term stability and/or excellent reusability and low-cost for tar reforming process is extremely critical for the development of viable hot gas clean-up technologies.

Table 1.11. Steam reforming of tar over Nickel-based catalysts

Catalyst	Metal loading (wt %)	Preparation method [a]	Reaction conditions	Conversion (%)	Ref
Ni/α-Al$_2$O$_3$	12	iw	Feed gas: C$_7$C$_8$/H$_2$O/N$_2$ W/F=0.003 g h/mol, S/C=0.5, T=923 K	54.2	[43]
Co/α-Al$_2$O$_3$	12			81.4	
Ni-Co/α-Al$_2$O$_3$	12			59.0	
Ni/AC	10	iw	Feed gas: C$_7$C$_8$/H$_2$O/N$_2$ LHSV=0.87 h^{-1}, S/C=2, T=473 K	98.0	[44]
Ni/olivine	10			46.2	
Ni/ α-Al$_2$O$_3$	10			65.5	
Ni/ α-Al$_2$O$_3$	12	iw	Feed gas: C$_7$C$_8$/H$_2$O/N$_2$ W/F=0.05 g h/mol, S/C=1.7, T=1123 K	26.5	[45]
Ni-Fe/α-Al$_2$O$_3$	12			26.3	
Ni/Mg/Al	12	cp		53.3	
Ni-Fe/Mg/Al	12			83.2	
Ni/Ca$_{12}$Al$_{14}$O$_{33}$	1	s.m	Feed gas: C$_7$C$_8$/H$_2$O/Ar GHSV=6000 h^{-1}, S/C=1.9, T=973 K	31.2	[46]
	3			64.8	
	5			100	
Ni/γ-Al$_2$O$_3$	15	imp	Feed gas: C$_6$H$_6$/H$_2$O/N$_2$ W/F=19.6 g h/mol, S/C=2.4, T=973 K	82.5	[47]
Ni/ZrO$_2$	15			38.8	
Ni/CeO$_2$	15			57.7	
Ni/CeO$_2$-ZrO$_2$	15			87.2	
Ni/LaAlO$_3$	10	imp	Feed gas: C$_7$H$_8$/H$_2$O/Ar W/F=13.5 g h/mol, S/C=3, T=873 K	81.0	[48]
Ni/LaFeO$_3$	10			55.0	
Ni/BaTiO$_3$	10			41.0	
Ni/SrTiO$_3$	10			65.0	
Ni/LaCeO$_3$	10			66.0	

[a] iw: incipient wetness method, imp: impregnation method, cp: co-precipitation method, s.m: solid mixing.

(4) Plasma-assisted tar removal

Recently, non-thermal plasma technology has been considered as a promising alternative approach to remove tars in the producer gas from the biomass gasification and convert them into clean fuels at relative low temperatures [49-53]. In non-thermal plasmas, the electrons are highly energetic with a typical energy of 1-10 eV, while the overall gas temperature can be as low as room temperature. This non-equilibrium characteristics enable non-thermal plasmas to easily break most chemical bonds and overcome the disadvantage of high temperature required by thermal or catalytic processes. As a result, thermodynamically unfavourable chemical reactions can occur under ambient conditions [54-59]. The basic principle of plasma and plasma-catalysis as well as the current state of the plasma assisted tar removal will be given in the following sections.

1.2 Plasma and plasma-catalysis

1.2.1 Basic principle, characteristics and classification of plasma

Plasma is defined as a neutral ionised gas, which contains a mixture of particles in permanent interaction: electrons, positive and negative ions, atoms, free radicals, photons, and excited and non-excited molecules. It was firstly found by William Crook in 1897 [60] and the term of plasma was introduced into physics by Irving Langmuir for the first time in 1929 [61]. In general, electrons and photons are designed as light species in plasma, while the other components are defined as heavy species. Plasma is electrically neutral, as the density of the positive charge carriers is equal to that of the negative ones [62]. It is also referred as the fourth state of matter. As shown in Figure 1.8 [63], the state of matter transfers in the sequence of solid, liquid, gas and finally plasma by increasing the energy level. Plasma is a state of matter similar to gas, as it does not have a definite shape or a definite volume unless enclosed in a container; however, it is quite different from the normal neutral gas, as it is strongly influenced by the electromagnetic field due to the non-negligible charge carriers. In nature, lightning and aurora are two examples of plasmas.
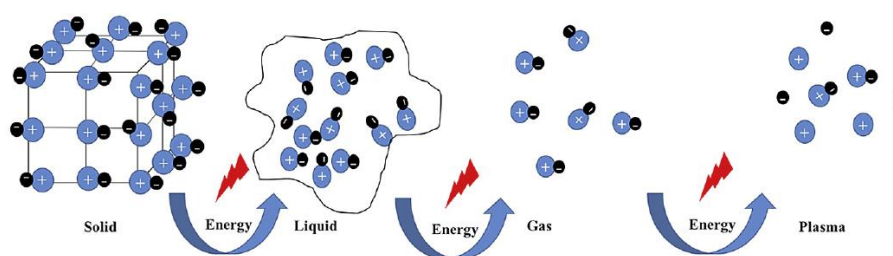
Figure 1.8 Schematic diagram of four state of matter [63].

Plasma can be generated by supplying energy in several forms (e.g. thermal energy, electron beams, electric or magnetic fields, radio or microwave frequencies, and so on) to a neutral gas to form the charge carriers [62, 64]. The most commonly used approach to generate and sustain plasma is gas discharge by applying an electric field to a neutral gas. Electric field increases the kinetic energy of electrons, which results in the enhancement in the collision between electrons and atoms (and molecules) in the gas or on the surface of electrode and reactor wall; and thus generate other new charge carriers and/or reactive species, such as electrons, ions, radicals, excited atoms and molecules, photon, etc. This leads to an avalanche of charge carriers, which is balanced by the annihilation of some charge carriers. As a result, a steady-state plasma is achieved [64, 65].

Gas pressure is an important characteristic parameter of plasma, which influences the total density of component particles and the probability of mutual collisions among these particles (known as collision frequency). In low pressure (10^{-6} – 10^{-4} bar) plasmas, the inelastic collisions between electrons and heavy species are excitative or ionising, which will not raise the temperature of the heavy particles. Therefore, the temperature of electrons is higher than those of the heavy particles. Increasing the pressure enhances the collision frequency, and hence a more efficient energy transfer is achieved, which increases the temperature of heavy particles and leads to a steady-state of energy equilibrium in the plasma [66].

Based on the temperature distribution among different components in the plasma system, plasma can be defined into two categories: thermal plasma and non-thermal plasma. In the thermal plasma, sufficient energy is required to induce the initial excitation in the working gas, followed by the ionisation and generation of various reactive species (e.g.

ionised and dissociated radials, etc.). In this process, the collision frequency between electron and other heavy species are extremely high, which leads to a high ionisation degrees (close to 100%) and provides thermalisation of different species to the thermodynamic equilibrium temperature [67]. That is to say, all the particles (including electrons, ions, atoms, molecules and so on) approximately have the same temperature and energy ($T_e \approx T_n \approx T_{gas}$). By contrast, the non-thermal plasma is characterised by the electron temperature being much higher than that of the bulk gas molecules [68]. Table 1.10 summaries the main characteristics of thermal plasmas and non-thermal plasmas [69, 70]. The overall temperature in thermal plasma is commonly in the order of 10^4 K [67]. The central part of lightning flashes and the core of the sun are examples of natural thermal plasmas; while nuclear fusion, laser fusion, arc torches used in waste incinerator and/or welding, etc. are typical man-made thermal plasmas [66, 71]. In the thermal plasma, the high temperatures enable it to be more powerful and achieve high specific productivity. Thermal plasma are normally adopted in the processes where high temperatures are required, such as cutting, welding, melting, purification, extractive metallurgy, transferred arc reclamation, spraying, etc. [72]. However, thermal plasma is energy intensity, which will consume a large amount of energy and induce the high energy cost. More energy is usually required to cool the electrodes because of the extremely high temperatures in the thermal plasma reactors. In addition, from the viewpoint of energy consumption, it has been reported that much higher energy consumption is required for the production of H_2 from plasma reforming of diesel in the thermal plasma compared to the non-thermal plasma, although the comparable H_2 yields were obtained with these two plasmas [73].

Table 1.10 Main characteristics of thermal plasmas and non-thermal plasmas [69, 70].

Plasmas	Thermal plasma	Non-thermal plasma
Properties	$T_e \approx T_n$ ($\approx 10,000$ K)	$T_e \gg T_n$ $T_e \approx 10,000 \sim 100,000$ K $T_n \approx 300 \sim 1000$ K
	High electron density $10^{21} - 10^{26}$ m^{-3}	Low electron density $< 10^{19}$ m^{-3}
	Inelastic collisions between electrons and heavy particles create reactive species; Elastic collisions heat the heavy particles and electron energy is consumed.	Inelastic collisions between electrons and heavy particles induce plasma chemistry; Heavy particles are slightly heated by only a few elastic collisions.

1.2.2 Non-thermal plasmas and corresponding generation methods

The non-thermal plasma has been applied for flue gas treatment and has been considered very promising for organic synthesis due to its non-equilibrium properties, low power requirement and its capacity to induce physical and chemical reactions within gases at relatively low temperatures. As mentioned in Section 1.2.1, gas discharge by applying an external electric field is the most common method to generate plasma. Electrical breakdown occurs when the external electric field exceeds a certain value. In non-thermal plasmas, although the breakdown is very complicated, they usually start with an electron avalanche [74]. Electrons are generated in the vicinity of cathode and drift down to the anode with the aid of the external electric field. Neutral particles are ionised by the collision with the sufficiently energetic electrons, leading to the production of the secondary electrons. Electron avalanche is the multiplication of primary electrons in cascade ionisation [74]. Compared with thermal plasmas, the ionisation degree in non-thermal plasmas is typically lower ($n_e/n \leq 10^{-6}$) [69, 75] and the electron density is also rather lower, as shown in Table 1.9. As a result, the electrons gain more energy from the external electric field via the successive collisions, which will decrease the electron-neutral interactions and consequently reduce the gas heating effect. That is to say, the input electrical energy can be selectively transferred to the electrons in non-thermal plasmas, which will generate free radicals by

collisions and induce the desired chemical reactions within the gases [76]. It is the high electron temperature that determines the unusual chemistry of non-thermal plasma [77], as the low temperature in the reaction system is not enough for thermal activation. Moreover, non-thermal plasmas are characterised by the low energy consumption, less electrode erosion, reduction of electrode cooling as well as compactness and low weight with relatively simple power supplies. All of these unique characteristics make the non-thermal plasmas potentially suitable in a wide range of applications [78]. One of the applications of non-thermal plasma chemistry was the ozone generation using dielectric barrier discharge, built by Siemens in the 19th century [79]. In recent decades, non-thermal plasmas have been widely investigated in the medical applications [80, 81], gas cleaning (e.g. VOC abatement, NO_x treatment and so on) [76, 82], water purification [68, 83, 84], soil remediation [71], food processing [62, 85], energy production and conversions (e.g. CO_2 conversion and utilisation, CH_4 activation, H_2 production, etc.) [86-91], surface treatment and modification [92-94] as well as catalyst preparations and activations [72, 95, 96].

The chemistry in non-thermal plasmas is usually complex and involves a large amount of elementary reactions. The chemical processes can be divided into a primary and a secondary process according to the timescale, shown in Figure 1.9 [97]. The primary process includes ionisation, excitation, and dissociation as well as light emission and charge transfer, whilst the subsequent chemical reaction between the products from the primary process (e.g. electrons, ions, excited molecules and radicals and so on). The typical time scale of the primary and secondary process is about 10^{-8} s and 10^{-3} s, respectively. The secondary process will produce the additional radicals and/or reactive molecules through radical-neutral recombination reactions [97].
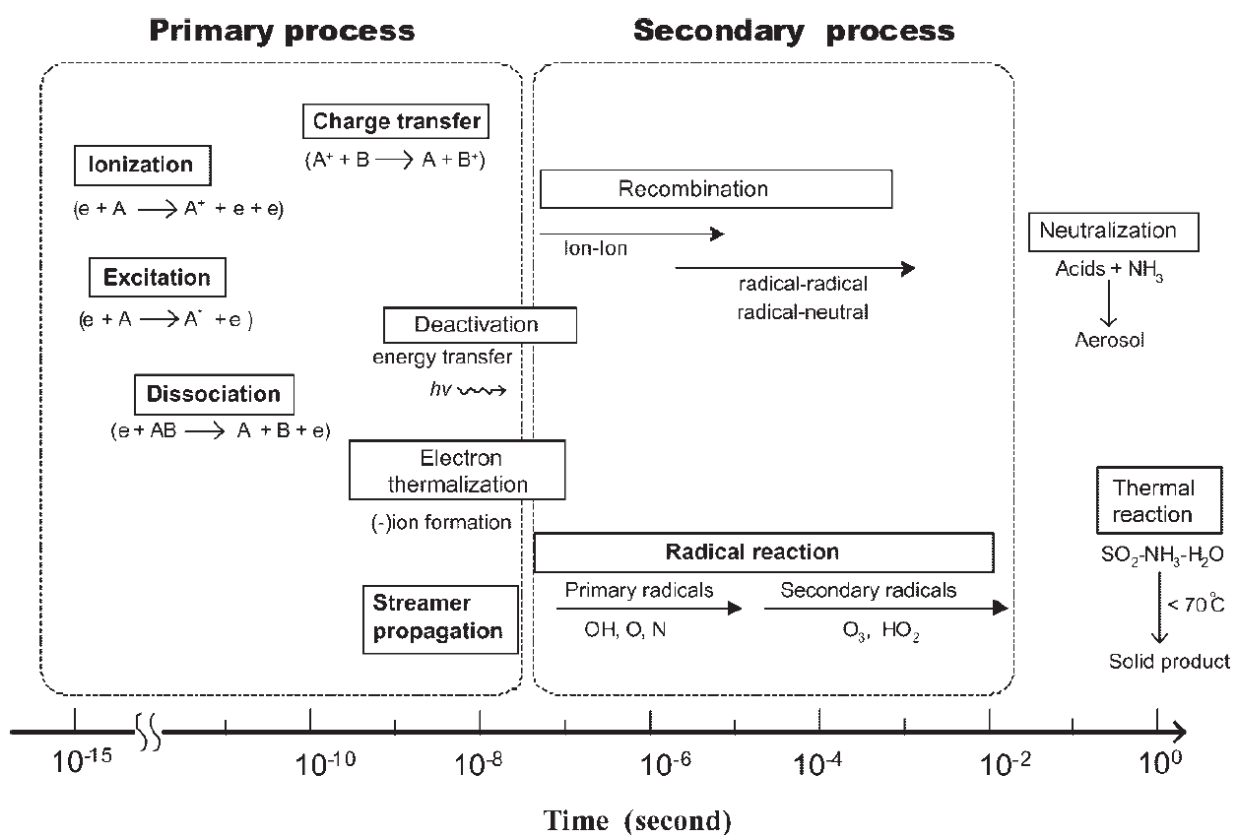
Figure 1.9 Timescale events of elementary processes in a non-thermal process [97].

The reactions in the plasma process can also be divided into homogeneous and heterogeneous reactions. Homogeneous reactions are the reactions take place between the species in the gas phase as a result of inelastic collisions between electrons and heavy species or the collisions between the heavy species. While the heterogeneous reactions occur between the plasma species and the solid surface which is immersed or in contact with the plasma [98]. The typical homogeneous and heterogeneous reactions are listed in Table 1.11 and 1.12, respectively.

Table 1.11 Gas phase reactions involving electrons and heavy species (A, B stand for atoms, A_2, B_2 for molecules; e represents an electron; M is a temporary collision partner; * marks the excited species and the species marked by + or – are ions) [98].

Name	Reactions	Description
Excitation of atoms or molecules	$e + A_2 \rightarrow A_2^* + e$ $e + A \rightarrow A^* + e$	Formation of the excited state of atoms and molecules by energetic electron impact.
De-excitation	$e + A_2^* \rightarrow A_2 + e + h\nu$	Electronically excited state emits electromagnetic radiations, back to the ground state.
Ionisation	$e + A_2 \rightarrow A_2^+ + 2e$	Energetic electrons ionise neutral species through electron detachment and positively charged particles are formed.
Dissociation	$e + A_2 \rightarrow 2A + e$	Molecules are dissociated by inelastic electron impact.
Dissociative attachment	$e + A_2 \rightarrow A + A^-$	Negative ions are formed by the dissociative electron attachment.
Dissociative ionisation	$e + A_2 \rightarrow A^+ + A + 2e$	Positive ions are formed by the dissociative electron ionisation.
Penning dissociation	$M^* + A_2 \rightarrow 2A + M$	Collision of energetic metastable species with neutral species leads to ionisation or dissociation.
Penning ionisation	$M^* + A_2 \rightarrow A_2^+ + M + e$	
Charge exchange	$A^{\pm} + B \rightarrow B^{\pm} + A$	Charge transfer from incident ion to the target neutral between two identical or dissimilar partners.
Ion-ion recombination	$A^- + B^+ \rightarrow AB$	Collision of two ions forms a molecule.
	$A^- + B^+ + M \rightarrow AB + M$	Three-body collision also forms ion-ion recombination.
Electron-ion recombination	$e + A^+ + B \rightarrow A + B$	Loss of charged particles from the plasma by recombination of opposite charges.
	$e + A_2^+ + M \rightarrow A_2 + M$	

Table 1.12 Reactions between the plasma species and the solid surface in the plasma (A, B stand for atoms; R represents a radical; M stands for a molecule; * marks the excited species and the species marked by + are ions) [98].

Name	Reactions	Description
Etching	$AB + C_{solid} \rightarrow A + BC_{vapour}$	Material erosion.
Adsorption	$M_g + S \rightarrow M_s$ $R_g + S \rightarrow R_s$	Molecules or radicals contact with a surface in the plasma and adsorbed on the surface.
Deposition	$AB \rightarrow A + B_{solid}$	Thin film formation.
Recombination	$S\text{-}A + A \rightarrow S + A_2$ $S\text{-}R + R \rightarrow S + M$	Atoms or radicals in the plasma react with the species already adsorbed on the surface to combine and form a compound.
Metastable de-excitation	$S + A^* \rightarrow A$	Excited species collide with a solid surface and return to the ground state.
Sputtering	$S\text{-}B + A^+ \rightarrow S^+ + B + A$	Positive ion accelerated with sufficient energy towards the surface can remove an atom from the surface.
Polymerisation	$R_g + R_s \rightarrow P_s$ $M_g + R_s \rightarrow P'_s$	Radicals or molecules in the plasma can react with radicals adsorbed on the surface to form polymers.

The classification of non-thermal plasma reactors is very complicated and depends on multiple characteristics. They can be divided into different categories according to the discharge mode (e.g. corona discharge, dielectric barrier discharge, gliding arc discharge, and so on), the type of power supply (AC, DC, pulsed, microwave, radio frequency, etc.), the presence of dielectric barriers and/or catalysts, reactor and electrode configurations, polarity, voltage level and gas composition [76, 99]. In the following sections, we will briefly describe the common non-thermal plasma reactors used in the field of environmental and energy applications. Only the atmospheric pressure plasma reactors will be considered in this study.

1.2.2.1 Corona discharge

Corona is a weakly luminous discharge, which is usually generated at atmospheric pressure near sharp points or thin wires when the electric field in the vicinity of the electrode is large enough to accelerate the randomly produced electrons up to the ionisation energy level of the surrounding gas atoms and molecules [100]. The strong electric field, ionisation and luminosity are mainly located near the sharp electrode; the electric current is transferred to the other electrode by the drift of charged particles with the aid of the relatively low electric field. As a result, a low current and thus a low discharge power can be achieved in the corona discharge.

Corona discharge can be generated in the DC and pulsed modes. In the DC corona, the formation mechanism of the electron avalanche is different depending on the polarity of the sharp electrode. Connecting the sharp electrode to the positive output of the power supply leads to the generation of the positive DC corona discharge, which is characterised by the presence of streamers [99]. The discharge would change from the stable corona mode to the unstable spark discharge regime when increasing the applied voltage to a certain threshold value. When the sharp electrode is connected to the negative output, a negative DC corona discharge is generated. The negative DC corona discharge initially form the Trichel pulse corona, followed by the pulseless corona and spark discharge when the applied voltage increases [101]. The formation of spark discharge in the DC corona discharge can be prevented using the pulsed power supply. With the short duration (in the order of $100 - 200$ ns) of a pulse voltage in the pulsed corona discharge, most of the input energy is transferred into the highly energetic electrons rather than dissipated by ions, which accounts for the production of the reactive species as well as the initiation and propagation of series of chemical reaction. Therefore, high energy efficiency can be obtained in the pulsed corona discharge [71]. However, for the large scale applications, corona discharges still suffer from the problems of the high cost for the pulsed power supply, the high malfunction rate and a short life of the electrodes [71].

According to the electrode structures, the corona discharge reactor can have different configurations, such as wire-cylinder, wire-plate, needle-plate, needle-needle types and so

on, as shown in Figure 1.10 [102]. Corona discharges are only generated around the electrode in the wire-cylinder and wire plate reactors, which leads to the small plasma region and weak discharge current. In addition, the stable discharge voltage range is narrow and the spark breakdown is easily formed in the wire-cylinder and wire plate reactors. Compared to the wire-cylinder and wire plate reactors, the spark breakdown voltage is higher and more stable discharge can be achieved in the needle-plate and needle-needle plasma reactors [102]. In the DC corona discharges, the needle-wire and needle-plate plasma reactors are mostly used configurations; however, their overall discharge efficiency is low [102]. Based on the principle of flow stabilised discharge, the DC corona radical shower system (see Figure 1.10) was developed and has been widely used for flue gas purification [103, 104]. In the corona radical shower system, pipe electrodes with nozzles are used and gas flow directly passes through the inside of the electrode. The corona discharge is generated at the tips of the nozzles; the additional gas is injected into discharge region from the nozzles and subsequently dissociated into various radicals.
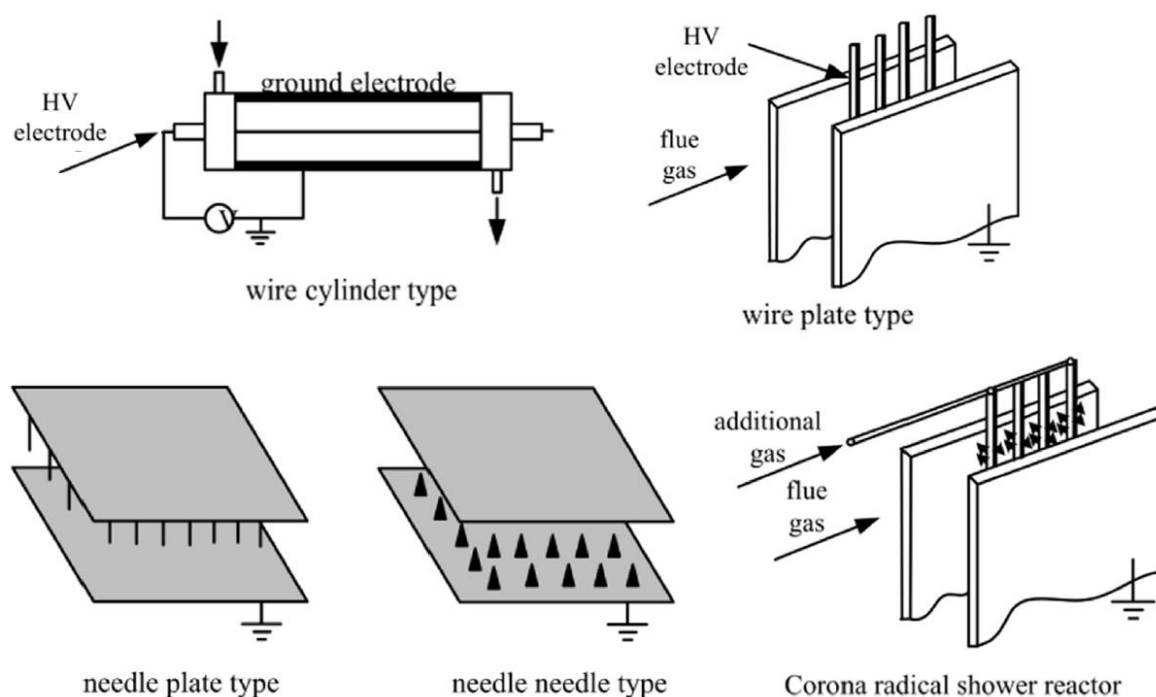
Figure 1.10 Different corona discharge reactor configurations [102].

1.2.2.2 Radio frequency (RF) discharge and Microwave (MW) discharge

RF discharge and MW discharge are two typical discharges that are sustained with high frequency electromagnetic field. They have a unique advantage that the electrodes are kept out of the discharge regions – plasma does not directly contact with electrodes. This electrode-less operation can avoid the electrode erosion and contamination of plasma by metal vapour and can eliminate the requirement for complicated cooling systems.

RF discharge can be obtained when subjecting the discharge gas to an oscillating electromagnetic field. It is named capacitive RF discharge when separate electrodes are arranged on the external surface of the reactor (Figure 1.11 (a) and (b)); while it is inductive RF discharge (Figure 1.11 (c)) if the oscillating electromagnetic field is generated by an induction coil which surrounds the reactor [79, 105]. The capacitive RF discharges are mainly generated at low pressures and form non-thermal plasma, while the inductive RF discharges are used to generate thermal plasma at the pressures of up to 1 bar. The frequencies used to generate the RF plasmas are typically in the range of 0.1 to 100 MHz with a commonly industrial frequency of 13.56 MHz [79].
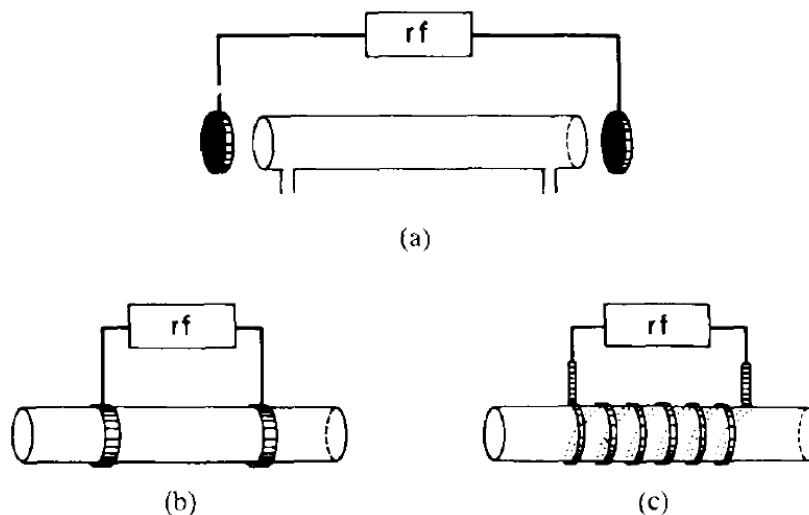
Figure 1.11 Typical arrangement of the RF discharge [79].

The MW discharge are generated by a magnetron (typically at 2.45 GHz) and guided to the process chamber by a wave-guide or a coaxial cable, without electrodes. Figure 1.12

shows a typical sketch of the wave-guide-based microwave plasma [78]. The wave guide is used to collect and concentrate the electromagnetic waves within the reactor. The kinetic energy of the electrons are increased by absorbing the microwave, which leads to the ionisation reactions by inelastic reactions. In the microwave discharge, good coupling between the electromagnetic field and the discharge will create a high degree of ionisation. The injected energy is used with high efficiency to produce a larger amount of highly energetic electrons along with higher amount of active species of interest, compared with other non-thermal plasmas.
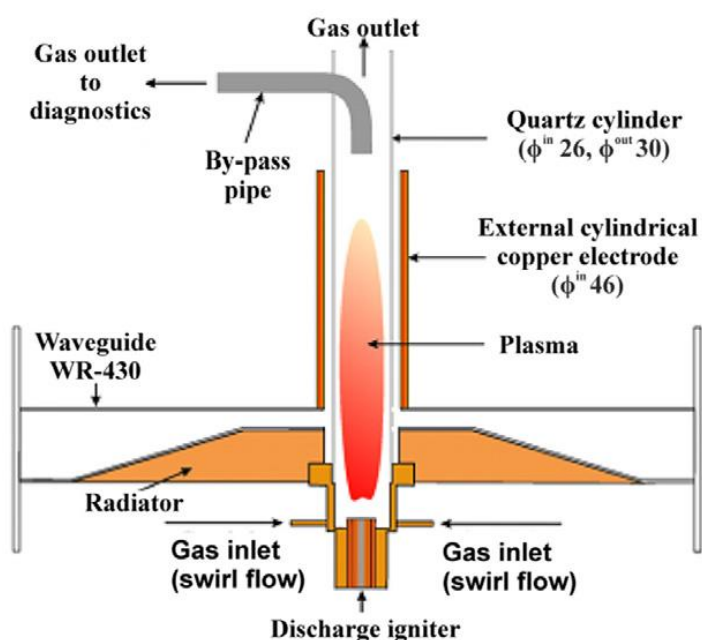
Figure 1.12 Wave guide-based microwave plasma used for H_2 production from hydrocarbon conversion [78].

Compared to the DC plasmas, initiating the high frequency plasmas is very challenging due to the more complex and expensive power supplies which contains the high frequency generators. In addition, the plasma must be coupled into the power circuit as a load. Poor coupling will lead to low efficiency of the power supply and the overall circuit.

1.2.2.3 Dielectric barrier discharge (DBD)

The DBDs are alternating current discharges with the typical electrical operation parameters in the range of several kV ignition voltage from line frequency to several MHz and the power consumption of several W/dm^2 [100]. DBD has a long history from the ozone synthesis, therefore, the fundamental physical and chemical properties and the industrial installation requirements have been widely investigated and are well understood [106]. DBDs usually can be generated in two different discharge modes – filamentary mode and glow (homogeneous) mode. The glow mode DBD can create the barrier discharge homogeneously without streamers and other spark –related phenomena [107]. It is very useful for the homogeneous treatment of surfaces and the deposition of thin films. While the filamentary mode DBD has been widely investigated during the past decades and most industrial DBD applications apply the filamentary mode [107]. Therefore, we only discuss the DBDs with the filamentary discharge mode in this study.

DBDs are usually generated in the planar or the cylindrical configurations, as show in Figure 1.13 (a) and (b). At least one dielectric barrier is placed (e.g. glass, quartz, ceramic materials, alumina and so on) between the two electrodes. The distance between the two electrodes can be micrometers up to centimeters depending on the used discharging gas and the applied voltage. The presence of the dielectric barrier leads to the formation of filamentary microdischarges. Being an insulator, the dielectric restricts the current flow when the discharge is ignited and limits the charge and energy conveyed to an individual microdischarge. It can also enable the microdischarges to distribute over the entire electrode area. With intact dielectric barriers, no spark or arc would occur in the discharge gap and electrode etching and/or corrosion could be avoided if the two electrodes are covered by the dielectric barriers. The amount of the total charge transferred in a microdischarge is influenced by the gas properties, the discharge gap and the properties of the dielectric barriers [108]. Different from corona discharge, DBD is bright. The thin currents are formed by channel streams with nanosecond duration and are statistically distributed in space and time [99, 109].
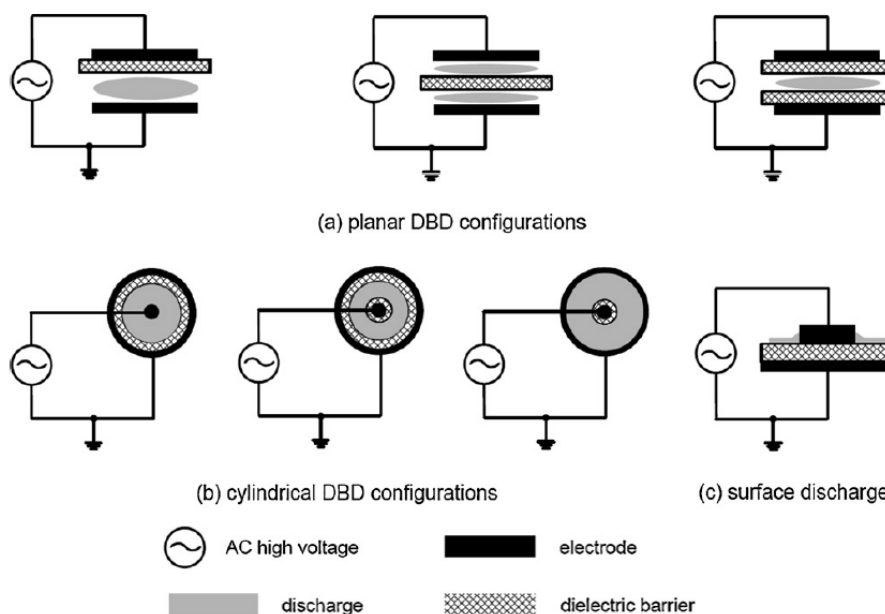
Figure 1.13 Typical configurations of DBDs [64].

In DBDs, the high voltage applied across the two electrodes is sufficient to establish a high electric field for the gas breakdown. The local electron density at certain locations in the discharge gap reaches a critical value and a large amount of separate and short-lived current filaments (also known as microdischarges) are formed. The microdischarges appear as spikes on the current waveform. Each microdischarge has an almost cylindrical plasma channel with a typical radius about 100 µm [108]. When one microdischarge reaches to the surface of the dielectric barrier material, it will spread into a surface discharge; and the transferred charge will accumulate on the dielectric surface, which will reduce the electric field. As the electric field is further reduced, electron attachment will prevail over ionisation and the microdischarge will be extinguished. When the polarity of the AC voltage changes, the microdischarge will be formed again at the same location if the electron density is high enough for electrical breakdown. As a result, the nanosecond microdischarges are continuously formed at a frequency which is double of the applied frequency [110]. The position of the microdischarge is closely related to the residual charge distribution on the dielectric surface due to memory effect [111]. There are three stages in the life cycle of one filamentary discharge – the electrical breakdown, the charge transportation across the gap and the excitation of atoms and molecules to initiate the reaction kinetics [108]. Surface

discharge is another form of DBD (see Figure 1.13 (c)). A thin and long electrode is placed on one of the dielectric barrier surface; while the reverse side of the dielectric surface is covered by an extended counter-electrode. In the cylindrical configuration, strip electrodes can be placed on the inner surface of the reactor [112].

Packed-bed DBD reactor is similar to the normal DBD reactor. Pellets of the dielectric materials are placed in the discharge gap between the dielectric barrier and the electrode, which results in the formation of the contact points between pellets as well as between pellets and electrode (dielectric barrier) surface, as shown in Figure 1.14. When applying the high electric field across the two electrodes, a spontaneous polarisation of the dielectric pellets occurs in the direction of the external electric field, which leads to a high electric field at the contact points [76]. The electric field at the contact points is significantly higher than the mean electric field between the two electrodes. This allows the production of partial discharges in the vicinity of each contact point. The enhanced electric field leads to a higher mean electron energy. The energetic electrons are beneficial to the generation of reactive species via dissociation and ionisation [99]. The presence of the dielectric materials in the discharge regions contributes to a uniform gas distribution and electrical discharge. Materials with different dielectric constants can be used as the dielectric pellets, including glass, quartz, alumina, ceramics and ferroelectrics. Dielectric pellets with high dielectric constants can reduce the critical breakdown voltage, which is favourable for industrial application [113]. For example, barium titanate ($BaTiO_3$) is one of the most widely used ferroelectric materials in the packed-bed DBD reactor for the environmental purposes due to its high dielectric constant (2000 ~ 10,000) [99]. The discharge performance of the packed-bed DBD reactor is significantly dependent on the material, dielectric constant, size and shape of the dielectric pellets. The dielectric material mainly affects the reactions between gas and solid phases, while the other parameters have a significant effect on the discharge characteristics [114]. In the packed-bed DBD reactor, catalyst pellets can also be used as the dielectric pellets and positioned in the discharge volume. This is one form of plasma-catalysis system. The details of the plasma-catalysis will be described in the following section.
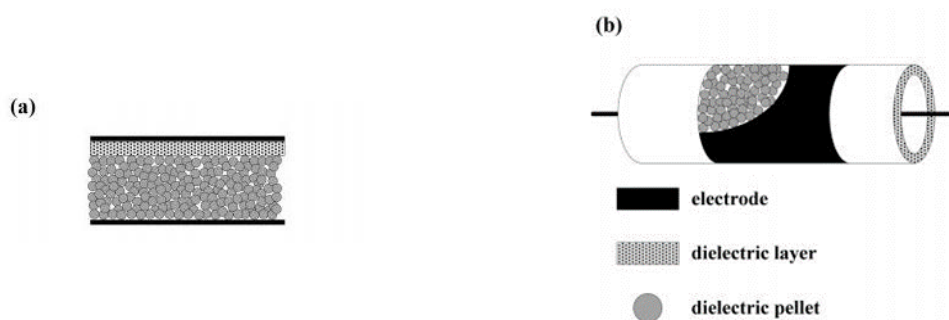
Figure 1.14 Illustration of packed-bed DBD reactor: (a) parallel-plate and (b) cylindrical types [114].

1.2.2.4 Gliding arc discharge (GAD)

GAD is non-equilibrium plasma generation method near atmospheric pressure. It was firstly proposed by A. Czernnichowski [115]. The typical quasi-two-dimensional bi-electrode gliding arc discharge device is illustrated in Figure 1.15. High voltage is applied between a pair of divergent flat electrodes to ignite the arc. The arc is firstly generated at the shortest distance between these two electrodes, and then moves with the gas flow from the inlet hole placed at the lower part of the axis of the two electrodes. The arc length elongates when it moves along the diverging electrode until the supplied power cannot sustain itself. Then the arc extinguishes, but immediately a new arc is generated at the narrowest gap. Through this ignition-evolution-extinction cycle, as shown in Figure 1.15(b) [116], the GAD region is formed.
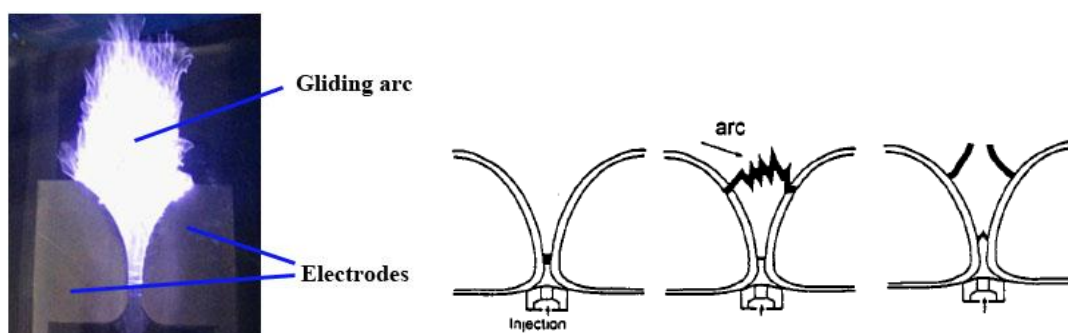
Figure 1.15 Phenomenon of gliding arc discharge: (a) photograph of gliding arc discharge; (b) ignition, evolution and extinction of the gliding arc discharge [116].

The evolution of GAD goes through three different stages [117, 118]: the initial break-down stage, the equilibrium stage and the non-equilibrium stage, as shown in Figure 1.16. In addition, there exists a fast transition between the equilibrium and the non-equilibrium stages, which is called Fast Equilibrium to Non-equilibrium (FENETRe). The physical characteristics of each particular stage will be described in the following sections.
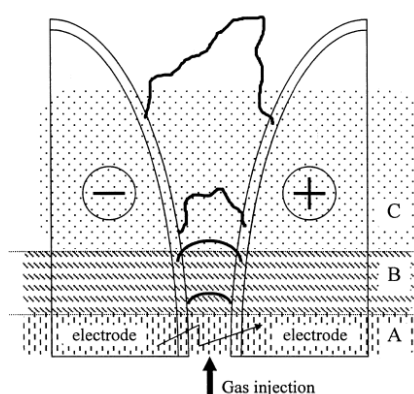
Figure 1.16 Gliding arc evolution process: (A) reagent gas break-down; (B) equilibrium heating phase; (C) non-equilibrium reaction phase [117]

(1) Initial break-down stage

The evolution process of the gliding arc commences when the gas between the two electrodes is broken down by the high external electric field. Immediately after breakdown, the discharge is formed at the shortest distance between the two electrodes. The characteristic time of the arc formation can be calculated by the kinetic equation for the electron concentration. This characteristic time is about 1 μs when the total arc electrical current is 1A [117]. During this period, a low resistance plasma is formed and the voltage between the electrodes falls rapidly.

(2) Equilibrium stage

In this stage, the equilibrium gas temperature T_0 does not change drastically, which lies in the range of $7000 \leq T_0 \leq 10000$ K [117] and would be different within the experiments with lower electric current and lower power. The quasi-equilibrium arc plasma column moves with the gas flow, and the gliding arc velocity is very close to that of the gas flow. As the arc motion is very complex, it cannot be well defined geometrically and no quantitative

models have been well developed for the description of the relative velocities of the arc and the gas flow. For relatively small power (200W) and gas flow velocity (10 m/s), the gliding arc velocity was equal to the gas flow velocity [117]. The difference in arc and gas velocities increases with the increase of the applied power and the absolute value of the flow velocities, while decreases with the increase of the arc length [119]. The main features of GAD in this stage are the relative high current (1~10000 A) and the rather low voltage (e.g. for air at 1 atm pressure and 10 A current, and the electric field is 20V/cm). With the increase of the plasma column length, the current decreases gradually, but the power dissipated per unit length of the arc column remains almost constant, resulting in the increase of the arc voltage.

In this stage, thermal ionisation is dominant and it is stable due to the peculiarity of both the heat and electric current balances of the arc discharge. The electron temperature T_e is close to the gas temperature T_0 and the ion temperature T_i. The electrical conductivity σ mainly depends on the gas temperature: a slight increase in the gas temperature will cause an obvious increment of the electron concentration n_e and the electrical conductivity σ. This can be compensated through declining the electrical field strength E, which will decrease the heating power σE^2 and thus the gas temperature, resulting a new equilibrium state. This can be briefly stated as: $T_0\uparrow \Rightarrow \sigma\uparrow \Rightarrow E\downarrow \Rightarrow \sigma E^2\downarrow \Rightarrow T_0\downarrow$.

(3) Fast Equilibrium to Non-equilibrium (FENETRe) stage

The equilibrium and the non-equilibrium stage simultaneously exist in the FENETRe stage. In this stage, the arc length exceeds the critical value and continues to increase, and the heat loss also increases. However, the applied electrical power cannot increase, which cannot sustain the gliding arc in the thermodynamic equilibrium state. The gas temperature reduces rapidly due to the heat transfer to the surrounding gases, while the electron temperature remains at a relative higher value. In this stage, the electron concentration reduces, while the plasma electrical conductivity is maintained by the high electron temperature ($T_e \approx 1$ eV) [117] and stepwise ionisation. In the transition stage, the ionisation pattern transforms from thermal to direct electron impact ionisation, which is usually not stable. In the case of fixed pressure and constant electric field E, a slight increase in the

temperature T_0 will lead to a reduction in the gas concentration n and an increment in the specific electric field E/n and the ionisation rate, which leads to an increase in the electric conductivity σ and the electron concentration n_e, thus increases the heating power σE^2. As a result, the gas temperature further increases, which induces a total discharge instability. This process can expressed briefly as follows: $T_0\uparrow \Longrightarrow \sigma\uparrow \Longrightarrow \sigma E^2\uparrow \Longrightarrow T_0\uparrow$.

(4) Non-equilibrium stage

      After the above fast transition, the gliding arc continues its evolution under the non-equilibrium conditions, where $T_e \gg T_0$. In this stage, the specific heat loss is numerically three time less than that in the equilibrium stage. The arc length can increase up to a new critical value, which about three times of that in the equilibrium stage. The plasma parameters are similar to those of the microwave discharge in the diffusive regimes at moderate pressure (30-200 torr): $T_0 \approx 1500\text{-}3000$ K, $T_e \approx 1$ eV [117].

      Based on the above analysis, it can be seen that the discharge is stable when the plasma conductivity mainly depends on the gas temperature; while the discharge becomes unstable when the electric field strength is relative high and the plasma conductivity mainly varies with the electric field strength. In the non-equilibrium stage, due to the strong sensibility of the plasma conductivity to the variation of electric field strength, the reduction of the electron concentration cannot be compensated by the growth of the electric field strength. This is the main physical reason for the quasi-unstable discharge behaviour in the FENETRe conditions. V. Liventsov et al. presented the physical parameters variation during GAD, as shown in 1.17 [117, 120]. At some specific condition, up to 75-80% of the gliding arc power can be dissipated in the non-equilibrium zone [117].
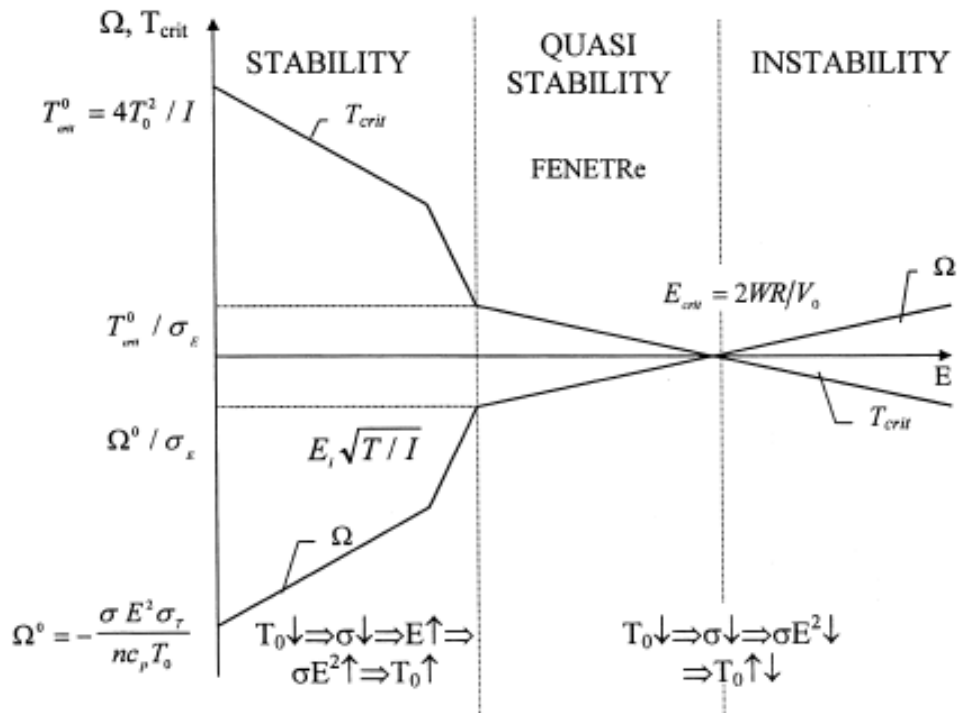
Figure 1.17 Characteristics of gliding arc evaluation parameters [120].

GAD has a relatively low electron temperature, but reasonably high electron density and neutral gas temperature. It has wide applications in the area of environmental pollution control and energy production due to its simple configurations and strong ability of inducing physical and chemical reactions [121]. Recently, several new GAD reactors have been developed based on the basic principles and characteristics of the traditional GAD reactor, such as multi-electrode GAD reactor [122], cone-shaped rotating GAD reactor [123], laval nozzle GAD reactor [124], magnetic GAD reactor [125], and reverse vortex GAD reactor [126], as shown in Figure 1.18.

(a) (b)

(c) (d)

(e)
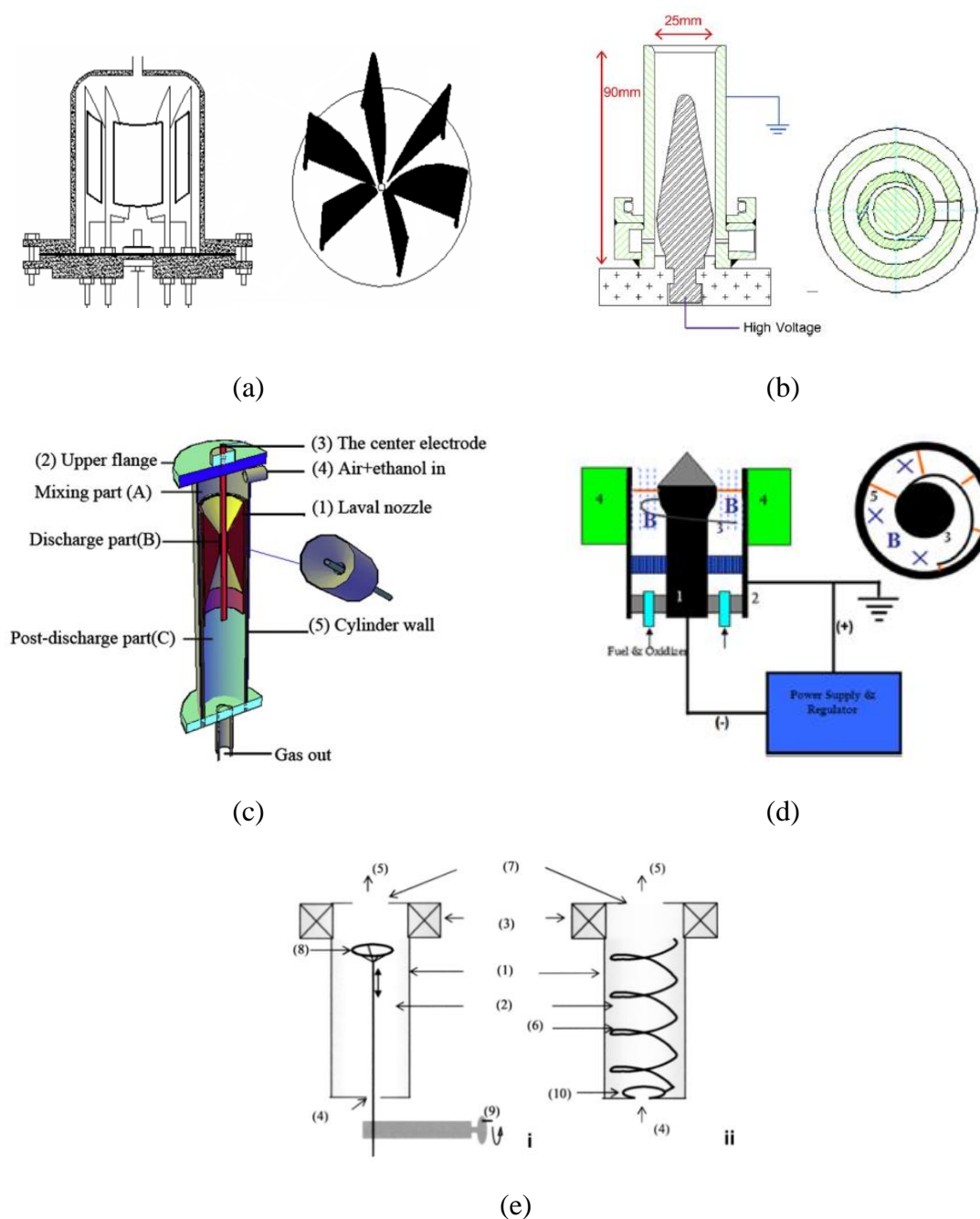
Figure 1.18 Different new GAD reactor configurations: (a) multi-electrode GAD reactor [122]; (b) cone-shaped rotating GAD reactor [123]; (c) laval nozzle GAD reactor [124]; (d) magnetic GAD reactor [125]; (e) reverse vortex GAD reactor [126].

1.2.3 Plasma-catalysis systems

The chemistry in the non-thermal plasma is very complicated and the selectivity of the desired product is typically low. It is possible to use the non-thermal plasma more effectively by exploiting its inherent synergistic effect by combining non-thermal plasmas with

heterogeneous catalysts, which is known as plasma-catalysis. Plasma-catalysis takes advantages of the low temperature activity, fast response and compactness of plasma reactor and the high selectivity of the catalytic reaction, which has the potential to increase the energy efficiency and optimise the by-product distribution. Figure 1.19 shows the common methods to combine non-thermal plasma and heterogeneous catalysts based on the position of the catalyst bed and plasma region [127, 128]. In the two-stage configuration, the catalyst bed is placed downstream of the plasma zone. In this method, chemically reactive species with long life times and easily formed products as well as the un-converted reactants interact with catalysts in the catalyst bed for further catalysis; this method is also called post plasma catalysis (PPC). It is the most applied configuration for two-stage plasma-catalysis. Actually, catalyst bed can also be located upstream of the plasma zone in the two-stage configuration. In this way, only the residual reactants and undesired by-products from the thermal catalysis are converted in the plasma region. In the single-stage configuration (also named in plasma catalysis: IPC), the catalyst bed can directly interact with plasma as it is completely or partially placed in the plasma zone. In this configuration, both short-lived (e.g. energetic electrons, excited atoms and molecules, radicals, photons and so on) and long-lived active species are involved in the plasma-catalytic reactions [129]. Figure 1.20 shows the common catalyst arrangement methods to place the catalyst in the IPC configuration [128]: (a) coating catalyst on the electrodes or on the reactor; (b) impregnating catalyst on honeycomb, foam and other porous materials (e.g. granulates, coated fibres, pellets), usually to form the fully packed-bed reactor; (c) a layer of catalyst materials (powder, pellets, granulates, coated fibres) to form the partially packed-bed configuration. It has been reported that in the fully packed configuration, the discharge mode changed from the typical filamentary microdischarge to a combination of spatially limited microdischarge and a predominant surface discharge on the catalysts surface; while in the partially packed configuration, strong filamentary discharge still could be observed, which significantly enhanced the interaction between the plasma and catalyst, and therefore result in the higher plasma catalysis performance of dry reforming of CH_4 than that in the fully packed configuration [55].
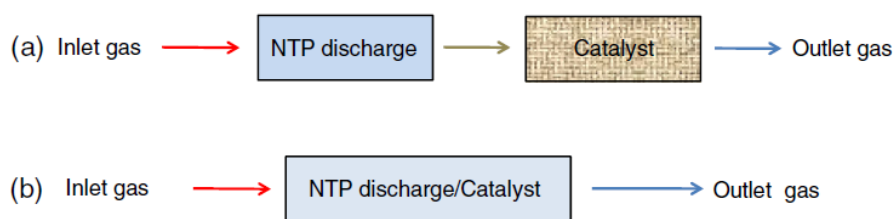
Figure 1.19 Schematic diagram of plasma-catalysis configurations: (a) two-stage configuration and (b) single-stage configuration [127, 128].
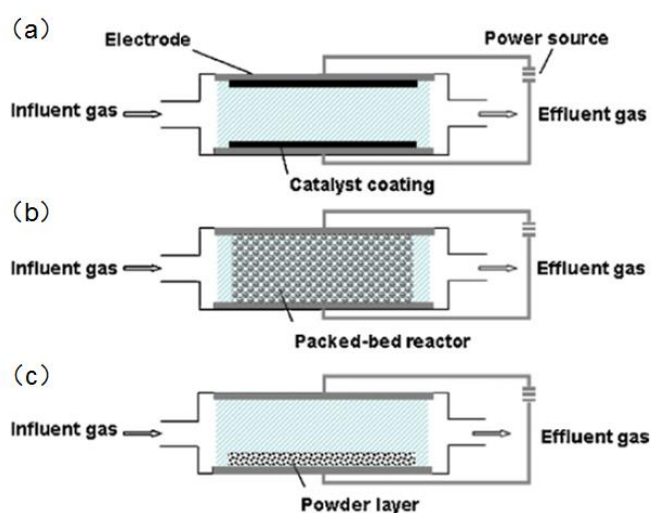
Figure 1.20 Common catalyst arrangement methods in the IPC plasma-catalysis configuration [128].

In the plasma-only process, a gas phase plasma gas discharge changes the chemistry of the bulk gas and involved reactions are mainly related to the gas phase activation. It is homogeneous reactions. Heterogeneous reactions are introduced into the reaction system when placing heterogeneous catalysts in the discharge region [127]. The presence of the catalysts can shorten the discharge gap and modify the plasma characteristics and the discharge behaviour; the reactive species generated in the plasma can be transported to and be adsorbed on the catalyst surface, which might change the chemical environment on the catalyst surface and react with the adsorbed molecules. In the single-stage plasma-catalysis configuration, the interaction between plasma and catalysts are very complicated, which can be discussed from two aspects: (1) the influence of catalysts on the plasma characteristics; (2) the changes in catalysis induced by the plasma. Figure 1.21 summarises the possible

plasma-catalyst interactions [130], which might generate the plasma-catalysis synergistic effect: the reaction performance in the plasma-catalysis process is higher than the sum of that in the plasma-only and catalysis-only process. As a result, the reactant conversion, product selectivity and energy efficiency of the plasma-catalysis process are significantly improved. The mechanism of plasma-catalysis has been discussed in the previous reviews in detail [130-133]. The plasma-catalysis synergy has been demonstrated in the VOC removal, NH_3 synthesis, dry reforming of CH_4 and CO_2 decomposition [55, 57, 134-136].
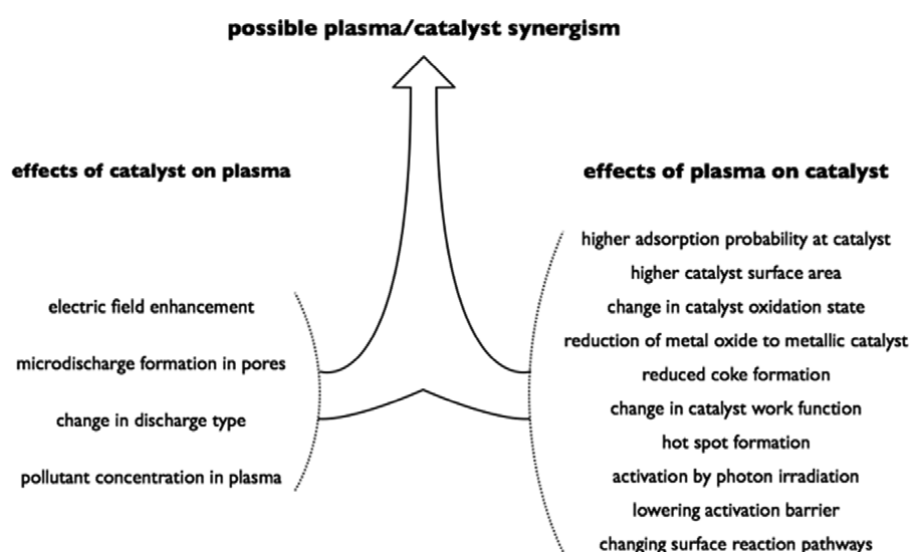
Figure 1.21 Overview of the various effects of the catalyst on the plasma and of the plasma on the catalyst [130].

1.3 Literature review of tar conversion using plasma systems

Different non-thermal plasma systems have been used for the conversion of tar from biomass gasification, including corona discharge [51, 137-141], MW discharge [50, 142], GAD [49, 53, 143, 144], DC pulsed plasma [52], etc. The state of the art will be briefly described in the following part.

Nair et al. developed a pulsed corona discharge system for the cracking of biomass tar [51, 137-141]. They investigated the tar removal in different background gases and found that a larger amount of energy was required for tar (e.g. naphthalene, toluene and phenol) removal in the N_2/fuel gas (20% CO, 12% CO_2, 17% H_2 and 1% CH_4) discharge than that in the pure N_2 discharge. This indicated that the radical termination reactions had a more

significant influence on the plasma tar removal process in the discharge containing fuel gas [51]. They also identified the primary processes for the plasma tar removal in biomass derived fuel gas at temperatures of 200°C and found that the tar (heavy aromatic hydrocarbons) was mainly removed via oxidation [137]. In addition, they extended their work at higher temperatures up to 500 °C and calculated the radical yields at different temperatures by chemical kinetic study. They found that the specific energy consumption for tar removal at 400 °C was around 200-250 J/L, whereas it was about 400-600 J/L at 200 °C. Further increasing the reaction temperature (e.g. 600 °C) led to production of more H radicals, which increased the energy consumption for complete removal due to regeneration of the dissociated naphthalene. Therefore, the optimum temperature for tar removal was around 400 °C [139, 141]. Furthermore, they developed the streamer corona generated by an alternative "DC/AC" power source to overcome the challenge of the availability of high power pulsed power sources for the pulsed corona. They found the chemical efficiency of the tar removal in the plasma process was similar in pulsed and streamer corona, although the difference in the energy consumption was observed [140]. In these investigations on the tar removal in the pulsed corona plasma processes, the final products from tar cracking were not discussed and the mechanisms of the plasma processes were not provided.

Chun et al. developed a GAD plasma reformer for the conversion of biomass tar (e.g. anthracene, naphthalene and benzene) into syngas [49, 143, 144]. The GAD reactor was made up of three blade-type electrodes mounted with 120°. In the plasma conversion of anthracene, the effect of steam flow rate, power input, total gas flow rate and input concentration of anthracene was investigated in terms of anthracene conversion and energy efficiency [143]. The conversion of anthracene was 61% in the absence of steam in the reaction. The highest conversion of anthracene of 96.1% was achieved in the optimal condition at a water steam flow rate of 0.63 L/min, a specific energy input (SEI) of 0.175 kWh/m^3, a total gas flow rate of 12.05 L/min and an input anthracene concentration of 0.21 g/Nm^3. The corresponding energy efficiency was 1.14 g/kWh. H_2, CO and CO_2 were the main gas products in their study. They also found that almost no carbon deposition was

observed when the flow rate of the water steam was higher than 0.37 L/min [143]. In the plasma conversion of naphthalene, they tested the effect of steam/carbon (S/C) ratio, SEI, total gas flow rate, input naphthalene concentration and the electrode length [144]. Through the parametric analysis, the optimal experimental condition (an S/C ratio of 2.5, an SEI of 1 kWh/m^3, a total gas flow of 18.4 L/min, an input naphthalene concentration of 1%, and an electrode length of 95 mm) was obtained for the highest naphthalene conversion. In this optimal condition, the naphthalene conversion and corresponding energy efficiency was 79% and 49 g/kWh [144]. In addition to the above influencing factors in the GAD reactors, they also considered the effect of nozzle diameter, the shortest gap between the electrodes and the electrode shape when carrying out the plasma conversion benzene in the GAD reactor [49]. They found that a smaller nozzle diameter, a longer electrode gap and a longer electrode length could result in a higher benzene conversion and energy efficiency in a stable plasma discharge condition. Zhu et al. developed a novel rotating GAD for tar destruction [53]. The rotating GAD reactor was composed of a conical inner electrode (anode) and a grounded cylindrical outer electrode (cathode). A ring magnet was situated coaxially with the electrodes to provide a magnetic field (approximately 2000 G) oriented along the reactor axis. Toluene in the N_2 flow was selected as the tar surrogate. The influence of the toluene concentration and the flow rate on tar destruction were investigated. A highest destruction efficiency of 95.2% was obtained in a toluene concentration of 10 g/Nm^3 and a total flow rate of 0.24 Nm^3/h. The products of toluene decomposition were mainly the valuable gases (e.g. H_2 and C_2H_2) and solid carbon. The highest selectivity of these two gas products were 39.4% and 27.0%, respectively. In addition, CH_4, C_2H_4 and C_2H_6 were minor products with a low total selectivity of no more than 5% and some small amounts of high-molecular by-products were also produced. The carbon deposition was the major negative factor in this plasma process for toluene destruction as no oxidants (e.g. CO_2 and H_2O) were used [53].

Eliott et al. developed a 1 kW MW plasma system for the destruction and reforming of tar from biomass gasification [50]. The system could run at atmospheric pressure using N_2 and Ar as carrier gas under a large range of flow rates. The injected tar was obtained from pine pyrolysis and was diluted in commercial ethanol (92.5% ethanol and 7.5% water) to

reduce its viscosity. Experiments were performed using a gas mixture of Ar, N_2, H_2O, ethanol and tar at controlled concentration (from 0.8 g/Nm^3 to 4.2 g/Nm^3) to simulate the producer gas from the gasifier. The results indicated that all supplied tar was destroyed in the plasma reactor as no tar content was detected at the reactor outlet. The main products were H_2, CO, O_2 and solid carbon (C(s)) and neither NO nor CO_2 were detected. In this MW discharge reactor, Ar cannot be totally replaced by N_2. The maximum nitrogen-argon (N/Ar) mass ratio obtained was 1.9, beyond which the torch became unstable and quenching was inevitable. The utilisation of Ar would increase the operation cost due to the high price of Ar. Additionally, the accumulation of carbon inside the torch reactor quartz tube would prevent the microwave from reaching and interacting with the gas molecules and also lead to quenching [50]. Wnukowski developed a MW plasma reactor for biomass tar destruction [142]. Toluene was selected as a tar surrogate and N_2 was used as a carrier gas. This reactor was proved effective for toluene decomposition as the high toluene conversion of > 95% were obtained. The main products from toluene decomposition were soot and hydrocarbons (e.g. CH_4 and C_6H_6) with molecular weight lighter than that of toluene [142].

For the plasma-catalytic conversion of biomass tar, Tao et al developed a non-thermal pulsed plasma reactor with a pin-pin configuration for the catalytic steam reforming of toluene as a model tar compound over a 5 wt.% Ni/SiO$_2$ catalyst [52]. The plasma was generated by applying a negative high voltage using a direct current (DC) power supply. For comparison, direct thermal decomposition, plasma-assisted decomposition and catalytic reforming of toluene were also investigated. Plasma enhanced catalytic steam reforming showed the best performance. The results indicated that the introduction of a plasma to the catalytic reforming reaction accelerated the conversion of toluene. The presence of the Ni/SiO$_2$ catalyst in the plasma region significantly enhanced the selectivity and the formation rate of CO and H_2. The plasma-catalytic reaction was performed using He as the carrier gas and with the aid of extra heating (773 K) [52].

1.4 Research objective and approach

As mentioned above, the depletion of fossil fuel sources and the global climate change due to CO_2 emissions from the combustion of fossil fuels has become a major concern for the sustainable development of human society. It is more and more important and urgent to develop and utilise new energy sources, which are abundant, environmentally friendly and with low carbon emissions, such as solar, wind, geothermal and biomass. Compared to the other new energy sources, biomass can provide stable power like fuel fuels as it depends less on the weather and geometrical conditions. Biomass gasification is gaining more and more attention as a promising biomass utilisation approach. However, tar formation in the producer gas with unacceptable levels is the main problem during the biomass gasification, as it will cause fouling, clogging and corrosion problems in downstream equipment upon cooling and condensing. It is also harmful to our health due to its carcinogenic character. Several strategies have been used for tar removal, including physical/mechanical, thermal cracking and catalytic tar elimination methods. However, these approaches usually have the drawbacks of high energy cost, low efficiency, deactivation of catalysts and/or secondary pollution.

Recently, non-thermal plasma technology has been widely investigated in the field of energy production and environmental protection due to its non-equilibrium properties and the unique capacity to induce both physical and chemical reactions at low temperatures as well as the compactness and flexibility of the plasma system. In addition, the use of non-thermal plasma in combination with solid catalysts has the potential to enhance the conversion of feed gases, improve the selectivity towards the desirable products and to reduce the operating temperature of the catalyst, and consequently increases the energy efficiency of the plasma process and improves the stability of the catalyst by reducing poisoning, coking and sintering. Therefore, non-thermal plasma provides an attractive alternative to the conventional routes for the conversion of biomass tar into value-added fuels and chemicals.

The present study focuses on steam and dry reforming of biomass tar, which aims to advance the current state of knowledge of plasma-assisted tar removal with the help of

fundamental study. The necessity of processing biomass tar to produce the clean fuels (H_2 and CO) cannot be satisfied with the existing knowledge from plasma treatment of the conventional producer gas. Therefore, a more depth knowledge of the reaction pathways undergone by the chemical structure present in these aromatic hydrocarbons in plasma reforming processing is required. Besides, mechanistic understanding of the reforming pathways requires the information of the active chemical species exists in the plasma zone as well as the primary reforming products. This was achieved by employing a system consisting a 2D gliding arc reactor directly coupled with the on-line analytical equipment, such as optical emission spectrometer and GC-MS, which was used to investigate the formation of different reactive species in the plasma reforming of tar and to identify the by-products, individually.

In addition, the reaction process was further simplified by considering the reforming of one component of biomass tar at a time. Two different model compounds, toluene and naphthalene were employed in this project because they are the typical light aromatic and poly-aromatic structures present in biomass tar. Using the model compound allows to gain a better understanding of the reaction pathways that occur in plasma reforming in a continuous reactor without having the interference of the mixture of complex polycyclic aromatic hydrocarbons that composes biomass tar.

The present work has two main objectives: the development of a new continuous plasma and plasma-catalyst reactor and the study of reaction pathways of toluene and/or naphthalene at different operating conditions, performed in the designed reactor.

Development, construction and commissioning of plasma and plasma-catalysts reactor
1. Develop a continuous plasma reactor and/or plasma-catalysis reactor that can operate at high temperatures, high inlet concentration of tar for a long time.
2. Perform a Hazard and Operability (HAZOP) study.
3. Implement all HAZOP decisions in a control system.

Steam and Dry Reforming Experiments on toluene and naphthalene

1. Investigate the role of steam and CO_2 in the process of tar reforming.

- Study the influence of H_2O and CO_2 on the conversion of toluene and naphthalene.

- Investigate 5 different inlet concentrations of H_2O and CO_2.

- Identify all reactive species formed in the plasma reforming reaction at these conditions.

- Compare the yield of products and energy efficiency of the reaction process at different conditions.

- Determine the gaseous and liquid products formed at these conditions.

- Determine potential reaction pathways for toluene and naphthalene by varying the concentration of H_2O and CO_2.

2. Study variation of reactant concentrations at different discharge powers.

3. Determine the nature and the effect of Ni-based catalysts in DBD plasma reactor

- Investigate the conversion of toluene at three nickel loading amounts.

- Identify all products formed.

- Determine possible reaction pathways for toluene in the plasma-catalysts system.

4. Investigate the role of Ni-Co bimetallic catalysts in GAD plasma reactor.

- Study the influence of the ratio of Ni and Co on the conversion of toluene and naphthalene.

- Evaluate the designed plasma-catalysts reaction system.

- Identify all products formed (liquid and gaseous).

- Determine the properties of the Ni-Co bimetallic catalyst.

5. Techno-economic analysis of clean fuels production based on biomass gasification.

1.5 Thesis outline

The contents of this thesis are arranged as 7 chapters. The first chapter primarily describes the current status of the utilisation of biomass energy and the tar issues during the process of biomass gasification, including the different approaches used for tar elimination.

Then, the basic principles, characteristics and classifications of plasma as well as the generation methods of non-thermal plasma are described, followed by the reviews of the research progress and the remaining problems in the plasma processes for biomass tar removal. The research scope of this thesis is provided in the last part of Chapter 1.

Chapter 2 describes the experimental system for the plasma reactions, measurement and analysis of electrical signals, catalyst preparation and characterisation methods, spectroscopic diagnostics as well as the analysis methods for the gas and liquid products.

In Chapter 3, the plasma steam reforming of toluene is investigated in a GAD reactor. The performance of the conversion of toluene in the GAD reactor is firstly discussed in the presence or absence of steam. Then, the influences of different processing parameters (S/C molar ratio, toluene feed rate and SEI) on the plasma process are systematically studied in terms of toluene conversion, energy efficiency of the plasma process and the yield of the gas products. The liquid products are quantitatively analysed using GC-MS. Optical emission spectroscopy (OES) is used to detect the reactive species in the during the plasma process under different conditions. Based on the analysis of OES and the gas and liquid products, the possible reaction mechanisms and pathways involved in the plasma conversion of toluene are deduced.

Chapter 4 performs the combined (CO_2 and steam) reforming of toluene in a GAD reactor. The effect of the CO_2 content in the feed gas on the performance of the plasma process is analysed in the absence of steam. The optimum CO_2 content is determined based on the conversion of toluene, energy efficiency of the plasma process and the yield of gas products. The role of CO_2 on the reaction pathways in the plasma conversion of toluene is discussed through OES analysis. Then, steam is added into the feed gas to investigate the combined effect of CO_2 and steam on the conversion of toluene in the GAD reactor. Two possible reaction pathways are discussed.

In Chapter 5, the plasma-catalytic steam reforming of toluene over the $Ni/\gamma-Al_2O_3$ catalysts is carried out in a coaxial DBD reactor. The effect of Ni loadings in $Ni/\gamma-Al_2O_3$ catalysts on the plasma-catalytic conversion of toluene is investigated in terms of toluene conversion, energy efficiency of the plasma-catalytic process as well as the distribution of

gas and liquid products. For comparison, the plasma steam reforming process is also performed in the same DBD reactor in the absence of the Ni catalysts. The possible reaction mechanism is discussed based on the quantitative and qualitative analysis of gas and liquid products.

Chapter 6 firstly studies the plasma process for the removal of a tar mixture (toluene and naphthalene) in a GAD reactor in the absence of catalysts. The effects of different process parameters (the S/C molar ratio, initial naphthalene concentration and the discharge power) on the performance of the plasma process are investigated in terms of toluene and naphthalene conversion, energy efficiency of the plasma process and the yield of the gas products. The reaction mechanisms are discussed in detail through the analysis of OES and the formation of gas and liquid products. Then, the γ-Al$_2$O$_3$ supported Ni, Ni-Co and Co catalysts are prepared for the plasma-catalytic steam reforming of the tar mixture in the GAD reactor. Catalyst characterization techniques, including N$_2$ adsorption–desorption, X-ray diffraction (XRD) and temperature-programmed reduction by H$_2$ (H$_2$-TPR), Transmission electron microscope (TEM) and thermo-gravimetric analysis (TGA) are used to investigate the catalyst properties and to understand the role of the catalysts in the plasma-catalytic steam reforming of tar in the GAD reactor. By comparing the conversion efficiency and energy efficiency, the performance of our system and other syngas cleaning approaches (thermal/catalytic cracking) are discussed. Based on non-stoichiometric Gibbs energy minimization approach, two models of gasification are developed for the utilization of various feedstock; there are plasma gasification and the conventional air gasification. The goal is to highlight the energy penalty of plasma gasification process when compared to the conventional gasification for different types of feedstock. The process matrices are assessed using energy balance, syngas distribution and the gas quality.

Finally, the summary of the work, gaps and results obtained in the thesis are discussed in chapter seven as well as the further work.

CHAPTER TWO EXPERIMENTAL SETUP AND ANAYTIC TECHNIQUES

2.1 Experiment system

2.1.1 GAD reactor systems for plasma-assisted conversion of biomass tar

Figure 2.1 shows GAD reactor system for steam reforming of toluene as a biomass tar compound. The GAD reactor consisted of two stainless steel semi-ellipsoidal electrodes (60 mm long and 18 mm wide) fixed in an insulating bracket and symmetrically placed on both sides of a gas nozzle with a diameter of 1.5 mm. The shortest electrode gap (electrode throat) was fixed at 2 mm, while the vertical distance between the nozzle exit and electrode throat was 3 mm. N_2 was used as a carrier gas (BOC, zero grade, 99.999% purity) and injected into the GAD reactor with a flow rate of 3.5 L/min. The flow rate was controlled by a mass flow controller (MFC) (Omega Engineering Limited, FMA5520A). Toluene (C_7H_8, purity >= 99%, Aldrich) and deionised water was controlled and injected into the gas line by high-resolution syringe pumps (KDS Legato, 100). In this way, the total feed flow rate of the mixed stream of 0.23 Nm^3/h and the input concentration of toluene (9.5 g/Nm^3-23.4 g/Nm^3) as well as the S/C molar ratio varying from 0 to 3 could be controlled. The mixed stream (toluene with water) was then heated to 160 ℃ in a copper pipe with an inner diameter of 4 mm (40 cm in length) equipped with a temperature controller system, to generate a steady-state vapour before flowing into the reactor. The plasma reactor was connected to an AC high voltage power supply with a maximum peak-to-peak voltage of 10 kV and a frequency of 50 Hz. The processing time was determined in the preliminary experiments when the discharge reaches a stable state, where the discharge was stable and the conversion of tar was almost unchanged. After 8 min of flow stabilization without any discharge, each experimental test was started and then carried out for 20 min when the steady-state condition was achieved. Prior to gas sampling, a condenser, which consists of a liquid trap placed inside of an ice water container was placed at the exit of the plasma reactor to condense and collect the condensable components in the effluent. Then the gaseous products were

collected by sampling bags. Before starting a fresh test, the electrodes and the quartz cover were cleaned to remove the solid carbon if formed.

In the experimental system for combined reforming of toluene (see Figure 2.2), CO_2 was mixed with the carrier gas (N_2) before entering the reactor. The flow rate of CO_2 was controlled by an MFC (Omega Engineering Limited, FMA-A2408). Similarly, toluene as well as deionised water were injected into the feeding line by using two high-resolution syringe pumps and mixed with the gas stream in a stainless steel pipe, pre-heated to 200 °C. The mixture of nitrogen, CO_2, toluene and steam vapour was then sprayed into the GAD reactor. In this work, the standard gas flow concentration was $16.1Ng/m^3$ of toluene, the total flow rate of the mixed steam was kept constant ($0.21~Nm^3/h$) in all experimental tests and the inlet concentration of CO_2 (0-10 % (vol/vol)) could be controlled. An AC high voltage power source was connected to the GAD reactor to generated plasma and the emission spectra of the plasma was recorded by an optical fibre connected to monochromatic equipped with an intensified charge coupled device (ICCD, Princeton Instruments, Model 320 PI) with the focal length of 320 mm. The gas flow leaving the GAD reactor passes through three successive absorption bottles placed in an iced waster with the first two containing dichloromethane (DCM) and the third empty, to collect entrained droplets. The gaseous products were collected by using sampling bags and determined qualitatively and quantitatively by a GC.

In the plasma steam reforming of toluene and naphthalene, naphthalene was dissolved in toluene to form the tar mixture sample and injected into the gas line by a high-resolution syringe pumps (KDS Legato, 100). Steam was added with the help of a high-resolution syringe pump with the flow rate of 2.3-13.8 ml/h. The mixed stream (including toluene, naphthalene, water and carrier gas N_2) was heated to 300 °C using a temperature controlled tube furnace (Carbolite Gero Ltd., MTF 12/38/250). In this study, toluene concentration in N_2 was fixed at 16.0 g /Nm^3, whiles the content of naphthalene was in the range of 0.48-1.83 g /Nm^3 and the S/C molar ratio was changed in the range of 0-3. The length of the heating section in the tube furnace was 250 mm. The gas line from the tube furnace was covered by

the insulation cotton to avoid the condensation of naphthalene before entering the reactor, as shown in Figure 2.3. Details of the setup can be found in the previous section.

In the plasma-catalytic steam reforming reaction, a support was used to place the catalysts below the electrodes (see Fig 2.3). The distance between the catalyst bed and the electrodes was adjusted to enable the discharge to contact the catalyst pellets. As mentioned before, the reactants (toluene, naphthalene, and H_2O) were added using the high-resolution syringe pumps and enter the GAD reactor though a tube furnace, preheated to 300 ℃. Toluene, naphthalene and water vapour were carried to the reactor by the carrier gas nitrogen with a flow rate of 3.5 L/min. During the whole experiment, the concentration of naphthalene and toluene was kept constant of 1.1 Ng/m^3 and 16.0 Ng/m^3 respectively, while the S/C molar ratio was a constant 1.5. Before sampling, the outlet gas flow passed through a liquid trap to condense out any condensable compounds present in the gas and a homemade cotton filter was added after the trap unit to remove moisture in the gas.
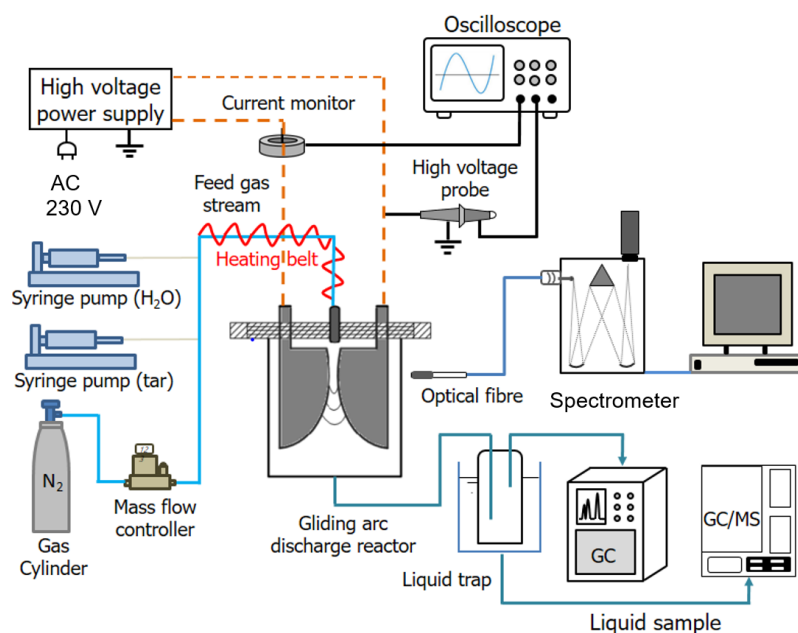
Figure 2.1 GAD reactor system for steam reforming of toluene as a biomass tar compound.
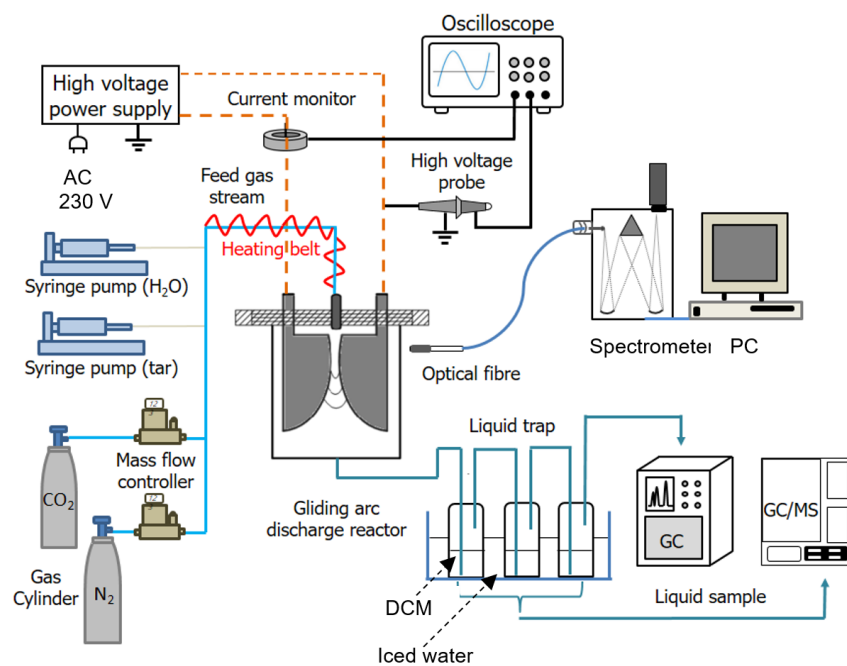
Figure 2.2 GAD reactor system for steam and CO_2 reforming of toluene as a biomass tar compound.
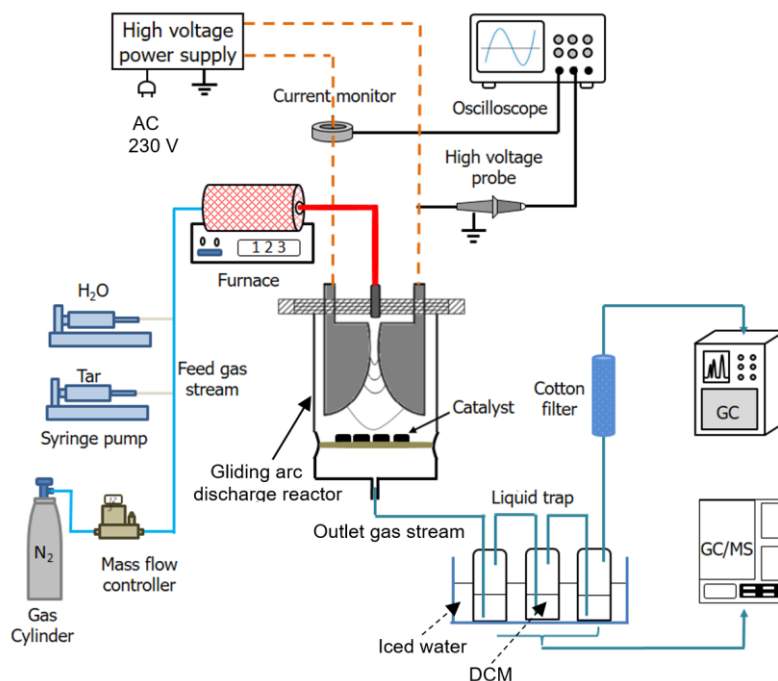
Figure 2.3 GAD reactor system for plasma catalytic steam reforming of toluene and naphthalene as biomass tar compounds.

2.1.2 DBD reactor system for plasma-catalytic conversion of biomass tar

Figure 2.4 shows the DBD reactor system for plasma catalytic steam reforming of toluene as biomass tar. The experiments were carried out in a coaxial DBD reactor (Figure 2.4 (a)). A 100 mm-long stainless steel (SS) mesh was wrapped over a quartz tube with an inner diameter of 18 mm and outer diameter of 21 mm. A SS rod with a diameter of 14 mm was used as an inner electrode and placed in the axis of the quartz tube. As a result, the length of the discharge region was 100 mm with a discharge gap of 2 mm. In the plasma reactor system (Figure 2.4 (b)), the inner electrode was connected to a high voltage output and the outer electrode was grounded via an external capacitor C_{ext} (0.47 µF). The DBD reactor was connected to an AC high voltage power supply with a maximum peak voltage of 30 kV and a frequency of 5-20 kHz. In this work, the frequency was fixed at 9 kHz.

In the plasma-catalytic reactions, catalyst pellets were packed into the plasma region along the bottom of the quartz tube, partially filling the discharge gap and held by quartz wood. The quartz wood was placed outside the plasma region to avoid its effect on the plasma chemical reactions. This partial packing method has been shown to effectively enhance the interactions between the plasma and catalyst in a DBD reactor and consequently promoted the plasma-catalytic chemical reactions in our previous studies [145]. Before the plasma-catalytic reaction, the calcined catalysts were in-situ reduced in a pure H_2 plasma at a discharge power of 60 W and a flow rate of 50 ml/min for 1 h in the same DBD reactor. In the plasma-catalytic reforming process, argon was used as a carrier gas at a flow rate of 150 ml/min. Toluene (C_7H_8, purity >= 99%, Aldrich) and deionised water were controlled and injected into the gas line by high-resolution syringe pumps (KDS Legato, 100) at a flow rate of 0.2ml/h and 0.6 ml/h, respectively. The mixed stream was heated to 160 ℃ in a copper pipe with an inner diameter of 4 mm (40 cm in length) controlled by a temperature controller system, to produce a continuous vapour before flowing into the plasma reactor. In this study, the initial concentration of toluene and the S/C molar ratio was fixed at 17.7 g/Nm^3 and 2.5, respectively throughout the experiment.

(a)

(b)
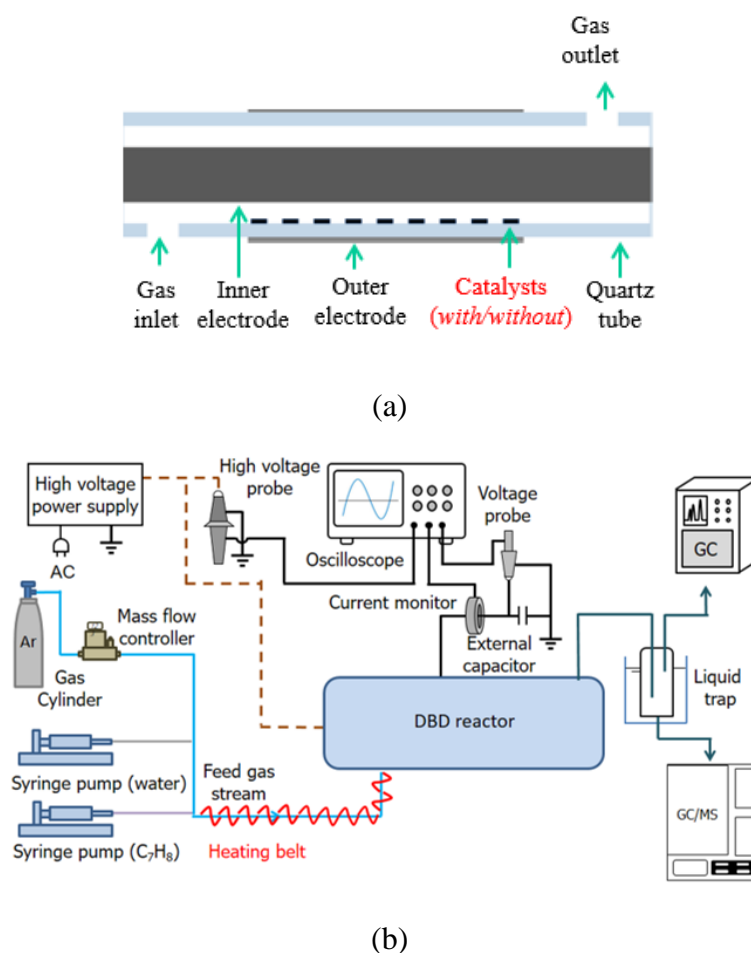
Figure 2.4 (a) DBD reactor and (b) plasma reactor system for steam reforming of toluene as a biomass tar compound.

2.2 Catalyst preparation

For the plasma-catalytic steam reforming of toluene in the DBD reactor, Ni/γ-Al$_2$O$_3$ catalysts with different Ni loadings (5, 10 and 20 wt. %) were prepared by impregnation method using Ni(NO$_3$)$_2$·6H$_2$O (Alfa Aesar) as the metal precursor. The appropriate weight of γ-Al$_2$O$_3$ (1 mm diameter beads) was added to the metal precursor solution and impregnated for 12 hours. The above solution was dried at 100 °C until most of water was evaporated. The obtained samples were heated at 100 °C for 24 h, followed by the calcination at 750 °C for 3 h. Prior to the plasma-catalytic reaction, the supported Ni catalysts were in-situ educed in a H$_2$ plasma at a discharge power of 60 W and a flow rate of 50 ml/min for 1 h in the same DBD reactor as descried in Section 2.1.2.

For the plasma-catalytic steam reforming of toluene and naphthalene in the GAD reactor, the x wt.%Ni- y wt.%Co/γ-Al$_2$O$_3$ (x = 0, 7.5 and 15; $x + y$ = 15) catalysts were prepared by the wetness impregnation method (co-impregnation) using Ni(NO$_3$)$_2$·6H$_2$O and Co(NO$_3$)$_2$·6H$_2$O (Alfa Aesar) as the metal precursors. The appropriate weight of γ-Al$_2$O$_3$ powder was added to the metal precursor solution and impregnated for 4 hours. The obtained samples were dried at 110 °C for 12 h, followed by the calcination at 500 °C for 5 h. Before each reaction, the calcined catalyst pellets were thermally reduced at 600 for 2 h in a tube furnace (Carbolite Gero Ltd., MTF 12/38/250). The obtained catalysts were denoted as 15Ni, 7.5Ni7.5Co and 15Co.

2.3 Analytic methods

2.3.1 Measurement and analysis of electrical signals

In the GAD experimental system, the applied voltage was measured by a high voltage probe (Testec, TT-HVP 15 HF, Figure 2.5 (a)), while the current in the discharge was measured by the current transformer (Magnelab, CT-E 0.5-BNC, Figure 2.5 (b)). All the electrical signals were recorded by a 4-channel digital oscilloscope (Tektronix, MDO 3024, Figure 2.5 (c)). The discharge power (P) of the plasma process was calculated by the integration of arc voltage and arc current, as shown in Equation (2-1):

$$P(\text{W}) = \frac{1}{T} \int_0^{t=T} U(t) \times I(t) \, \mathrm{d}t \tag{2-1}$$

(a)   (b)

<div align="center">(c)</div>

<div align="center">(d)</div>

Figure 2.5 (a) High voltage probe; (b) Current transformer; (c) Four channel digital oscilloscope; (d) Voltage probe.

In the DBD experiments, the applied voltage and current in the discharge were measured by the above high voltage probe and current transformer, respectively; while the voltage on the external capacitor was recorded by a voltage probe (Tektronix P5100, Figure 2.5 (d)) to obtain the charge generated in the discharge. The *Q-U* Lissajous method was used to determine the discharge power (*P*) of the DBD reactor, as expressed in Equation (2-2). The details of the *Q-U* Lissajous method can be found elsewhere [65, 146]. A homemade online power measurement system was used to monitor and control the discharge power in real time [147].

$$P(\text{W}) = f(\text{Hz}) \cdot C_{\text{ext}}(\text{F}) \cdot A(\text{m}^2) \tag{2-2}$$

where C_{ext} is the capacitance of the external capacitor, *f* is the discharge frequency and *A* is the area of the Lissajous figure.

For both GAD and DBD experimental system, the specific energy input (SEI) was determined by

$$\text{SEI}\left(\text{kWh}/\text{m}^3\right) = \frac{P(\text{kW})}{\text{Total gas flow rate } \left(\text{m}^3/\text{h}\right)} \tag{2-3}$$

2.3.2 Catalyst characterisation

The N_2 physisorption was carried out at 77 K using the ASAP 2000 analyser to measure the pore size and the specific surface area of the catalyst. Before each measurement, the samples were dried at 100 ºC for 5 h outgassed at 300 ºC for 5 h under a vacuum to remove any moisture and other adsorbed gases. The specific surface area was calculated

using the Brunauer-Emmett-Teller (BET) method, while the pore size distribution was determined via the Barrett-Joyner- Halenda (BJH) model from the data of the desorption branch of the N_2 isotherm.

The crystallinity of the catalyst was identified through XRD analysis using an X-ray diffractometer (Empyrean, Panalytical) equipped with Mo and Ag sources (60 kV tube voltage and 40 mA tube current) in the scanning range 2θ between 5° and 80° with a scanning rate of 4 °/min and a scanning step size of 0.02°.

The morphology and the dispersion of the freshly reduced catalysts were observed with transmission electron microscopy (TEM: JEOL 2010). The samples for the TEM analysis was ultrasonically treated in ethanol to form a suspension and then transferred to a carbon-coated copper grid.

The reducibility of the catalysts was evaluated by H_2-TPR using a fully automated chemisorption analyser (AutoChem II 2920). Prior to each run, the 90 mg catalyst sample was pre-treated at 400 °C for 60 min under Ar flow to remove physically adsorbed and/or weakly bound species. After cooling to room temperature, the sample was heated from 20 °C to 800 °C with a heating rate of 5 °C min^{-1} using a H_2/Ar gas mixture (V/V, 10/90) with a flow rate of 30 ml/min.

The coke deposition on the spent catalyst is analysed via TGA in air atmosphere using TA Instruments SDT-Q600 (simultaneous TGA/DSC). The spent catalyst (20 mg) is heated from 60 to 800 °C at a heating rate of 10 °C/min with an air flow of 30 ml/min.

2.3.3 Spectroscopic diagnostics

Emission spectra of the gliding arc discharges under different conditions were recorded by an optical fibre connected to a Princeton Instruments ICCD spectrometer (Model 320 PI) with a focal length of 320 mm.

2.3.4 Analysis of gas and liquid products

In this study, gas chromatography (GC) was used for the analysis of the gas mixtures during the experiments. The feed and product gases were analysed by a two-channel gas

chromatograph (Shimadzu GC-2014) equipped with a thermal conductivity detector (TCD) and a flame ionization detector (FID). Both detectors are sensitive to a variety of components and can work over a wide range of concentrations. TCD is used to detect any component other than the carrier gas, as long as their thermal conductivities are different from that of the carrier gas at the detector temperature, while FID is primarily used to detect organic compounds. Ar was used as the carrier gas in this study. The first channel in the GC contains a Molecular Sieve 5A (60-80 mesh) column for the separation of H_2 and CO, while the second channel is equipped with a HayeSep N (60-80 mesh) column for the measurement of CO_2, CH_4 and C_2-C_4 hydrocarbons. The GC was calibrated for each gaseous component with a wide range of concentrations using standard gas mixtures (Air Liquid) and other calibrated gas mixtures.

A liquid trap was placed at the exit of the plasma reactor to collect the condensable products in the effluent. Details can be found in the section of experimental set up. The collected liquid samples were analysed by a gas chromatography – mass spectrometry (GC-MS, Agilent GC 7820A, MSD) and qualitatively identified using the mass spectral library from the National Institutes for Standards and Technology (NIST). H_2 was used as a carrier gas for the GC-MS, which was produced by a hydrogen generator (Parker, 20H-MD). The GC-MS was calibrated for tar components (e.g. toluene and naphthalene) with different concentrations. As a result, calibration lines were obtained to calculate the tar content in the collected liquid samples.

For the plasma steam reforming toluene (Chapter 3 and Chapter 5), the conversion of toluene ($X_{C_7H_8}$) was defined as the ratio of the carbon in the carbon-containing gas products (CO, C_2H_2, C_2H_4, C_2H_6 and C_3H_8) to the carbon in the input toluene,

$$X_{C_7H_8}\,(\%) = \frac{\text{Moles of carbon in the produced gas}}{\text{Moles of carbon in the feed}} \times 100 \tag{2-4}$$

The yield (Y) of the products can be calculated:

$$Y_{H_2}\,(\%) = \frac{\text{moles of } H_2 \text{ produced}}{4\times\text{moles of } C_7H_8 \text{ input} + \text{moles of } H_2O \text{ input}} \times 100 \tag{2-5}$$

$$Y_{CO}\left(\%\right)=\frac{\text{moles of CO produced}}{7\times\text{moles of C}_7\text{H}_8\text{ input}}\times100 \tag{2-6}$$

$$Y_{C_xH_y}\left(\%\right)=\frac{x\times\text{moles of C}_x\text{H}_y\text{ produced}}{7\times\text{moles of C}_7\text{H}_8\text{ input}}\times100 \tag{2-7}$$

For the plasma combined reforming of toluene (Chapter 4), the conversion of toluene was determined by

$$X_{tar}\left(\%\right)=\frac{C_i-C_o}{C_i}\times100 \tag{2-8}$$

where C_i and C_o are the tar concentration in the feed and the effluent, respectively. Here, tar is toluene. The definition of H_2 yield was the same as Equation (2-5), while the yield of CO and C_xH_y were calculated by

$$Y_{CO}\left(\%\right)=\frac{\text{moles of CO produced}}{7\times\text{moles of C}_7\text{H}_8\text{ input}+\text{moles of CO}_2\text{ input}}\times100 \tag{2-9}$$

$$Y_{C_xH_y}\left(\%\right)=\frac{x\times\text{moles of C}_x\text{H}_y\text{ produced}}{7\times\text{moles of C}_7\text{H}_8\text{ input}+\text{moles of CO}_2\text{ input}}\times100 \tag{2-10}$$

For the plasma steam reforming of tar mixture (toluene and naphthalene), the definition of tar conversion was the same as Equation (2-8), while the yield of the gas products was determined by the following equations.

$$Y_{H_2}\left(\%\right)=\frac{H_2\text{ produced}\left(\text{mol/s}\right)}{4\times(\text{C}_7\text{H}_8+\text{C}_{10}\text{H}_8)\text{ input }\left(\text{mol/s}\right)+\text{H}_2\text{O input}\left(\text{mol/s}\right)}\times100 \tag{2-11}$$

$$Y_{CO_x}\left(\%\right)=\frac{CO_x\text{ produced }\left(\text{mol/s}\right)}{7\times\text{C}_7\text{H}_8+10\times\text{C}_{10}\text{H}_8\text{ input }\left(\text{mol/s}\right)}\times100 \tag{2-12}$$

$$Y_{C_xH_y}\left(\%\right)=\frac{x\times\text{C}_x\text{H}_y\text{ produced }\left(\text{mol/s}\right)}{7\times\text{C}_7\text{H}_8+10\times\text{C}_{10}\text{H}_8\text{ input }\left(\text{mol/s}\right)}\times100 \tag{2-13}$$

The energy efficiency (E) of the plasma reforming toluene conversion was defined as the mass of converted toluene per unit of discharge power, as shown in Equation (2-14).

$$E\left(\text{g/kWh}\right)=\frac{\text{mass of converted tar (g/h)}}{\text{discharge power (kW)}} \tag{2-14}$$

The reproducibility was demonstrated in the preliminary experiments. To quantify the reliability and repeatability of the operation system, each test under the same condition was repeated for three times. The relative error of the reactant conversions and product yields under one test was less than 5%. The uncertainty in the measurement of the gas and liquid concentrations by using GC and GC/MS was less than 4% and 5%, respectively, whilst the uncertainty in the calculation of conversion, yield and energy efficiency is less than 4%.

CHAPTER THREE   STEAM REFORMING OF TOLUENE AS MODEL BIOMASS TAR IN A GAD REACTOR

3.1 Introduction

GAD has been considered as a transitional plasma and can be generated by applying an electrical field across two or more electrodes in a laminar or turbulent gas flow [148]. A gliding arc system offers high flexibility for working in a wide range of flow rates and elevated power levels (up to several kW) efficiently. It is worth noting that the electron density (10^{23} -10^{24} m^{-3}) in a gliding arc is close to that of a thermal plasma and is significantly higher than that of other non-thermal plasmas (e.g. DBD and corona) [149]. These distinguishing features result in high energy efficiency of the plasma process for chemical reactions, and have great potential for the removal of tars from biomass gasification [150]. Most previous studies focused on the effect of different operating parameters had on the performance of the plasma tar removal process. However, few analyzed the by-products and intermediates in the plasma reforming of tar to better understand the underlying reaction pathways and mechanisms in the plasma process.

In this paper, an AC gliding arc plasma gas cleaning system has been developed for the removal of tars from biomass gasification. The configuration of the GAD reactor and the experimental system is shown in Figure 2.1 and the corresponding details are described in Section 2.1.1. Toluene has been chosen as a model tar compound since it represents a major stable aromatic product in the tars formed in high temperature biomass gasification processes [151]. N_2 (BOC, zero grade, 99.999% purity) has been used as a carrier gas in the plasma gas cleaning process. It was injected into the GAD reactor with a flow rate of 3.5 L/min. Toluene (C_7H_8, purity >= 99%, Aldrich) with a flow rate of 3.6 - 9.6 ml/h and water (0 - 20 ml/h) were injected into a pipe by high-resolution syringe pumps (KDS Legato, 100). As a result, the concentration of toluene can be changed from 9.5 g/Nm^3 to 23.4 g/Nm^3, which is within the range of tar concentrations from the gasification process using different gasifiers [37]. The mixed stream (toluene with water) was then heated to 160 $^\circ$C in a copper pipe with

an inner diameter of 4 mm (40 cm in length), equipped with a temperature controller system, to generate a steady-state vapour before flowing into the reactor.

The effect of different processing parameters (e.g. steam-to-carbon (S/C) molar ratio, toluene feed rate and specific energy input (SEI)) on the reaction performance (e.g. toluene conversion, yield of products and energy efficiency) has been investigated. Optical emission spectroscopy (OES) has been used to understand the role of steam on the formation of reactive species (e.g. CH, CN, NH and OH) in the plasma chemical reactions. In addition, the possible reaction mechanisms and pathways involved in the plasma conversion of toluene have been discussed by combined means of OES and the analysis of gas and liquid products. The conversion of toluene is calculated by Equation (2-4); the yield of the products is determined by Equations (2-5) to (2-7); while the energy efficiency of the plasma process is defined as Equation (2-14).

3.2 Steam reforming of toluene in GAD reactor

3.2.1   Effect of steam on the plasma conversion of toluene

The plasma conversion of toluene was carried out at a constant toluene flow rate of 4.8 ml/min and a discharge power of 43.5 W with and without steam, as shown in Figure 3.1 (a). Clearly, introducing steam into the plasma reaction significantly enhanced the toluene conversion from 5.4 % without steam to 41.6 % with steam, whilst the energy efficiency of the plasma process was increased by a factor of 8. A similar effect on the plasma chemical reactions from the introduction of water has also been reported in previous studies. Chun et al reported the presence of water promoted the decomposition of benzene in a gliding arc reactor [49]. Yang et al. also found that a humid N_2 plasma exhibited a better performance for the destruction of naphthalene compared to the plasma reaction using dry N_2 as a carrier gas [144]. Reactions R3-1 to R3-8 describe the possible reactions leading to toluene conversion in dry nitrogen environment.

$$C_6H_5 \cdot CH_3 + e \rightarrow C_6H_5 \cdot CH_2 + H + e \qquad \text{(R3-1)}$$

$$C_6H_5 \cdot CH_3 + e \rightarrow C_6H_4 \cdot CH_3 + H + e \qquad \text{(R3-2)}$$

$$C_6H_5 \cdot CH_3 + e \rightarrow C_6H_5 + CH_3 + e \tag{R3-3}$$

$$C_6H_5 \cdot CH_3 + e \rightarrow C_5H_6 + C_2H_2 + e \tag{R3-4}$$

$$C_6H_5 \cdot CH_3 + N_2^* \rightarrow C_6H_5 \cdot CH_2 + H + N_2 \tag{R3-5}$$

$$C_6H_5 \cdot CH_3 + N_2^* \rightarrow C_6H_4 \cdot CH_3 + H + N_2 \tag{R3-6}$$

$$C_6H_5 \cdot CH_3 + N_2^* \rightarrow C_6H_5 + CH_3 + N_2 \tag{R3-7}$$

$$C_6H_5 \cdot CH_3 + N_2^* \rightarrow C_5H_6 + C_2H_2 + N_2 \tag{R3-8}$$
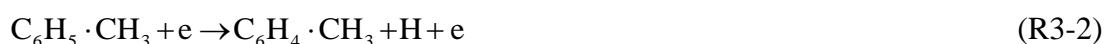
Adding steam in the N_2 plasma leads to the formation of OH radicals through electron-impact dissociation of H_2O (R3-9) and collisions of H_2O with N_2 excited species (R3-10),

$$H_2O + e \rightarrow H + OH + e \tag{R3-9}$$

$$H_2O + N_2^* \rightarrow N_2 + H + OH \tag{R3-10}$$

where N_2^* refers to nitrogen excited species $N_2 (A^3)$, $N_2 (a^{'})$ and $N_2 (B)$.

The generated OH radicals could oxidize toluene (R3-11 and R3-12) and intermediates, which provides a new reaction pathway for direct and indirect decomposition of toluene, resulting in a significantly enhanced toluene conversion and energy efficiency compared to the plasma toluene conversion without steam. The formation of OH in the plasma steam reforming of toluene can be confirmed by the presence of OH bands in the spectrum of the $N_2/C_7H_8/H_2O$ GAD (Figure 3.2).

$$C_6H_5 \cdot CH_3 + OH \rightarrow C_6H_5 \cdot CH_2 + H_2O \tag{R3-11}$$

$$C_6H_5 \cdot CH_3 + OH + N_2 \rightarrow C_6H_5(OH)CH_3 + N_2 \tag{R3-12}$$
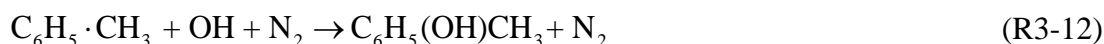
In addition, the presence of steam in the plasma conversion of toluene generated more gas products including H_2, CO, C_2H_6, C_2H_4, C_2H_2 and C_3H_8. For instance, the yield of H_2 (6.3 %) was significantly increased by a factor of 5 when adding steam in this reaction, as shown in Figure 3.1 (b). No CO was detected in the plasma toluene conversion without steam. However, a high yield of CO (29.8 %) was achieved in the plasma steam reforming of toluene, which suggests that OH might play an important role in the stepwise oxidation

reactions, eventually forming CO. It is also interesting to note that no CO_2 was detected in the gas products regardless of whether steam was used in the reaction, while CO_2 is a common by-product in the oxidation of toluene using air plasmas [152].

H_2, CO and C_2H_2 were the major gaseous products in this study (see Figure 3.1 (b)). Hydrogen can be formed through the recombination of two H atoms, which are more likely generated from a methyl group (R3-1 and R3-5) than that from a benzene ring (R3-4 and R3-8) as the dissociation energy of C-H bonds (3.7 eV) in the methyl group are the weakest bonds in the toluene molecules [53]. Besides, water molecules could offer the H radicals to form molecule hydrogens as well through the reaction R3-9. The appreciable yield of C_2H_2 generated in the plasma-chemical progress reveals that the conversion of toluene at N_2 GAD reactor is accompanied by reactions with benzene ring cleavage, which can be represented by the reaction R3-4 and R3-8. Generally, C_2H_4, C_2H_6 and C_3H_8 hydrocarbons are formed through the neutral-neutral recombination of radicals (e.g. CH_3, CH_2, C_2H_5, etc.), as shown in R3-13 to R3-15. However, only trace amounts of these gaseous products were detected in the plasma reforming of toluene, which suggests the occurrence of R3-13 to R3-15 is negligible.

$$CH_3 + CH_3 \rightarrow C_2H_6 \tag{R3-13}$$

$$CH_2 + CH_2 \rightarrow C_2H_4 \tag{R3-14}$$

$$CH_3 + C_2H_5 \rightarrow C_3H_8 \tag{R3-15}$$
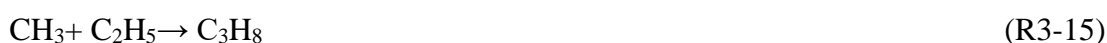
The recombination of CH_3 with H can form CH_4 (R3-24). However, no CH_4 was detected in the plasma conversion of toluene with or without steam, suggesting that this reaction is ineligible.

$$H + CH_3 \rightarrow CH_4 \tag{R3-16}$$

(a)

(b)
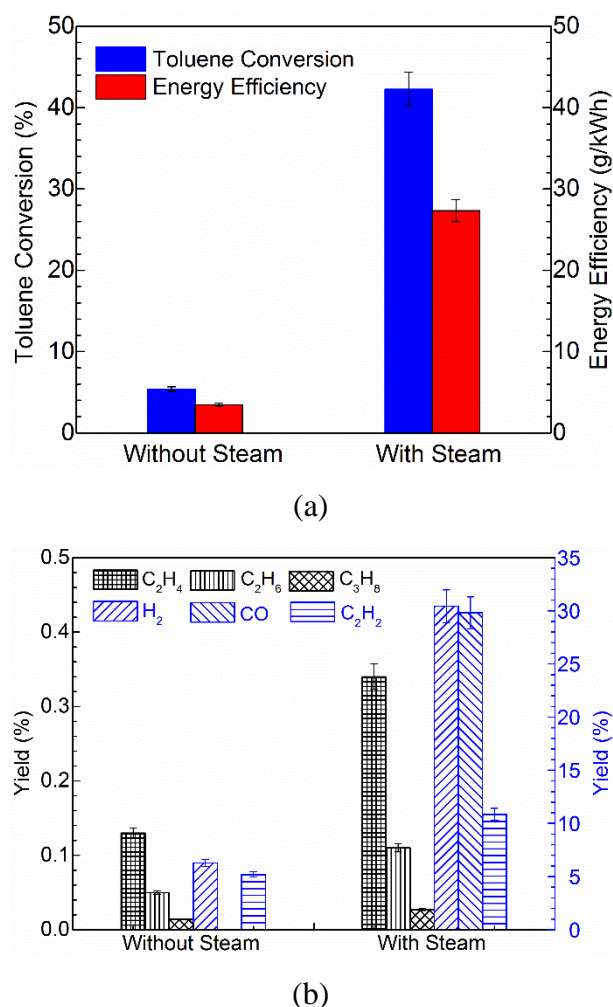
Figure 3.1 Effect of steam on (a) toluene conversion and energy efficiency; (b) yields of primary gaseous products (toluene flow rate: 4.8 ml/h; discharge power 43.5 W).

3.2.2 Optical analysis

Optical emission spectroscopy was used to investigate the formation of different reactive species in the plasma reforming of toluene with and without steam. Figure 3.2 shows the typical spectra of the GAD plasmas using pure N_2, N_2/C_7H_8 and $N_2/H_2O/C_7H_8$. In the N_2/C_7H_8 plasma without steam, strong CN ($B^2\Sigma \to X^2\Sigma$) violet and second order violet bands can be clearly observed, which might be generated through the following reactions (R3-17 to R3-19):

$$N_2 + C_2 \to CN + CN \tag{R3-17}$$

$$N + CH_2 \to CN + H_2 \tag{R3-18}$$

$$N + CH \to CN + H \tag{R3-19}$$
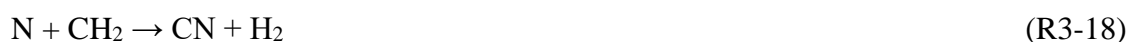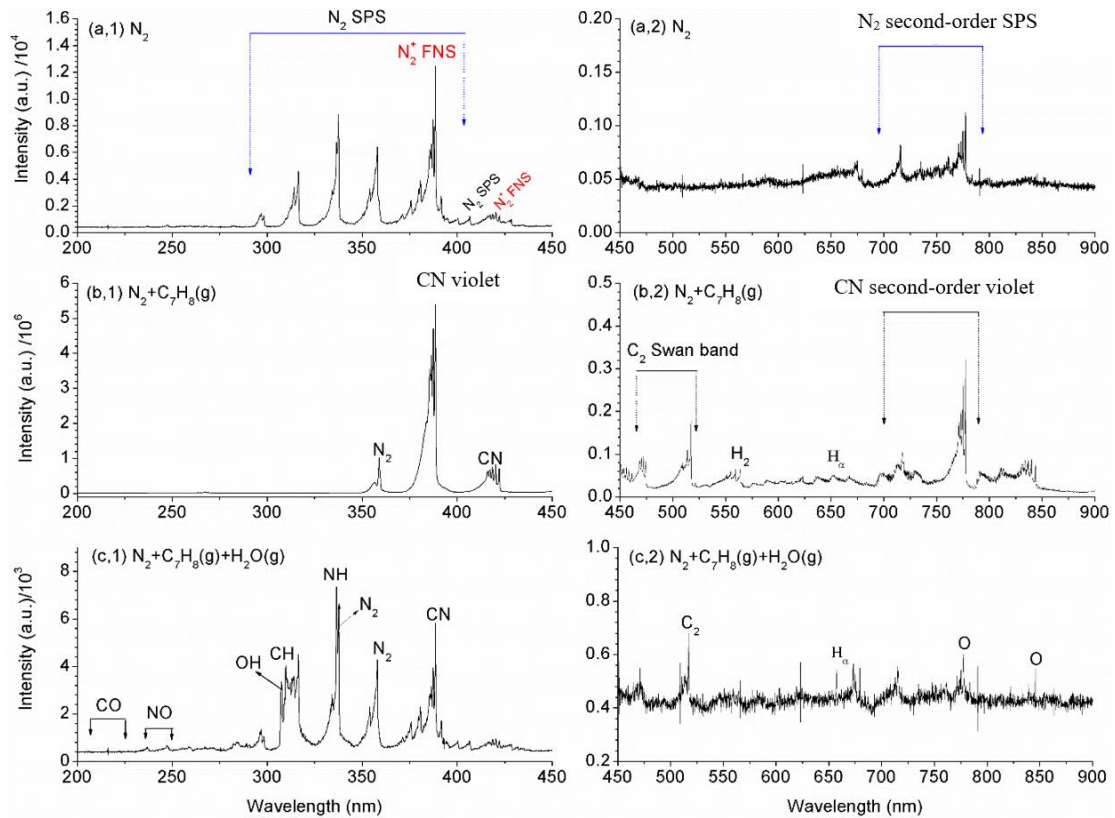
Figure 3.2 Spectra of optical emission from GAD (a) N_2 GAD plasma; (b) N_2/C_7H_8 GAD plasma; and (c) $N_2/C_7H_8/H_2O$ GAD plasma (C_7H_8 flow rate: 4.8 ml/h; N_2 flow rate: 3.5 l/min; H_2O flow rate: 14.3 ml/h) (600 G/mm grating, exposure time 0.3 s).

The formation of CN might also be linked with carbon deposition in the plasma reaction [153].

$$N_2 + C \rightarrow CN + N \tag{R3-20}$$

The hydrogen Balmer series H_α centred at 653.3 nm and C_2 swan bands in the spectral range of 460-520 nm can also be found, while the intensity of Fulcher band H_2 ($d^3 \prod_u \rightarrow a^3\Sigma_g^+$) in the range of 580-650 nm was much weaker compared to that of CN bands.

Adding steam in the plasma reforming of toluene significantly changed the emission spectrum of the plasma due to the formation of different reactive species in the plasma process. The presence of the OH ($A^2\Sigma^+ \rightarrow X^2\prod$) band in the spectrum of the $N_2/C_7H_8/H_2O$ GAD confirms the dissociation of water through the major reactions R3-9 and R3-10.

Introducing steam into the plasma reforming of toluene significantly reduced the relative intensity of the CN bands but increased the intensity of N_2 ($C^3\prod u \to B^3\prod g$) second positive system (350-360 nm). In addition, the spectrum showed a NH ($A^2\sum \to X^2\sum$) band at 336.1 nm, which could be produced from the reactions of N atoms with H_2O or OH radicals via reactions R3-20 and R3-21 as NH band did not appear in the spectrum of the N_2/C_7H_8 plasma without steam [154]. This phenomenon also suggests that the formation of NH via direct reactions between N_2 and H_2 might be negligible. Moreover, the emissions of CO ($A^1\prod \to X^1\sum$) at 200-220 nm and CH ($C^2\Pi^+ \to X^2\Pi$) at 314.3 nm were also observed. The presence of NO ($A^2\sum^+ \to X^2\Pi$) bands in the range of 230-250 nm suggests that the following reaction might be possible (R3-22 and R3-23).

$$N + H_2O \to NH + OH \qquad\qquad (R3-21)$$

$$N + OH \to NH + O \qquad\qquad (R3-22)$$

$$N + OH \to NO + H \qquad\qquad (R3-23)$$

$$NH + O \to NO + H \qquad\qquad (R3-24)$$
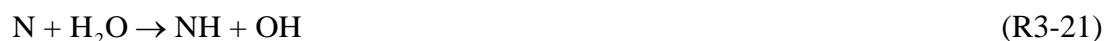
3.2.3 Effect of S/C molar ratio on the reforming process

The effect of S/C molar ratio on the performance of the plasma reforming of toluene has been investigated to better understand the role of steam in this reaction. Figure 3.3 (a) presents the variation of toluene conversion and energy efficiency when changing the S/C molar ratio from 1 to 3.5 at a fixed toluene feed rate of 4.8 ml/h. Clearly, increasing the S/C molar ratio initially enhanced the toluene conversion of the plasma steam reforming of toluene and reached a maximum value of ~42.2% at an S/C molar ratio of 2-3, beyond which the toluene conversion gradually decreased to 38.3% at an S/C molar ratio of 3.5. Lim et al. also reported an optimal S/C molar ratio of 2-2.5 to achieve the maximum conversion of naphthalene and benzene in the conversion of light tars using a GAD [155]. The energy efficiency of the plasma process showed a similar evolution and reached the maximum (~27.3 g/kWh) at the S/C molar ratio of 2-3. The yield of gaseous products strongly depends on the S/C molar ratio with the optimal S/C molar ratio being 2-3, as show in Figure 3.3 (b).

For instance, the highest yields of H_2 and CO were 30.4% and 35.1%, respectively, obtained at an S/C molar ratio of 2-3. However, increasing the S/C molar ratio gradually decreased the yield of C_2H_2 from 12.8% to 5.3%. A higher S/C molar ratio could generate more OH radicals which participate in the oxidation of toluene and intermediates, thus reducing the chance of toluene ring cleavage by free electrons and N_2 excited species to release C_2H_2. Trushkin et al also reported that an increase in flow humidity leads to a noticeable increase in the yield of CO and a suppression of acetylene yield [156]. Compared with major gas products H_2, CO and C_2H_2, only a small amount of C_2H_4, C_2H_6 and C_3H_8 were formed in the plasma steam reforming of toluene with a total yield of no more than 1% under all experimental conditions (see Figure 3.3 (b)).
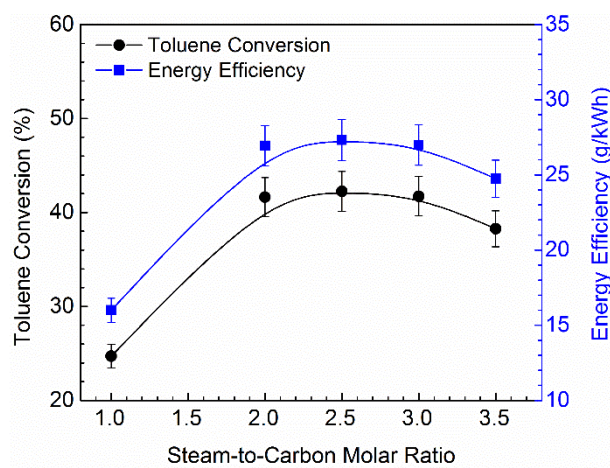
(a)
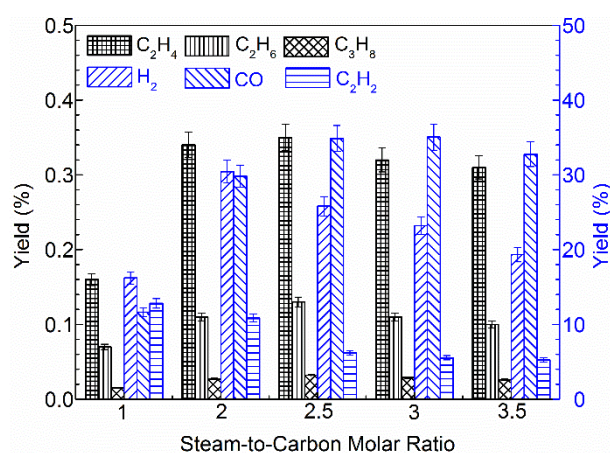
(b)

Figure 3.3 Effect of S/C molar ratio on (a) toluene conversion and energy efficiency; (b) yields of primary gaseous products (C_7H_8 feed rate: 4.8 ml/h; SEI: 0.19 kWh/m^3).

Clearly, humidity has a significant effect on toluene conversion in the plasma process. To better understand the role of S/C molar ratio on the reaction pathways in the plasma steam reforming of toluene, the effect of different S/C molar ratios on the relative intensity of three key radicals (CH, CN and OH) was investigated, as presented in Figure 3.4. Clearly, increasing the S/C molar ratio from 1 to 3.5 significantly increased the relative intensity of OH. The presence of OH radicals in the plasma reaction opens a new route for toluene decomposition through step-wise oxidation of toluene and intermediates, resulting in an enhanced conversion and energy efficiency, as shown in Figure 3.1. Meanwhile, the relative intensity of CN dropped significantly when increasing the S/C molar ratio. CN radicals could be produced from the reactions of N_2 with C_2 (R3-5). Figure 3.3 shows that increasing the S/C molar ratio suppressed the formation of C_2 in the plasma reaction, which might also limit the formation of CN radicals. In addition, less carbon deposition was observed when adding steam into the plasma reforming of toluene, which might also reduce the production of CN as one possible route for CN formation could be the reaction between N and carbon (R3-8). The intensity of CH radical initially increased with the S/C molar ratio and reached a peak at an S/C ratio of 2.5, and then dropped with further increase of the S/C ratio. The evolution of the CH intensity with the S/C molar ratio is very similar to the effect of S/C ratio on the conversion of toluene (Figure 3.3), which indicates that CH might be mainly produced from the dissociation of CH_3 and CH_2 by electrons and N_2 excited states, and closely associated with the decomposition of toluene in this reaction.
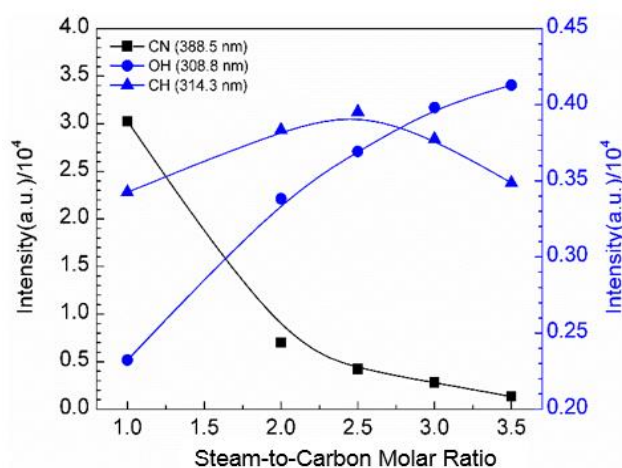
Figure 3.4 Optical emission intensity of three species in $N_2/H_2O/C_7H_8$ plasma as a function of water vapour amount (C_7H_8 feed rate: 4.8 ml/h; SEI: 0.19 kWh/m^3).

3.2.4 Effect of toluene feed rate on the steam reforming process

Figure 3.5 (a) shows the effect of toluene feed rate on the toluene conversion and energy efficiency of the plasma process at a constant discharge power of 43.5 W. The conversion of toluene decreased from 47.7 % to 35.8 % when increasing the toluene feed rate from 3.6 to 9.6 ml/h, whereas the energy efficiency of the plasma process was doubled (from 23.1 to 46.3 g/kWh), which means more toluene was decomposed at a higher toluene feed rate. The yield of H_2 and CO followed the same tendency as the toluene conversion, and decreased from 31.9 % and 33.4 % to 22.6 % and 25 %, respectively, with the increase of toluene feed rate from 3.6 to 9.6 ml/h. C_2H_2 was found to be a major gas product with a maximum yield of 13.3 %, while the total yield of other hydrocarbons was lower than 1%.
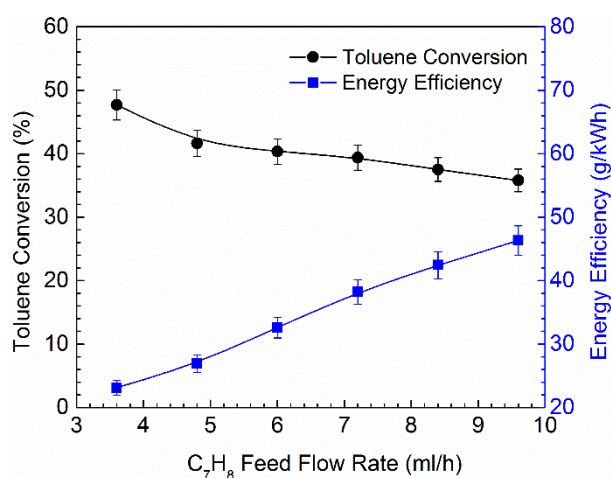
(a)
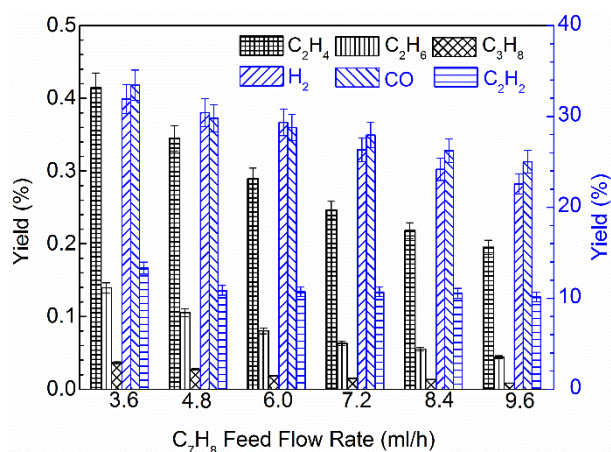
(b)

Figure 3.5 Effect of toluene feed rate on: (a) toluene conversion and energy efficiency; (b) yields of main gaseous products (discharge power: 43.5 W; S/C=2).

3.2.5 Effect of SEI on the reforming progress

SEI is one of the most important parameters affecting plasma chemical reactions as it is closely related to the power input to the plasma process. The influence of SEI on the reaction performance of the plasma toluene reforming is shown in Figure 3.6. The SEI of the plasma is varied in the range of 0.17 - 0.30 kWh/m^3 by changing the discharge power from 37 to 68 W at a constant total flow rate of 0.23 Nm^3/h. The toluene conversion increased continuously up to 51.8% at a SEI of 0.30 kWh/m^3. A similar tendency was reported in tar conversion either using plasma alone or using plasma-catalysis [155, 157, 158].
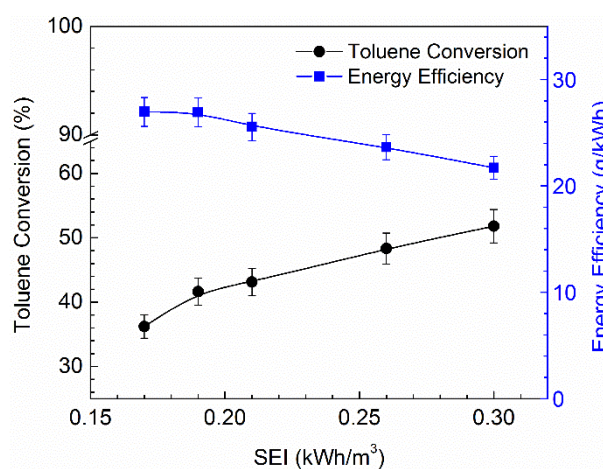

(a)
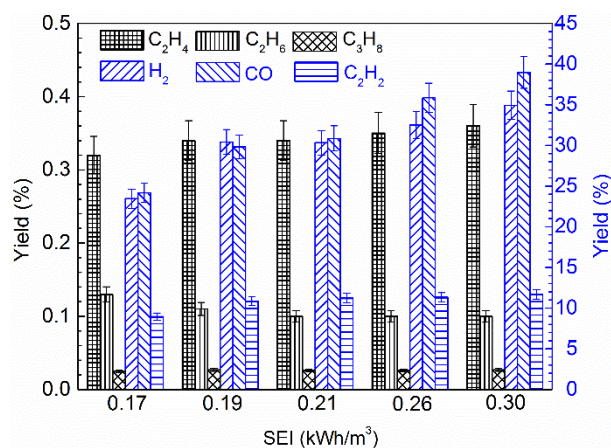
(b)

Figure 3.6 Effect of SEI on (a) toluene conversion and energy efficiency; (b) yields of main gaseous products (toluene flow rate: 4.8 ml/h; S/C=2).

Increasing SEI also enhanced the production of syngas. For instance, the yield of H_2 was enhanced by about 36 % when the SEI increased from 0.17 to 0.3 kWh/m^3. Note that the yield of C_3 saturated hydrocarbon was almost independent of SEI in the tested range. Previous studies showed that increasing plasma power at a constant excitation frequency effectively enhances the electric field, electron energy and gas temperature in the discharge zone [149]. All of these properties may contribute in different ways to the enhanced toluene conversion and syngas production. In addition, increasing the discharge power produces more chemically reactive species (e.g. OH, N and N_2 excited states) which participate in the conversion of toluene and intermediates in the plasma reaction. The maximum energy efficiency of 27.0 g/kWh was obtained at the lowest SEI of 0.17 kWh/m^3, which is greater than that obtained using a microwave plasma (4.52 g/kWh) [50] and a GAD plasma (20.9 g/kWh) in previous studies [49]. In addition, increasing SEI resulted in a reduction in energy efficiency of the plasma reaction, although the conversion of toluene was increased.

3.2.6 Possible reaction mechanism of toluene reforming

To understand the reaction mechanisms and pathways in the plasma steam reforming of toluene, liquid-phase end-products were qualitatively analyzed using GC-MS, as shown in Figure 3.7 and Table 3.1. In this reaction, benzonitrile, benzene (butoxymethyl),

benzenpropanenitrile and benzene were identified as the major liquid compound. The production of these N-containing organic compounds suggests that NH_x (x=1 and 2) and CN radicals participate in the reactions through their recombination with intermediates from toluene decomposition. In addition, naphthalene was clearly identified as a dominant polycyclic product, which might be formed from the combination of cyclopentadienyl radicals [159]. Remarkably, linear product panaxynone was also detected, resulting from the cleavage of a toluene ring followed by the recombination or hydrogenation of the intermediates, including methyl, bi-radical HC=CH and acetylene.
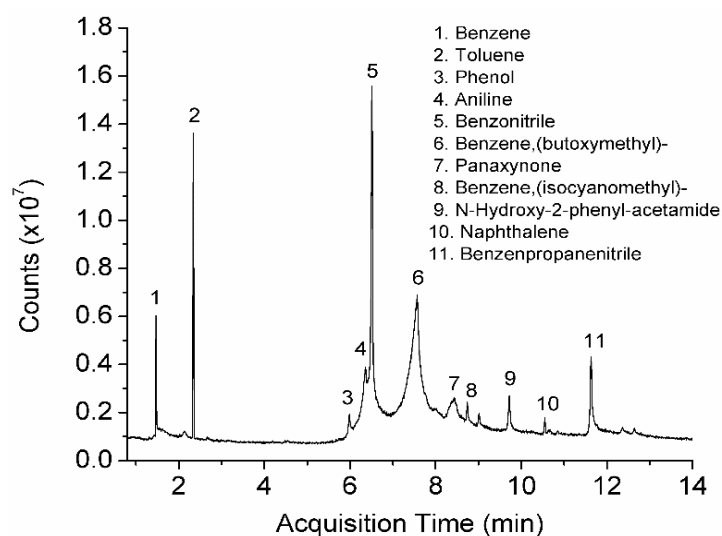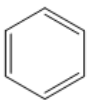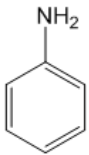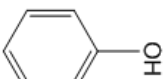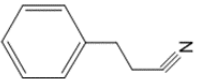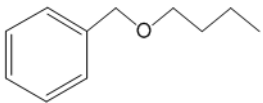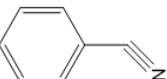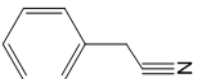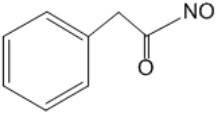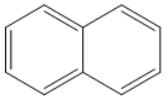
Figure 3.7 GC/MS analysis of liquid sample after plasma steam reforming of toluene (toluene flow rate: 4.8 ml/h; S/C=2; SEI: 0.19 kWh/m^3).

Table 3.1 Products identified in liquid sample by GC-MS.

Benzene	Aniline	Phenol	Benzenpropanenitrile	Benzene (butoxymethyl)

Benzonitrile	Benzene (isocyanomethyl)	N-hydroxy-2-phenyl-acetamide	Naphthalene

Based on the observed results and identified species, the possible mechanism of toluene decomposition is schematically shown in Figure 3.8. The dissociation energy of the C-H bond in methyl is 3.7 eV, which is smaller than that of the C-H bond in the aromatic ring (4.3 eV), the C-C bond between methyl group and aromatic ring (4.4 eV), the C-C bond in the aromatic ring (5.0-5.3eV) and the C=C bond in the aromatic ring (5.5 eV) [160]. Mean energy of the electrons generated by gliding arc discharge generally ranges from 1-3 eV and high energy electrons abounds in the discharge area [161]. Therefore, in dry nitrogen discharge with low concentration or in absence of any oxidations, the primary pathway of toluene decomposition should be the H-abstraction from the methyl group by nitrogen excited species or energetic electrons [162]. The generated benzyl radicals (I) from the H-abstraction of methyl could react with excited methyl radical, OH radical and CN radical to form ethylphenyl(II), benzyl-alcohol(III) and benzyl-cyanide (IV), respectively. Afterward, a series of dehydrogenation of the ethylphenyl radical followed by the recombination of CN radical, leading to the formation of benzenpropanenitrile(V). Benzyl-alcohol could be further oxidized to benzaldehyde (VI) and later onto benzoic acid, which in turn decomposes via a photo-kolbe mechanism, giving rise to phenyl radicals (VII) and CO_2 [163]. Additionally, the C-C bond between the methyl group and the aromatic group can be easily destructed by energetic electrons beyond 4.4 eV and the metastable nitrogen molecules, generating a phenyl radical (VII) and a methyl radical. As shown in Figure 3.8, phenyl radicals could react with H, OH, NH_2 and CN radicals, forming benzene (VIII), phenol (IX), aniline (X) and benzonitrile (XI), respectively, all of which were identified by GC-MS after the plasma reaction. Blin-Simiand et al. reported that the possibility of the reaction between CN and phenyl was higher than that between CN and methyl-phenyl in the destruction of toluene using a DBD [164]. Toluene can also be ruptured by the dissociation of C-C bonds of the aromatic ring with a dissociation energy of 6.0 eV, resulting in the direct cleavage of the aromatic ring to produce the ring-opening products, such as acetylene and C_5H_6 [164]. Those generated intermediates are further react with active species or energetic electrons, finally converted into H_2, H_2O, CO and CO_2. Several studies have proposed the similar conclusions that the destruction of low concentration toluene in the nitrogen plasma

discharge can be initialized through two major reaction pathways: H-abstraction of the methyl group and breaking the benzene ring through reactions induced by energetic electrons and N_2 excited states such as N_2 (A^3) and N_2 ($a^'$), shown in R3-1 to R3-8 . Concerning the small electron cross section of aromatic hydrocarbons molecules, it could be concluded that the direct electron impact has a low contribution to the toluene destruction process [165]. Previous experimental and modelling studies showed the importance of N_2 excited states in the destruction of low concentration gas pollutants in nitrogen or air plasmas [166, 167]. Trushkin et al. developed a kinetic model to understand the decomposition of toluene (100-400 ppm) in a nitrogen pulsed discharge. Their results showed that toluene is mainly decomposed via its reactions with N_2 excited species, such as N_2 (A^3) and N_2 ($a^'$) [168]. Yu et al. demonstrated that the destruction of naphthalene (20-140 ppm) in a gliding arc reactor is mainly initialized through its reactions with nitrogen-excited states, while the electron impact reactions play a weak role in the decomposition of naphthalene. This can be evidenced by a lower naphthalene decomposition in the Ar/O_2 gliding arc compared to that using the N_2/O_2 GAD [161].

Simultaneously with the channels described above, there also exists the other mechanism of toluene decomposition associated with the formation of oxidation species. In the plasma steam reforming of toluene, the produced OH radicals from steam can oxidize toluene and intermediates, opening a new reaction pathway for the destruction of toluene, which results in the enhanced conversion and energy efficiency of the plasma process. This pathway seems to be minor at low humid level, whereas at significant humid level it is enhanced by the increase in population of active radicals (i.e. OH radical, O and H atom). The arc discharges are quenched at higher moisture content in the gas streams, which leads to vanish of the electrons and the ions. As a result, the active radicals with longer lifetimes take over the process of toluene decomposition. Durne et al indicated that the first step in toluene steam reforming is either hydrogen atom abstraction from side methyl group by OH radical, resulting in the production of benzyl alcohol, or OH radical addition to the aromatic ring of toluene molecule and leads to the formation of the radical $C_6H_5OHCH_3$ [152]. As discussed above, benzyl alcohol can be oxidized to benzaldehyde and then transferred to

benzoic acid, which undergoes a photo-kolbe reaction to generate benzene and carbon dioxide. The other route of toluene conversion induced by the oxidation of the aromatic ring, would lead to the formation of an intricate hydroxyl-cyclohexadienyl type peroxy radical (XII), which has been confirmed in the previous modelling and experimental studies [152, 163, 169, 170]. Those generated aromatic intermediates rather actively interact with molecular oxygen radicals via H-abstraction and results in the formation of a peroxide bridge radical, which is a precursor for both the carbonyl and epoxide routes. The carbonyl reaction route opens a ring of toluene via a series of oxidation steps by O/OH radicals to form a relatively stable oxygen-enriched compound (XIII) [152]. Meanwhile, the ring-cleavage aromatic compounds might be further fragmented and consequently mineralized into syngas and H_2O. The possible reactions could be the scission of 2, 3-carbon or 1, 2-carbon bond of oxygen-enriched chemicals, leading to the formation of oxalic acid (XIV), formic acid (XIV), and eventually producing CO and H_2. For the conditions in non-equilibrium low-temperature plasma, the contribution of the latter channel (OH radical directly reacts with the aromatic ring of toluene molecule and leads to the formation of the radical $C_6H_5OHCH_3$) to toluene destruction roughly 90%, which is the more prevalent pathways [156]
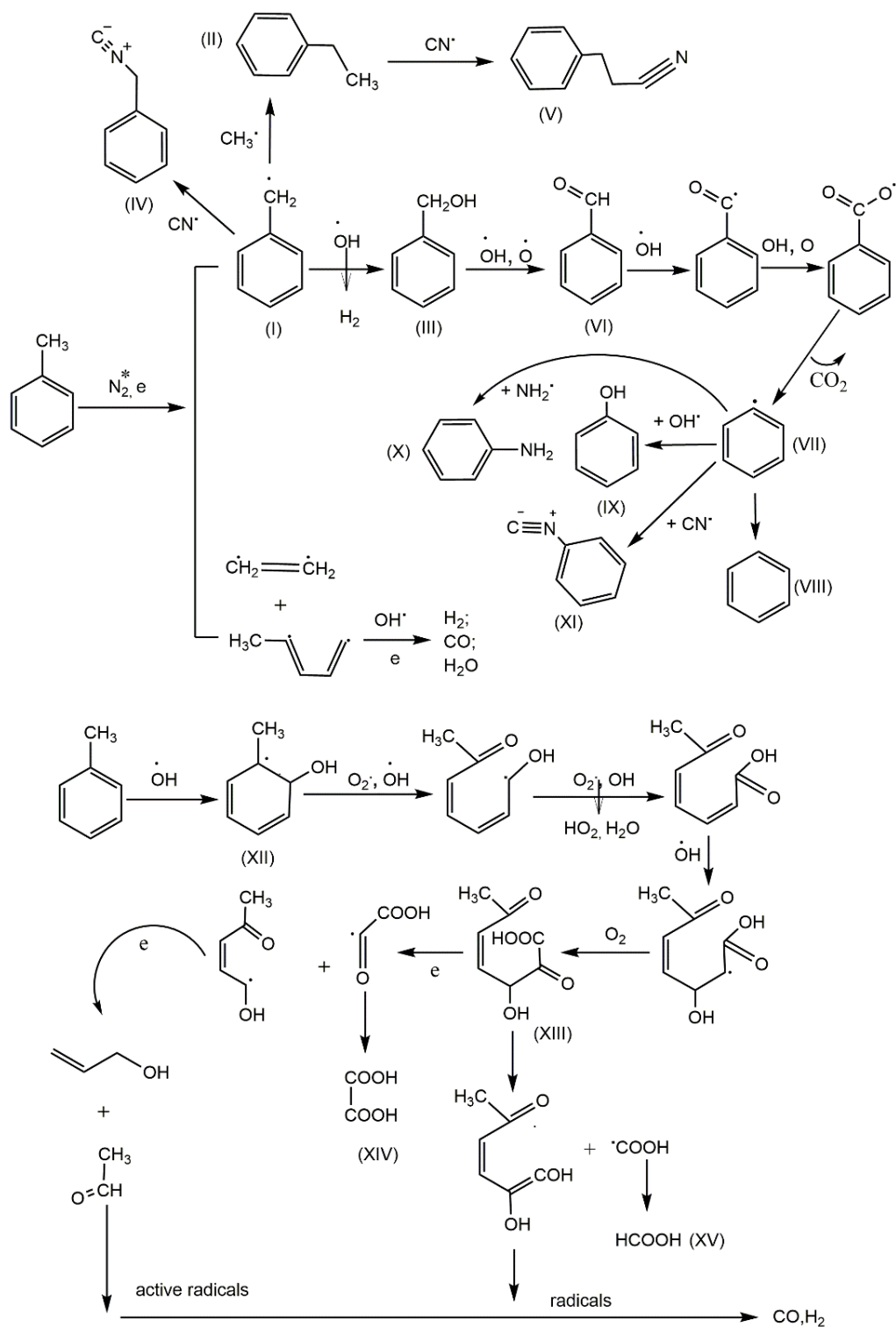
Figure 3.8 Possible reaction pathways for toluene destruction.

3.3. Conclusions

In this chapter, the conversion of toluene as a model tar compound from biomass gasification was carried out in an AC gliding arc discharge reactor at atmosphere pressure. Adding steam in the plasma toluene reaction significantly enhanced the conversion of toluene and energy efficiency of the plasma process due to the formation of OH radicals which open a new reaction route for the decomposition of toluene through a stepwise oxidation of toluene and intermediates. The effect of different process parameters on the performance of the plasma steam reforming of toluene was also investigated in terms of the toluene conversion, yield of products and energy efficiency of the plasma process. The performance of the plasma process strongly depends on the S/C molar ratio with the optimal S/C molar ratio being 2-3 for both high toluene conversion and energy efficiency. The maximum toluene conversion of 51.8% was achieved at an optimal S/C molar ratio of 2, a toluene feed flow rate of 4.8 ml/h and a SEI of 0.3 kWh/m^3, while the energy efficiency of the plasma process reached the maximum (~46.3 g/kWh) at the same S/C molar ratio, but a higher toluene feed flow rate (9.6 ml/h) and a lower SEI (0.19 kWh/m^3). H_2, CO and C_2H_2 were identified as the major gas products, while a trace amount of hydrocarbons (C_2H_4, C_2H_6 and C_3H_8) with a total yield of less than 1% were also detected in the effluent. The S/C molar ratio also has a significant influence on the yield of gaseous products. The maximum syngas production (73.9% gas yield) was achieved at the same condition as that for the maximum toluene conversion. However, increasing the S/C molar ratio gradually decreased the yield of C_2H_2 from 12.8% to 5.3% at a toluene feed flow rate of 4.8 ml/h and a SEI of 0.19 kWh/m^3. Higher S/C molar ratio could generate more OH radicals for the stepwise oxidation of toluene and intermediates, reducing the chance of toluene ring cleavage by free electrons and N_2 excited species to release C_2H_2. In addition, a small amount of liquid by-products were also collected after the plasma steam reforming of toluene. The possible mechanisms and reaction pathways in the plasma conversion of toluene was proposed and discussed in details based on the analysis of the gas and liquid samples and the formation of reactive species (e.g. CH, OH, CN and NH) using OES under different experimental conditions.

CHAPTER FOUR COMBINED (CARBON DIOXIDE AND STEAM) REFORMING OF TOLUENE IN A GAD REACTOR

4.1 Introduction

In Chapter 3, the challenge concept of direct conversion of toluene with humid nitrogen was explored by using an AC gliding arc discharge system [171]. The experimental results showed that the addition of a small amount of steam effectively minimised carbon deposition on the electrode surface and also enhanced the yield of syngas and the energy efficiency. Actually in the raw syngas produced from biomass gasification, typically, CO_2 accounts for 10-13 vol.%, higher than the content of H_2O 10 vol.% [172]. Thereby, carbon dioxide reforming of tar might be a good choice to improve the effective transformation of tar by generating more syngas, which also benefits environmental protection. From an industrial application point of view, gas humidity is one of the most important factors affecting the effectiveness of plasma gas cleaning applications since the producer gas emitted from gasification processes generally contains water. To the best of our knowledge, there is very limited work focused on the use of greenhouse gas CO_2 for tar conversion, while information on the interaction of heavy hydrocarbons with CO_2 and H_2O is rather scarce. The mechanistic interpretation on the compositions of producer gas and formations of the aromatic hydrocarbons are of great importance in understanding the characteristics of tar removing in the biomass thermochemical conversion, which will contribute better to the design of the process and optimization of the operation.

In this present work, an AC gliding arc discharge reactor has been employed for syngas production from CO_2 reforming of tar. The configuration of the GAD reactor and the experimental system is shown in Figure 2.2 and the corresponding details are described in Section 2.1.1. Toluene was chosen as a model biomass tar compound because it is found in significant quantities in biomass gasification, especially at low reaction temperature, being clearly surpassed by benzene as the major component of tar [173]. A tube furnace and an electrical heating-jacket were coupled to produce toluene and water vapour. Toluene with

the purity of 99.5% (Sigma) and deionized water were fed into the evaporator preheated in the tube furnace at 200 $^{\circ}$C through the high-resolution syringe pumps (KDS Legato, 100). Toluene and water vapour at a steady state were then fed into the reactor by the carrier gas. Both pure N_2 and the mixture of N_2 and CO_2 were used as the carrier gas in the reforming test. The steam-to-biomass carbon molar ratio (S/C$_T$) was varied from 0 to 2.5. The total flow rate of the feed gas mixture was fixed at 3.5 L/min with a constant toluene concentration of 16 g/Nm^3 during the whole experiment. The effects of different operating parameters (e.g. CO_2 concentration and steam-to-tar carbon (S/C$_T$) molar ratio) on the performance of plasma decomposition of toluene were assessed in terms of toluene conversion, energy efficiency and the yield of gaseous products. Optical emission spectroscopy (OES) was used to identify the active species generated in the plasma process. In addition, the role of the nitrogen excited species and oxygen-containing active species derived from CO_2 dissociation has been evaluated at different humidity levels. The possible reaction mechanisms and pathways involved in the plasma gas processing have been discussed by combined means of OES diagnose and the analysis of gas and liquid products. The conversion of toluene is calculated by Equation (2-8); the yield of the products is determined by Equations (2-5), (2-9) and (2-10); while the energy efficiency of the plasma process is defined as Equation (2-14).

4.2 CO$_2$ reforming of toluene in a GAD reactor

4.2.1 Effect of CO$_2$ content on the conversion of toluene

In order to investigate the effect of CO_2 on the plasma conversion of toluene, CO_2 was injected into the reaction system. The total flow of N_2 and CO_2 was kept constant at 3.5 L/min when varying the initial CO_2 concentration in the gas mixture (CO_2 and N_2). Figure 4.1 shows the effect of the initial CO_2 concentration on the performance of plasma conversion of toluene at a constant toluene content of 16.1 g/Nm^3 and a SIE of 0.25 kWh/m^3. Clearly, the conversion of toluene was initially increased by increasing the content of CO_2 and reached a maximum value of 59.9% when the initial CO_2 concentration increased to 3%, beyond which the toluene conversion started to decrease gradually. A minimum toluene of

56.2% was observed at an initial CO_2 concentration of 12%. The energy efficiency of the plasma process followed the same tendency as the toluene conversion and reached a maximum value of 38.7 g/kWh at an initial CO_2 concentration of 3vol. %.
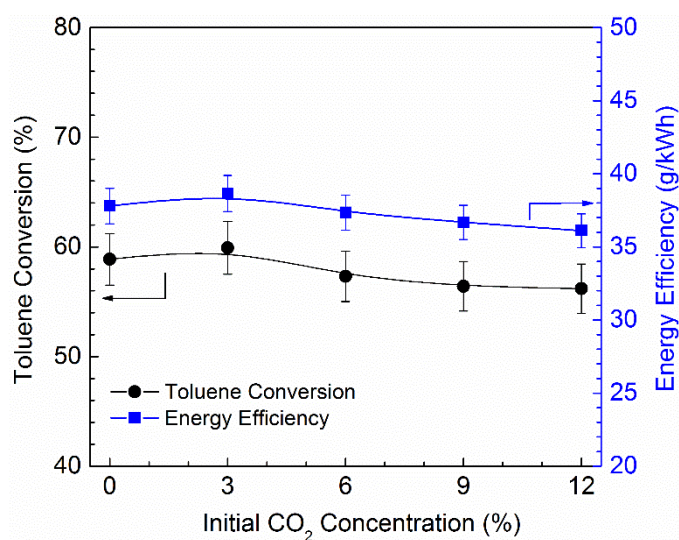
(a)
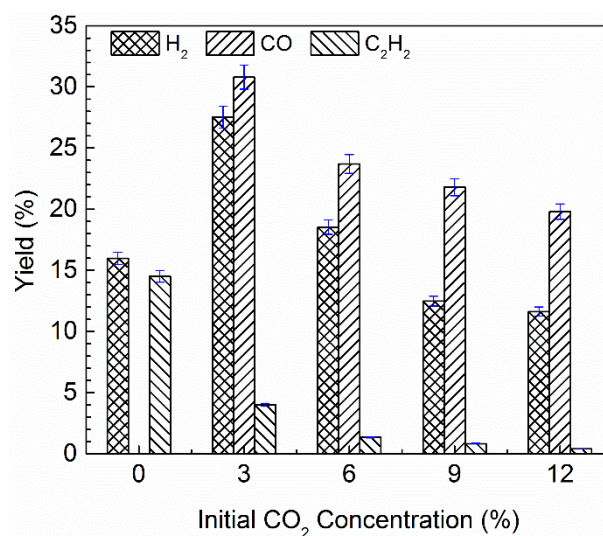
(b)

Figure 4.1 Effect of the initial CO_2 concentration on (a) toluene conversion and energy efficiency; (b) yields of primary gaseous products. (C_7H_8 concentration: 16.1 g/m^3; SEI: 0.25 kWh/m^3)

It was reported that the major pathways leading to toluene decomposition in N_2 plasma can be either direct electron impact dissociation or collision with the excited nitrogenous species (shown in R4-1 to R4-5), especially the metastable state of the nitrogen molecules $N_2\left(A^3\Sigma_u^+\right)$ which have been considered as the energy reservoirs for their higher reaction rates [164].

$$C_6H_5\cdot CH_3 + e \rightarrow C_6H_5\cdot CH_2 + H + e \tag{R4-1}$$

$$C_6H_5\cdot CH_3 + e \rightarrow C_6H_5 + CH_3 + e \tag{R4-2}$$

$$C_6H_5\cdot CH_3 + N_2^* \rightarrow C_6H_5\cdot CH_2 + H + N_2 \tag{R4-3}$$

$$C_6H_5\cdot CH_3 + N_2^* \rightarrow C_6H_4\cdot CH_3 + H + N_2 \tag{R4-4}$$

$$C_6H_5\cdot CH_3 + N_2^* \rightarrow C_6H_5 + CH_3 + N_2 \tag{R4-5}$$

$$e + N_2 \rightarrow N_2^* + e \tag{R4-6}$$

where N_2^* represents the excited nitrogen species, it can be either nitrogen metastable states $N_2\left(A^3\Sigma_u^+\right)$ or the excited states $N_2\left(a^1\Pi_g\right)$ and $N_2\left(B^3\Pi_g\right)$, with excitation threshold energy of 6.17 eV, 8.4 eV and 7.35 eV, respectively.

Introducing CO_2 into the reaction system generated active oxygen species O via dissociation of CO_2 molecules impacted by energetic electrons (R4-7) and excited N_2 species (R4-8). The active oxygen species O were also generated by exciting the ground state O using excited nitrogen species (R4-9). The active oxygen species O were beneficial to the conversion of toluene through R4-10 and could generate hydroxyl radicals OH by the recombination of O and H (see R4-11) [156]. The hydroxyl radicals OH are more reactive with toluene than atomic O, resulting in an increase of the toluene conversion and the energy efficiency compared to that in pure nitrogen. The lower toluene conversion in the higher CO_2 initial concentration can be attributed to the quenching of excited nitrogen species by CO_2 and its derivatives O, as shown in R4-7 and R4-8. In addition, in the CO_2/N_2 mixtures, the energetic electrons are more likely to be consumed to produce CO and O due to its relative low dissociation energy 2.94 eV (R4-9), which reduced the possibility of collision between electrons and N_2 and thus decreased the amount of the excited nitrogen species in the reaction

system [174]. Meanwhile, the contribution of excited nitrogen species in the decomposition process diminished due to the fast quenching of N_2 ($A^3\sum$) by CO (R4-12) [175]. All of these behaviours indicated that the increase of toluene conversion caused by the oxidation reactions (i.e., R4-10) cannot compensate its decrease due to the loss of nitrogen metastable states or loss of a fraction of the input energy for decomposing CO_2 directly.

$$CO_2 + N_2^* \rightarrow CO + O + N_2 \qquad\qquad\text{(R4-7)}$$

$$O + N_2^* \rightarrow O + N_2 \qquad\qquad\text{(R4-8)}$$

$$CO_2 + e \rightarrow CO + O + e \qquad\qquad\text{(R4-9)}$$

$$C_6H_5 \cdot CH_3 + O \rightarrow C_6H_5CH_2 + OH \qquad\qquad\text{(R4-10)}$$

$$H + O + N_2 \rightarrow OH + N_2 \qquad\qquad\text{(R4-11)}$$

$$CO + N_2(A^3\Sigma) \rightarrow N_2 + CO \qquad\qquad\text{(R4-12)}$$

The presence of CO_2 in the plasma process of toluene decomposition significantly affected the distribution of the gaseous products, as shown in Figure 4.1(b). Apparently, in the absence of CO_2, the major gaseous products were H_2 and C_2H_2 with the yield of 15.9% and 14.5%, respectively. When the initial CO_2 concentration increased to 12%, the yield of C_2H_2 significantly was decreased by a factor of 37; while the maximum H_2 yield of 27.5% was achieved at an initial CO_2 concentration of 3%. The presence of CO_2 generated CO as the main gas product. The yield of CO reached its maximum value (30.8%) at an initial CO_2 concentration of 3% and decreased to 19.8% when the initial CO_2 concentration increased to 12%. CO are mainly formed via the CO_2 dissociation reactions (R4-7 and R4-9). Simultaneously, CO could be formed in another pathway, initialized by the reaction R4-13. Hydrogen can be formed through the recombination of two H atoms, which are more likely to be produced in the process of methyl group dehydrogenation, since the dissociation energy of C-H bonds (3.7 eV) in the methyl group are the weakest bonds in the toluene molecules [53]. The recombination of CH_3 radical with H can form methane, as described by reaction R4-14. However, no CH_4 was detected in the plasma conversion of toluene with or without CO_2, suggesting that this reaction is negligible in our plasma system. The production of an appreciable amount of acetylene in the nitrogen plasma discharge indicates that toluene

conversion is accompanied by the reactions of benzene ring cleavage, which is originated mainly in the following reaction R4-15 [156]. Studies on homogeneous discharges have shown that the active molecular nitrogen has a non-negligible influence on ring cleavage of aromatic hydrocarbons in non-thermal plasmas at near atmospheric pressure [176].

$$CO_2 + H \rightarrow CO + OH \tag{R4-13}$$

$$CH_3 + H \rightarrow CH_4 \tag{R4-14}$$

$$C_6H_5CH_3 + N_2^* \rightarrow C_5H_6 + C_2H_2 + N_2 \tag{R4-15}$$
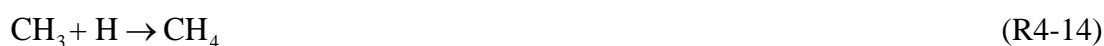
4.2.2 Optical diagnostics

To better understand the role of CO_2 on the reaction pathways in the GAD plasma dry reforming of toluene, optical emission spectroscopy was used to investigate the formation of different reactive species in the plasma process. Figure 4.2 shows the emission spectra of N_2, N_2/C_7H_8 and $N_2/CO_2/C_7H_8$ plasma in the visible spectral range of 200-900 nm. The spectrum of the active particles suggests that the plasma-chemical conversion of toluene is strongly affected by the composition of the gas mixture. In the N_2 discharge, the spectra is characterized by the second positive band system (SPS) of N_2 ($C^3\Pi_u \rightarrow B^3\Pi_g$) and the N_2 first negative system (FNS) ($B^2\Sigma_u^+ \rightarrow X^2\Sigma_g^+$), which are distributed in the range of 280 to 430 nm. This indicates that in the N_2 discharge; initially formed highly energetic electrons can interact with N_2 molecules to produce a cascade yield of a variety of chemically reactive species, such as the electronically excited metastable $N_2\left(A^3\Sigma_u^+\right)$ and vibrationally excited $N_2\left(X^2\Sigma_g^+\right)$ .These species are believed to substantially contribute to the toluene decomposition via reactions R4-3 to R4-5. Other excited nitrogen species (e.g. N (^{2}D)) might be generated in the plasma, but the intensity of these emission spectra is too low to be measured due to low concentration of these active particles. Xiao et al. reported that nitrogen could be pre-dissociated into the ground state N(^{4}S) and the metastable state N(^{2}D) [177]. Previous studies reported that the reaction channels of toluene decomposition initiated by nitrogen plasma are associated with the reactions between the toluene molecules and the

metastable electronically excited nitrogen N_2 ($A^3\Sigma$) molecules and nitrogen N (^{2}D) atoms. The latter reaction is expressed in R4-16 [156].

$$C_6H_5 \cdot CH_3 + N(^2D) \rightarrow C_6H_5CH_2 + NH \qquad\qquad (R4\text{-}16)$$
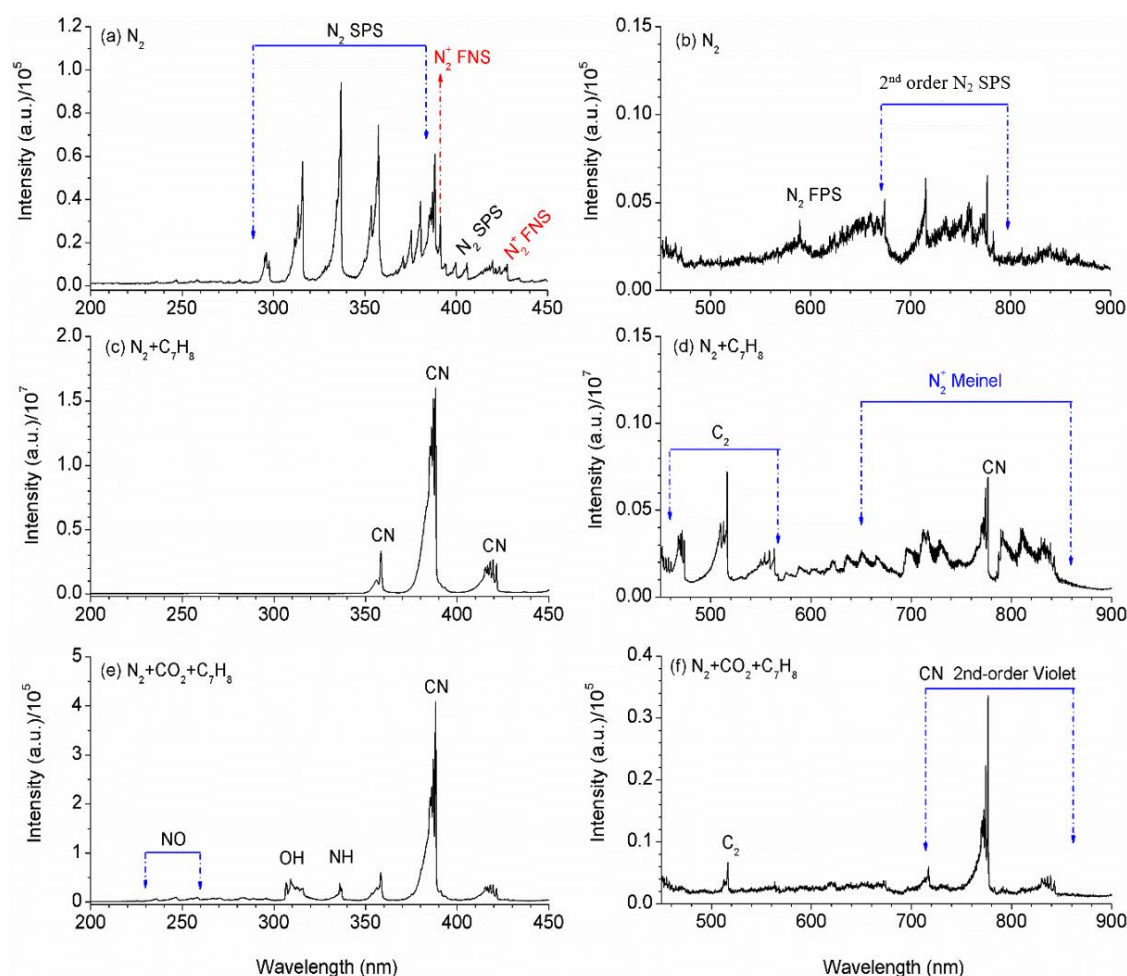
Figure 4.2 Spectra of optical emission from GAD (a)-(b) N_2 GAD plasma; (c)-(d) N_2/C_7H_8 GAD plasma; and (e)-(f) N_2/C_7H_8 /CO_2 GAD plasma (C_7H_8 concentration:16.1 g/m^3; CO_2 content: 12%, SEI: 0.25 kWh/m^3) (600 G/mm grating, exposure time 0.2 s).

Clearly, the spectrum of N_2 and toluene mixture discharge is dominated by the CN ($B^2\Sigma \rightarrow X^2\Sigma$) violet system and C_2 swan bands, which might be generated through R4-17 and R4-18. These observations indicate that toluene decomposition takes place via a mechanism involving nitrogen-excited radicals and also supports the assumption that the

electronic excited state of nitrogen molecules abound in a N_2 gliding discharge. In the plasma toluene decomposition using N_2 as a carrier gas, non-volatile products with dark brown colour were always observed in the form of deposits on the metallic electrodes and the reactor wall, which indicates that aromatic hydrocarbons agglomeration reaction and soot formation took place in the decomposition process [178]. However, no spectra from carbon were observed within the wavelength range 200-900 nm. This might be attributed to the sensitivity limitation of the spectrometer.

$$N_2^* + CH_x \rightarrow CN + N + H_y + H_z \tag{R4-17}$$

$$N + CH_x \rightarrow CN + H_y + H_z \, (x \, (\leq 4) = y + z) \tag{R4-18}$$
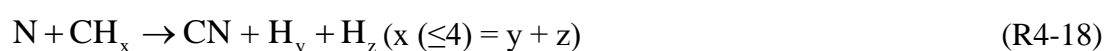
The introduction of CO_2 into the initial gas mixture (N_2/toluene) results in a generation of new chemically active particles. For instance, the spectral emission of OH radical ($A^2 \sum^+ \rightarrow X^2 \prod$) appears at 308.8 nm can be observed in the $N_2/C_7H_8/CO_2$ GAD plasma. It should be noted that the initial gas mixture does not contain water vapour, the hydroxyl radical OH is generated exclusively due to plasma-chemical reactions between toluene and CO_2 decomposition products (i.e., R4-10 and R4-11). In the presence of CO_2, the carbon deposition on the electrode and reactor wall was reduced. In addition, the relative intensity of CN dropped significantly when introducing CO_2 in the reaction system. Such behaviours suggested that the formation of CN might be associated with carbon deposition in the processing of toluene decomposition, as shown in R4-19 and R4-20.

$$N_2 + C \rightarrow CN + N \tag{R4-19}$$

$$N_2 + C + N \rightarrow CN + N_2 \tag{R4-20}$$

The spectrum of the $N_2/C_7H_8/CO_2$ discharge showed a NH ($A^2 \sum \rightarrow X^2 \sum$) band at 336.1 nm. The main channel for NH formation might be associated with the hydroxyl radical OH (i.e., R4-21), as the NH radical was not observed in the spectrum of nitrogen discharge [154]. This phenomenon also suggests that the formation of NH via direct reactions between N_2 and H_2 might be negligible and nitrogen atoms make an insignificant contribution to C_7H_8 removal (see R4-16).

$$N_2 + OH \rightarrow NH + NO \qquad\qquad (R4\text{-}21)$$

$$CH + NO \rightarrow NH + CO \qquad\qquad (R4\text{-}22)$$
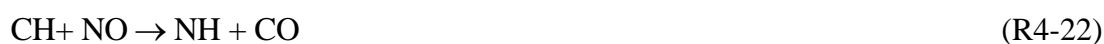
The presence of NO ($A^2\Sigma^+ \rightarrow X^2\Pi$) bands in the range of 230-250 nm indicates that the reaction R4-21 to R4-24 might be involved [153].

$$N_2^* + O \rightarrow NO + N \qquad\qquad (R4\text{-}23)$$

$$N + CO_2 \rightarrow NO + CO \qquad\qquad (R4\text{-}24)$$

Although the presence of CO_2 in the plasma system could generate O or OH radicals to provide additional destroy channels for toluene, CO_2 has an adverse effect on the processing of toluene destruction, especially in the high initial CO_2 concentration. Increasing the content of CO_2 in the gas stream gradually dropped the relative intensity of N_2^+ and C_2 radicals (shown in Figure 4.3), which indicated that the presence of CO_2 limits the density of nitrogen excited states and consequentially decreases the contribution of metastable nitrogen molecules to toluene decomposition. The similar evolutions of C_2 and N_2^+ in the plasma toluene conversion process also suggest that the formation of C_2H_2 is mainly related to the interaction between toluene molecules and excited nitrogen molecules.
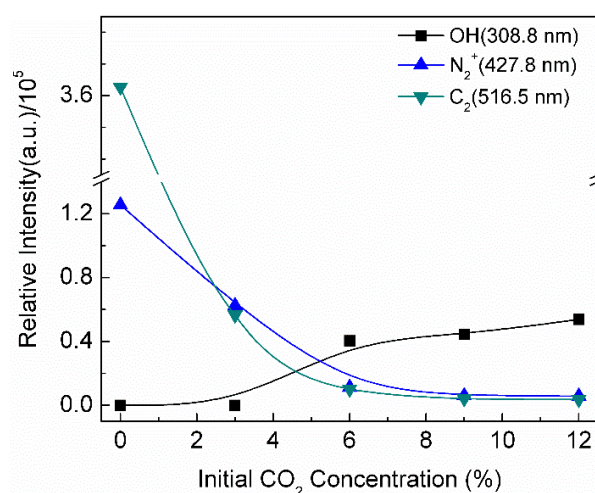
Figure 4.3 Optical emission intensity of three species in $N_2/CO_2/C_7H_8$ plasma as a function of CO_2 concentration in the feed gas (C_7H_8 concentration: 16.1 g/m^3; SEI: 0.25 kWh/m^3).

4.2.3 Combined effect of steam and CO_2 on the conversion of toluene

In order to determine how moisture content in the gas stream affects the performance of plasma dry reforming of toluene in the GAD reactor, the experiments were conducted in dry and humid mixtures of N_2 and CO_2. It was reported that the concentration of CO_2 in the producer gas is in the range of 10-13 vol.% [179]; therefore, the concentration of CO_2 in the feed was fixed at 12 vol.% in this study. Figure 4.4 (a) presents the dependence of toluene conversion and the energy efficiency on the steam to biomass carbon molar ratio S/C_T at a fixed SIE of 0.25 kWh/m^3. Obviously, there is an optimum S/C_T molar ratio of 1 in the feed gas, at which the maximum toluene conversion 63.3% and the highest energy efficiency 40.5 g/kWh were achieved. Lu et al. also found that increasing the concentration of H_2O up to 300 mg/m^3 in the feed (which is equivalent to a steam-to-biomass carbon molar ratio of 1in the feed stream) could improve the removal efficiency of toluene by a rotating gliding discharge reactor [170].
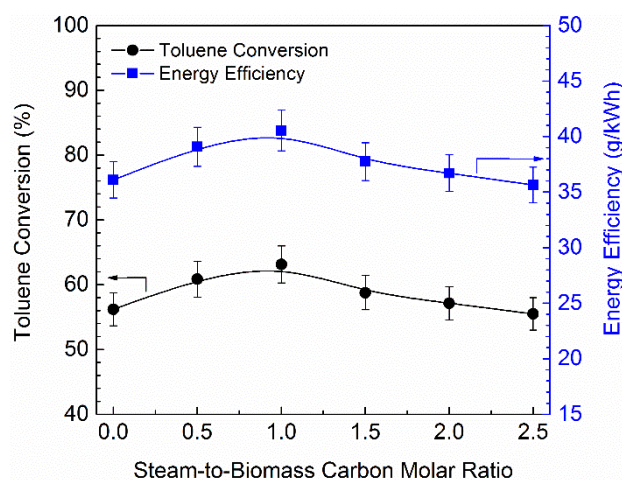
(a)
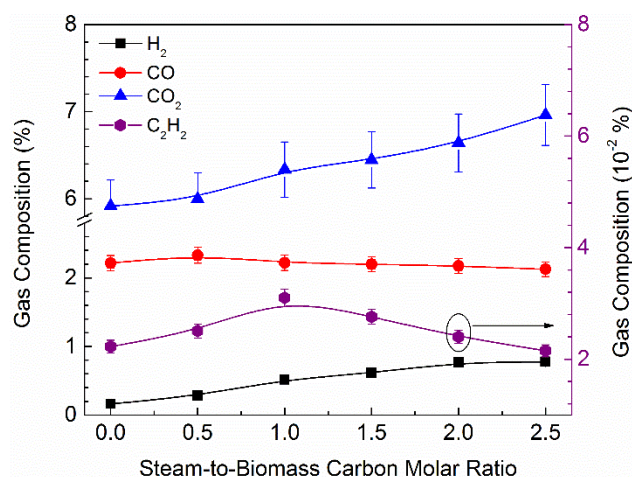
(b)
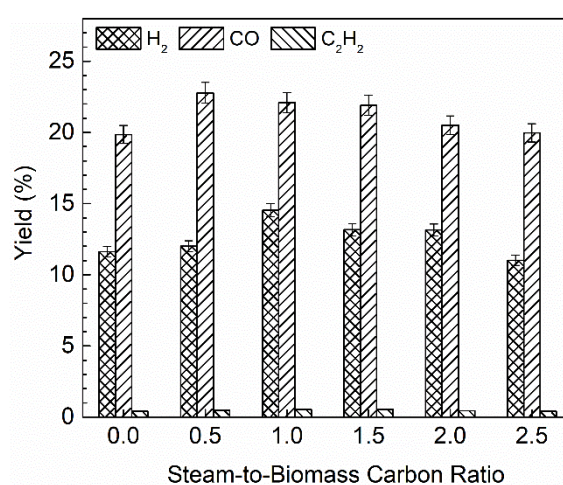
(c)

Figure 4.4 Effect of S/C_T molar ratio on (a) toluene conversion and energy efficiency; (b) the distribution and (c) the yield of gaseous products (C_7H_8 concentration: 16.1 g/m^3; SEI: 0.25 kWh/m^3; CO_2 concentration: 12%. Here, C_T means the carbon in toluene).

The concentration of water vapour in the feed gas also played a significant role in the distribution on the final gaseous products from plasma dry reforming of toluene, as shown in Figure 4.4 (b), whilst the yield of the major gaseous products (H_2, CO and C_2H_2) was shown in Figure 4.4 (c). Increasing the S/C_T molar ratio from 0 to 2.5 leads to a noticeable increase in the volume fraction of H_2 and CO_2 in the gaseous products, whereas the content of CO gradually decreases with the S/C_T molar ratio. This phenomenon can be attributed to the water-gas shift reaction R4-25, which is responsible for the increase in the concentration

of H_2 and CO_2 and the decrease in the concentration of CO. In contrast, the evolution of the C_2H_2 concentration with the S/C_T molar ratio is very similar to the effect of S/C_T molar ratio on the conversion of toluene. The highest concentration of C_2H_2 (0.032%) was obtained at the optimum S/C_T molar ratio of 1. This suggests that acetylene might be produced from the recombination of CH or CH_2 radicals (R4-26 and R4-27), which are closely associated with the decomposition of toluene.

$$H_2O + CO \rightarrow H_2 + CO_2 \tag{R4-25}$$

$$CH + CH \rightarrow C_2H_2 \tag{R4-26}$$

$$CH_2 + CH_2 \rightarrow C_2H_2 + H + H \tag{R4-27}$$
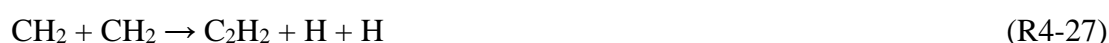
The introduction of water vapour into the discharge volume opens the direct mechanisms of hydroxyl radical production from electron-impact dissociation of H_2O molecules (R4-28) and collisions of water vapour with electronically excited nitrogen molecules (R4-29). The interaction rate of OH radicals with toluene molecules is about two orders of magnitude higher than that of O radical [164], which suggests that the hydroxyl radical OH is much more reactive with toluene than atomic oxygen at low temperature. Reactions R4-30 to R4-31 describe the possible reactions leading to toluene conversion in the humid environment. Increasing the concentration of water vapour in the feed can increase the number of produced OH radicals in the reaction system, as shown in Figure 4.5, which should promote the removal efficiency of toluene. Previous theoretical and experimental works on the destruction of toluene using a pulse-periodic discharge indicated that the main channel of the interaction of toluene molecules with radical OH occurs according to reaction R4-30 and R4-31 at low temperatures [156].

$$H_2O + e \rightarrow H + OH + e \tag{R4-28}$$

$$H_2O + N_2^* \rightarrow N_2 + H + OH \tag{R4-29}$$

$$C_6H_5CH_3 + OH \rightarrow C_6H_5CH_2 + H_2O \tag{R4-30}$$

$$\begin{aligned} C_6H_5CH_2 + O &\rightarrow C_6H_5CHO + OH \\ &\rightarrow C_6H_5CO + H_2O \end{aligned} \tag{R4-31}$$

$$C_6H_5CH_3 + OH + N_2 \rightarrow C_6H_5OHCH_3 + N_2 \tag{R4-32}$$
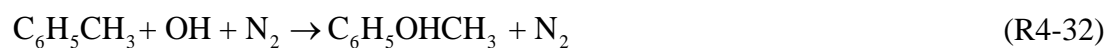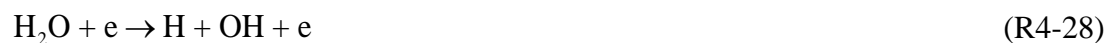
However, the further increase in S/C_T molar ratio caused a considerable drop in the toluene conversion. This might be attributed to the electronegative property of H_2O, which activates additional channel of electrons consumption via electron impact dissociative attachment as shown in R4-33 [180]. At the low S/C_T molar ratio, the effect of electron attachment is insignificant; while raising the concentration of water vapour led to an appreciable reduction in the electron density and the electrical energy contributed to the discharge, and consequently reduce the conversion of toluene.

$$H_2O + e \rightarrow H^- + OH \tag{R4-33}$$
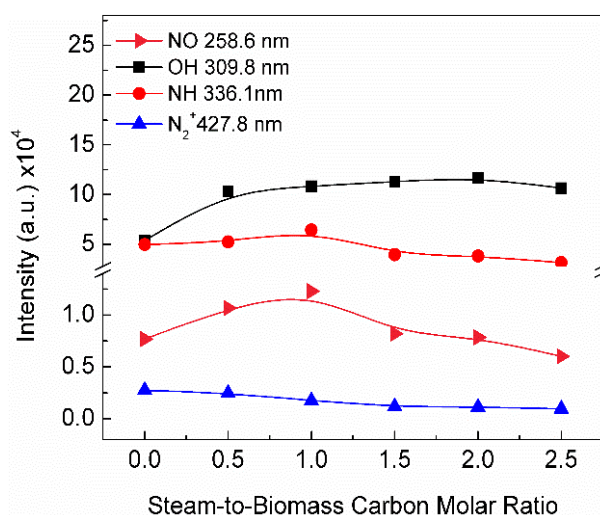
Figure 4.5 Optical emission intensity of essential species in $N_2/CO_2/H_2O/C_7H_8$ plasma as a function of S/C_T molar ratio (C_7H_8 concentration: 16.1 g/m^3; SEI: 0.25 kWh/m^3; CO_2 concentration: 12%).

In addition, the other adverse effect of H_2O on toluene conversion can be described by the ability of quenching the electronically excited nitrogen species by the water vapour and its derivatives, as described by the reaction R4-29 [181]. Increasing the humidity of the plasma-working gas considerably accelerated this contribution and consequently less availability of the excited nitrogen species were generated for the subsequent decompositions, which resulted in a decrease of the conversion of toluene. This can be

confirmed by the OES analysis results shown in Figure 4.5 - the intensity of N_2^+ metastable state monotonically decreases with an increase in the S/C_T molar ratio.

4.3 By-products analysis

To get a better insight into the decomposition mechanisms of toluene and the role of the reactive species in the decomposition process, the collected liquid by-products at different experimental conditions were studied by GC-MS method. Figure 4.6 presents the GC-MS chromatogram of the organic by-products of toluene destruction in the GAD reactor and the structures of relevant products are list in Table 4.1. In case of nitrogen discharge, 19 types of organic by-products from toluene destruction by GAD plasma were identified by GC-MS. The abundance of 1-butene, 3-methyl, benzene, ethylbenzene, phenylethyne, benzo- nitrile and naphthalene were detected as the major by-products. It should be noted that the presence of N-containing compounds in the N_2 discharge such as benzonitrile, benzylcyanide, and 1-Isocyano-4-methylbenzene indicates that the CN radicals would recombine with the benzyl intermediates. Remarkably, the presence of CO_2 molecules in the incident mixture, less N-containing substituent compounds were detected compared with that in the case of nitrogen discharge, which confirms that the contribution of nitrogen to the toluene destruction process was decreased with the presence of oxygen-containing compounds in the feed gas. Trushkin and co-workers developed a kinetic model of plasma chemical decomposition of toluene in a gas mixture of nitrogen and oxygen [156]. They found that the metastable molecules of nitrogen played the key role in decomposition of toluene in pure nitrogen and made a substantial contribution when the oxygen content was less than 5% in the O_2/N_2 gas mixture; however, it exhibited weak influence on the decomposition of toluene in humid air.

When the toluene destruction was carried out in the humid CO_2/N_2 environment, the by-products were distinct from those in the nitrogen discharge, as shown in Figure 4.6. Only three main byproducts were identified, they were benzene, ethylbenzene and dodecane. At the humid N_2/CO_2 discharge, due to the combination of strong oxidation of oxygen-derived radicals and electron impact, more oxidized polycyclic aromatics were detected during the

experiments. The detected liquid by-products in $N_2/CO_2/H_2O$ discharge could be divided mainly into three group (see in Figure 4.6). The first group containing one-ringed compounds, such as styrene, ethylbenzene and phenylethyne, resulting apparently from an alkylation of benzene with either ethylene, ethane or ethyne. The oxygen-containing substituents monocyclic aromatic compounds such as 4-aminobenzoic acid and Benzeneacetamide were also observed, which indicates that the formation of NH_3 via the reactions between the NH radicals and H atoms took place in the destruction process. This result suggests that some reactive nitrogen, oxygen and hydroxyl radicals do not directly react with toluene molecules but are consumed to produce carboxyl acid, hydroxylamine (-N-OH) and carboxamide (-CO-NR) compounds. Naphthalene, biphenyl, bibenzyl and diphenylmethane belong to the second group (polycyclic hydrocarbon group). The intermediate molecular fragments of toluene would recombine by radical impact and lead to the formation of high-molecular polymer compounds. It is interesting to note that no products with more than two aromatic rings were observed in the liquid by-products. Linear organic by-products were representatives in the third group compound, such as 1, 3-Butadyne, 3-methyl-1-butene and oxalic acid. These linear products might come from the cleavage of toluene ring, followed by the hydrogenation and oxidation of the resulting intermediates. The presence of aliphatic compound dodecane implies that the reactive C_2- and C_3-entities tend to polymerise to linear hydrocarbons, in the range of kerosene to light diesel oil.

It is generally accepted that the generation of high-molecular products might depress the toluene destruction and in some cases, they could be more harmful than the original pollutants [182]. For instance, biphenyl is 2.5 times more toxic than benzene. Although unable to quantify the diverse liquid by-products, it is clear from Figure 4.6 that the concentration of the aforementioned compounds are several orders of magnitudes lower than that of toluene. This means the polymerisation reactions only contribute to a very small proportion of total reactivity in the toluene destruction process. Further study will be conducted to improve the reactor structure and optimise the operation parameters, and consequently convert tar compounds into value-added gaseous products (e.g. syngas) with high efficiency.
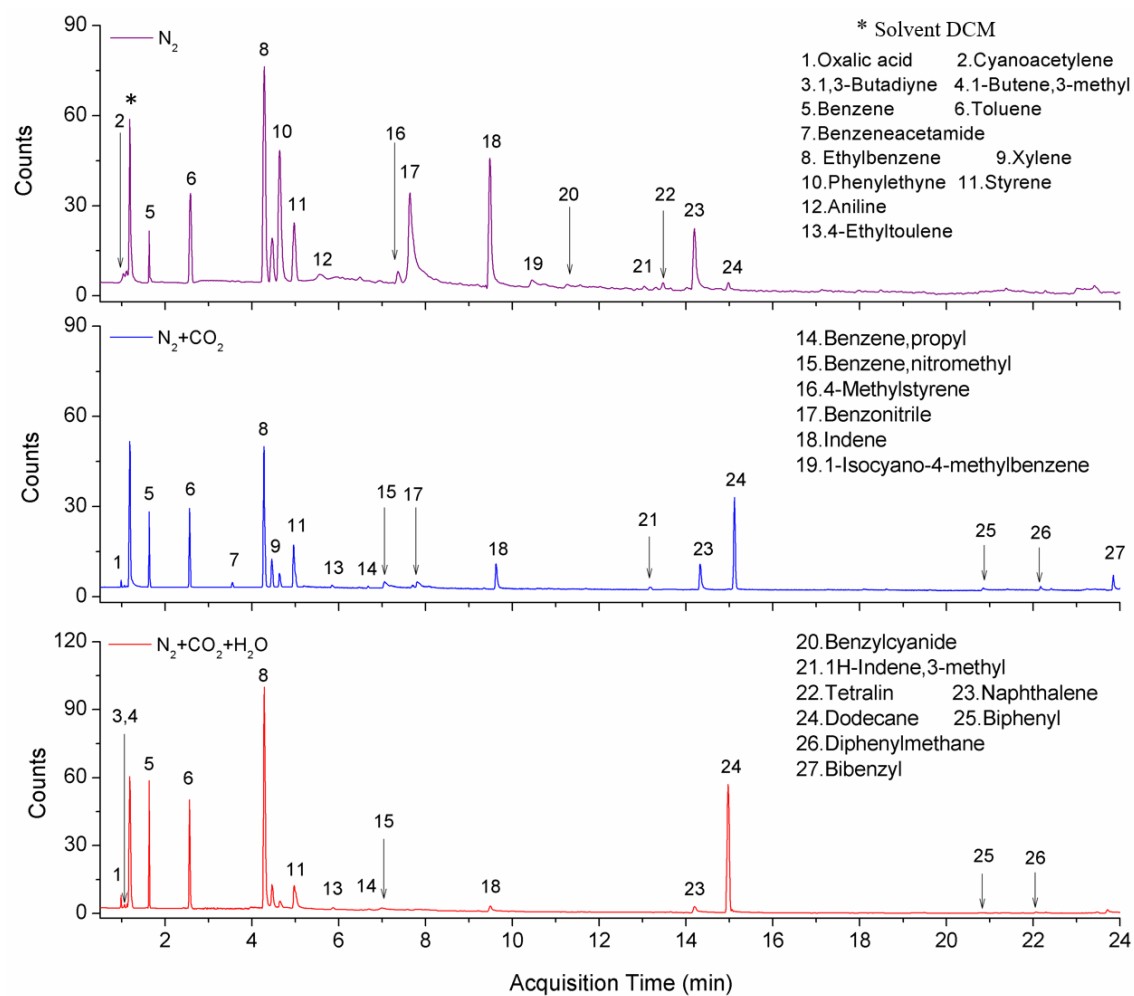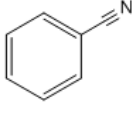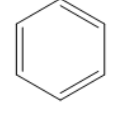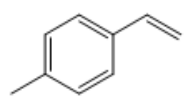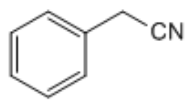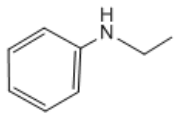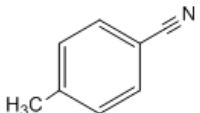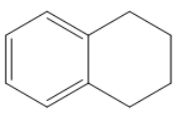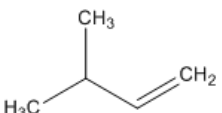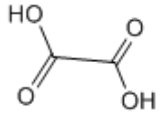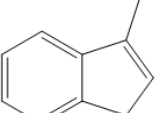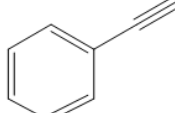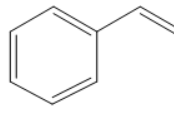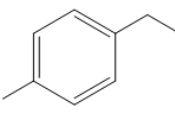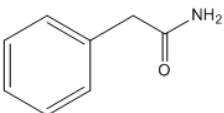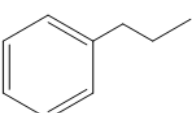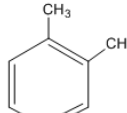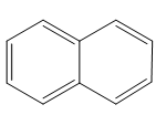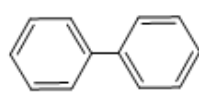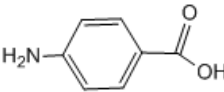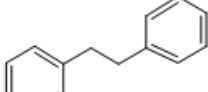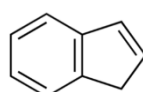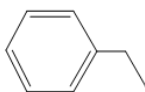
Figure 4.6 GC-MS chromatogram of liquid by-products collected in the toluene plasma reforming (C_7H_8 concentration: 16.1 g/m^3, CO_2 concentration: 12%; SEI: 0.25 kWh/m^3; S/C$_T$: 1.5).

Table 4.1 Liquid compounds identified after plasma treatment.

Specific by-products			General byproducts	
Background gas: N_2				
HC≡C−C≡N				
Cyanoacetylene	4-Methylstyrene	Benzylcyanide	Benzonitrile	Benzene

N-Ethylaniline	1-Isicyano-4-methylbenzene	Tetralin	3-Methyl-1-butene	
Background gas: $N_2+CO_2+H_2O$				
1,3-Butadyne	Oxalic acid	1H-Indene-3-methyl	Phenylethyne	Styrene
4-Ethyltoluene	Benzeneacetamide	Propylbenzene	Xylene	Naphthalene
Biphenyl	4-Aminobenzoic acid	Bibenzyl	Indene	Ethylbenzene

4.4 Possible reaction mechanism

Various by-products were identified from toluene conversion in the presence of different gaseous components, indicating the existence of a complex destruction network involving reactions between toluene molecules, reactant gases, reactive species and produced intermediates. It is generally accepted that the decomposition of toluene in the GAD plasma could technically be achieved through three channels, i.e., (1) electron-impacts, (2) gas-phases radical attacks, and (3) ion collisions [152]. Previous experimental and modelling studies indicated that the most important role of electron impact is during the discharge stage, the radical mechanism is predominant in the afterglow period, while the contribution of ions is negligible [183]. It is noteworthy that the concentration of toluene is

several orders of magnitude lower than that of main gas molecules (such as N_2, CO_2, or H_2O), therefore the probability for direct ionisation of toluene molecule is very small. The accelerated electrons have more chance to collide with other gas molecules (e.g. nitrogen, carbon dioxide or H_2O molecules), resulting in the formation of active species, such as excited N_2 species, atomic oxygen or hydroxyl radicals [184]. The direct electron impact has a low contribution to the toluene destruction process due to the small electron cross section of aromatic hydrocarbons [165]. All of these factors suggests that the collision with active species (e.g. nitrogen excited species, OH radicals) is the most important channel for the initial reaction of toluene decomposition.

4.4.1 Reaction pathways of toluene decomposition (I)

On the basis of the experimental results and literature data, two different reaction mechanisms of toluene removal occur according to the content of oxidants: (1) collision with the excited nitrogen species as well as the energetic electrons, and (2) the step-by-step oxidation via the OH/O radicals. Figure 4.7 presents a tentative reaction scheme for the abatement of toluene in gas phase. In the GAD, mean energy of the electrons is in the range of 1-3 eV and high energy electrons abounds in the discharge area [178]. In the dry mixtures containing CO_2 with low concentration or in absence of any oxidations, the reaction is mainly initiated via an electron transfer from toluene molecule with the formation of either an aromatic radical cation or a benzyl radical [171]. The benzyl radical interacts with excited methyl radical, OH radical and CN radical, with the forming of ethyl-benzene, benzyl-alcohol and benzyl-cyanide, respectively. Afterward, a series of dehydrogenation of the ethylphenyl radical would take place and form the styrene and phenylethyne. The presence of propybenzene indicates an alkylation of benzyl radical with either ethyne or ethane. Benzyl-alcohol could be oxidized to benzaldehyde and later onto benzoic acid, which in turn decomposes via a photo-kolbe mechanism giving rise to benzene and CO_2 [185]. Meanwhile, the aromatic radical cation can also react with a methyl radical and a CN radical, which leads to the formation of xylene isomers and 1-Isicyano-4-methylbenzene, respectively. Under the plasma environment, the collision of isomeric xylenes with energetic particles would

produce various aromatic products, such as m-xylene, p-xylene, 4-ethyltoluene and 4-methylstyrene. Lee and Liu reported that o-xylene and m-xylem radicals can undergo rearrangement and convert to p-xylyl radicals in pyrolysis experiments [182]. Additionally, the C-C bond between the methyl group and the aromatic group can be easily destructed by energetic electrons beyond 4.4 eV and the metastable nitrogen molecules, generating a phenyl radical and a methyl radical. As shown in Figure 4.7, the phenyl radical can react with excited H and CN, forming benzene and benzo nitrile, respectively. Blin- Simiand et al. also reported the possibility of reactions between CN radical and phenyl or between CN and methyl-phenyl in toluene destruction process by DBD discharge [164]. Furthermore, the highly energetic electrons beyond 5.5 eV and metastable molecules of nitrogen provide another possibility leading to direct cleavage of the aromatic ring, which contributes to the formation of ring-opening products, such as acetylene and C_5H_6. Liang et al described the possible ring-opening reactions of toluene as shown in R4-34 and R4-35 [186].

$$C_7H_8 + e \rightarrow C_2H_2 + HC=CH-CH(CH_3)=CH \qquad \text{(R4-34)}$$

$$C_7H_8 + e \rightarrow CH=CH-CH=CH + CH=CH(CH_3) \qquad \text{(R4-35)}$$
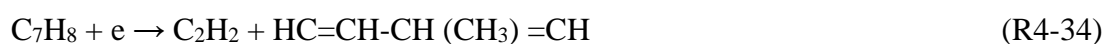
Those generated aromatic intermediates are further attacked by the energetic electrons, leading to the rupture of aromatic ring. The active or partial decomposed species are further react with active species or energetic electrons, and are finally converted to H_2O, CO and CO_2.

Simultaneously with the above channels, there exists other mechanism of toluene decomposition, associated with the formation of polycyclic aromatic compounds, mainly 2-ring compounds. During our measurements, biphenyl, bibenzyl and diphenylmethane were identified as trace products in both dry and humid CO_2/N_2 discharges. These compounds might be generated by direct combination of phenyl and benzyl radicals. For example, the recombination of two phenyl radicals or two benzyl radicals form a biphenyl molecule or a bizenzyl molecule, respectively; whilst, the diphenylmethane molecule could be produced by coupling a benzyl radical and a phenyl radial together in toluene plasma [152]. Previous studies have demonstrated that recombination reactions play important roles in the formation of polycyclic compounds from benzene and toluene plasmas [152, 182]. The formation of

indene and tetralin molecules can be explained by H-abstraction of toluene and its decomposed product o-xylene forming benzyl and o-xylyl radical, respectively, followed by acetylene addition and hydrogenation which propagates molecular growth by cyclisation. Similarly, the recombination of a benzyl radical with an intermediate product propene could result in the production of a naphthalene molecule, initiating a polymerization reaction. Additionally, recombination of two cyclopentadienyl radicals that is mainly formed by the combination of allyl radicals with acetylene, resulting in the formation of naphthalene molecule [187]. It is believed that the cyclopentadienyl radical is mainly formed through combination of acetylene with propyne. Acceptable content of acetylene demonstrated in Figure 4.1 supported the proposed mechanism for naphthalene formation.
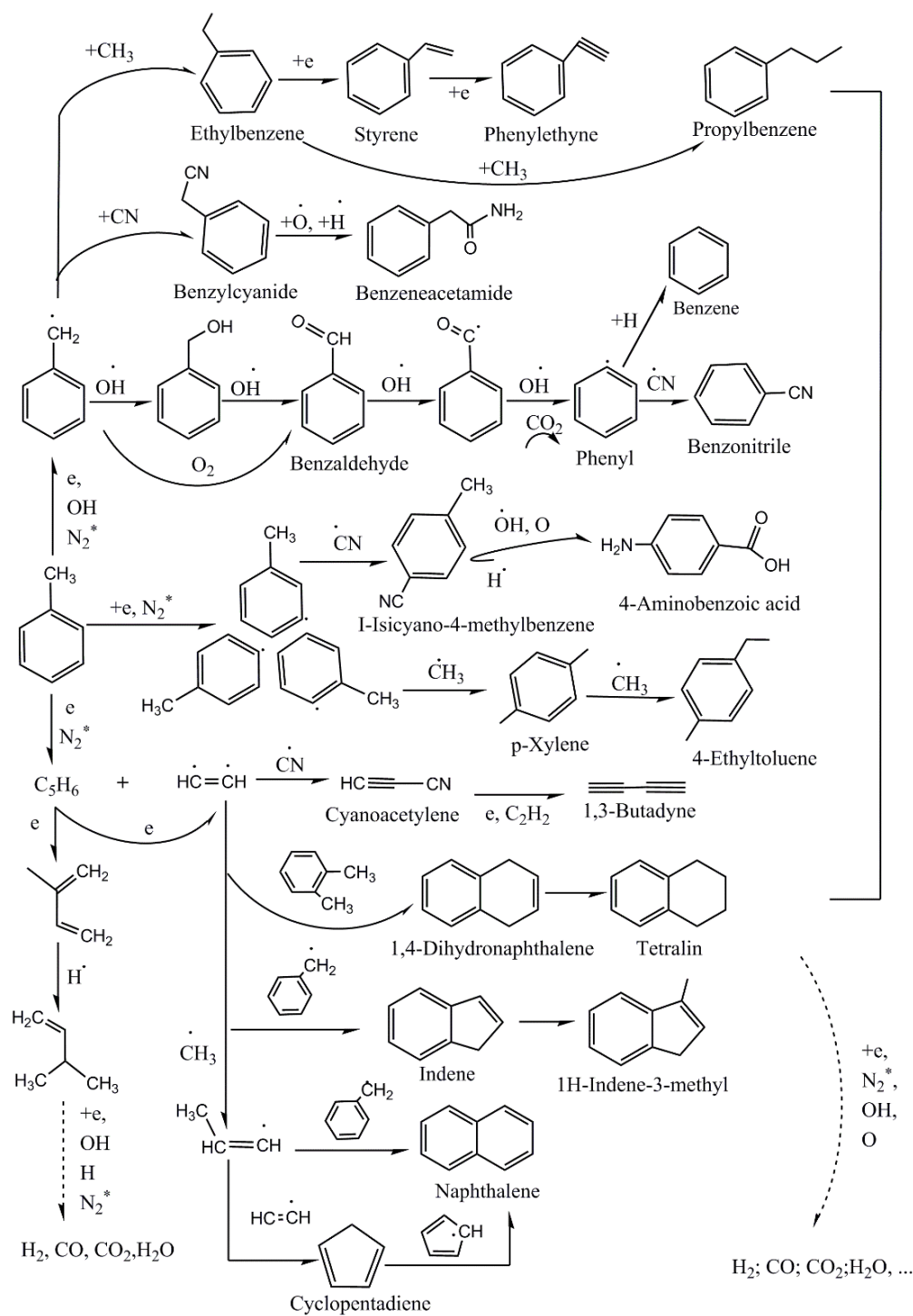
Figure 4.7 Possible reaction pathways for toluene destruction initialled by electron impacts.

4.4.2 Reaction pathways of toluene decomposition (II)

The reaction network of toluene oxidation seems to be minor at the low humid level, whereas it is significantly enhanced by the increase in the population of active radicals (i.e. OH radical, O and H atom) at a significant humid level. In the presence of high humid level,

the electrical arcs are quenched due to the higher moisture content in the gas streams, resulting in vanish of the electrons and the ions. Therefore, the active radicals with longer lifetimes take over the process of toluene decomposition. Due to the high reaction rate with the toluene molecule, the OH radical has a significant effect on the process of toluene removal even if its content is low in the reaction system. Durme et al. [152] indicated that the first step in this route is either the abstraction of hydrogen atom from side methyl group by OH radical, resulting in the production of benzyl alcohol; or OH radical addition to the aromatic ring of toluene molecule, leading to the formation of the radical $C_6H_5OHCH_3$. As discussed above, benzyl alcohol can be oxidized to benzaldehyde and then transferred to benzoic acid, which undergoes a photo-kolbe reaction to generate benzene and carbon dioxide. Previous experimental results have indicated that aldehydes were the common products for the atmospheric reactions of aromatic compounds. For instance, HCHO formaldehyde and CH_3CHO were identified as the major products for the OH-toluene reactions [188]. Our measurements demonstrate that some carbonyl derivative, notably oxalic acid, 4-Aminobenzoic acid and benzeneacetamide were formed during the abatement of toluene by $N_2/CO_2/H_2O$ GAD plasma; however, aldehydes were not detected. This phenomenon might be attributed to the OH radical-rich environment, in which the generated HCHO was further oxidised to form carboxylic acid and finally to H_2O and CO_2. In the non-equilibrium low-temperature plasma, the contribution of the latter channel to toluene destruction is roughly 90% [156]. Possible pathways for toluene-OH reactions are summarized in Figure 4.8. According to this mechanism, an intricate oxygen-enriched peroxide radical $C_6H_5OHOOCH_3$ was produced, which rather actively interacted with molecular oxygen radicals via H-abstraction and resulted in the formation of carbonyl derivative, notably aldehydes and ketones. Finally, the ring-cleavage aromatic compounds may be further fragmented and finally mineralized into CO and CO_2.
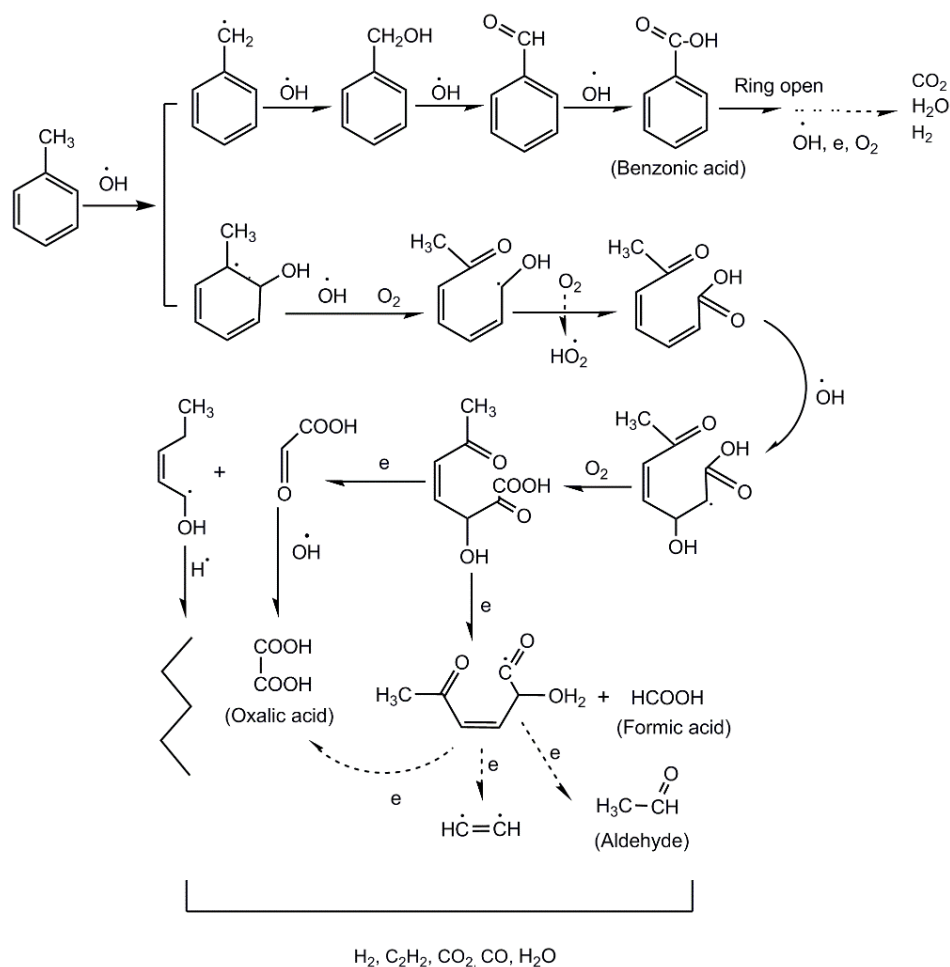
Figure 4.8 Possible pathways of toluene destruction initialled by OH radical attack.

4.5 Conclusions

The influence of carrier gas on the decomposition of toluene, as a model compound of tar was investigated in an AC GAD reactor. The presence of water vapour and CO_2 in the feed gas mixture had a significantly influence on toluene decomposition reactions. A low concentration of CO_2 (3 vol.%) in the gas mixture enhanced the decomposition of toluene and led to a high toluene conversion (59.9%), whereas a slight decrease in toluene conversion was observed by increasing CO_2 concentration ($\geq$ 4 vol.%).

The beneficial role of OH radicals for toluene removal process was clear as higher decomposition efficiency were gained in humid CO_2/N_2 mixtures. The highest toluene conversion (63.1%) and energy efficiency (40.5 g/kWh) were obtained in a nitrogen-based mixtures containing 12 vol. % CO_2, 16.1 g/Nm^3 toluene and S/C_T molar ratio of 1.0 with a

total flow rate of 3.5 L/min and an SEI of 0.25 kWh/m^3. The influence of biomass derived producer gas mixture composition was found to be significant for syngas production from toluene destruction. In the case of toluene destruction without steam or CO_2, the yield of syngas was 16.0%, while it increased to 58.4% when adding 3% CO_2 and 37.3% water into the feed gas mixtures. Based on the analysis of the gaseous products and the absorbed liquid by-products together with the spectrum diagnostics for active species, it is suggested that in humid producer gas, tar decomposition process is initialised predominantly by the reaction with OH radicals while the other pathways play a minor role.

CHAPTER FIVE   HYBRID PLASMA-CATALYTIC STEAM REFORMING OF TOLUENE OVER Ni/γ-Al$_2$O$_3$ CATALYSTS IN A COAXIAL DBD REACTOR

5.1 Introduction

A more effective use of plasma is to integrate plasma process with heterogeneous catalysis, combining the advantages of fast and low temperature reaction by non-thermal plasmas and selective synthesis from catalysis. The combined plasma-catalytic process has great potential to produce a synergy, which can low the activation energy of catalysts and enhance the conversion of reactants, the selectivity and yield of desirable products, and the efficiency of the plasma process [57, 189]. This novel hybrid process has attracted significant interest for gas clean-up, methane activation, CO$_2$ conversion, synthesis of carbon nanomaterials and catalysts [129]. However, very limited work has been focused on the use of non-thermal plasma for the removal of tars from the gasification of biomass or waste. To the best of our knowledge, no work has been dedicated to the investigation of hybrid plasma-catalytic process for the removal of tars from biomass gasification. So far, a range of catalysts have been evaluated in thermal-catalytic reforming of tars at high temperatures, such as calcined rocks, clay minerals, ferrous metal oxides, activated alumina and supported-metal catalysts (e.g. nickel, cobalt and other noble metals) [31]. Nickel catalysts mainly supported on alumina, have been extensively investigated for thermal catalytic tar reforming because of its high initial activity, abundance and low cost. However, catalyst deactivation due to coke deposition remains a major challenge in catalytic reforming of tars. Previous works showed that the coupling of plasma with Ni/Al$_2$O$_3$ catalysts can significantly reduce carbon deposition in plasma-catalytic reforming of biogas compared to thermal catalytic reactions [190]. However, it is not clear how a catalyst (e.g. Ni/Al$_2$O$_3$) present in the plasma process affects the reforming of tars or a tar model compound at low temperatures. Furthermore, previous studies mainly investigated the effect of different operating parameters on the performance of the plasma tar removal process [51, 191], whereas few

analyzed the by-products and intermediates in the plasma reforming of tar to better understand the underlying reaction pathways and mechanisms in the plasma process.

In addition, a detailed understanding of the underlying reaction pathways and mechanisms in the plasma processing of tars is still missing. It is of primary importance to analyze both the gas and condensed liquid products in the plasma-catalytic steam reforming process to get new insights into the reaction pathways, which would provide valuable information for the further optimization of the plasma-catalytic process.

The present study aimed to demonstrate the effectiveness of the hybrid plasma-catalytic process for the removal of a tar model compound and provide an insight of toluene destruction pathways in the plasma-catalytic process. In this work, an IPC system based on a coaxial DBD reactor was developed for the steam reforming of toluene, a typical model tar compound representing a major stable aromatic product in the tars formed in high temperature biomass gasification processes. The configuration of the DBD reactor and the experimental system is shown in Figure 2.4 and the corresponding details are described in Section 2.1.2. The effect of $Ni/\gamma-Al_2O_3$ catalysts with different Ni loadings (5 to 20 wt.%) on the plasma-catalytic removal of toluene was investigated. The plasma steam reforming process without a catalyst was also carried out for comparison. The possible reaction pathways involved in the plasma reactions were proposed and discussed through combined quantitative and qualitative analysis of gas and liquid products. The conversion of toluene is calculated by Equation (2-4); the yield of the products is determined by Equations (2-5) to (2-6); while the energy efficiency of the plasma process is defined as Equation (2-14).

5.2 Plasma-catalytic steam reforming of toluene

Plasma steam reforming of toluene was carried out in the DBD reactor with and without the Ni catalysts, as shown in Figure 5.1. Compared with the plasma reaction without a catalyst, the presence of the 10 wt.% $Ni/\gamma-Al_2O_3$ catalyst in the plasma significantly enhanced the carbon conversion by around 20% (from 39.5 % to 47.1%), whilst the energy efficiency of the process was increased by 18.0 %. Tao et al reported similar findings in a plasma-catalytic steam reforming of high content toluene (~200 g/Nm^3) over a 5 wt.%

Ni/SiO$_2$ catalyst in a DC plasma reactor [52]. However, extra thermal heating (at 773 K) was used to heat the plasma-catalytic process in their experiments. Therefore, it was extremely difficult to identify whether the effect of the Ni/SiO$_2$ catalyst on the enhanced toluene conversion was driven by the plasma or thermal heating or both [52].
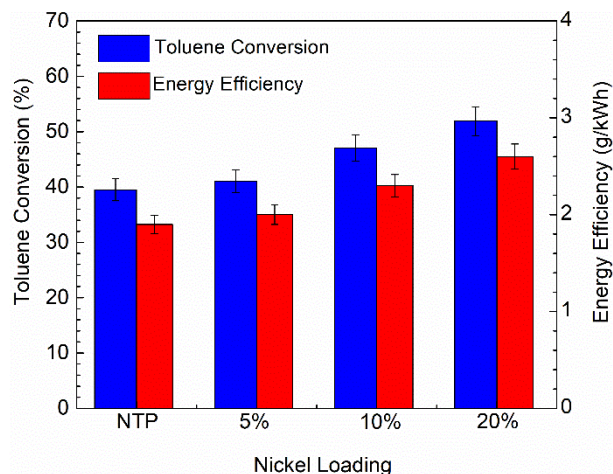
Figure 5.1 Toluene conversion and energy efficiency of the plasma process with and without catalysts (toluene concentrate: 17.7 g/Nm^3, discharge power: 35 W, S/C ratio: 2.5, catalyst: 10 wt.% Ni/γ-Al$_2$O$_3$).

In this study, the Ni catalysts were placed along the bottom of the discharge region in the DBD reactor, while the plasma-catalytic steam reforming reaction was carried out at low temperatures (<200 °C) without any external heating. Therefore, heating effect from the plasma on the catalyst activation and plasma-catalytic reaction was negligible. As shown in Figure 5.2, this partial packing method could still generate a strong filamentary discharge in the DBD reactor due to the presence of large void fraction in the discharge gap, resulted in strong physical and chemical interactions between the discharge and Ni catalysts [145]. Compared to the plasma reaction without packing, the shape of the Lissajous figure was almost same when the catalysts were partially packed into the discharge region (Figure 5.3). Moreover, when a catalyst is placed in the discharge, polarisation of the catalyst leads to the charge accumulation on the catalyst surface, increasing the local or average electrical field and therefore the number of energetic electrons and reactive species, characterized by the formation of intensified microdischarges around the contact points between the catalyst

pellets and those between the catalyst pellet and quartz wall [130, 192]. Previous studies demonstrated that placing a 10 wt.% Ni/γ-Al$_2$O$_3$ along the bottom of a DBD reactor enhanced the intensity of current pulses in the plasma-catalytic dry reforming of CH$_4$ [145], while the mean electric field and mean electron energy of the DBD were enhanced by 9-11% when BaTiO$_3$ and TiO$_2$ photocatalysts were partially packed in the DBD reactor in the plasma-catalytic conversion of CO$_2$ [57]. These physical effects have been shown to enhance the conversion of reactants in plasma-catalytic chemical reactions. Similar phenomenon was also observed in Figure 5.1. Clearly, in this study, the enhanced toluene conversion and energy efficiency in the plasma-catalytic steam reforming of toluene can be partly attributed to the physical effects induced by the presence of the Ni catalyst pellets in the plasma.

(a)

(b)
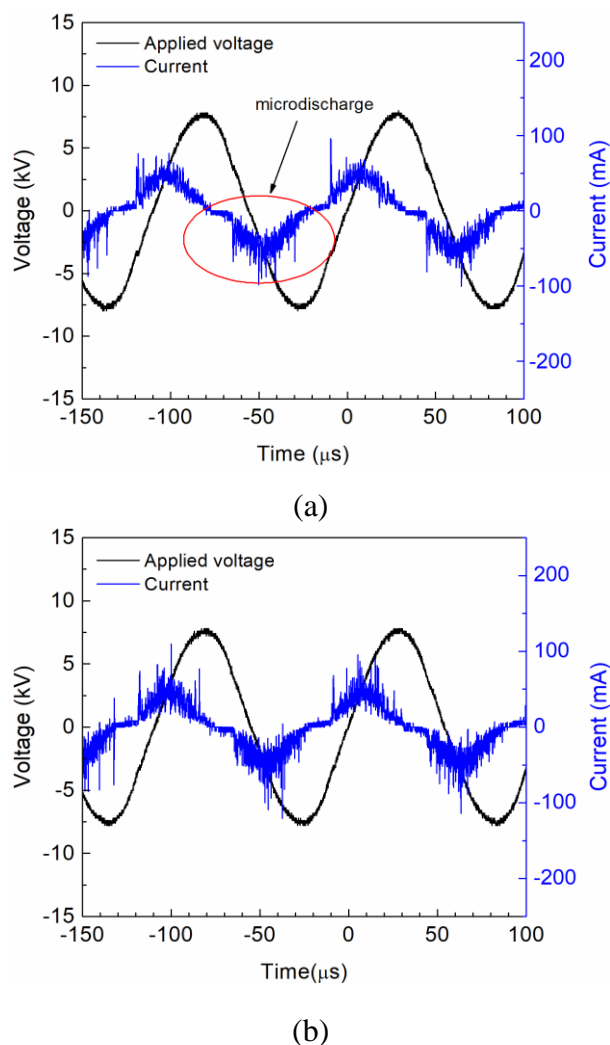
Figure 5.2 Electrical signals of the DBD (a) without packing; (b) with 10 wt% Ni/γ-Al$_2$O$_3$ catalyst.
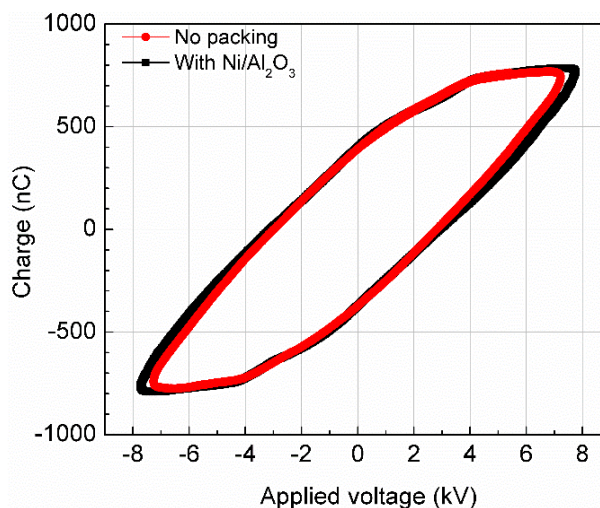
Figure 5.3 Lissajous figures of DBD plasma with and without Ni/γ-Al$_2$O$_3$ catalyst at a constant discharge power of 35 W.

In addition, increasing the Ni loading from 5% to 20% increased the conversion of toluene and energy efficiency of the plasma-catalytic process, as shown in Figure 5.1. For example, the combination of the DBD with the 20 wt.% Ni/γ-Al$_2$O$_3$ catalyst showed the highest toluene conversion of ~51.9 % and energy efficiency of 2.6 g/kWh. In the plasma-catalytic reforming reaction at low temperatures, increasing the Ni loading over γ-Al$_2$O$_3$ could effectively enhance the catalyst activity owing to the formation of more active Ni sites on the catalyst surface. Aziznia et al. also showed that higher conversions of CO$_2$ and CH$_4$ were obtained in the low temperature plasma-catalytic dry reforming of CH$_4$ when a 20 wt.% Ni/γ-Al$_2$O$_3$ catalyst was placed in a corona discharge compared with Ni/γ-Al$_2$O$_3$ catalysts with a lower Ni loading (5 wt.% and 10 wt.%) [193]. Similar phenomenon was also observed in thermal catalytic chemical reactions. Wang reported that the removal efficiency of tar and hydrogen production increased with increasing Ni loading from 5 wt.% to 20 wt.% [194]. Aziz et al investigated the effect of Ni loading (1-10 wt. %) on CO$_2$ methanation over Ni/mesoporous silica nanoparticles (MSN) catalysts at different reaction temperatures [195]. They found that increasing the Ni loading enhanced the catalytic activity for CO$_2$ methanation at low temperatures (<623 K). However, the 10 wt. % Ni/MSN catalyst showed a similar activity as the 5 wt. % Ni/MSN catalyst in CO$_2$ methanation at high temperatures (>673 K). Similarly, Liu et at reported that there was an optimum Ni loading of 10 wt.% of

activated carbon (AC) supported Ni catalysts in thermal catalytic steam reforming of toluene at 200 °C. They found that further increasing the Ni loading to 15 wt.% increased the nickel particle size and lowered the nickel particle dispersion on the catalyst surface, resulted in the aggregation of Ni particles and increased carbon deposition, and consequently decreased the conversion of toluene. Compared to relatively high temperature thermal catalytic reactions, placing supported metal catalysts in low temperature plasma process can effectively reduce the metal particle size and enhance the metal dispersion on the catalyst surface due to low temperature effect [44]. In this experiment, low temperature plasma reaction is believed to avoid the aggregation of Ni particles on the catalyst surface but increase the catalytic activity for toluene conversion when increasing the Ni loading from 5 wt. % to 20 wt. %. In addition, the presence of conductive Ni species on the catalyst also contribute to the expansion of the plasma over the catalyst surface, which may be favourable to the expansion of discharge volume and intensity in the DBD-catalytic process [196].

These results clearly demonstrated that the catalytic effect (e.g. catalyst activity) also plays an important role in enhancing the conversion of toluene and efficiency of the plasma-catalytic process besides the physical effects. In the hybrid plasma-catalytic process, the adsorption of reactants on the catalyst surface could be enhanced [130], which would increase the retention time of toluene and its intermediates in the plasma and therefore improve the collision probability between these pollutants and chemically reactive species, leading to a higher toluene conversion in the plasma-catalytic process.

5.3 Gaseous products

H_2, CO_2 and CH_4 were found as the main gas products in the plasma steam reforming of toluene with and without the Ni catalyst. A small amount of hydrocarbons (C_2H_2, C_2H_4, C_2H_6, C_3H_8 and C_4H_{10}) were also detected. Clearly, the presence of the Ni catalysts in the DBD reactor enhanced the production of H_2 and CO_2, as shown in Figure 5.4. Increasing the Ni loading from 5 to 20 wt.% steadily increased the yield of H_2 and CO_2 by 15% and 16%, respectively. It is worth to note that no CO was detected in the gas products. The occurrence of water gas shift reaction (R5-1) might be the major reason to inhibit the generation of CO

in the steam reforming of toluene in the DBD. Moreover, the presence of reactive oxide species (e.g. OH, O radicals) through the dissociation of water by energetic electrons (R5-2 and R5-3) and metastable argon might be able to further oxidize CO (R5-4 and R5-5), toluene and its intermediates into CO_2. This plasma reaction might be considered as an attractive hydrogen production process without CO formation suitable for fuel cell applications.

$$H_2O + CO \rightarrow CO_2 + H_2 \tag{R5-1}$$

$$H_2O + e \rightarrow H^- + OH \tag{R5-2}$$

$$H_2O + e \rightarrow 2H + O^- \tag{R5-3}$$

$$OH + CO \rightarrow CO_2 + H \tag{R5-4}$$

$$O + CO \rightarrow CO_2 \tag{R5-5}$$

As shown in Figure 5.4, the yield of CH_4 was nearly constant (~10%) when changing the Ni loading, whereas the yield of C_3-C_4 hydrocarbons (less than 1.6 %) increased by increasing the Ni content. Compared to the plasma reaction with no catalyst, placing the 5 wt. % Ni/γ-Al$_2$O$_3$ catalyst in the DBD reactor almost did not change the production of C_2H_2 and C_2H_6. However, increasing Ni content from 5 to 20 wt. % enhanced the yield of C_2H_2 and C_2H_6. The highest C_2H_2 yield of 5.2% was achieved when the 20 wt.% Ni/γ-Al$_2$O$_3$ catalyst was placed in the plasma steam reforming of toluene.
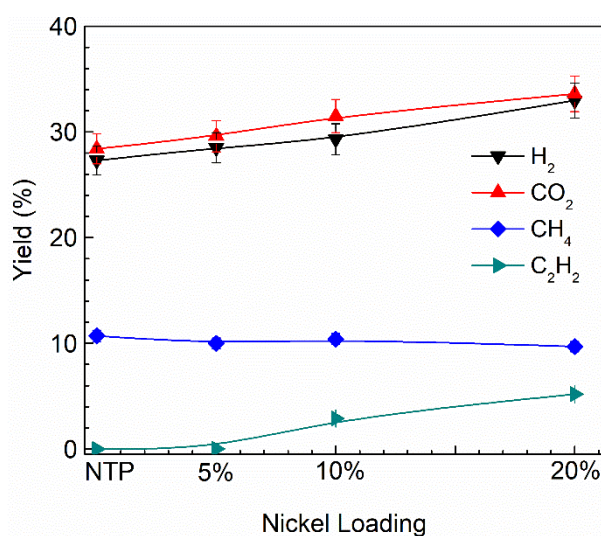
(a)
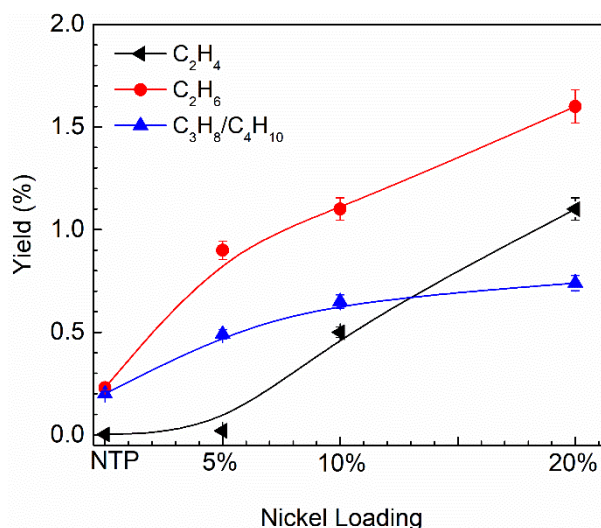
(b)

Figure 5.4. The effect of Ni loading on the yield of gaseous products (toluene concentrate: 17.7 g/Nm^3, discharge power: 35 W, S/C: 2.5).

5.4 Formation of condensed by-products

Figure 5.5 shows the GC-MS chromatogram of condensed by-products collected in the plasma steam reforming of toluene with and without the catalyst. In the plasma reaction without a catalyst, 11 types of organic by-products were detected, including major compounds such as benzene, phenol and (butoxymethyl)-benzene. Additionally, aliphatic compounds such as methyl ester, diol, octadecadienoic acid and the linear compounds 5, 7-Dodecadiyn-1, 12-diol were also detected, which could be generated from the cleavage of toluene ring, and the recombination and hydrogenation of the resulting fragments of intermediates. The presence of the 5 wt.% Ni/γ-Al$_2$O$_3$ catalyst in the plasma process significantly inhibited the formation of organic by-products. As shown in Figure 5.5(b), only six types of condensed compounds were detected, among which phenol, 2,4-Hexadien-1-ol and (butoxymethyl)-benzene were identified as the major organic by-products. It is worth noting that the amount of phenol and (butoxymethyl)-benzene formed in the plasma-catalytic reforming reaction was several orders of magnitude lower than those generated in the plasma reaction without the Ni catalyst. These results clearly demonstrated that the coupling of the DBD and the Ni/γ-Al$_2$O$_3$ catalyst promoted the conversion of toluene into gas products (e.g.

H$_2$), whilst significantly minimized the formation of undesirable organic by-products (Figure 3.5).
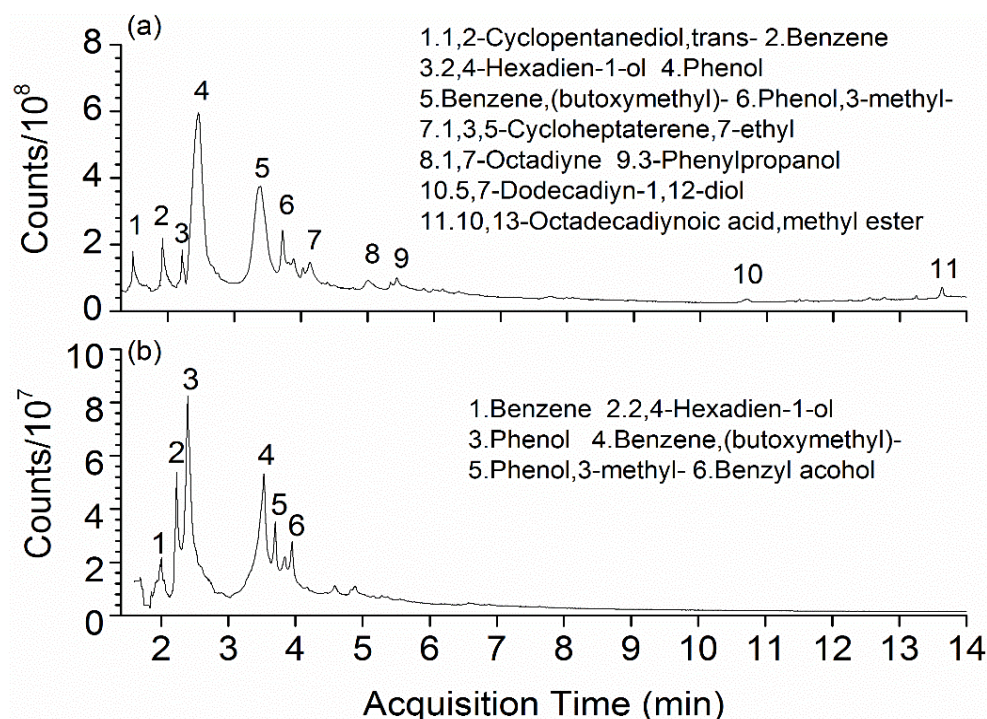
Figure 5.5 GC-MS chromatogram of condensed by-products collected in the plasma steam reforming of toluene (a) without a catalyst, and (b) with the 5 wt. % Ni/γ-Al$_2$O$_3$ catalyst (toluene concentration: 17.7 g/Nm^3, discharge power: 35 W, S/C: 2.5, catalyst: 0.5 g).

5.5 Possible reaction mechanisms

The reaction mechanism in the destruction of toluene (50 -500 ppm) as a model VOC in air or nitrogen plasmas without a catalyst has been investigated and proposed in previous studies [162, 197]. However, very limited work has focused on the understanding of the reaction routes in the plasma reforming of toluene as a model tar compound, especially in the presence of a catalyst. Compared to the removal of toluene as a model VOC, the reaction pathways present in the plasma steam reforming of toluene could be different due to the presence of high content toluene and steam. To get new insights into the possible reaction routes in this plasma process, the analysis of both gaseous and condensed liquid by-products were carried out in the plasma reaction with and without the Ni catalyst. It is well known that only gas-phase reactions are involved in the plasma reforming of toluene without the Ni

catalyst. However, placing the Ni catalyst in the DBD makes the reaction more complicated as plasma driven surface reactions occur besides the gas-phase reactions.

The destruction of toluene as a model tar compound in the argon DBD can be initiated through two major reaction routes: (i) direct electron impact dissociation of toluene and (ii) reaction with chemically reactive species including OH and Ar metastable species. The ionization of Ar requires a much higher electron energy (15.76 eV) compared to the excitation of Ar to its metastable states Ar^* (e.g. 11.55 eV). Therefore, in the Ar DBD, Ar is more likely to be excited to its metstable states rather than being ionized [198]. Previous studies have shown that metastable Ar species play an important role in initiating chemical reactions [199]. The presence of steam in the plasma could generate OH radicals from the dissociation of water by electrons and Ar*. The generated OH radicals can oxidize toluene and its intermediates, opening a new reaction route for the conversion of toluene, resulting in the enhanced conversion and energy efficiency of the plasma process [171].

Different bond energies of chemical bonds in toluene determine the reaction pathways involved in the plasma conversion of toluene. The dissociation energy of C-H bond in methyl is 3.7 eV, which is smaller than that of C-H bond in aromatic ring (4.3 eV), C-C bond between aromatic ring and methyl group (4.4 eV), C-C bond (5.0-5.3 eV) and C=C bond in aromatic ring (5.5 eV). Therefore, the primary reaction pathway of toluene decomposition could be the H-abstraction from methyl group by energetic electrons or reactive species such as Ar* and OH [160]. The H-abstraction from the methyl group forms a benzyl radical, which could further react with OH to generate benzyl alcohol. The formed benzyl alcohol can be converted to benzaldehyde, followed by further reactions with electrons and reactive species to form a phenyl radical [163]. In addition, the C-C bond between methyl and aromatic ring and C-H bond in the aromatic ring can be broken through the reactions with energetic electrons and metastable Ar species, generating phenyl, methyl, and toluene radicals [162]. As shown in Figure 5.6 (a), the recombination of phenyl with H and OH radicals could produce benzene and phenol, respectively, while adding OH to the aromatic ring of toluene radicals produces 3-methyl phenol, as identified by GC-MS. Moreover, ring opening and cracking of phenol via electron impact dissociation forms butyl alcohol, which

then reacts with benzyl to generate benzene, (butoxymethyl). These aromatic intermediates can be further ruptured by electrons and Ar^* species to form ring-opening by-products and then oxidized by OH to end-products such as CO_2 and H_2O.

Toluene can also be decomposed by the cleavage of benzene ring through collisions with reactive species, e.g. OH radicals, producing hydroxycyclohexadienyl type peroxy radicals (Figure 5.6 (b)), which has been confirmed in the previous modelling and experimental studies [152, 163, 169]. This reactive compound is unstable and can form a peroxide bridge radical, a precursor for the formation carbonyl and the oxygen-enriched chemical [169]. The carbonyl reaction route opens the benzene ring of toluene via a stepwise oxidation by OH species to form a relatively stable epoxide, which can be further decomposed by electrons or active species, forming small molecules, such as oxalic acid and acetic acid.

The presence of the Ni catalysts in the plasma steam reforming of toluene enhanced the production of most gas products, whilst significantly reduced the formation of condensed organic by-products. These findings suggest that the combination of the plasma with the Ni catalysts shifted the primary reaction pathways of toluene destruction from the dehydrogenation or oxygenation of methyl group to direct cleavage of toluene ring, which can be evidenced by the enhanced yield of hydrogen and C_2H_2. Previous experimental and theoretical studies showed that acetylene was most likely formed by rupturing the toluene ring through the collisions with electrons and Ar^* species [164]. Recently, Zhu et al. also reported that high energetic electrons could breakdown toluene ring, forming acetylene and methyl-cyclobutadiene in the plasma decomposition of toluene as a tar surrogate using a rotating gliding arc discharge [53]. In this work, the detected C_5H_6 might be 1, 3-pentadiene, which sequentially reacted with methyl and OH radicals to form linear hydrocarbons such as 2, 4-hexadien-1-ol. In the hybrid plasma-catalytic reforming of toluene, plasma-assisted surface reactions also contributed to the enhanced reaction performance. In our experiment, the Ni catalyst pellets were placed along the button of the quartz tube in the discharge region and can directly interact with the plasma. Partial packing of the Ni catalyst pellets in the DBD still formed predominant micro-discharges across the electrode gap and induced strong

interactions between the plasma and Ni catalyst, which is favourable for the plasma induced surface reactions on the surface of the Ni catalyst [145]. In this plasma-catalysis configuration, both toluene and its intermediates formed in the gas phase reactions can be adsorbed on the surface of the Ni catalyst. Short-lived reactive species (e.g. O, OH) initially generated close to or on the catalyst surface can also be involved in the surface reactions. The excited species generated in the plasma might accelerate the adsorption of toluene and intermediates onto the catalyst surface [200]. The residence time of toluene and intermediates in the plasma reaction region could be prolonged due to the catalyst effect. The enhanced adsorption increases the collisions of toluene with energetic species, consequently accelerates the plasma reactions, both in the gas phase and on the catalyst surface. The adsorbed species could also react with oxidative radicals, forming intermediates such as benzoic acid, before finally oxidized to produce end-products such as CO_2 and H_2O.
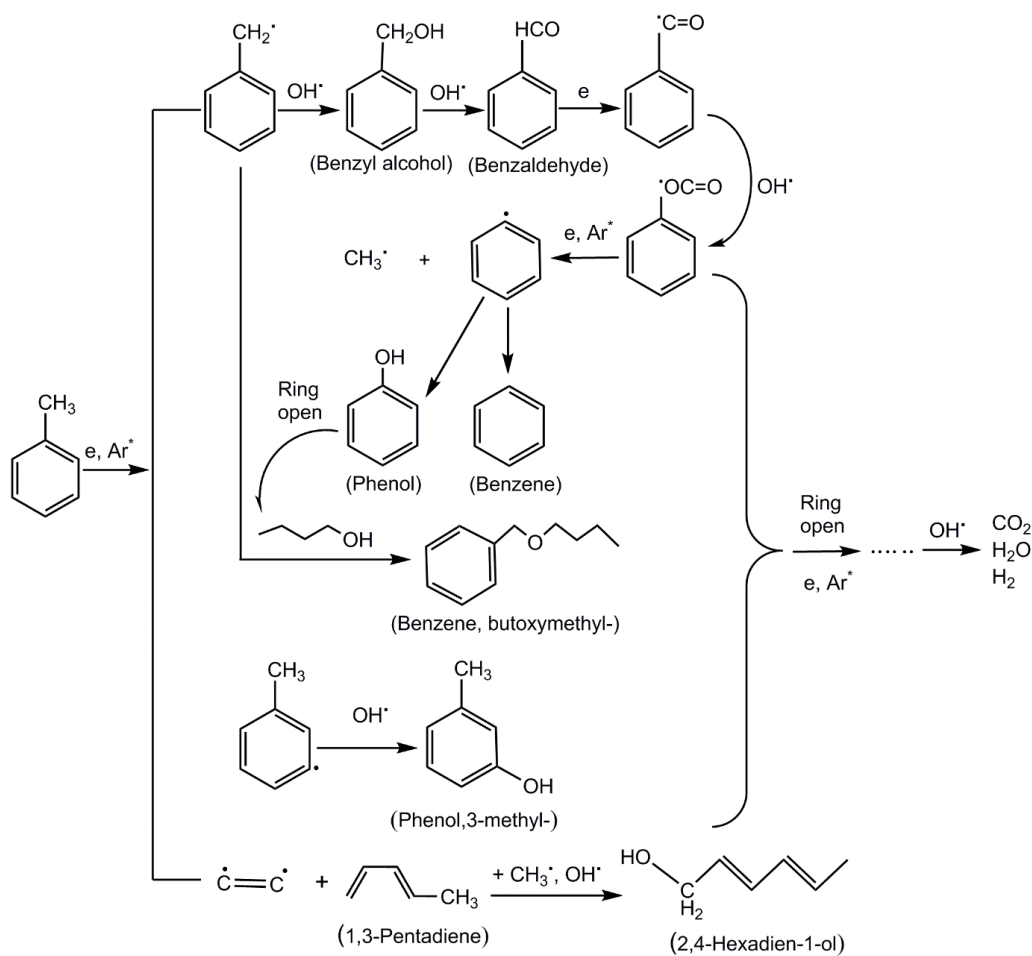
(a)
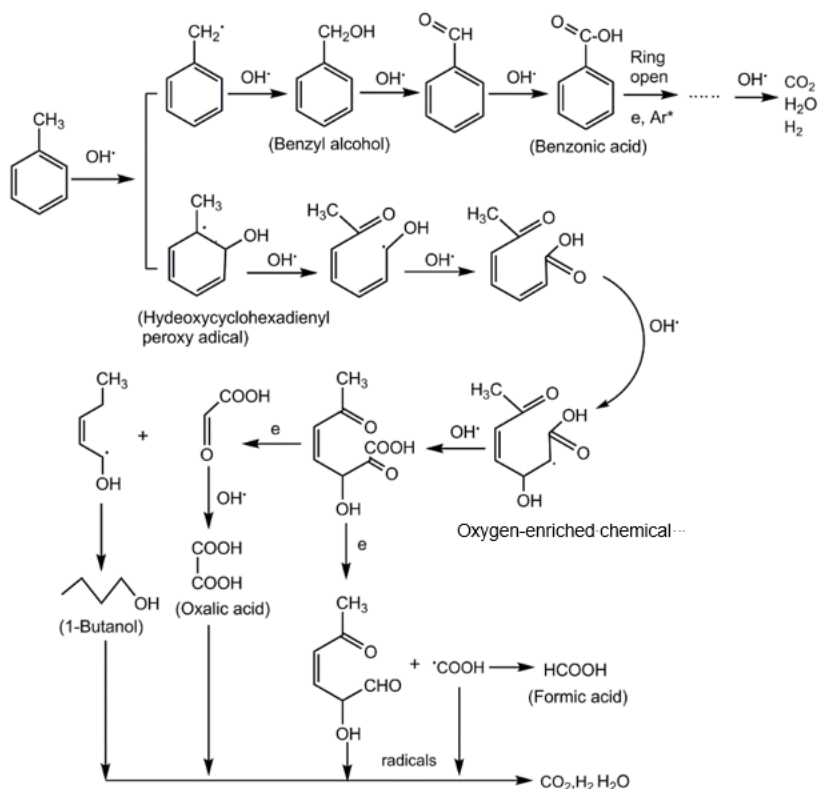
(b)

Figure 5.6 Possible reaction pathways for toluene destruction initiated by (a) energetic electrons and Ar*, and (b) OH radicals.

5.6 Conclusions

In this chapter, the effect of Ni/γ-Al$_2$O$_3$ catalysts on the plasma-catalytic steam reforming of toluene as a model tar compound was carried out in a DBD plasma reactor. The possible reaction mechanisms and pathways involved in the plasma-catalysis reforming of toluene were proposed and discussed. Compared to the plasma process without catalyst, the coupling of plasma with the Ni catalysts enhanced the conversion of toluene and H$_2$ yield, while significantly suppressed the formation of undesirable by-products. Increasing the Ni content from 5 wt.% to 20 wt.% considerably enhanced the performance of the hybrid process, which can be attributed to the enhanced catalytic activity due to enhanced dispersion of Ni species on the catalyst surface. These findings suggest that the combination of the plasma with the Ni catalysts shifted the primary reaction pathways of toluene destruction from the dehydrogenation or oxygenation of methyl group to direct cleavage of toluene ring, which can be evidenced by the enhanced yield of hydrogen and C$_2$H$_2$.

CHAPTER SIX   STEAM REFORMING OF TOLUENE AND NAPHTHALENE IN A GAD REACTOR

6.1 Introduction

In the previous chapters, only individual model biomass tar compound (toluene) was used to investigate the effectiveness of the non-thermal plasma process for reforming of biomass tar into value-added fuels and chemicals. This is similar with most of the previous studies related to the thermal-catalytic process and plasma process for the conversion of the biomass tar, in which toluene, benzene, phenol or naphthalene was selected as the model tar compound [10, 49, 144, 201, 202]. In the practical conditions, tar is a mixture of organic compounds with different structures and molecular weights, which will affect the performance of the conversion of biomass tar (e.g. tar conversion, product distribution, carbon deposition on the catalysts and so on). To the best our knowledge, the understanding on the behaviour of the tar mixture in the plasma steam reforming process is very limited, although the tar mixture (e.g. phenol, toluene, methyl naphthalene, indene, anisole and furfural) was used in the thermal catalytic steam reforming process [203].

One drawback of the plasma-only process for steam reforming of tar is the formation of undesired by-products. This problem can be alleviated by combining the plasma process with the heterogeneous catalysts, which has been demonstrated by the investigation in Chapter 5. We found that the presence of the Ni/γ-Al$_2$O$_3$ catalyst significantly reduced the composition and the amount of by-products from the steam reforming of toluene as a biomass compound in a coaxial DBD reactor [204]. However, the energy efficiency of the plasma-process using the DBD reactor was typically low due to the small treatment capacity. Far less has been done to significantly enhance the energy efficiency of the plasma-catalytic steam reforming of biomass tar.

In this work, an AC gliding arc discharge reactor has been employed for syngas production from steam reforming of tar mixture. The configuration of the GAD reactor and the experimental system is shown in Figure 2.3 and the corresponding details are described

in Section 2.1.1. The mixture of toluene and naphthalene were chosen as the model biomass tar mixture because these two compounds were used as typical light monoaromatic and light polyaromatic model tar compound, respectively [205]. A tube furnace and an electrical heating-jacket were coupled to produce tar mixture and water vapour. Naphthalene was dissolved in toluene. The tar mixture solution and deionized water were fed into the evaporator preheated in the tube furnace at 300 °C through the high-resolution syringe pumps (KDS Legato, 100). The tar and water vapour were then fed into the reactor by the carrier gas after they reached a steady state. Pure N_2 was used as the carrier gas in the steam reforming process.

In the plasma-only process, the S/C molar ratio was varied from 0 to 3.0, the initial naphthalene concentration changed from 0.48 to 1.83 g/Nm^3 and the discharge power increased from 54.2 to 72.9 W with a constant total flow rate of 3.5 L/min and a constant initial toluene concentration of 16.0 g/Nm^3 during the experiment. The effects of different operating parameters (e.g. the S/C molar ratio, the initial naphthalene concentration and the discharge power) on the performance of plasma steam reforming of tar mixture were assessed in terms of the conversion of toluene and naphthalene, the energy efficiency for the tar conversion and the yield of gaseous products. Optical emission spectroscopy (OES) was used to identify the active species generated in the plasma process. The possible reaction mechanisms and pathways involved in the plasma steam reforming process have been discussed by combined means of OES diagnostics and the analysis of gas and liquid products.

In the plasma-catalytic process for steam reforming of toluene and naphthalene mixture, the effect of the 15Ni, 7.5Ni7.5Co and 15Co catalysts on the performance on the plasma steam reforming process was investigated. Details of these catalysts including the preparation procedure and characterisation techniques are described in Chapter 2. The conversion of biomass tar is calculated by Equation (2-8); the yield of the products is determined by Equations (2-11) to (2-13); while the energy efficiency of the plasma process is defined as Equation (2-14).

6.2 Thermodynamic equilibrium calculation for steam reforming of toluene and naphthalene

Thermodynamic equilibrium calculation of tar steam reforming progress has been carried out by the method based on the minimization of Gibbs free energy in a closed system. In this study, it is supposed that 1 mole of tar is injected into the closed system and the molar ratio of toluene and naphthalene is 25. To evaluate the effect of H_2O on the destruction process, water vapour is also added into the system at the S/C molar ratio of 1-2. The assumed products include H_2, CO, CO_2 and CH_4. The C_2-C_4 hydrocarbons is ignored as their total equilibrium concentration of is very low (<0.1%). Figure 6.1 shows the effect of temperature on the gaseous products of thermodynamic equilibrium conversions of naphthalene and toluene at 1 atm.
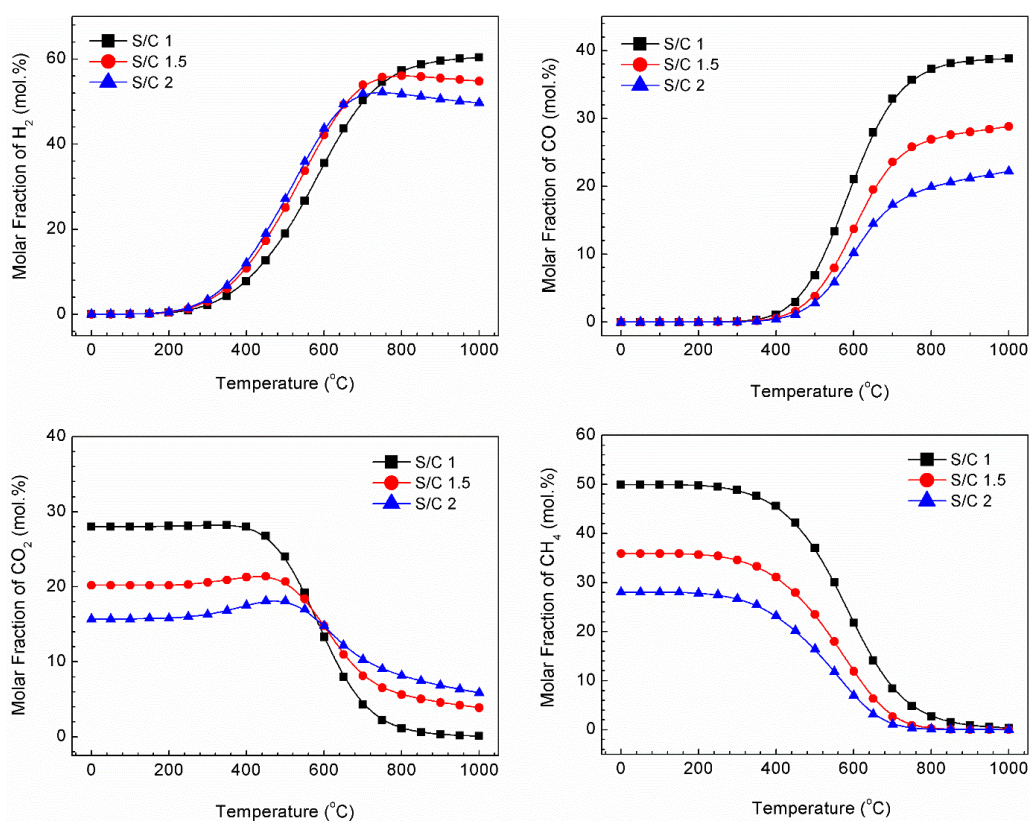
Figure 6.1 Thermodynamic equilibrium calculation for steam reforming of naphthalene and toluene as a function of operating temperature at 1 atm (C_7H_8 /$C_{10}H_8$ molar ratio: 25).

It is clear that the molar fraction of syngas is very low (<1%) when the operating temperature is below 400 °C. Reasonable formation of syngas (~ 50 %) can only be obtained at extraordinarily high temperatures (> 600 °C), resulting in high energy cost for thermal conversion of tar into syngas. The distribution of gaseous products also depend on the S/C molar ratio. It can be noted that the increasing the S/C molar ratio significantly decreases the molar fraction of syngas, but enhances the formation of CO_2 when the operating temperature is higher than 600 °C.

6.3 Plasma steam reforming toluene and naphthalene without catalysts

6.3.1 Effect of S/C molar ratio

The effect of humidity is of great interest as the producer gas usually contains large amounts of water (~15 vol. %) in practical conditions. To characterise and optimise the role of water in the decomposition process of the tar model compound, the conversion of naphthalene/toluene was determined at different S/C molar ratios (from 0 to 3) in nitrogen gas flow at a constant total flow rate of 3.5 L/min and a discharge power of 60 W. As shown in Figure 6.2 (a), the naphthalene conversion increases initially with the increase of the S/C molar ratio reaching a maximum value of 63.2% at an S/C molar ratio of 1, and then decreases at higher S/C molar ratio. Meanwhile, the highest toluene conversion 79.2% was achieved at an optimal S/C molar ratio of 1.5. This is probably due to the formation of the active species OH, which could oxidise the tar molecules and intermediates with high interaction rate at low temperature, resulting in a boost of the conversion compared to the plasma progress without steam. In the GAD discharge, the production of OH radical is mainly due to the dissociation of water molecules by the electronic dissociative excitations and collisions with excited states of nitrogen, as described by reactions R6-1 and R6-3. The destruction of the naphthalene/toluene molecule by the OH radicals can be explained by the following scheme, in which both generated H and OH radicals participate to respectively produce intermediate H and OH adducts of naphthalene/toluene, such as styrene, xylene, and benzene.

$$H_2O + e \rightarrow H + OH + e \tag{R6-1}$$

$$N_2 + e \rightarrow N_2^* + e \tag{R6-2}$$

$$H_2O + N_2^* \rightarrow N_2 + H + OH \tag{R6-3}$$

$$C_{10}H_8/C_7H_8 + OH \rightarrow \text{Intermediate byproducts} + H_2O \tag{R6-4}$$

$$C_7H_8 + H \rightarrow C_6H_6 + CH_3 \tag{R6-5}$$

$$C_{10}H_8 + H \rightarrow \text{products} \tag{R6-6}$$

$$H_2O + e \rightarrow OH + H^- \tag{R6-7}$$
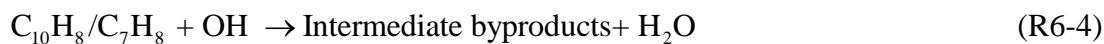
where N_2^* represents the nitrogen excited species, it can be either nitrogen metastable states $N_2\left(A^3 \Sigma_u^+\right)$ or the excited state $N_2\left(a^1\Pi_g\right)$ and $N_2\left(B^3\Pi_g\right)$, the corresponded excitation threshold energy are 6.17 eV, 8.4 eV and 7.35 eV, respectively. However, the humidity exhibited an adverse effect on the reforming reaction in the present reactor, despite of the importance of water molecules to generate the reactive species OH, which contributes to the enhancement of conversion efficiency due to the presence of stepwise oxidation reaction pathways. Lu et al. reported that increasing the concentration of H_2O up to 300 mg/m^3 in the feed gas stream could improve the removal efficiency of toluene in a rotating gliding discharge reactor [170]. Nunnally et al. found that there existed an optimal moisture content of 30% to achieve the highest conversion of naphthalene and toluene in the conversion of tar molecules using a RGA reactor [174]. This phenomenon could be described by the electronegative property of water molecules, which can trap energetic electrons via electron impact dissociated attachment as expressed by the reaction R6-7. Literatures revealed that the probability of electron attachment reaction is proportional to the gas humidity when the applied voltage is a constant [180]. Therefore, increasing the S/C molar ratio could increase the electrons decay in the discharge zone with a subsequent less availability to generate the metastable species, i.e. OH/H radical and excited states of nitrogen and then supresses the destruction of naphthalene/toluene. The energy efficiency of the plasma naphthalene/toluene reforming process showed the similar evolution trend and the maximum energy efficiency for naphthalene and toluene was about 2.2 g/kWh for naphthalene and 48.1 g/kWh,

respectively, at the S/C molar ratio of 1-1.5. These results indicated that the present reactor has the ability to destroy polyaromatic hydrocarbons with high treatment capacity and high energy efficiency.

Figure 6-2 (c) shows the yield of primary gaseous products in nitrogen discharge as a function of the S/C molar ratio. The highest yield of H_2 and CO was obtained at an S/C molar ratio of 1.5. The yield of H_2 and CO gradually reduced from 31.0% to 20.7% and from 27.4% to 23.1% by increasing the S/C molar ratio to 3. CO_2 was generated at a relative high S/C molar ratio of 1.5 and the yield increased up to 7.7% when the S/C molar ratio was increased to 3. Hence, increasing the humidity of the working gas in the GAD reactor leads not only to an increase in the amount of decomposed naphthalene/toluene, but also to a more complete oxidation of intermediate products to stable CO_x oxides (x =1, 2). The numerical plasma modelling work has demonstrated that reaction R6-8 is the major factor causing an increase in CO_2 yield in the plasma naphthalene/toluene conversion process [168]. In addition, CO_2 could also be formed through the Boudouard reaction (R6-9) and the water gas shift reaction (R6-10) [206]. Interestingly, a high C_2H_2 yield of 12.8% was achieved in nitrogen discharge, which was higher than that in humid environment. The appreciable yield of C_2H_2 generated in the plasma-chemical process reveals that the conversion of naphthalene/toluene at dry N_2 GAD reactor is accompanied by reactions with benzene ring cleavage, which can be represented by the reaction R6-11. The lower C_2H_2 yield in humidity condition could be ascribed to the formation of substantial OH radicals, which participate in the destruction progress through direct and indirect oxidation of naphthalene/toluene, thus reducing the chance of benzene ring cleavage by energetic electrons and excited nitrogen species to release acetylene. Similar evolution behaviour of the gas product in the plasma-assisted tar reforming process has also been reported in previous studies. Trushikn et al reported that an increase in the humidity of the gas streams led to a noticeable increase in the yield of CO and a suppression in the yield of C_2H_2 [207].

$$CO + OH \rightarrow CO_2 + H \qquad\qquad (R6-8)$$

$$2CO \rightarrow CO_2 + C \qquad\qquad (R6-9)$$

$$CO + H_2O \rightarrow CO_2 + H_2 \tag{R6-10}$$

$$C_{10}H_8/C_7H_8 + N_2^*/e \rightarrow C_8H_6/C_5H_6 + C_2H_2 + N_2 \tag{R6-11}$$
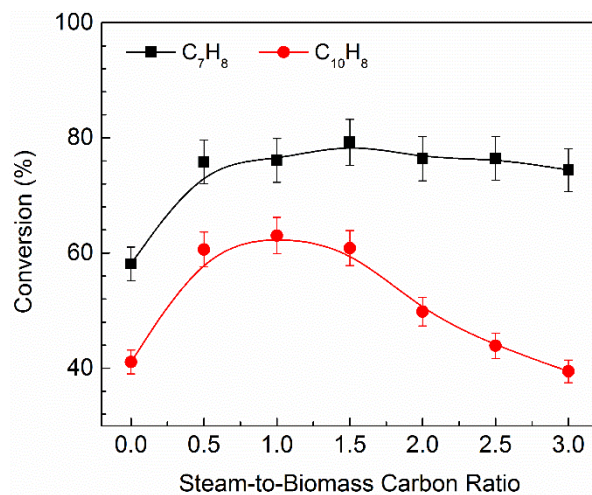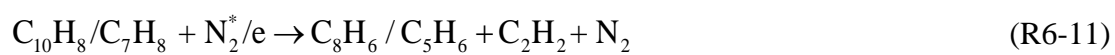
(a)
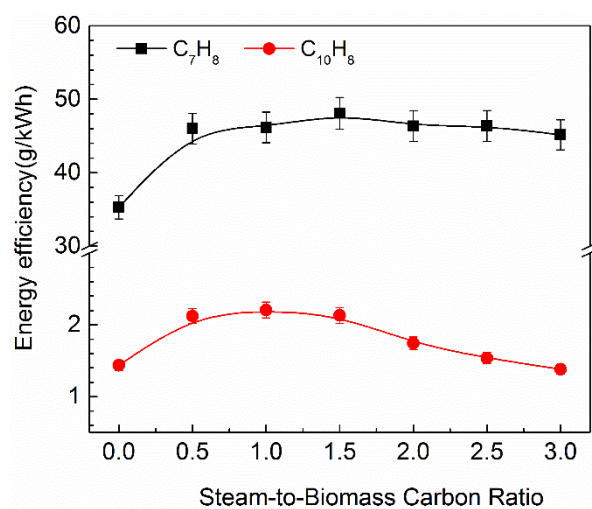
(b)
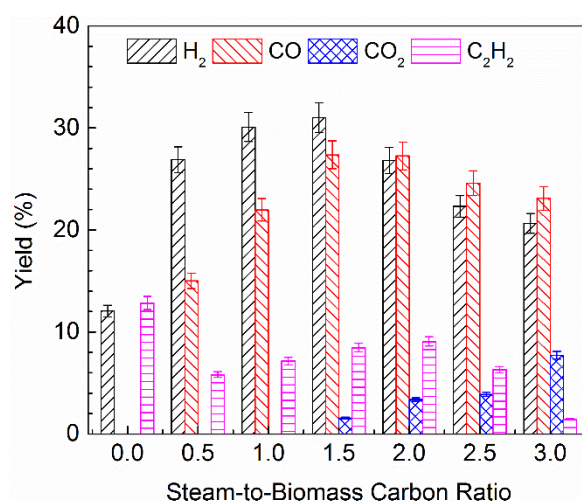
(c)

Figure 6.2 Effect of S/C molar ratio on (a) conversion efficiency of tar; (b) energy efficiency of plasma decomposition process and (c) yields of primary gaseous products (C_7H_8 Content: 16.0 g/Nm^3; $C_{10}H_8$ concentration: 1.1 g/Nm^3; Discharge power: 60 W; Q: 3.5 L/min).

6.3.2 Effect of initial naphthalene concentration

Figure 6.3 shows the influence of the initial naphthalene concentration on the performance of the plasma steam reforming of naphthalene/toluene in humid N_2 at a constant discharge power of 60 W. The conversion of naphthalene significantly decreased from 72.9% to 48.9%, when increasing the initial naphthalene concentration from 0.48-1.83 g/Nm^3, while the toluene conversion slightly declined from 79.8% to 68.5%. The mean energy and density of the electrons are almost constant regardless the inlet concentration changes at the same discharge power, and thus the energy dissipated to destroy per unit tar molecule would be decreased by increasing the initial naphthalene concentration. Consequently, a higher inlet concentrations led to a lower conversion. This result is different to that obtained in the naphthalene removal using surface dielectric barrier discharge reactor in dry N_2 conditions, where the decomposition efficiency of naphthalene was nearly independent of the initial concentration [165]. It can be seen from Figure 6.3 (b) that the energy efficiency of plasma naphthalene reforming linearly increased by a factor of 3 with the increase of the initial naphthalene concentration to 1.83 g/Nm^3, whereas the energy efficiency of toluene destruction gradually drops from 52.2 to 41.1 g/kWh. The converted amount (g/Nm^3) of

naphthalene was increased by increasing its initial concentration although its conversion (%) is reduced, which is the main reason for the increase in the energy efficiency of plasma reforming of naphthalene; whereas the amount of the converted toluene dropped in the destruction process due to the declined toluene conversion at a constant toluene initial concentration, which reduces the energy efficiency of toluene conversion.

For the gaseous products, the yield of H_2 initially increased slightly with rising the initial naphthalene concentration, and peaked (32.6%) at an initial naphthalene concentration of 1.08 g/Nm^3, beyond which the H_2 yield decreased gradually. Similarly, the highest yield of CO (28.8%) was obtained at an initial naphthalene concentration of 1.4 g/Nm^3. C_2H_2 was identified as a major hydrocarbon gas product with a maximum yield of 10.2%, while trace amount of other hydrocarbons (e.g. C_2H_4, C_2H_6 and C_3H_8) were detected with a total yield below 1%.
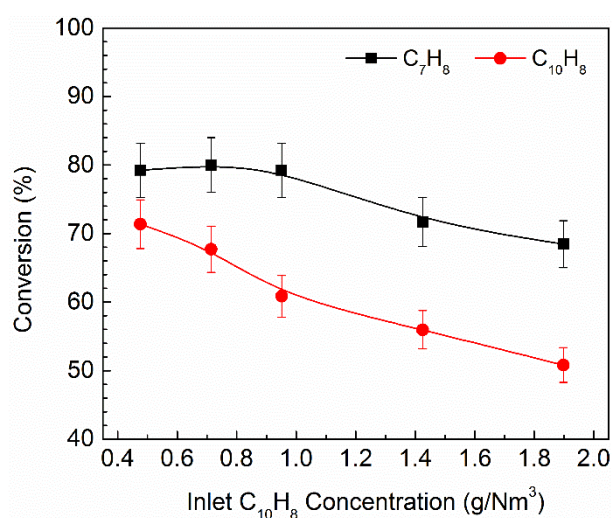
(a)
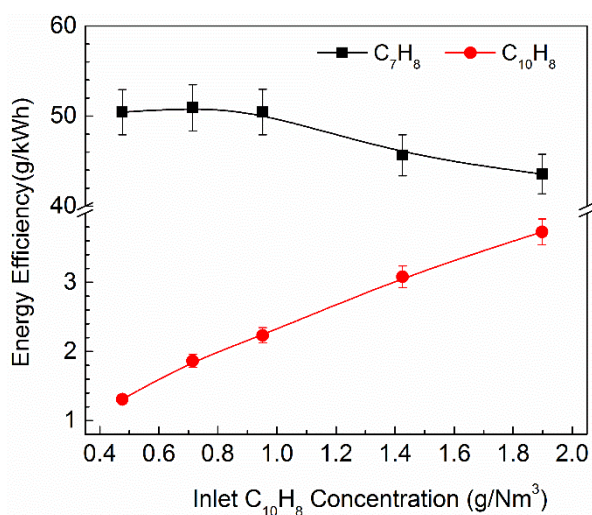
(b)
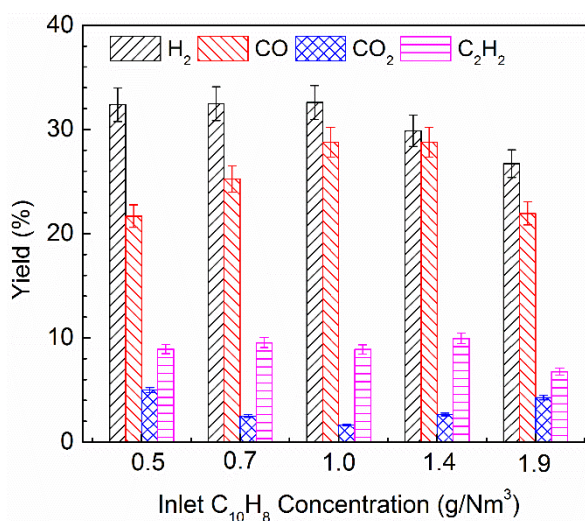
(c)

Figure 6.3 Effect of initial naphthalene concentration on (a) conversion efficiency of tar (b) energy efficiency of plasma decomposition process and (c) yields of primary gaseous products (C_7H_8 content: 16.5 g/Nm^3; Discharge power: 60 W; Q: 3.5 L/min; S/C: 1.5).

6.3.3 Effect of discharge power

Figure 6.4 (a) shows the effect of discharge power on the destruction efficiency of naphthalene/toluene at a flow rate of 3.5 L/min, an initial naphthalene concentration of 1.08 g/Nm^3 and an S/C molar ratio of 1.5. Increasing the discharge power from 54 to 73 W increased the conversion of toluene by 23%, whiles the conversion rate of naphthalene was remarkably boosted by a factor of 1.6. This phenomenon can be explained by the fact that

both the electric field strength between the electrodes and the power deposited into the gas stream increase with the increase in the discharge power, which generates more energetic electrons to initiate the destruction of naphthalene/toluene by collision and leads to the enhanced naphthalene and toluene conversion. The energy efficiency for the conversion of naphthalene and toluene reached a maximum value of 48.6 g/kWh and 2.2 g/kWh, respectively, at the discharge power of 60 W and gradually decreased with the increase in the plasma discharge power even if a higher conversion efficiency can be obtained at a high discharge power.
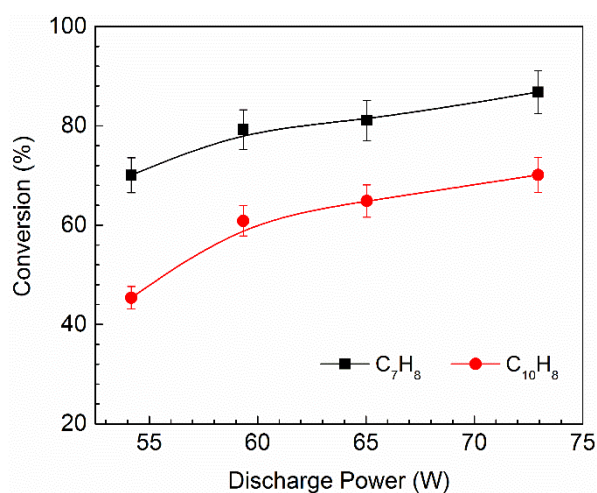
(a)
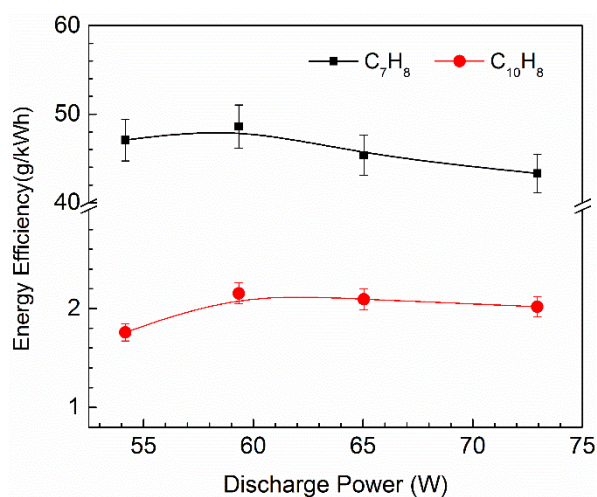
(b)
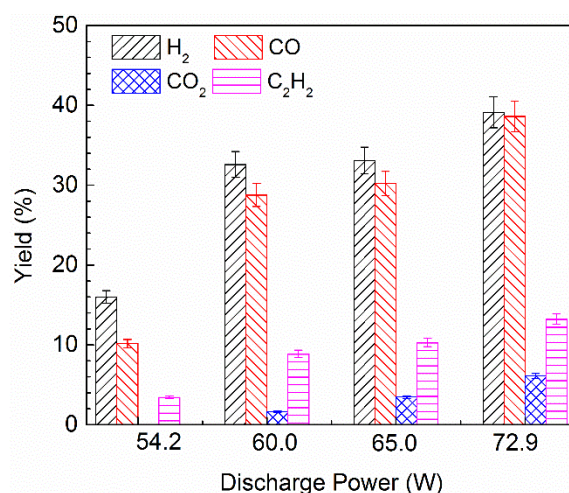
(c)

Figure 6.4 Effect of discharge power on (a) reactant conversions and, (b) energy efficiency and (c) yields of primary gaseous products (C_7H_8 Content: 16.0 g/Nm^3; $C_{10}H_8$ Content: 1.1 g/Nm^3; Q: 3.5 L/min, S/C: 1.5).

Increasing the discharge power led to the high yield of the H_2, CO and C_2H_2. The respective highest yield of these three gas products were 39.1%, 38.6% and 13.2% at the highest discharge power of 73 W, as shown in Figure 6.4 (c). It should be noted that CO_2 was obtained only at high discharge powers, and its yield followed the same tendency as the conversion of naphthalene with the increase in discharge power. Previous result reported that the quantity of charge transfer between electrode increases by increasing applied voltage (discharge power) with fixed geometry of the electrode [144]. Therefore, the toluene, naphthalene, water and nitrogen molecules could dissociate more efficiently at a higher discharge power, resulting in more chemically reactive species (e.g. O, OH, and N_2 excited states). The reactive species participated in the destruction process and enhance the oxidisation of naphthalene/toluene and their intermediates, yielding lower molecular weight products (e.g. CO and CO_2) in the plasma reaction.

6.3.4 Optical diagnostics

In order to get better understanding of the decomposition mechanism of naphthalene/toluene in the GAD and to determine the role of the reactive species on the

decomposition process, the spectroscopic technique was carried out to measure the emission spectra of the discharges under different conditions. The typical emission spectrum of the nitrogen/naphthalene/toluene discharges with and without water vapour are shown in Figure 6.5. Obviously, the spectra of N$_2$/tar were clearly dominated by the CN ($B^2\sum^+ \rightarrow X^2\sum^+$) violet system between 350 and 420 nm and the CN second-order violet system due to the low activation energies of CN ($B^2\sum^+$) (3.2 eV) [206]. Several band sequences of C$_2$ swan system ($d^3\Pi_g \rightarrow a^3\Pi_u$) around 470-520 nm were also clearly observed. In experiments of the decomposition process in nitrogen discharge, non-voltaic products of dark brown colour were always observed in the form of deposits on the metallic electrodes and the internal surface of the reactor, which indicated aromatic hydrocarbons agglomeration and soot formation occurred in the decomposition process. This phenomenon was also evidenced by detecting the spectral line of atomic C1 at around 560 nm in nitrogen discharge.
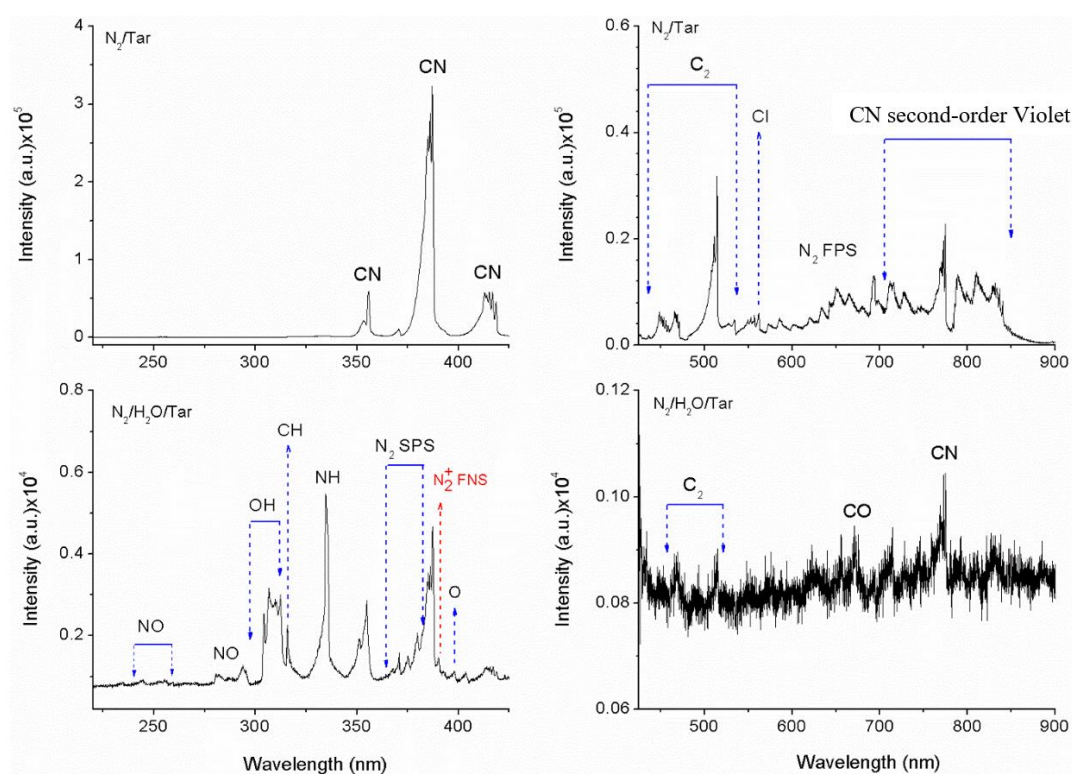
Figure 6.5 Optical emission spectra (OES) of naphthalene/toluene discharges with and without H$_2$O. (C$_7$H$_8$, C$_{10}$H$_8$ concentration: 16.0 g/m^3, 1.1 g/m^3; SEI: 0.29 kWh/m^3) (600 g/mm grating, exposure time 0.2 s).

In N_2 discharge, most of the input electrical energy to the plasma is utilised to dissociate the nitrogen molecules and three primary active species, excited N_2 molecules, N atoms in ground and excited states are produced during the discharge process. The dominating channels of nitrogen dissociation are assumed to be R6-2 and R6-12 [208]. The direct electron impact with the naphthalene/toluene molecules has low contribution in the destruction process due to the low concentration of the reactants and the small electron cross section of hydrocarbons. Therefore, it is believed that the excited nitrogen molecules and atoms formed in the plasma zone probably substantially contributed to the decomposition of naphthalene/toluene molecules, where the leading reactions are represented by R6-13 and R6-14 [181, 184]. Bityurin.et al reported that H atoms can be released through the reaction R6-14 [183]. It is interesting to note that the excited states of nitrogen are generally quenched rapidly at atmospheric pressure (see R6-15) and do not contribute significantly to the destruction process of naphthalene/toluene. Some authors demonstrated that the relative contribution of reaction R6-15 to the loss of excited nitrogen species $N_2(A^3\Sigma)$ increases with a decrease of naphthalene concentration [175]. A similar conclusion was reported by Aerts et al that the direct electron impact dissociation reactions are negligible, while the quenching reactions with metastable $N_2(A^3\Sigma)$ appear to be important in the destruction of very low concentration ethylene (10-1000 ppm) using an air DBD plasma [183].

$$N_2 + e \rightarrow N(^2D) + N(^4S) + e \tag{R6-12}$$

$$C_{10}H_8/C_7H_8 + N_2(A^3\Sigma_u^+) \rightarrow \text{Intermediate byproducts} + N_2 \tag{R6-13}$$

$$C_{10}H_8/C_7H_8 + N(^2D) \rightarrow \text{products} \tag{R6-14}$$

$$N_2(A^3\Sigma_u^+) + N_2(A^3\Sigma_u^+) \rightarrow N_2 + N_2(C^3\Pi_u, B^3\Pi_g) \tag{R6-15}$$
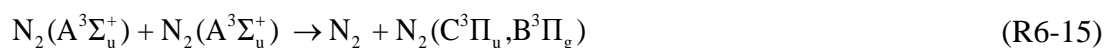
In addition to the CN violet system and C_2 swan band, the OH ($A^2\Sigma^+ \rightarrow X^2\Pi$) systems in 305-310 nm and a strong NH ($A^2\Sigma \rightarrow X^2\Sigma$) transition centred at 336 nm were detected in the humid N_2 discharge plasma. These results suggest that the main channel of the formation of NH radical was associated with the hydroxyl radical OH, as NH radical was not found in the spectrum of nitrogen discharge. The NH radical is originated mainly in

following reactions R6-16 and R6-17. NH$_3$ was probably formed through the coupling reactions of NH with H or H$_2$ (see R6-18). The emission of CH ($C^2\Pi^+ \to X^2\Pi$) band at 314 nm, a weak CO band at 283 nm can be clearly seen in the N$_2$ discharges containing water vapour. The N$_2$ second positive system (SPS) ($C^3\Pi_u \to B^3\Pi_g$) and N$_2^+$ first negative system (FNS) ($B^2\Sigma_u^+ \to X^2\Sigma_g^+$) was detected as well, which indicate that the electron energy of the GAD plasma is sufficient as the threshold energies of the metastable N$_2$ or N$_2^+$ species, N$_2$ ($A^3\Sigma_u^+$), N$_2$ ($B^3\Pi_g$), N$_2$ ($C^3\Pi_u$) and N$_2^+$ ($B^2\Pi_u^+$) are 6.2, 7.4, 11.0 and 18.7 eV, respectively. In addition, several weak NO γ ($A^2\Sigma^+ \to X^2\Pi$) bands in the range of 230-250 nm also appear in the N$_2$/Tar/H$_2$O spectra, illustrating the presence of the nitrogen metastable state N$_2$ ($A^3\Sigma_u^+$) since the formation of NO radicals in plasma discharge region mainly produced from the reaction of N$_2$ ($A^3\Sigma_u^+$) and NO ($X^2\Pi$) through R6-19 [154]:

$$N + H_2O \to OH + NH \tag{R6-16}$$

$$N + OH \to O + NH \tag{R6-17}$$

$$NH + 2H/H_2 \to NH_3 \tag{R6-18}$$

$$N_2\left(A^3\Sigma_u^+\right) + NO\left(X^2\Pi\right) \to N_2\left(X^1\right) + NO\left(A^2\right) \tag{R6-19}$$
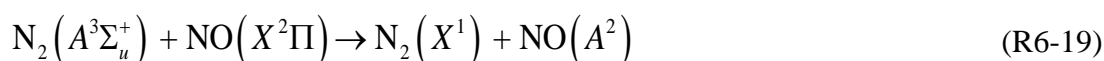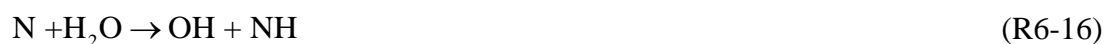
Moreover, in the plasma naphthalene/toluene reforming process, the presence of NO is beneficial to the formation of more active species (e.g. O, OH and H), as shown in R6-20 to R6-22. These active species enhanced the conversion of toluene/naphthalene trough R6-4 to R6-6.

$$NO + NH \to H + N_2O \tag{R6-20}$$

$$NO + NH \to OH + N_2 \tag{R6-21}$$

$$NO + NH \to O + N_2H \tag{R6-22}$$

It is noteworthy that the main gaseous product of the naphthalene/toluene reforming process, hydrogen molecules were not observed in the spectra, but can be generated via the following reactions [209].

$$H_2O + H \to OH + H_2 \tag{R6-23}$$

$$OH + H \rightarrow O + H_2 \qquad\qquad\qquad\qquad (R6\text{-}24)$$

$$H + H + M \rightarrow H_2 + M \qquad\qquad\qquad\qquad (R6\text{-}25)$$
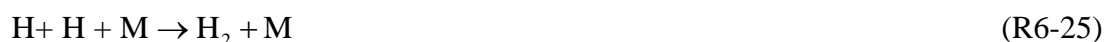
Although C_2 emission lines were observed in the N_2/H_2O/Tar spectra, its relative intensity significantly decreased when adding steam into the feed gas of the plasma reforming of naphthalene/toluene process. In addition, the CH radicals were observed in the N_2/H_2O/Tar spectra, but not in the N_2/Tar spectra. These phenomena indicate that the mechanism of C_2H_2 formation in the N_2/H_2O/Tar plasma process might be different from that in the N_2/Tar plasmas process. The possible reactions for acetylene formation in the N_2/H_2O/Tar plasma process are listed below;

$$CH_3 + e \rightarrow CH_x + yH + e \quad\quad (x + y = 3) \qquad\qquad (R6\text{-}26)$$

$$CH_3 + OH \rightarrow CH_2 + H_2O \qquad\qquad\qquad\qquad (R6\text{-}27)$$

$$CH + CH \rightarrow C_2H_2 \qquad\qquad\qquad\qquad (R6\text{-}28)$$

$$CH + CH_2 \rightarrow C_2H_2 + H \qquad\qquad\qquad\qquad (R6\text{-}29)$$

$$CH_2 + CH_2 \rightarrow C_2H_2 + H + H \qquad\qquad\qquad\qquad (R6\text{-}30)$$

6.3.4.1 Effect of S/C molar ratio on the emission intensities of observed species

Previous literatures reported that the optical emission intensity of chemical radicals could be used to study the concentrations of the corresponding species [210]. The emission bands of the OH radical at 309 nm, NH (A→X) transition at 336 nm, N_2 SPS (C→B) at 337 nm and the N_2^+ FNS ($B^2\Sigma_u^+$) band at 391 nm were selected to investigate the effects of the S/C molar ratio on the emission intensities of these species. Figure 6.6 shows the relative intensity of observed species as a function of S/C molar ration at the SEI of 0.29 kWh/m^3. Clearly, the addition of steam into the N_2 plasma led to the formation of OH and NH and the decline in the relative intensity of N_2 and N_2^+. The intensity of OH was gradually increased with the increase in the S/C molar ratio, while the highest intensity of NH was obtained at an S/C molar ratio of 0.5, beyond which the intensity of NH was decreased. Increasing the S/C molar ratio result in a further decrease in the relative intensity of N_2 and N_2^+ species.

Previous works also demonstrated that increasing the inlet concentration of H_2O into the plasma process could lead to a continuous rise in the OH intensity [154]. In addition to the direct electron impact dissociation of H_2O, the reactions between the excited N_2 species and H_2O molecules are also considered to play a key role in the generation of OH radicals, which can be explained by the following two aspects. Firstly, the nitrogen metastable state molecules N_2 ($A^3\Sigma$) are abundant in the plasma zone, inferring from the high intensity of the N_2 SPS transitions, therefore the collision probability between the H_2O molecules and excited nitrogen molecules should be quite high . Secondly, increasing the S/C molar ration slightly increased the OH intensity and decreased the intensity of N_2 species (see Figure 6.6), which revealed that the loss of N_2 species affected the formation of OH radicals. As mentioned above, the OH radical has a strong ability to oxidise naphthalene /toluene, which plays an important role in the destruction process in humid environment as it opens a new route for naphthalene/toluene decomposition through step-wise oxidation of reactants and their intermediates. Therefore, the addition of H_2O into the N_2 plasma results in an enhanced conversion and energy efficiency, as shown in Figure 6.2. In addition, the mean electron energy is considered to decrease with the increases of S/C molar ratio due to the electronegative property of water molecules (see R6-7) and the quenching effect of H_2O molecules (see R6-3) in the discharge system. This can be evidenced by the drop of N_2 and N_2^+ intensities with increasing the S/C molar ratio in the plasma process. Meanwhile, the emission intensity of N_2^+ species is very sensitive to the electron temperature due to the high ionisation energy of N_2 molecules (15.58 eV), which indicates that the increase of the S/C molar ratio might contribute to the decrease of electron temperature [211].
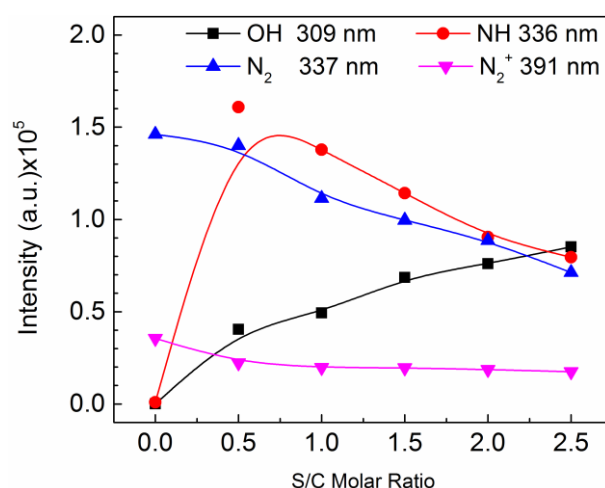
Figure 6.6 Relative intensity of OH, NH, N_2 and N_2^+ as a function of the S/C molar ratio (C_7H_8, and $C_{10}H_8$ concentration: 16.0 g/m^3 and 1.1 g/m^3, respectively; SEI: 0.29 kWh/m^3)

Besides, the relative intensity of NH radical peaked at the S/C molar ratio of 0.5. This might be attributed to the fact that the OH-containing species (e.g. H_2O and OH) could react with N atoms to produce NH via reactions R6-16 and R6-17. Further increasing the S/C molar ratio, the decrease in the electron temperature and recline in the concentration of active nitrogen molecules and atoms could contribute the decrease of NH intensity. All of these phenomena suggest that the electronegative property and quenching effect of H_2O molecules compete with the oxidation ability of OH radicals in the destruction process of naphthalene/toluene, which led to the highest naphthalene/toluene conversion, yield of gas products and the energy efficiency in the plasma process at an S/C molar ratio of 0.5.

6.3.4.2 Determination of the rotational temperatures

In this study, the N_2^+ FNS (B→X)(0,0) transition in the range of 380 - 394 nm was selected to determine the rotational temperature of the GAD plasma, based on finding the best fit between experimental and simulated spectra using SPECAIR software [154]. Figure 6.7 represents the effect of the S/C molar ratio on the rotational temperatures of N_2 in the GAD reactor. Clearly, the rotational temperature of the vibrationally excited nitrogen N_2^+ (B) is gradually decreased by increasing the S/C molar ratio, which follows the similar evolution of the emission intensity of N_2 species (see Figure 6.6).
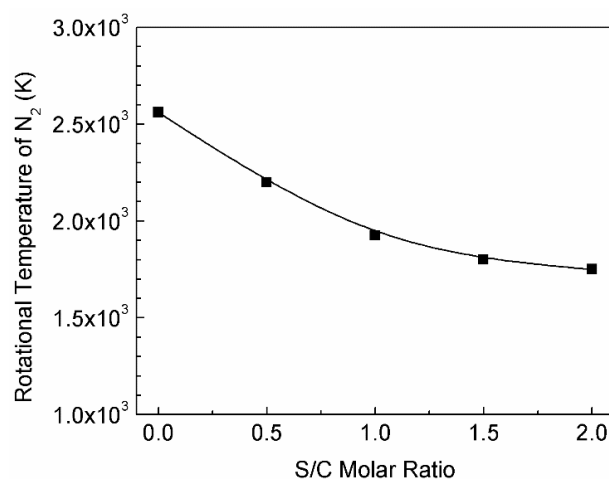
Figure 6.7 Rotational temperature of N_2 as a function of the S/C molar ratio (C_7H_8, and $C_{10}H_8$ concentration: 16.0 g/m^3 and 1.1 g/m^3, respectively; SEI: 0.29 kWh/m^3).

Increasing the S/C molar ratio from 0 to 2 leads to a continuous drop of the rotational temperature from 2560±100 to 1745 ±45 K, which might be caused by the strong cooling effect of H_2O molecules that have large heat capacity. This phenomenon also indicates that the heat loss in the plasma at a lower humid level could make a remarkable contribution to the decrease of the rotational temperature of N_2 since the rotational temperature drops with a relatively faster rate when the S/C molar ratio varied from 0 to 0.5. Previous studies have demonstrated that the rotational temperature of N_2 in the GAD plasmas was decreased by increasing the water vapour content [154].

The rotational temperature of N_2^+ molecules approximately equals the gas temperature in atmospheric pressure plasmas, due to the sufficiently fast rotational-translational relaxation of N_2^+ molecules to equilibrate the rotational temperature and the gas kinetic temperature before the rotationally excited nitrogen species undergo the radiative decay [211]. Thus, the addition of water vapour into the plasma zone leads to a declining of the gas temperature, which may restrict the steam reforming process since it is an endothermic reaction. It is interesting to note that a better performance of our plasma reactor could be obtained in terms of a comparison of the rotational temperature with others. For instance, Czernichowski et al. observed the rotational temperature (~1000-1500 K) and the vibrational

temperature (~3200-3700 K) of a non-thermal gliding arc discharge by simulating the experimental N_2 (C-B, Δv=-2,-1, 0) bands using a computer program Lifbase [212].

6.3.5 Formation of by-products

In order to understand the related mechanism in the steam reforming of the mixture of toluene and naphthalene in a GAD plasma, the organic by-products generated in this study were captured and analysed by GC/MS, the corresponding results are described in Figure 6.8. Table 6.1 presents the liquid by-products with the molecular weight smaller than that of ethyl-benzene detected by GC/MS. As the boiling points of the liquid products are different, a GC-temperature programmed method was used to separate and detect these organic compounds. The initial temperature of the oven was 47 $^{\circ}$C, holding for 2 min; then the temperature increased to 100 $^{\circ}$C at a rate of 5 $^{\circ}$C/min. After that, the temperature increasing rate was increased to 10 $^{\circ}$C/min until the oven temperature reached 270 $^{\circ}$. The temperature was kept at 270 $^{\circ}$C for 20 min. The temperatures of injector and detector were set to 250 $^{\circ}$C and 280 $^{\circ}$C, respectively.
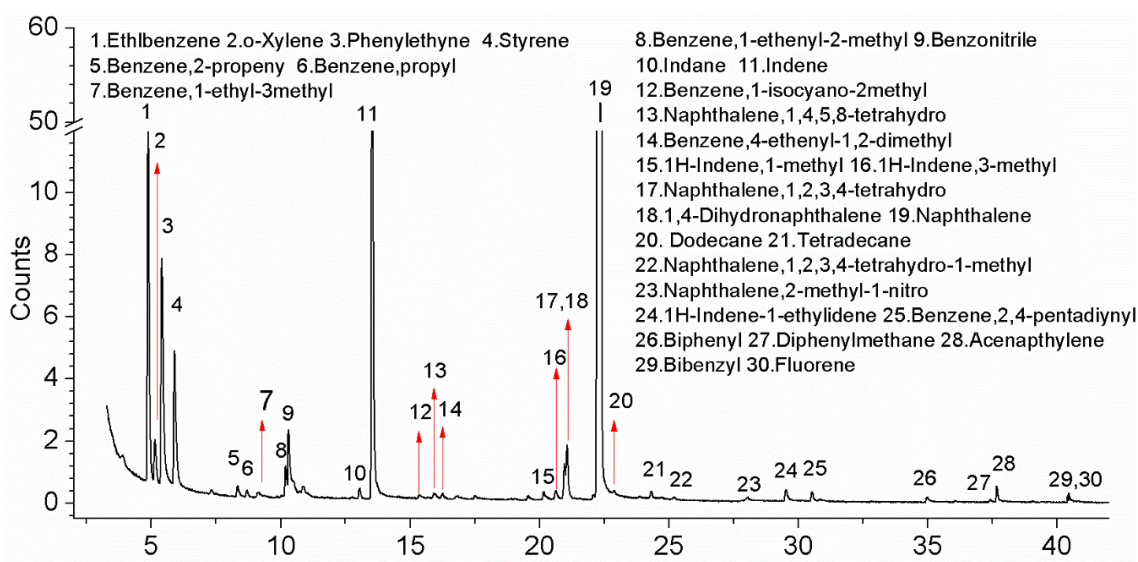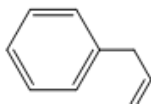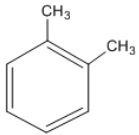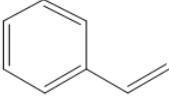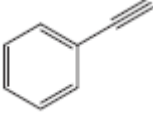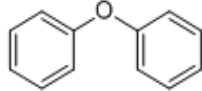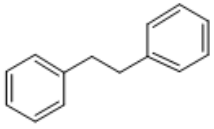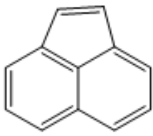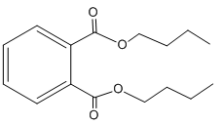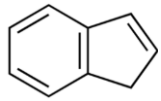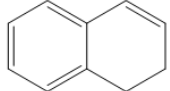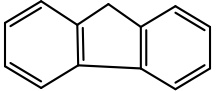
Figure 6.8 Chromatogram of GC/MS analysis for the identification of the tar model compounds degradation products (C_7H_8 concentration: 16.0 g/m^3; $C_{10}H_8$ concentration: 1.1 g/m^3; SEI: 0.29 kWh/m^3; S/C: 1.0).

Table 6.1 Liquid by-products with the molecular weight smaller than ethyl-benzene detected by GC/MS.

Retention time (min)	Compound & Formula	Retention time (min)	Compound & Formula
0.72	Glyoxylic acid, $C_2H_2O_3$	2.74	Toluene, C_7H_8
0.84	Oxalic acid, $C_2H_2O_4$	3.02	Heptane, 3-methylene, C_8H_{16}
1.07	2-Butene, C_4H_8	3.19	Hexane, 2-methyl-4-methylene, C_8H_{16}
1.16	1-Butene, 3-methyl, C_5H_{10}	3.38	2-Octene-(E), C_8H_{16}
1.84	Benzene, C_6H_6		

Table 6.2 Structures of relevant liquid by-products.

Benzene,2-propenyl	Xylene	Styrene	Phenylethyne
Diphenyl ether	Bibenzyl	Acenaphthalene	Dibutyl phthalate
Indene	1,2-Dihydronaphthalene		Fluorene

The process of naphthalene/toluene steam reforming is very complex as a large number of reactions take place simultaneously. This could be confirmed by the various by-products that were identified in the liquid samples. Some relevant product structures are shown in Table 6.2. Although the by-products were not quantitatively analysed in this study, it is clear from the chromatogram that benzene, ethylbenzene, phenylethyne, styrene, and indene were

the major by-products. The organic by-products in humid N_2 discharges included various oxygen- and nitrogen-containing substituents, such as glyoxalic acid, benzonitrile, biphenyl ether and naphthalene, 2-methyl-1-ntro, which indicated that both OH/O radicals and excited nitrogen species were involved in the naphthalene/toluene conversion process. Remarkably, the presence of aliphatic compounds (e.g. 2-butene, 1-butene, 3-methyl, hexane, 2-methyl-4-methylene and tetradecane) suggested that the ring-opening reactions were induced during the steam reforming of toluene and naphthalene mixture. The polymerization reactions also took place in the plasma region due to the present of diphenyl ether, bibenzyl and fluorine.

For the better understanding on the reaction scheme, it is essential to analyse the chemical and physical properties of naphthalene molecules. Figure 6.9 illustrates the characteristics of naphthalene molecules. Clearly, the bond lengths of naphthalene molecule are different (I=0.136 nm, II=0.140 nm, III=0.139 nm, IV=0.142 nm) because of the different carbon atom positions. The carbon atoms with the number of 1, 4, 5 and 8 are called α position carbon, and the rest positions are named β position carbon. It has been demonstrated that the electron cloud density is higher at α position in naphthalene molecules than that in β position [213]. Therefore, the decomposition of naphthalene is most likely initialled by breaking the C-H bond at α position via reacting with the excited species and the active radicals formed in the GAD plasma reactor (e.g. H or OH radicals). Once the naphthalene molecule is destroyed, the unstable intermediate products would undergo a variety of reactions. These intermediate products are fragments or radicals, which can further react with OH, and O to form carbon oxides and the stable intermediate organic compounds. Under different experimental conditions, the process of naphthalene/toluene steam reforming mostly leads to the formation of permanent gases (e.g. hydrogen, CO and C_2H_2). Previous study also reported that the first step reaction in the decomposition of any non-substituted aromatic compound is the C-H or C-C bond cleavage [214], followed by the cleavage reaction, which results in the ring opening or breakage of the aromatic compounds to form the lower aliphatic or aromatic hydrocarbons. Consecutive reactions of these lower hydrocarbons could contribute to the production of the permanent gases.

I=0.136 nm II=0.140 nm III=0.139 nm IV=0.142 nm
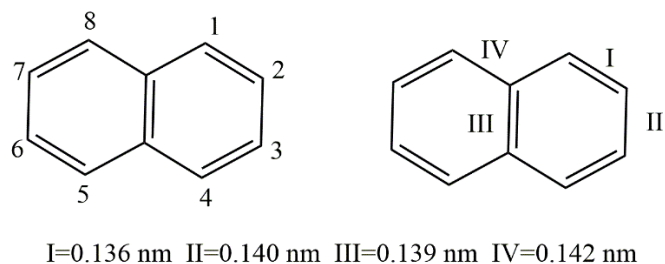
Figure 6.9 Structure of the naphthalene molecule.

6.3.6 Possible reaction mechanisms

Toluene destruction via NTP has been discussed in detail in previous chapters. Therefore, we focus on the reactions between active radicals and naphthalene molecules in this chapter. Concerning the distribution of the organic by-products, it is believed that naphthalene steam reforming by GAD plasma can generally be realized by two pathways – the collision process with the nitrogen excited species and the oxidation process with the OH radicals and O atoms. Figure 6.10 shows a possible reaction scheme of the plasma steam reforming of toluene and naphthalene in the humidity N_2 plasma a GAD reactor based on the product distribution.

As we mentioned in the part of optical diagnostics, the GAD plasma could generate abundant excited nitrogen species, which can easily dissociate C-H bonds of naphthalene molecule, forming napthyl radical. The excited napthyl can react with species such as OH, CH_3 and C_2H_2 to produce naphthol, 1 or 2-methylnaphthalene and acenaphthylene, respectively. The intramolecular rearrangement of acenaphthylene via tautomerization leads to the formation of naphthalene-1-ethynyl. The methylation process of naphthalene molecules might generate acenaphthalene.
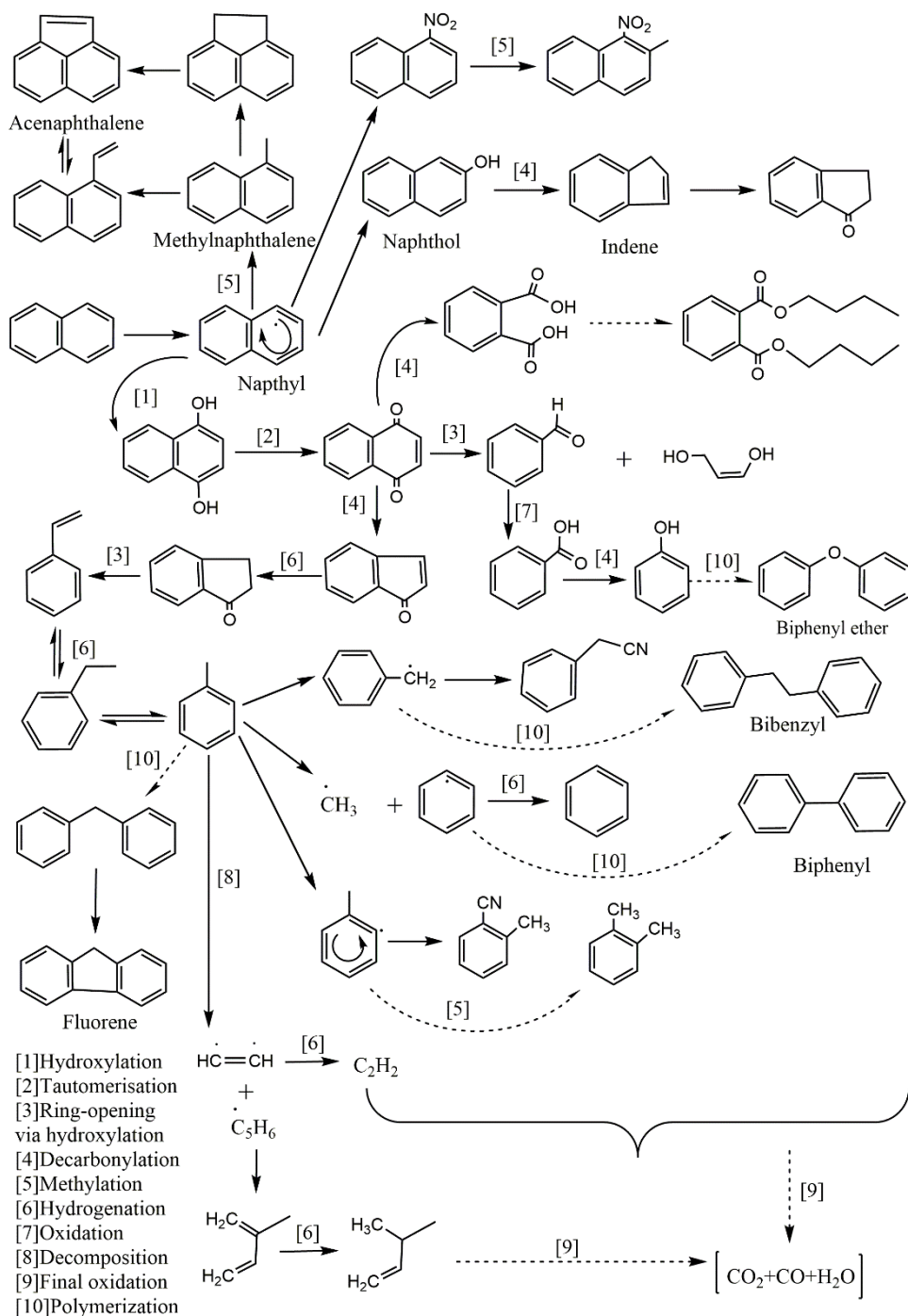
Figure 6.10 Proposed reaction mechanism for the plasma conversion of naphthalene and toluene under studied humid conditions.

The naphthalene conversion process can also proceed mainly through the formation of a naphthoxy radical [215]. The oxidation process proceed via dehydrogenation of one or two of the aromatic rings to form naphthol or 1, 4-dihydroxynaphthalene, and the rearrangement of the later compound via tautomerization results in the formation of 1, 4-naphthoquinone [216]. In case of naphthol, parallel reactions (namely decarbonylation and oxidation) take

place, which generate carbon monoxide and hydrogen. The corresponding reaction product is indene and 2-3-dihydroindenone, respectively. The chemical compound 2-3-dihydroindenone may also be generated by decarbonylation from 1, 4-naphthoquinone, followed by hydrogen addition [217]. Further reactions of the intermediates indene and 2,3-dihydroindeneone with or without water molecules lead to ethenylbenzene, ethylbenzene and toluene. Indene is an intermediate compound for the production of other stable (aromatic) compounds, as suggested by Devi [217]. Remarkably, oxidation of 1, 4-naphthoquinone together with the loss of oxalic acid leads to aromatic ring opening and contributes to the formation of phthalic acid, which can further react with active C_2 or C_3 entities to generate the stable compound dibutyl phthalate. Moreover, the formation of benzaldehyde follows the pattern of hydroxylation and decarbonylation. The main reaction pathways for the formation of benzaldehyde and phthalic acid are illustrated in Figure 6.11. At the same time, water molecules can decompose to produce OH and O radicals. The combination of OH and oxygen radicals leads to the formation of perhydroxy radical, which can react with hydrogen radicals to reform hydrogen peroxide in the system, as suggested by Croiset et al [218]. At the same time, peroxy and perhydroxy radicals can decompose to produce molecular oxygen, where the possible reaction network is shown below. In a strongly oxidising environment, for instance, benzaldehydes are converted to benzoin acid. The decomposition of phenols would occur by loss of CO, which could be further oxidised to CO_2.

$$2OH \rightleftarrows H_2O_2 \tag{R6-31}$$

$$H^{\cdot} + {}^{\cdot}OOH \rightleftarrows H_2O_2 \tag{R6-32}$$

$${}^{\cdot}OOH \rightarrow O_2 + H \tag{R6-33}$$

Previous studies also showed that the intermediate products of naphthalene oxidation to include phthalic acid, benzoin acid, benzaldehyde, phenol and other substituted aromatic alcohols [219]. Diphenyl ether and biphenyl were detected in the liquid products from the steam reforming of naphthalene/toluene, which could be formed probably by the dimerization of phenol and benzene, respectively. The hydrogenation of the product from the combination of benzene with benzyl radical leads to the formation of fluorine. With the

aid of the active radicals (e.g. O and OH), these intermediates formed during the decomposition process can be oxidised continuously into other small permanent molecules, such as CO, CO_2 and H_2O.
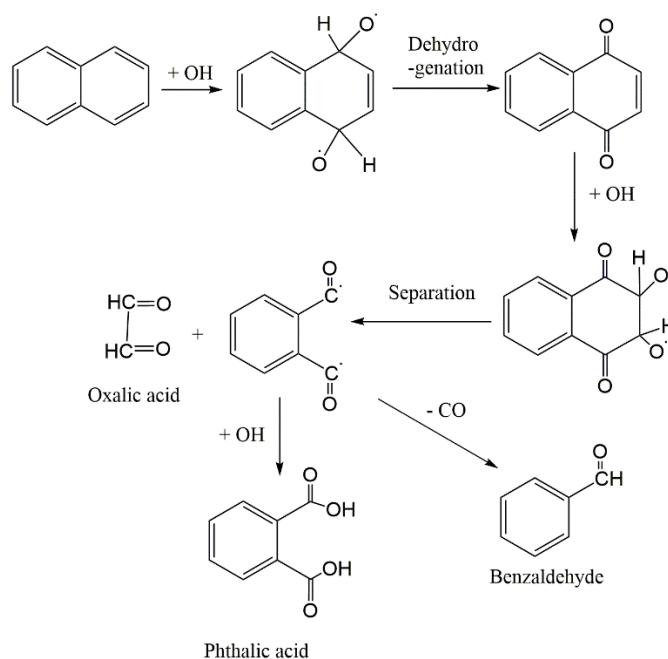
Figure 6.11 Main reactions for the formation of benzaldehyde and phthalic acid.

6.4 Plasma-catalytic steam reforming of toluene and naphthalene using Ni-Co bimetallic catalysts

6.4.1 Catalyst properties

(1) Surface structure of the catalysts

Table 6.3 shows the physicochemical properties of the support and the reduced catalysts, determined by N_2 adsorption–desorption isotherms. The Brunauer–Emmett–Teller (BET) specific surface area (S_{BET}) of pure γ-Al_2O_3 is 368.0 m^2/g, whilst the specific surface area of all the supported catalysts is much lower. The 7.5Ni7.5Co catalyst shows the highest specific surface area of 224.9 m^2/g; while the specific surface area of the 15Co catalyst is less than half of the support. In addition, the pore volume of the catalysts (0.37 – 0.45 cm^3/g) is smaller than that of the γ-Al_2O_3 support (0.54 cm^3/g). The lower specific surface area and the pore volume is due to the coverage of γ-Al_2O_3 surface by deposited metals and/or partial

blockage of pores in the catalyst samples [220, 221]. The average pore diameters of the reduced catalysts (6.38 – 6.74 nm) is larger than that of the γ-Al_2O_3 support, which can be attributed to the clogging of pores with a small diameter (e.g. micropores) after loading active metals on the support with the meso- and macro-pores unaffected [221].

Table 6.3 Physicochemical properties of the catalyst support and reduced catalyst.

Sample	S_{BET} (m^2/g)	Pore volume (cm^3/g)	Average pore diameter (nm)
γ-Al_2O_3	368.0	0.54	5.45
15Ni	201.4	0.41	6.53
7.5Ni7.5Co	224.9	0.45	6.38
15Co	172.8	0.37	6.74

Figure 6.12 shows the XRD patterns of the catalyst support, calcined catalysts and the reduced catalysts. The XRD spectrum of the γ-Al_2O_3 support shows six diffraction peaks at $2\theta = 14.5°$, $28.3°$, $38.5°$, $45.8°$, $49.7°$ and $67.1°$ (see Figure 6.12 (a)). These peaks can also be observed in the XRD patterns of the reduced catalysts. However, the intensities of the γ-Al_2O_3 peaks in the reduced catalysts are much lower than that of the support. The diffraction peaks of Co_3O_4 and NiO are shown in the calcined 15Co and 15Ni catalysts (see Figure 6.12 (a)), which indicate the formation of metal oxide crystallites. No obvious $NiAl_2O_4$ and $CoAl_2O_4$ spinel aluminates are observed in the XRD patterns of the calcined catalysts as the diffraction peaks of the cubic spinel species easily overlap with that of the cubic phase NiO and the spinel phase Co_3O_4 [222, 223]. However, the H_2-TPR analysis in the following section indicates that spinel aluminates are formed in the calcined catalysts, especially for the 15Ni catalyst. Similar findings were reported by Liao et al. using similar Ni/Al_2O_3, Co/Al_2O_3 and bimetallic Ni-Co/Al_2O_3 for dry reforming of methane [224].
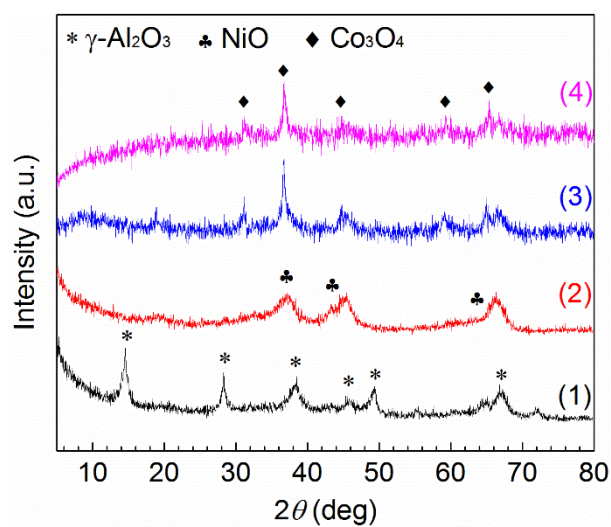
(a)
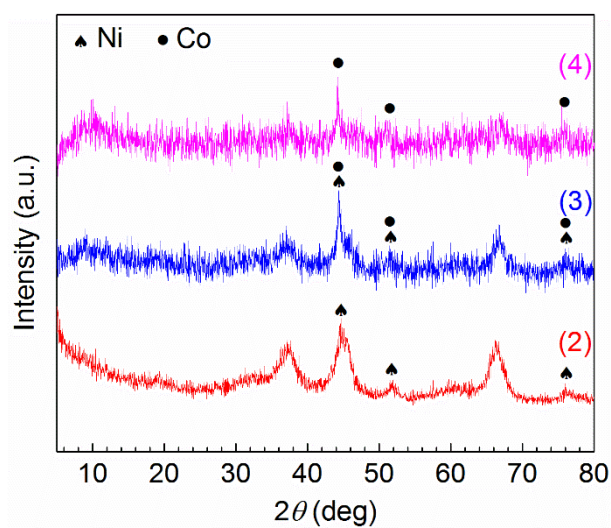
(b)
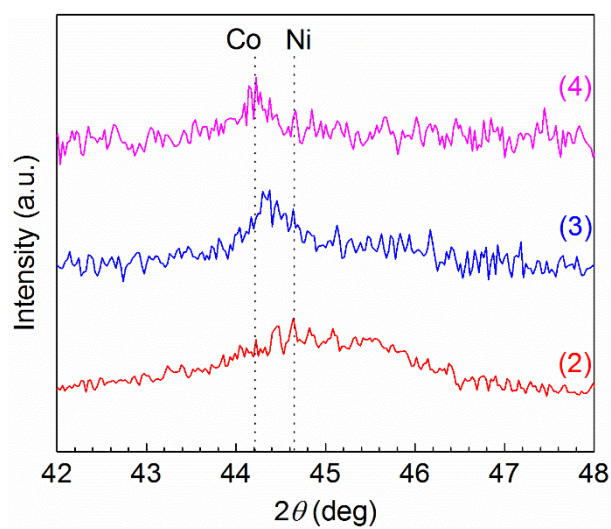
(c)

Figure 6.12 XRD patterns of (a) the catalyst support and calcined catalysts, (b) the reduced catalysts before reaction and (c) the reduced catalysts with 2θ range of $42° – 48°$: (1) γ-Al$_2$O$_3$; (2) 15Ni; (3) 7.5Ni7.5Co; (4) 15Co.

For the reduced 15Ni catalyst (see Figure 6.12 (b)), the diffraction peaks at $2\theta = 44.6°$, $51.8°$ and $76.5°$ are assigned to the diffraction of the Ni metal phase; while the diffraction peaks at $2\theta = 44.2°$, $51.4°$ and $75.7°$ in the XRD spectrum of the 15Co catalyst indicates the existence of the characteristics of the Co metal phase [225]. The reduced 7.5Ni7.5Co catalyst displays the similar XRD diffraction patterns as that of 15Ni and 15Co catalyst. It is difficult to distinguish the Ni and Co metal phase in the reduced 7.5Ni7.5Co catalyst, as the Ni-Co might be formed during the reduction process [226]. The XRD spectrum of the reduced 15Ni, 7.5Ni7.5Co and 15Co catalysts in the 2θ range of $42°$ and $48°$ is shown in Figure 6.12 (c). Clearly, the XRD pattern of the reduced 7.5Ni7.5Co catalyst only shows one diffraction peak at a 2θ value of $44.4°$. This 2θ value shifts from that of 15Ni catalyst to a lower value close to that of the 15Co catalyst, which demonstrates that the Ni-Co alloy is formed [226]. Previous studies also indicated that the presence of a single peak around $2\theta = 44.5°$ in the XRD patterns of the supported Ni-Co catalysts was due to the formation of a homogeneous phase (Ni-Co alloy) [227-229]. The weak peak intensities in the reduced catalysts indicates the high dispersion and small crystallite size of the active metal particles. This can be confirmed by the TEM images of the reduced catalysts, as shown in Figure 6.13. The average particle size in these reduced catalysts is around 20 nm.
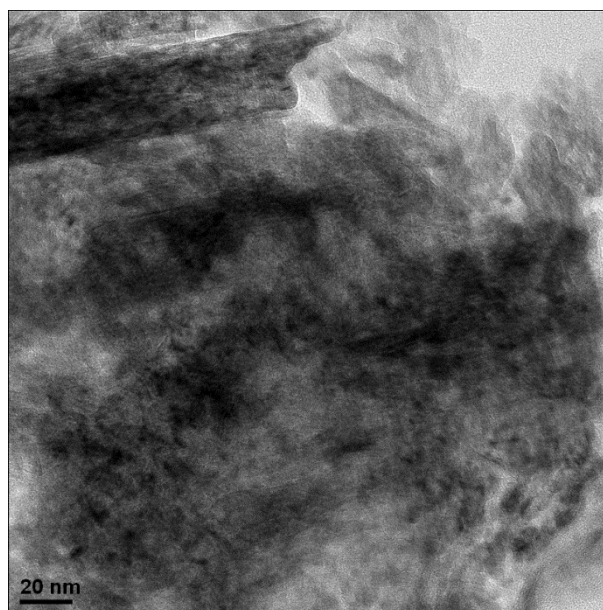
(a)
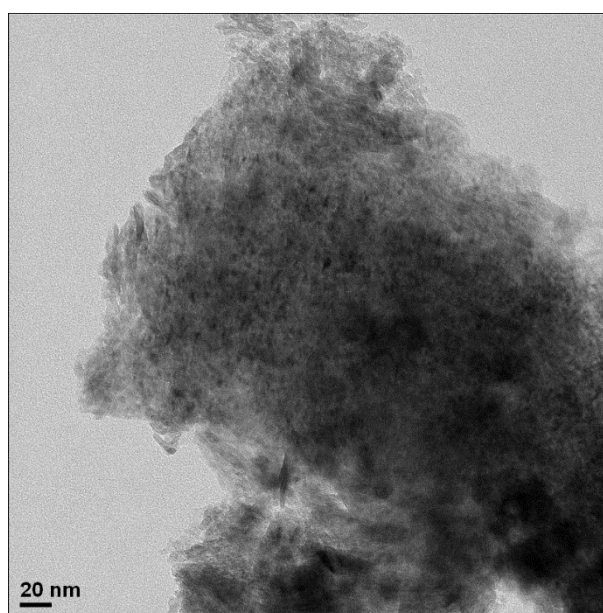
(b)
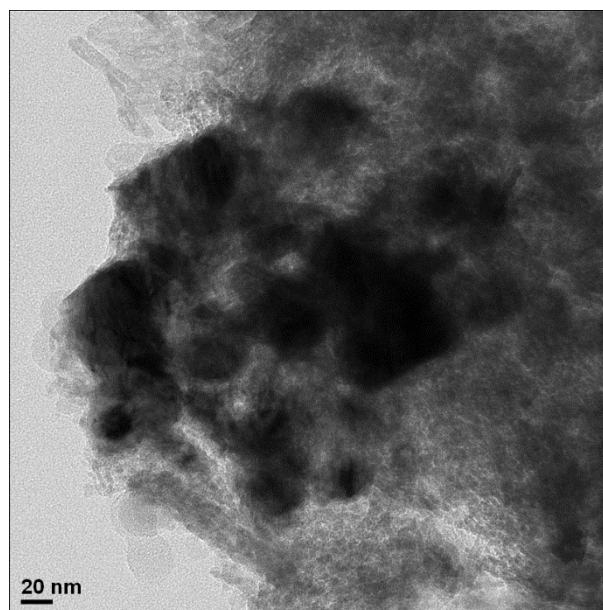
(c)

Figure 6.13 TEM images of the reduced 15Ni (a), 7.5Ni7.5Co (b) and 15Co (c) catalysts.

(2) H_2-TPR

Figure 6.14 show the H_2-TPR patterns of the calcined 15Ni, 7.5Ni7.5Co and 15Co catalysts. Two major peaks are observed in the H_2-TPR profile of the calcined 15Ni catalyst. The first peak at 413.3 ^{o}C is attributed to the reduction of the bulk NiO; while the second peak at 638.5 is mainly related to the reduction of the NiO species which have medium-strength interaction with the γ-Al_2O_3 support. From the H_2-TPR profiles of the 15Ni catalyst, H_2 consumption occurs when the temperature is higher than 700 ^{o}C, which indicates the formation of a small amount of $NiAl_2O_4$ associated with the high temperature (>700 ^{o}C) reduction [221, 230]. The $NiAl_2O_4$ is formed in the calcination process due to the strong interaction between the γ-Al_2O_3 support and the Ni precursor. The H_2-TPR profile of the calcined 15Co catalyst shows a high peak at 311.3 ^{o}C and a broad pear starting at 408.8 ^{o}C, which indicates the two-step reduction of the Co species. The first peak is associated with the reduction of Co_3O_4 to CoO, while the second one is assigned to the further reduction of CoO to Co [227, 231]. The H_2-TPR profile of the calcined 7.5Ni7.5Co catalyst is different from that of the calcined 10Ni and 10Co catalysts. The reduction process of the calcined bimetallic catalyst starts at an earlier temperature of 266.7 ^{o}C. This shift of the reduction

peak to a lower temperature indicates an easier reducibility of the calcined 7.5Ni7.5Co catalyst, suggesting that the presence of Co decreases the reduction temperature of the surface metal oxide species in the supported catalysts. Similar phenomenon has been reported by Zhao et al. using the similar Ni/Al_2O_3, Co/Al_2O_3 and bimetallic $Ni-Co/Al_2O_3$ catalyst for steam reforming of ethanol [225]. The reducibility of the supported catalysts follows the order of 7.5Ni7.5Co > 15Co > 15Ni in this study.
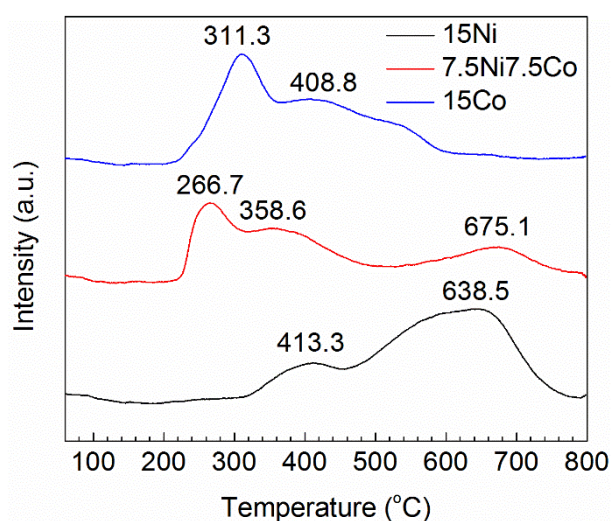
Figure 6.14 H_2-TPR patterns of the calcined 15Ni, 7.5Ni7.5Co and 15Co catalysts.

6.4.2 Reactant conversions and energy efficiency

Figure 6.15 presents the effect of different catalysts on the plasma process for biomass tar conversion in terms of the conversion of toluene and naphthalene and the energy efficiency of converting toluene and naphthalene in the plasma process. Clearly, the presence of the supported catalysts increased both the tar conversion and the energy efficiency of the plasma process. The combination of the 7.5Ni7.5Co catalyst exhibited the best reaction performance. The conversion of toluene and naphthalene was increased by 7.6% (from 87.1% to 93.7%) and 11.8% (from 73.5% to 82.2%), respectively, in the presence of the 7.5Ni7.5Co catalyst, compared to that in the plasma-only process. The corresponding energy efficiency of the plasma process was enhanced from 34.4 to 37.0 g/kWh and from 2.0 to 2.3 g/kWh, respectively.

(a)

(b)
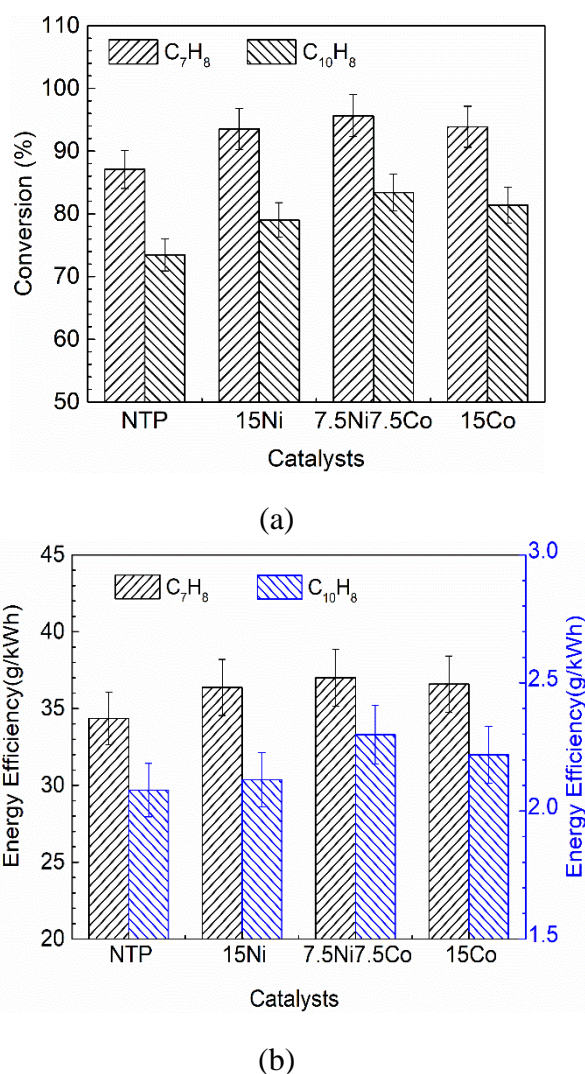
Figure 6.15 Effect of the supported catalysts on (a) the conversion of toluene and naphthalene and (b) the energy efficiency of converting toluene and naphthalene in the plasma process (C_7H_8 content: 16.0 g/Nm^3; $C_{10}H_8$ content: 1.1 g/Nm^3; Discharge power: 86 W; Q: 3.5 L/min; S/C molar ratio: 1.5).

The performance of the plasma-catalytic conversion of biomass tar is mainly dependent on the properties of the catalysts and on the interaction between the active metals and the support. In this study, the 7.5Ni7.5Co catalyst was found to be the best catalyst for the plasma-catalytic conversion of toluene and naphthalene, followed by the 15Co and the 15Ni catalysts. However, the specific surface areas of these three catalysts followed the order of 7.5Ni7.5Co > 15Ni > 15Co (see Table 6.2), which suggest that the specific surface areas might not be the dominant factor for the plasma-catalytic conversion of toluene and

naphthalene. While the effect of the catalysts on the plasma-catalytic process for biomass tar conversion was in good agreement with the reducibility of these catalysts, decreasing in the sequence of 7.5Ni7.5Co > 15Co > 15Ni, which indicates that the reducibility of the supported catalysts plays an important role in the plasma-catalytic conversion of biomass tar. In addition, the synergy between the Ni and Co atoms in the Ni-Co alloy would enhance the catalytic activity and reduce the coke deposition, and consequently improve the conversion of toluene and naphthalene [43, 232]. The enhancement in the reaction performance due to the Ni-Co bimetallic catalyst was also reported in the thermal-catalytic reforming of hydrocarbons. Wang et al. performed the thermal steam reforming of toluene as a biomass tar over the Ni-Co/Al_2O_3 catalysts in a laboratory-scale continuous feeding dual-bed reactor [43]. They found that the steam reforming of toluene showed the highest conversion and the lowest coke formation using the 12Ni3Co/Al_2O_3 catalyst. Xiao et al. used the Ce-promoted Ni-Co/Al_2O_3 catalysts for the thermal catalytic steam reforming of n-docecane at 700 ^{o}C and atmospheric pressure in a fixed-bed tubular reactor [232]. The results indicated that the presence of the Ce-promoted Ni-Co/Al_2O_3 catalysts could enhance the catalytic activity and the stability due to the Ni-Co alloying and the CeO_2 promotion. The highest conversion of n-dodecane (89%) was achieved using the 5 wt.% Ce-promoted 12Ni3Co/Al_2O_3 catalyst.

The stabilities of these Ni-Co catalysts in the hybrid plasma-catalysts system were also investigated (not shown in here). The conversion efficiency of naphthalene/toluene kept almost unchanged during 1 h of reaction. Unfortunately, it is impossible to operate the system for a long time (over 1.5 h) due to the poor thermal resistance of the GAD reactor. (Long running process will melt the insulator where close to the electrodes, leading the gas leakage.)

6.4.3 Analysis of gas and liquid products

In the plasma process with and without any catalysts, H_2, CO, CO_2, CH_4 and C_2H_2 were the main gas products while trace amount of C_2H_4, C_2H_6, C_3H_8 and C_4H_{10} were also detected. The distribution and the amount of the gas products strongly depends on the reactor types. Chun et al. reported that H_2, CO and CO_2 were the main gas products from the steam

reforming of benzene as a surrogate tar in a GAD reactor with three blade-shaped electrodes in the absence of any catalyst [49]. Zhu et al. reported that H_2 and C_2H_2 were main products from the destruction of toluene in a rotating GAD reactor equipped a ring magnet without a catalyst, while the selectivities of CH_4, C_2H_4 and C_2H_6 were much lower than that of H_2 and C_2H_2 [53]. In the plasma-catalytic conversion of biomass tar, Tao et al. reported that H_2 and CO were main gas products from plasma-catalytic steam reforming of toluene as a model tar compound over the Ni/SiO_2 catalyst in a pin-to-pin DC pulsed plasma reactor [52].

Figure 6.16 shows the effect of different catalysts on the yield of the main gaseous products in the plasma-catalytic steam reforming of toluene and naphthalene in this study. Compared to the plasma-only process, the combination of GAD plasma with the supported catalysts enhanced the yield of syngas, CO_2 and CH_4. The highest yield of H_2 and CO was 42.2% and 37.3%, respectively, in the presence of the 7.5Ni7.5Co catalyst, followed by that using the 15Co and 15Ni catalysts. The highest yield of H_2 and CO was increased by 49.1% and 33.7% compared to that in the plasma only process. A highest CH_4 yield of 1.6% was achieved when using the 7.5Ni7.5Co catalyst, while the yield of CH_4 was similar in the case of the 15Ni and 15Co catalysts (1.2%). Although the introduction of the supported catalysts in the GAD reactor increased the yield of the CO_2, the CO_2 yield in the monometallic 15Ni and 15Co catalysts (around 7.8%) was higher than that in the bimetallic 7.5Ni7.5Co catalyst (5.6%), which was different from the variation of the yield of H_2, CO and CH_4. It is interesting to note that only the 7.5Ni7.5Co catalyst enhanced the yield of C_2H_2, which was increases by 24.4% (from 9.0% to 11.2%) compared to the plasma-only process, while the C_2H_2 yield was decreased by 34.4% and 44.4% by combing the 15Ni and 15Co catalysts with the GAD reactor, respectively.
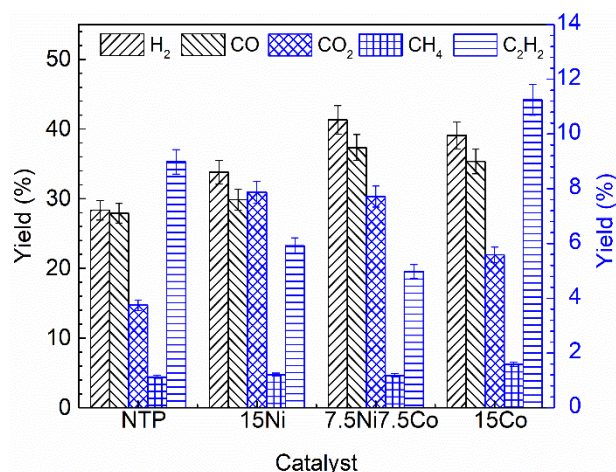
Figure 6.16 Effect of the supported catalysts on the yield of the gaseous products in the plasma process (C_7H_8 content: 16.0 g/Nm^3; $C_{10}H_8$ content: 1.1 g/Nm^3; Discharge power: 86 W; Q: 3.5 L/min; S/C molar ratio: 1.5).

Figure 6.17 shows the liquid by-products in the plasma steam reforming of toluene and naphthalene mixture with and without catalysts. The corresponding name of these by-products is listed in the Table 6.4. In the plasma process without a catalyst, ethlbenzene, phenylethyne, styrene, indane, benzene, 1-isocyano-2methyl and 1,4-Dihydronaphthalene were detected as the major liquid by-products. The combination of the GAD plasma and the supported catalysts significantly reduced the amount of these by-products, which could be due to the fact that in the presence of the supported catalyst, toluene and naphthalene were more selectively converted into gaseous products (e.g. CO, CO_2 and CH_4), as shown in Figure 6.16. In Chapter 5, we also found that introducing the Ni/γ-Al_2O_3 catalyst into the discharge gap of the DBD reactor significantly decreased the composition and amount of the liquid by-products from the plasma-catalytic steam reforming of toluene [204].
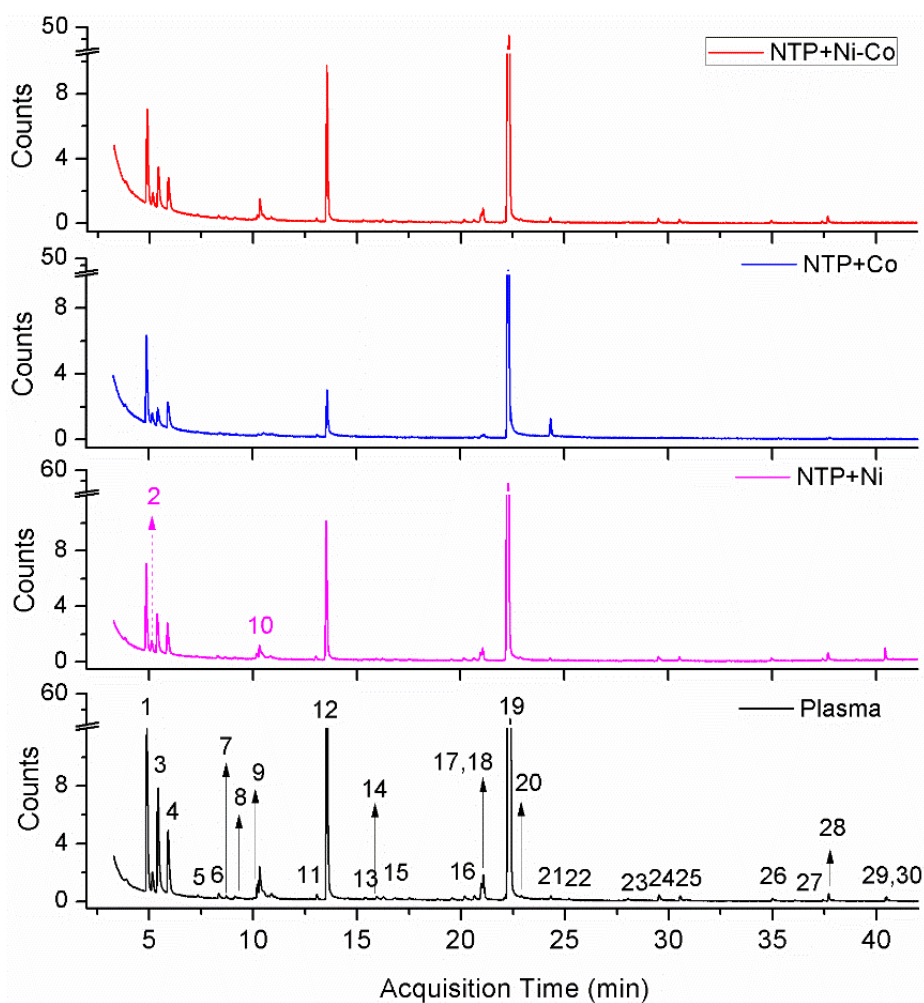
Figure 6.17 GC-MS chromatogram of condensed by-products collected in the plasma steam reforming of toluene and naphthalene with and without catalysts (C_7H_8 content: 16.0 g/Nm^3; $C_{10}H_8$ content: 1.1 g/Nm^3; Discharge power: 86 W; Q: 3.5 L/min; S/C molar ratio: 1.5).

Table 6.4 By-products collected in the plasma steam reforming of toluene and naphthalene corresponding to Figure 6.17.

No	Compound	No	Compound	No	Compound
1	Ethlbenzene	11	Indene	21	Tetradecane
2	o-Xylene	12	Benzene,1-isocyano-2methyl	22	Naphthalene,1,2,3,4-tetrahydro-1-methyl
3	Phenylethyne	13	Naphthalene,1,4,5,8-tetrahydro	23	Naphthalene,2-methyl-1-nitro
4	Styrene	14	Benzene,4-ethenyl-1,2-dimethyl	24	1H-Indene-1-ethylidene

5	Benzene,2-propeny	15	1H-Indene,1-methyl	25	Benzene,2,4-pentadiynyl
6	Benzene,propyl	16	1H-Indene,3-methyl	26	Biphenyl
7	Benzene,1-ethyl-3methyl	17	Naphthalene,1,2,3,4-tetrahydro	27	Diphenylmethane
8	Benzene,1-ethenyl-2-methyl	18	1,4-Dihydronaphthalene	28	Acenapthylene
9	Benzonitrile	19	Naphthalene	29	Bibenzyl
10	Indane	20	Dodecane	30	Fluorene

6.4.4 Catalyst characterisation after reaction

Figure 6.18 shows the TG results of the spent catalysts after the plasma-catalytic reaction running for 30 min. The initial weight reduction occurred over the temperature over 100 $^{\circ}$C, which was the thermal desorption of H_2O and/or adsorbed CO_2 [225]. The weight loss at around 240 $^{\circ}$C and 440 $^{\circ}$C was assigned to the removal of carbonaceous species which were mainly composed of the easily oxidisable amorphous coke [233]; while the weight loss at the temperature higher than 500 $^{\circ}$C was associated with the removal of the whisker and graphitic carbon [234]. In this study, the temperature inside the GAD reactor was around 300 $^{\circ}$C. Therefore, most of the amorphous coke was removed during the reaction process, which would not result in the catalyst deactivation; while the whisker and graphitic carbon was hard to be removed due to the relatively low temperature and would accumulate on the catalyst surface, and consequently led to the catalyst deactivation when the plasma-catalytic reaction lasted for a long time. Among the three catalysts, the 7.5Ni7.5Co catalyst exhibited the smallest amount of carbon deposition (below 4.5%) and most of the carbon deposition was the oxidisable amorphous carbon (around 240 $^{\circ}$C). The high carbon resistance of the 7.5Ni7.5Co catalyst was mainly due to the generation of synergy between the Ni and Co in the Ni-Co alloying. The long stability of the Ni-Co bimetallic catalyst was also reported by Hu et al. using the Ni-Co catalyst for the thermal catalytic steam reforming of acetic acid [235].
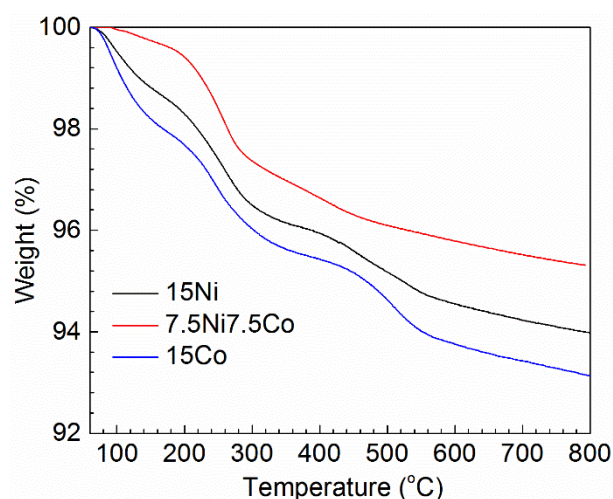
Figure 6.18 TG results for the spent 15Ni, 7.5Ni7.5Co and 15Co catalysts after reaction at a discharge power of 86 W for 30 min.

6.5 Performance comparison for plasma assisted tar reduction

In order to evaluate the effectiveness of the GAD reactor for the plasma tar reduction, the performance in terms of the energy efficiency and conversion efficiency for the conversion of model tar compounds (toluene, benzene and naphthalene) using different non-thermal plasmas was summarized, as shown in Table 6.5. It is clear that the energy efficiency (48.1 g/kWh) for the conversion of tar in this work is much higher than that of most of other plasma processes. Notably, the energy efficiency of the process using gliding arc is significantly higher than that using DBD or corona discharge, which might be attributed to higher electron density in the gliding arc discharge. Previous study showed that the electron density ($\sim 10^{23}$ m^{-3}) in the gliding arc discharge is several orders of magnitude higher than that in the DBD (10^{16}-10^{19} m^{-3}) and corona discharge (10^{15}-10^{19} m^{-3}) [149]. High tar removal efficiency could be obtained using plasma technique and it has the potential to be used in the field of industries. Van Heesch et al. tested the effectiveness of a pulsed corona system for real tar conversion in industrial biogas conditions obtaining a relatively high efficiency of heavy tar reduction (62%) [236]. However, plasma along process also has many disadvantages for industrial purposes, such as being expensive, having a limited lifetime for power supplies and a high-energy demand from overall process. As shown in Table 6.5, very

high toluene conversion efficiency (99%) can be achieved using the microwave plasma at a relatively low inlet toluene concentration of 4.2 g/Nm^3. However, the corresponding energy efficiency of this process was only 4.5 g/kWh, which is significantly lower than that obtained in this work. A balance between tar conversion and energy efficiency in the plasma process is significantly important for the development and deployment of an efficient and cost-effective plasma process for tar removal.

Further enhancement in the conversion and energy efficiency of tar reforming using a gliding arc plasma can be expected from the optimization of reactor geometry, power supply and plasma operating parameters. For instance, developing a rotating gliding arc reformer with a 3-dimendional configuration can ensure that all the reactants pass through the plasma area, which can increase the reaction time of the reactants in the plasma and significantly enhance the reaction performance [144, 149]. Furthermore, the reaction conditions, such as the power source and electrode material, as well as the types and concentration of the carrier gas, can be better controlled to optimise the performance of gliding arc plasmas. Previous studies have demonstrated that the waveform of applied voltage can not only control the applied electric field, which affects the density of the energetic electrons and the reactive species generated, but can also improve the energy transfer with subsequent improvement of the energy efficiency of the plasma process [237]. Nair et al and co-workers revealed that a DC/AC corona system requires higher levels of energy to complete tar removal than pulsed system [238]. This conclusion was also supported by a simulation study, which showed that the energy efficiency of a plasma reactor can be enhanced by a factor of 4 when using rectangular pulse instead of a sinusoidal voltage [239]. From an overall process point of view, a combination of pulsed power supplies and GAD reactors would be ideal.

Table 6.5 Comparison of reaction performance of tar removal by different plasmas.

Process	Tar	Working Gas	Tar Content (g/Nm^3)	Q (m^3/h)	SEI (kWh/m^3)	X (%)	E (g/kWh)	Ref
AC GAD	C_6H_6	Humid N_2	4.3	1.0	0.17	82.6	20.9	[49]
Microwave Torch	C_7H_8	20%Ar+N_2	4.2	1.07	0.93	99.0	4.5	[191]
DBD	$C_{10}H_8$	10% O_2+ N_2	0.46	0.03	0.02	83.0	12.7	[240]
Pulsed Corona	Real tar	Real producer gas	0.72	~15.0	0.04	62.0	11.16	[241]
Positive Corona	C_7H_8	Dry Air	0.8	0.02	0.19	15.0	2.5	[242]
DC GAD	$C_{10}H_8$	O_2	1.3	0.40	0.47	92.0	3.6	[161]
3-electrode GAD	$C_{10}H_8$	Humid N_2	14.3	1.1	1	79.0	47	[144]
AC GAD	C_7H_8	Humid N_2 with CO_2	16.1	0.21	0.25	63.1	40.5	This work
AC GAD	C_7H_8	Humid N_2	23.5	0.23	0.19	35.8	48.1	This work

The combination of plasma with highly active catalysts might provide a promising solution to realize the efficient conversion of tar to high valued-added energy products, since catalysts could increase the production of syngas by promoting the steam reforming reaction and water-gas shift reactions. A synergistic effect may be obtained through the combination of plasma with a desirable catalyst. To evaluate the effectiveness of the synergistic effect of our system, a comparison of reaction and energy performance for both thermal-catalytic and plasma-catalytic tar reduction technologies were summarized, as shown in Table 6.6. It is worth noting that in the conventional thermal catalytic process, a relatively high temperature (over 500 ^{o}C) is required to active the reaction of tar reforming and the type of the reactor is an essential factor as well (single or two-stage process). However, the corresponding tar conversion efficiency by using catalytic steam reforming was limited, less than 70 % [203]. Besides, the high-energy consumption and operation costs as well as fast deactivation of catalysts caused by carbon deposition limit its application in a large scale [53, 203].

Compared with conventional thermal-catalytic steam reforming process, non-thermal plasma can increase the conversion efficiency and reduce the required temperature of tar conversion, leading to a higher energy efficiency. Tao et al. conducted a comparative investigation on the effectiveness of four different gas-cleaning systems for toluene steam reforming, including direct thermal decomposition (DD), plasma-assisted decomposition (PD), catalytic steam reforming (CR) and plasma enhanced catalytic steam reforming (PCR) [52]. The conversion of toluene conversions were performed at a temperature of 773 K in these four different systems, 0.5 g of Ni/SiO$_2$ catalyst was used in both CR and PCR process. It was reported that the PCR process exhibited the best performance and the effectiveness order in terms of conversion efficiency was: DD (5.4 %) < CR (32.8%) < PD (34%) < PCR (57%). They also indicated that Ni/SiO$_2$ catalyst was deactivated rapidly after a 2 h reaction in the case of CR, while in the PCR process the toluene conversion kept almost stable during 6h of reaction. More recently, Liu et al. investigated the interactions between plasma and solid catalyst involved in the steam reforming of toluene [243]. They used three different plasma-catalyst reactors: (i) a coaxial DBD plasma without catalysts, (ii) a Ni-based catalyst placed in plasma discharge zone (IPC) and (iii) a two-stage plasma-catalyst reactor (PPC). The performance of IPC system in terms of toluene conversion, selectivity and yield of syngas as well the unwanted liquid products is much better than that of plasma only process. Both high toluene conversion (86.5%) and energy efficiency (22.5 g/kWh) were obtained simultaneously when the Ni/ZSM-5 catalysts was integrated into the DBD reactor. These experimental results reveal the hybrid plasma-catalysis process system has potential in both the removal efficiency of biomass tar and the economic efficiency. However, compared with the hybrid DBD-catalyst system, the proposed GAD plasma-catalysts system offers more benefits, such as lower energy consumption and wide range of feed flow rate, which is more suitable for the industry applications. Further efforts can be applied for the improvement of the tar removal efficiency, energy efficiency and the production of syngas by developing the catalysts with high activity, coke-resistant and relatively low costs,

Table 6.6 Performance comparison of reforming biomass tar by different technologies.

Process	Tar	Working Gas	Tar Content (g/Nm^3)	Q (m^3/h)	SEI (kWh/m^3)	X (%)	E (g/kWh)	Ref
One-stage furnace with Rh/α- Al$_2$O$_3$	C_6H_6	Humid N$_2$ T=1023 K S/C =0.4	82	0.12	-	9.7	-	
Two-stage furnace with Ni/α- Al$_2$O$_3$	C_7H_8	Humid N$_2$ T=1023 K S/C =3	175	0.017	-	67.0	-	[203]
DBD + MnO$_2$/γ-Al$_2$O$_3$	C_7H_8	Dry Air RT	1.0	0.12	0.01	98.0	0.7	[244]
DBD+ Ni/CaO (IPC)	C_7H_8	Humid N$_2$ T=573 K	51.9	0.03	2	66.6	17.3	[243]
DBD + Ni/ZSM-5 (IPC)						86.5	22.5	
DBD+ Ni/CaO (PPC)						67.0	17.4	
DBD + Ni/ZSM-5 (PPC)						79.5	20.7	
DBD along	C_7H_8	Humid N$_2$ T=573 K S/C =1	51.9	0.03	2	64.0	16.7	[245]
DBD + Al$_2$O$_3$						68.0	17.7	
DBD + Ni-Al						96.0	25.0	
DBD + Fe-Al						81.0	21.0	
Thermal cracking, DD	C_7H_8	Humid He T=773 K S/C =1	258.6	0.0024	-	5.4	-	[52]
Ni/SiO$_2$ reforming, CD					-	32.8	-	
Plasma reforming, PD					~7.2	34.0	12.2	
Plasma + Ni/SiO$_2$,PCR						57.0	20.5	
DBD + Ni/γ-Al$_2$O$_3$ (IPC)	C_7H_8	Humid Ar RT S/C =2.5	17.7	0.015	2.33	47.1	2.6	This work
AC GAD + Ni-Co/γ-Al$_2$O$_3$	C_7H_8/ $C_{10}H_8$	Humid N$_2$ RT S/C =1.5	16.0/1.1	0.21	0.41	93.7/ 82.2	37.0/ 2.2	This work

RT: room temperature

6.6 Conclusions

In this chapter, the plasma steam reforming tar mixture (toluene and naphthalene) was carried out in a GAD reactor. The effects of different reaction conditions (e.g. S/C molar ration, initial naphthalene concentration and discharge power) and the supported catalysts (15Ni, 7.5Ni7.5Co and 15Co) were investigated. In the plasma process without a catalyst, it was found that there was an optimum S/C molar ratio for high reaction performance, which was due to the competing effects of the generation of the reactive species OH from H_2O dissociation and the electronegative property of water molecules. The optimum S/C molar for highest conversion and energy efficiency of converting toluene and naphthalene was 1.5 and 1.0, respectively. Increasing the initial naphthalene concentration decreased the conversion of toluene and naphthalene as well as the energy efficiency for toluene conversion in the plasma process, but increased the energy efficiency for naphthalene conversion due to the enhancement in the amount of the converted naphthalene when increasing the naphthalene concentration. As the major gas products, the highest CO and H_2 yield was achieved at an initial naphthalene concentration of 1.4 and 1.1 g/Nm^3, respectively, when the toluene concentration, discharge power, total flow rate and the S/C molar ratio were kept at 16.5 g/Nm^3, 60 W, 3.5 L/min and 1.5. Increasing the discharge power increased both the conversion of toluene and naphthalene and the yield of the gas products (e.g. H_2, CO, CO_2 and C_2H_2); while the energy efficiency for the conversion of toluene and naphthalene in the plasma process was initially increased by increasing the discharge power, and then decreased after it peaked at a certain discharge power. The possible reaction mechanism in the plasma-only process was deduced by the combination of OES diagnostics and the analysis of the gas and liquid products.

In the plasma-catalytic process, the presence of the γ-Al_2O_3 supported catalysts played a significant role in the steam reforming of toluene and naphthalene. The 7.5Ni7.5Co catalysts exhibited the best performance in terms of tar conversion, energy efficiency, the yield of the gas products and the amount of the carbon deposition, followed by the 15Co and 15Ni catalysts. This was mainly due to the easy reducibility of the 7.5Ni7.5Co catalysts and

the synergy between Ni and Co in the Ni-Co alloying. In the presence of the 7.5Ni7.5Co catalyst, the conversion of toluene and the corresponding energy efficiency were increased by 7.6% compared to these in the plasma-only process, whilst the conversion of naphthalene and its energy efficiency were enhanced by 11.8%. Similarly, the highest yield of H_2 and CO was increased by 49.1% and 33.7%, respectively, in comparison with that obtained in the plasma-only process. The combination of the GAD plasma with the supported catalysts also significantly reduced the amount of the liquid by-products.

Moreover, based on non-stoichiometric chemical equilibrium model, a plasma-based gasification process has been introduced to evaluate the techno-economic performance in terms of product gas composition and the process efficiencies of the plasma-assisted gasification and the conventional air gasification for a broad range of feedstock. Although, the average efficiency clear shows a higher value for the conventional air gasification (over 70%) as compare to the plasma gasification (around 42 %). When the gas qualities (concentrations of contaminant species) and the distribution of syngas are considered, obviously plasma gasification contributes more. The results of plasma gasification showed that using high calorific value feedstock could accommodate high amounts of steam as plasma gas, which result in a hydrogen-enriched syngas with high heating value. However, the enhancement in the gas quality attributions of this plasma gasification usually at the expense of process efficiencies due to high-energy consumption of the plasma system in the moist condition.

CHAPTER SEVEN   CONCLUSIONS AND FUTURE WORK

7.1 Conclusions

Biomass gasification is one of the most promising approaches for the utilisation of biomass, which has considered as a renewable and CO_2-neutral energy source. The utilisation of biomass has the potential to alleviate the dependence on the conventional fossil fuels and reduce the emission of greenhouse gases, and consequently make a significant contribution to the low carbon economy. The formation of tar is one of the great challenges during the biomass gasification process. Any effective methods to remove and convert the biomass tar into the value-added fuels and chemicals will be beneficial to the large scale utilisation of biomass. In this study, the non-thermal plasma technology is employed for the conversion of biomass tar. Specifically, steam reforming and combined (CO_2 and steam) reforming of toluene as a model tar from biomass gasification are performed in a GAD reactor, while the plasma-catalytic steam reforming of toluene is carried out in a coaxial DBD reactor.

Investigating the influence of steam-to-carbon (S/C) molar ratio (steam concentration), CO_2 concentration, initial tar concentration, specific energy input (energy density) on the removal efficiency of toluene resulted in the following findings:

(1) The removal efficiency of toluene at room temperature and atmospheric pressure non-thermal plasma generated in a 2D gliding arc discharge reactor with humid nitrogen was better than that conducted in dry discharge conditions. The presence of steam generated reactive OH radicals, which opened a new reaction route for the decomposition of toluene through a stepwise oxidation of toluene and intermediates, and consequently significantly enhanced the conversion of toluene and the energy efficiency of the plasma process while decreasing the amount of carbon formation.

(2) The optimal S/C molar ratio was around 2-3 for the high performance of the plasma process. The highest toluene conversion of 51.8% was achieved at an S/C molar ratio of 2, a toluene concentration of 9.5 g/m^3 and a SEI of 0.3 kWh/m^3, while the energy efficiency of

the plasma process peaked (~46.3 g/kWh) at the same S/C molar ratio, but a higher toluene feed flow rate of 20.8 ml/h and a lower SEI 0.19 kWh/m^3.

(3) In the plasma process without steam, the removal efficiency of toluene in nitrogen-CO2 plasma decreased with increasing CO_2 concentrations above 3 percent as a result of the formation of CO and nitrogen oxygen in the plasma. Considering the CO_2 concentration in the practical condition (12 vol.%), the presence of steam would further enhance the conversion of toluene and the energy efficiency of the plasma process and there existed an optimum S/C_T molar ratio. The highest higher toluene conversion of 63.1% and the highest energy efficiency of 40.5 g/kWh were obtained at a S/C_T molar ratio of 1.0 with the toluene concentration, the total flow rate and the SEI was fixed at 16.1 g/Nm^3, 3.5 L/min and 0.25 kWh/m^3, respectively.

(4) The combination of the non-thermal plasma and the catalysts could enhance the tar conversion, the energy efficiency for converting tar and the yield of the gas products in the plasma-catalytic process for steam reforming of biomass tar. This was demonstrated by the improvement in the performance of plasma-catalytic steam reforming of toluene over the Ni/γ-Al$_2$O$_3$ catalyst in a coaxial DBD reactor. The performance of the plasma-catalysis hybrid process was further increased by increasing the Ni content from 5 wt.% to 20 wt.%. However, the energy efficiency of the plasma-catalytic process in the DBD reactor was limited due to the small feed flow rate.

As the gas exhaust from industries contains a mixture of tar, it is important to evaluate the influence of concentration and composition of tar on the conversion efficiency for plasma reforming process, a toluene and naphthalene additive was used. Both plasma-only and plasma-catalytic processes for conversion of tar mixture samples were performed in the GAD reactor. The plasma-catalytic process in the GAD reactor aims to investigate the feasibility of combining GAD with catalysts for the conversion of tar.

(1) For the plasma steam reforming of toluene and naphthalene, the conversion of toluene was higher than that of naphthalene. Increasing the initial concentration of toluene and naphthalene in the feed gas resulted in decreasing their removal efficiency in a GAD plasma with nitrogen and steam gas mixture. While increasing the inlet concentration of

naphthalene was in favour of energy efficiency due to the enhancement in the amount of the converted naphthalene.

(2) Increasing the specific energy input of the plasma system increased the conversion efficiency of toluene and naphthalene in a GAD plasma reactor with nitrogen-H_2O gas stream. The decomposition of tars in any plasma system is expected to increase with increasing the specific energy input as a result of increasing the active species generated in the plasma zone.

(3) H_2, CO and C_2H_2 were identified as the major gas products in the plasma reforming biomass tar, either the individual tar compound (toluene) or the tar mixture (toluene and naphthalene), with a trace amount of hydrocarbons (e.g. C_2H_4, C_2H_6 and C_3H_8). The yield of the main gas products strongly depended on the S/C molar ratio.

(4) The feasibility of the plasma-catalytic conversion of biomass tar in the GAD reactor was investigated using the 15Ni, 7.5Ni7.5Co and 15Co catalysts for steam reforming of toluene and naphthalene. The 7.5Ni7.5Co catalyst was found to be the best catalyst due to the easy reducibility of calcined 7.5Ni7.5Co catalyst and the synergy between Ni and Co in the Ni-Co alloying.

(5) The possible mechanisms and reaction pathways in the plasma process for the biomass tar conversion were proposed and discussed in detail based on the analysis of the gas and liquid samples and the formation of reactive species using OES under different experimental conditions.

To conclude, this work add a better understanding of the decomposition of biomass tar in GAD plasma in general and plasma-catalyst reactors in particular. Compared with other non-thermal plasma, such as corona and DBD, the GAD plasma could offer higher energy efficiency and has more potential to be used in industries. Besides, the current work also highlights the important effect of tar mixtures on the decomposition of these mixtures as well as the possible reaction mechanism in the plasma process.

7.2 Future work

This thesis mainly aims to investigate the performance of the plasma process for the conversion of the biomass tar (toluene and naphthalene) into value-added fuels and chemicals in the non-thermal plasma reactor (DBD and GAD). There is still much room for the improvement to develop a cost-effective and environmentally friendly approach of removal of the tar compound and re-utilisation of the carbon sources in the biomass tar. Based on the current experimental facilities, the following tasks are strongly recommended for steam reforming of tar within the current system:

(1) Currently, the plasma process for biomass conversion was generally performed using the individual tar compound and the simple carrier gas. This is far from the practical condition of the tar from the biomass gasification. It is suggested that the real composition of the producer gas is firstly used as the discharge gas for the plasma conversion of individual tar compound and /or the tar mixture. Then, it is important to investigate the performance of the plasma reactor under the practical biomass gasification condition by combing the plasma reactor with the biomass gasifier before the large-scale utilisation of the plasma reactor for biomass tar conversion.

(2) Although the igniter showed a good performance in the experiments reported here, its long exposure to high temperatures caused the connector between the electrodes and the bracket to melt. Hence, a ceramic connector could be adapted in this part to main the high temperature. Selection of the pipe material is also essential since high temperature are required to avoid the condensation of tar.

(3) The understanding on the detailed mechanism in the plasma-catalytic conversion of biomass tar is very limited. Much work is required to reveal the interaction between the plasma and the catalyst using the different catalyst characterisation approaches (e.g. in situ IR). Based on this information, suitable and cost-effective catalysts should be developed to enhance the conversion of tar and the corresponding energy efficiency, selectively produce the useful compounds and inhibit the formation of un-desired by-products.

(4) The energy efficiency of the plasma process in this study was still low for the large scale utilisation of this technology, although the enhancement in both tar conversion and

energy efficiency was achieved when combining the plasma process with catalysts. Therefore, in addition to the exploitation of the cost effective catalyst, measures should be taken to develop reactor with new design (e.g. 3D rotating GAD reactor) and optimise the reactor geometry, power supply and the plasma processing parameters.

REFERENCES

[1] U.S. Energy Information Administration. International Energy Outlook 2013 With Projections to 2040. 2013.

[2] Climate Change 2014 Synthesis Report. Intergovernmental Panel on Climate Change; 2015.

[3] Sikarwar VS, Zhao M, Clough P, Yao J, Zhong X, Memon MZ, et al. An overview of advances in biomass gasification. Energy & Environmental Science. 2016;9:2939-77.

[4] Hall DO. Biomass energy. Energy Policy. 1991;19:711-37.

[5] Sansaniwal SK, Pal K, Rosen MA, Tyagi SK. Recent advances in the development of biomass gasification technology: A comprehensive review. Renewable & Sustainable Energy Reviews. 2017;72:363-84.

[6] HM Government. The UK Low Carbon Transition Plan - National Strategy for Climate and Energy. London2009.

[7] Forestry Commission. A Woodfuel Strategy for England. Bristol2007.

[8] RCEP. Energy - The Changing Climate. London, Royal Commission on Environmental Pollution (RCEP). 2000.

[9] Pornmai K, Jindanin A, Sekiguchi H, Chavadej S. Synthesis gas production from CO_2-containing natural gas by combined steam reforming and partial oxidation in an AC gliding arc discharge. Plasma Chem Plasma P. 2012;32:723-42.

[10] Guan GQ, Kaewpanha M, Hao XG, Abudula A. Catalytic steam reforming of biomass tar: Prospects and challenges. Renewable & Sustainable Energy Reviews. 2016;58:450-61.

[11] Shahbaz M, Yusup S, Inayat A, Patrick DO, Ammar M. The influence of catalysts in biomass steam gasification and catalytic potential of coal bottom ash in biomass steam gasification: A review. Renewable & Sustainable Energy Reviews. 2017;73:468-76.

[12] Anis S, Zainal ZA. Tar reduction in biomass producer gas via mechanical, catalytic and thermal methods: Renewable & Sustainable Energy Reviews. 2011;15:2355-77.

[13] Claude V, Courson C, Kohler M, Lambert SD. Overview and essentials of biomass gasification technologies and their catalytic cleaning methods. Energy & Fuels. 2016;30:8791-814.

[14] Molino A, Chianese S, Musmarra D. Biomass gasification technology: The state of the art overview. Journal of Energy Chemistry. 2016;25:10-25.

[15] Sharma M, Rakesh N, Dasappa S. Solid oxide fuel cell operating with biomass derived producer gas: Status and challenges. Renewable & Sustainable Energy Reviews. 2016;60:450-63.

[16] Aravind PV, de Jong W. Evaluation of high temperature gas cleaning options for biomass gasification product gas for Solid Oxide Fuel Cells. Progress in Energy and Combustion Science. 2012;38:737-64.

[17] Li CS, Suzuki K. Tar property, analysis, reforming mechanism and model for biomass gasification: An overview. Renewable & Sustainable Energy Reviews. 2009; 13:594-604.

[18] Ahmed AMA, Salmiaton A, Choong TSY, Azlina W. Review of kinetic and equilibrium concepts for biomass tar modeling by using Aspen Plus. Renewable & Sustainable Energ Reviews. 2015;52:1623-44.

[19] Shen YF, Wang JF, Ge XL, Chen MD. By-products recycling for syngas cleanup in biomass pyrolysis: An overview. Renewable & Sustainable Energ Reviews. 2016;59:1246-68.

[20] Din ZU, Zainal ZA. Biomass integrated gasification-SOFC systems: Technology overview. Renewable & Sustainable Energ Reviews. 2016;53:1356-76.

[21] Din ZU, Zainal ZA. The fate of SOFC anodes under biomass producer gas contaminants. Renewable & Sustainable Energ Reviews. 2017;72:1050-66.

[22] Han J, Kim H. The reduction and control technology of tar during biomass gasification/pyrolysis: An overview. Renewable & Sustainable Energ Reviews. 2008;12:397-416.

[23] Shen YF, Yoshikawa K. Recent progresses in catalytic tar elimination during biomass gasification or pyrolysis: A review. Renewable & Sustainable Energ Reviews. 2013;21:371-92.

[24] Asadullah M. Barriers of commercial power generation using biomass gasification gas: A review. Renewable & Sustainable Energ Reviews. 2014;29:201-15.

[25] Shen YF. Chars as carbonaceous adsorbents/catalysts for tar elimination during biomass pyrolysis or gasification. Renewable & Sustainable Energ Reviews. 2015; 43:281-95.

[26] The chemistry behind the plasma display. Chemical Engirneering News. 2002;80:26-.

[27] Shen Y, Wang J, Ge X, Chen M. By-products recycling for syngas cleanup in biomass pyrolysis: An overview. Renewable & Sustainable Energ Reviews. 2016; 59:1246-68.

[28] Simell P, Ståhlberg P, Kurkela E, Albrecht J, Deutsch S, Sjöström K. Provisional protocol for the sampling and anlaysis of tar and particulates in the gas from large-scale biomass gasifiers. Version 1998. Biomass and Bioenergy. 2000;18:19-38.

[29] Simell P, Kurkela E, Ståhlberg P, Hepola J. Catalytic hot gas cleaning of gasification gas. Catalst Today. 1996;27:55-62.

[30] Corella J, Aznar M, Caballero M, Molina G, Toledo J. 140g H_2/kg biomass d.a.f. by a CO-shift reactor downstream from a FB biomass gasifier and a catalytic steam reformer. Int J Hydrogen Energ. 2008;33:1820-6.

[31] Li D, Tamura M, Nakagawa Y, Tomishige K. Metal catalysts for steam reforming of tar derived from the gasification of lignocellulosic biomass. Bioresour Technol. 2015;178:53-64.

[32] Polychronopoulou K, Fierro JLG, Efstathiou AM. The phenol steam reforming reaction over MgO-based supported Rh catalysts. J Catal. 2004;228:417-32.

[33] Furusawa T, Saito K, Kori Y, Miura Y, Sato M, Suzuki N. Steam reforming of naphthalene/benzene with various types of Pt- and Ni-based catalysts for hydrogen production. Fuel. 2013;103:111-21.

[34] Tomishige K, Asadullah M, Kunimori K. Syngas production by biomass gasification using $Rh/CeO_2/SiO_2$ catalysts and fluidized bed reactor. Catalyst Today. 2004;89:389-403.

[35] Guan G, Kaewpanha M, Hao X, Abudula A. Catalytic steam reforming of biomass tar: Prospects and challenges. Renewable & Sustainable Energy Reviews. 2016;58:450-61.

[36] Virginie M, Courson C, Niznansky D, Chaoui N, Kiennemann A. Characterization and reactivity in toluene reforming of a Fe/olivine catalyst designed for gas cleanup in biomass gasification. Applied Catalysis B: Environmental. 2010;101:90-100.

[37] Anis S, Zainal ZA. Tar reduction in biomass producer gas via mechanical, catalytic and thermal methods: A review. Renewable and Sustainable Energy Reviews. 2011; 15:2355-77.

[38] Dou B, Gao J, Sha X, Baek SW. Catalytic cracking of tar component from high-temperature fuel gas. Applied Thermal Engineers. 2003;23:2229-39.

[39] Abu El-Rub Z, Bramer EA, Brem G. Review of catalysts for tar elimination in biomass gasification processes. Ind Eng Chem Res. 2004;43:6911-9.

[40] Bhandari PN, Kumar A, Bellmer DD, Huhnke RL. Synthesis and evaluation of biochar-derived catalysts for removal of toluene (model tar) from biomass-generated producer gas. Renew Energ. 2014;66:346-53.

[41] Wang Y, Hu X, Song Y, Min ZH, Mourant D, Li TT, et al. Catalytic steam reforming of cellulose-derived compounds using a char-supported iron catalyst. Fuel Process Technol. 2013;116:234-40.

[42] Min Z, Yimsiri P, Asadullah M, Zhang S, Li C-Z. Catalytic reforming of tar during gasification. Part II. Char as a catalyst or as a catalyst support for tar reforming. Fuel. 2011;90:2545-52.

[43] Wang L, Li D, Koike M, Watanabe H, Xu Y, Nakagawa Y, et al. Catalytic performance and characterization of Ni–Co catalysts for the steam reforming of biomass tar to synthesis gas. Fuel. 2013;112:654-61.

[44] Liu XJ, Yang XQ, Liu C, Chen P, Yue XM, Zhang SQ. Low-temperature catalytic steam reforming of toluene over activated carbon supported nickel catalysts. Journal of the Taiwan Institute of Chemical Engineers. 2016;65:233-41.

[45] Koike M, Li D, Nakagawa Y, Tomishige K. A highly active and coke-resistant steam reforming catalyst comprising uniform nickel-iron alloy nanoparticles. Chemsuschem. 2012;5:2312-4.

[46] Li C, Hirabayashi D, Suzuki K. A crucial role of O_2^- and O_{22}^- on mayenite structure for biomass tar steam reforming over $Ni/Ca_{12}Al_{14}O_{33}$. Applied Catalysis B: Environmental. 2009;88:351-60.

[47] Park HJ, Park SH, Sohn JM, Park J, Jeon JK, Kim SS, et al. Steam reforming of biomass gasification tar using benzene as a model compound over various Ni supported metal oxide catalysts. Bioresour Technol. 2010;101 Suppl 1:S101-3.

[48] Sekine Y, Mukai D, Murai Y, Tochiya S, Izutsu Y, Sekiguchi K, et al. Steam reforming of toluene over perovskite-supported Ni catalysts. Applied Catalysis A: General. 2013;451:160-7.

[49] Chun YN, Kim SC, Yoshikawa K. Decomposition of benzene as a surrogate tar in a gliding arc plasma. Environment Prog Sustain Energy. 2013;32:837-45.

[50] Eliott RM, Nogueira MFM, Sobrinho ASS, Couto BAP, Maciel HS, Lacava PT. Tar reforming under a microwave plasma torch. Energy Fuels. 2013;27:1174-81.

[51] Nair SA, Pemen AJM, Yan K, van Gompel FM, van Leuken HEM, van Heesch EJM, et al. Tar removal from biomass-derived fuel gas by pulsed corona discharges. Fuel Process Technol. 2003;84:161-73.

[52] Tao K, Ohta N, Liu GQ, Yoneyama Y, Wang T, Tsubaki N. Plasma enhanced catalytic reforming of biomass tar model compound to syngas. Fuel. 2013;104:53-7.

[53] Zhu FS, Li XD, Zhang H, Wu AJ, Yan JH, Ni MJ, et al. Destruction of toluene by rotating gliding arc discharge. Fuel. 2016;176:78-85.

[54] Liu SY, Mei DH, Shen Z, Tu X. Nonoxidative conversion of methane in a dielectric barrier discharge reactor: Prediction of reaction performance based on neural network model. The Journal of Physical Chemistry C. 2014;118:10686-93.

[55] Tu X, Whitehead JC. Plasma-catalytic dry reforming of methane in an atmospheric dielectric barrier discharge: Understanding the synergistic effect at low temperature. Applied Catalysis B: Environmental. 2012;125:439-48.

[56] Mei DH, Zhu XB, He YL, Yan JD, Tu X. Plasma-assisted conversion of CO_2 in a dielectric barrier discharge reactor: Understanding the effect of packing materials. Plasma Sources Science & Technology. 2015;24.

[57] Mei D, Zhu X, Wu C, Ashford B, Williams PT, Tu X. Plasma-photocatalytic conversion of CO_2 at low temperatures: Understanding the synergistic effect of plasma-catalysis. Applied Catalysis B: Environmental. 2016;182:525-32.

[58] Zhang H, Zhu F, Li X, Cen K, Du C, Tu X. Enhanced hydrogen production by methanol decomposition using a novel rotating gliding arc discharge plasma. Rsc Advances. 2016;6:12770-81.

[59] Wang L, Liu SY, Xu C, Tu X. Direct conversion of methanol to n-C_4H_{10} and H_2 in a dielectric barrier discharge reactor. Green Chemistry. 2016;18:5658-66.

[60] Crookes W. Contributions to molecular physics in high vacua. magnetic deflection of molecular trajectory. Laws of magnetic rotation in high and low vacua. Phosphorogenic properties of molecular discharge. Philosophical Transactions of the Royal Society of London. 1879;170:641-62.

[61] Tonks L, Langmuir I. Oscillations in ionized gases. Physical Review. 1929;33:195-210.

[62] Mir SA, Shah MA, Mir MM. Understanding the role of plasma technology in food industry. Food Bioprocess Technol. 2016;9:734-50.

[63] Liao XY, Liu DH, Xiang QS, Ahn J, Chen SG, Ye XQ, et al. Inactivation mechanisms of non-thermal plasma on microbes: A review. Food Control. 2017;75:83-91.

[64] Conrads H, Schmidt M. Plasma generation and plasma sources. Plasma Sources Science & Technology. 2000;9:441-54.

[65] Mei D. Plasma-catalytic conversion of greenhouse gas into value-added fuels and chemicals. Liverpool: University of Liverpool; 2016.

[66] Bardos L, Barankova H. Cold atmospheric plasma: Sources, processes, and applications. Thin Solid Films. 2010;518:6705-13.

[67] Surowsky B, Schlüter O, Knorr D. Interactions of non-thermal atmospheric pressure plasma with solid and liquid food systems: A Review. Food Engineeering Reviews. 2015;7:82-108.

[68] Jiang B, Zheng JT, Qiu S, Wu MB, Zhang QH, Yan ZF, et al. Review on electrical discharge plasma technology for wastewater remediation. Chemical Engineering Journal. 2014;236:348-68.

[69] Fridman A, Kennedy LA. Plasma physics and engineering. New York: Taylor & Francis Inc.; 2004.

[70] Prantsidou M. Plasma methods for the clean-up of organic liquid waste. Manchester: The University of Manchester; 2013.

[71] Zhang H, Ma DY, Qiu RL, Tang YT, Du CM. Non-thermal plasma technology for organic contaminated soil remediation: A review. Chemical Engineering Journal. 2017;313:157-70.

[72] Witvrouwen T, Paulussen S, Sels B. The use of non-equilibrium plasmas for the synthesis of heterogeneous catalysts. Plasma Processes and Polymers. 2012;9:750-60.

[73] Petitpas G, Rollier JD, Darmon A, Gonzalez-Aguilar J, Metkemeijer R, Fulcheri L. A comparative study of non-thermal plasma assisted reforming technologies. International Journal of Hydrogen Energy. 2007;32:2848-67.

[74] Randeniya LK, de Groot G. Non-thermal plasma treatment of agricultural seeds for stimulation of germination, removal of surface contamination and other benefits: A review. Plasma Processes and Polymers. 2015;12:608-23.

[75] Raizer YP. Gas Discharge Physics: Springer; 1991.

[76] Talebizadeh P, Babaie M, Brown R, Rahimzadeh H, Ristovski Z, Arai M. The role of non-thermal plasma technique in NO_x treatment: Renewable and Sustainable Energy Reviews. 2014;40:886-901.

[77] Liu CJ, Xu GH, Wang TM. Non-thermal plasma approaches in CO_2 utilization. Fuel Processing Technology. 1999;58.

[78] Tatarova E, Bundaleska N, Sarrette JP, Ferreira CM. Plasmas for environmental issues: from hydrogen production to 2D materials assembly. Plasma Sources Science & Technology. 2014;23:52.

[79] Eliasson B, Kogelschatz U. Nonequilibrium volume plasma chemical-processing. IEEE Transactions on Plasma Science. 1991;19:1063-77.

[80] Kajiyama H, Utsumi F, Nakamura K, Tanaka H, Toyokuni S, Hori M, et al. Future perspective of strategic non-thermal plasma therapy for cancer treatment. Journal of Clinical Biochemistry and Nutrition. 2017;60:33-8.

[81] Tanaka H, Hori M. Medical applications of non-thermal atmospheric pressure plasma. Journal of Clinical Biochemistry and Nutrition. 2017;60:29-32.

[82] Thevenet F, Sivachandiran L, Guaitella O, Barakat C, Rousseau A. Plasma-catalyst coupling for volatile organic compound removal and indoor air treatment: A review. Journal of Physics D: Applied Physics. 2014;47:224011.

[83] Locke BR, Sato M, Sunka P, Hoffmann MR, Chang JS. Electrohydraulic discharge and nonthermal plasma for water treatment. Industrial & Engineering Chemistry Research. 2006;45:882-905.

[84] Brisset JL, Moussa D, Doubla A, Hnatiuc E, Hnatiuc B, Youbi GK, et al. Chemical reactivity of discharges and temporal post-discharges in plasma treatment of aqueous media: Examples of gliding discharge treated solutions. Industrial & Engineering Chemistry Research. 2008;47:5761-81.

[85] Misra NN, Koubaa M, Roohinejad S, Juliano P, Alpas H, Inacio RS, et al. Landmarks in the historical development of twenty first century food processing technologies. Food Research International. 2017;97:318-39.

[86] Chung WC, Chang MB. Review of catalysis and plasma performance on dry reforming of CH_4 and possible synergistic effects. Renewable & Sustainable Energy Reviews. 2016;62:13-31.

[87] Srivastava MPK, Akira. Carbon dioxide decomposition by plasma methods and application of high energy and high density plasma in material processing and nanostructures. Transaction of JWRI. 2010;39:11-25.

[88] Tatarova E, Bundaleska N, Sarrette JP, Ferreira CM. Plasmas for environmental issues: from hydrogen production to 2D materials assembly. Plasma Sources Science & Technology. 2014;23:063002.

[89] Chen FQ, Huang XY, Cheng DG, Zhan XL. Hydrogen production from alcohols and ethers cold plasma: A review. International Journal of Hydrogen Energy. 2014;39:9036-46.

[90] Du CM, Mo JM, Li HX. Renewable Hydrogen Production by Alcohols Reforming Using Plasma and Plasma-Catalytic Technologies: Challenges and Opportunities. Chem Rev. 2015;115:1503-42.

[91] Ashford B, Tu X. Non-thermal plasma technology for the conversion of CO_2. Current Opinion in Green and Sustainable Chemistry. 2017;3:45-9.

[92] Zille A, Oliveira FR, Souto AP. Plasma treatment in textile industry. Plasma Processes and Polymers. 2015;12:98-131.

[93] Geyter ND, Morent R. Nonthermal plasma sterilization of living and nonliving surfaces. Annu Reviwe of Biomedical Engineering. 2012;14:255-74.

[94] Cheng YL, Wang YK, Chen P, Deng SB, Ruan R. Non-thermal plasma assisted polymer surface modification and synthesis: A review. International Journal of Agricultural and Biological Engineering. 2014;7:1-9.

[95] Kortshagen UR, Sankaran RM, Pereira RN, Girshick SL, Wu JJ, Aydil ES. Nonthermal plasma synthesis of nanocrystals: Fundamental principles, materials, and applications. Chemical Reviews. 2016;116:11061-127.

[96] Liu CJ, Li MY, Wang JQ, Zhou XT, Guo QT, Yan JM, et al. Plasma methods for preparing green catalysts: Current status and perspective. Chinese Journal of Catalysis. 2016;37:340-8.

[97] Kim HH. Nonthermal plasma processing for air-pollution control: A historical review, current issues, and future prospects. Plasma Processes and Polymers. 2004; 1: 91-110.

[98] Nehra V, Kumar A, Dwivedi HK. Atmospheric Non-thermal plasma sources. International Journal of Engineering. 2008;2:53-68.

[99] Vandenbroucke AM, Morent R, De Geyter N, Leys C. Non-thermal plasmas for non-catalytic and catalytic VOC abatement. Journal of Hazardous Materials. 2011; 195: 30-54.

[100] Ehlbeck J, Schnabel U, Polak M, Winter J, von Woedtke T, Brandenburg R, Low temperature atmospheric pressure plasma sources for microbial decontamination. Journal of Physics D: Applied Physics. 2011;44:013002.

[101] Chang JS, Lawless PA, Yamamoto T. Corona discharge processes. IEEE Transactions on Plasma Science. 1991;19:1152-66.

[102] Ma SM, Zhao YC, Yang JP, Zhang SB, Zhang JY, Zheng CG. Research progress of pollutants removal from coal-fired flue gas using non-thermal plasma. Renewable and Sustainable Energy Reviews. 2017;67:791-810.

[103] Ohkubo T, Kanazawa S, Nomoto Y, Jen-Shih C, Adachi T. NO_x removal by a pipe with nozzle-plate electrode corona discharge system. IEEE Transactions on Industry Applications. 1994;30:856-61.

[104] Ohkubo T, Kanazawa S, Nomoto Y, Chang JS, Adachi T. Time dependence of NO_x removal rate by a corona radical shower system. IEEE Transactions on Industry Applications. 1996;32:1058-62.

[105] Moreau M, Orange N, Feuilloley MGJ. Non-thermal plasma technologies: New tools for bio-decontamination. Biotechnology Advances. 2008;26:610-7.

[106] Kogelschatz U. Dielectric-barrier discharges: Their history, discharge physics, and industrial applications. Plasma Chemistry and Plasma Processing. 2003;23:1-46.

[107] Fridman A, Chirokov A, Gutsol A. Non-thermal atmospheric pressure discharges. Journal of Physics D: Applied Physics. 2005;38:R1-R24.

[108] Istadi, Amin NAS. Co-generation of synthesis gas and C_{2+} hydrocarbons from methane and carbon dioxide in a hybrid catalytic-plasma reactor: A review. Fuel. 2006;85:577-92.

[109] Eliasson B, Hirth M, Kogelschatz U. Ozone synthesis from oxygen in dielectric barrier discharges. Journal of Physics D: Applied Physics. 1987;20:1421-37.

[110] Kogelschatz U, Eliasson B, Egli W. From ozone generators to flat television screens: history and future potential of dielectric-barrier discharges. Pure and Applied Chemistry. 1999:1819-28.

[111] Kogelschatz U. Filamentary, patterned, and diffuse barrier discharges. IEEE Transactions on Plasma Science. 2002;30:1400-8.

[112] Urashima K, Chang JS, Ito T. Reduction of NO_x from combustion flue gases by superimposed barrier discharge plasma reactors. IEEE Transactions on Industry Applications. 1997;33:879-86.

[113] Xiao G, Xu WP, Wu RB, Ni MJ, Du CM, Gao X, et al. Non-thermal plasmas for VOCs abatement. Plasma Chemistry and Plasma Processing. 2014;34:1033-65.

[114] Chen HL, Lee HM, Chen SH, Chang MB. Review of packed-bed plasma reactor for ozone generation and air pollution control. Industrial & Engineering Chemistry Research. 2008;47:2122-30.

[115] Lesueur H, Czernichowshi A, Chapelle, J. Design for generating low-temperature plasmas by formation of sliding electric discharges. French1988.

[116] Czernichowski A. Gliding arc applications to engineering and environment control. Pure and Applied Chemistry. 1994;66:1301-10.

[117] Fridman A, Nester S, Kennedy LA, Saveliev A, Mutaf-Yardimci O. Gliding arc gas discharge. Progress in Energy and Combustion Science. 1999;25:211-31.

[118] Mutaf-Yardimci O, Saveliev AV, Fridman AA, Kennedy LA. Thermal and nonthermal regimes of gliding arc discharge in air flow. Journal of Applied Physics. 2000;87:1632-41.

[119] Richard F, Cormier JM, Pellerin S, Chapelle J. Physical study of a gliding arc discharge. Journal of Applied Physics. 1996;79: 10.1063/1.361188.

[120] Liventsov VP, B.; Raddatis, V.;Rusanov, V.; Sevalnikov, A.; Fridman A. . Discharge scaling in plasma chemistry. Sov Phys High Temp Thermophys. 1989;27:220-5.

[121] Ju YG, Sun WT. Plasma assisted combustion: Dynamics and chemistry. Progress in Energy and Combustion Science. 2015;48:21-83.

[122] Bo Z. Fundamental research of the treatment of volatile organic compounds with gliding arc discharge plasma. Hangzhou, Zhejiang: Zhejiang University; 2008.

[123] Lee DH, Kim KT, Cha MS, Song YH. Plasma-controlled chemistry in plasma reforming of methane. International Journal of Hydrogen Energy. 2010;35:10967-76.

[124] Du C, Li H, Zhang L, Wang J, Huang D, Xiao M, et al. Hydrogen production by steam-oxidative reforming of bio-ethanol assisted by Laval nozzle arc discharge. International Journal of Hydrogen Energy. 2012;37:8318-29.

[125] Gangoli SP, Gutsol AF, Fridman AA. A non-equilibrium plasma source: magnetically stabilized gliding arc discharge: I. Design and diagnostics. Plasma Sources Science & Technology. 2010;19: 065003.

[126] Kalra CS, Cho YI, Gutsol A, Fridman A, Rufael TS. Gliding arc in tornado using a reverse vortex flow. Review of Scientific Instruments. 2005;76: 025110.

[127] Thevenet F, Sivachandiran L, Guaitella O, Barakat C, Rousseau A. Plasma-catalyst coupling for volatile organic compound removal and indoor air treatment: A review. Journal of Physics D: Applied Physics. 2014;47:14.

[128] Van Durme J, Dewulf J, Leys C, Van Langenhove H. Combining non-thermal plasma with heterogeneous catalysis in waste gas treatment: A review. Applied Catalysis B: Environmental. 2008;78:324-33.

[129] Whitehead JC. Plasma catalysis: A solution for environmental problems. Pure and Applied Chemistry. 2010;82.

[130] Neyts EC, A B. Understanding plasma catalysis through modelling and simulation-a review. Journal of Physics D: Applied Physics. 2014;47:224010.

[131] Neyts EC. Plasma-surface interactions in plasma catalysis. Plasma Chemistry and Plasma Processing. 2015;36:185-212.

[132] Neyts EC, Ostrikov K, Sunkara MK, Bogaerts A. Plasma catalysis: Synergistic effects at the Nnanoscale. Chemical Reviews. 2015;115:13408-46.

[133] Whitehead JC. Plasma–catalysis: the known knowns, the known unknowns and the unknown unknowns. Journal of Physics D: Applied Physics. 2016;49:243001.

[134] Whitehead JC. Plasma catalysis: A solution for environmental problems. Pure and Applied Chemistry. 2010;82:1329-36.

[135] Futamura S, Einaga H, Kabashima H, Hwan LY. Synergistic effect of silent discharge plasma and catalysts on benzene decomposition. Catalysis Today. 2004;89:89-95.

[136] Mizushima T, Matsumoto K, Sugoh J, Ohkita H, Kakuta N. Tubular membrane-like catalyst for reactor with dielectric-barrier-discharge plasma and its performance in ammonia synthesis. Applied Catalysis A: General. 2004;265:53-9.

[137] Nair SA, Pemen AJM, Yan K, van Heesch EJM, Ptasinski KJ, Drinkenburg AAH. Chemical processes in tar removal from biomass derived fuel gas by pulsed corona discharges. Plasma Chemistry and Plasma Processing. 2003;23:665-80.

[138] Pemen AJM, Nair SA, Yan K, van Heesch EJM, Ptasinski KJ, Drinkenburg AAH. Pulsed corona discharges for tar removal from biomass derived fuel gas. Plasmas and Polymers. 2003;8:209-24.

[139] Nair SA, Yan K, Pemen AJM, Winands GJJ, van Gompel FM, van Leuken HEM. A high-temperature pulsed corona plasma system for fuel gas cleaning. Journal of Electrostatics. 2004;61:117-27.

[140] Nair SA, Yan K, Safitri A, Pemen AJM, van Heesch EJM, Ptasinski KJ, et al. Streamer corona plasma for fuel gas cleaning: comparison of energization techniques. Journal of Electrostatics. 2005;63:1105-14.

[141] Nair SA, Yan K, Pemen AJM, van Heesch EJM, Ptasinski KJ, Drinkenburg AAH. Tar removal from biomass derived fuel gas by pulsed corona discharges: Chemical kinetic study II. Industrial & Engineering Chemistry Research. 2005;44:1734–41.

[142] Wnukowski M. Decomposition of tars in microwave plasma – preliminary results. Journal of Ecological Engineering. 2014;15:23-8.

[143] Chun YN, Kim SC, Yoshikawa K. Destruction of anthracene using a gliding arc plasma reformer. Korean Journal of Chemical Engineering. 2011;28:1713-20.

[144] Yang YC, Chun YN. Naphthalene destruction performance from tar model compound using a gliding arc plasma reformer. Korean Journal of Chemical Engineering. 2011;28:539-43.

[145] Tu X, Whitehead JC. Plasma-catalytic dry reforming of methane in an atmospheric dielectric barrier discharge: Understanding the synergistic effect at low temperature. Applied Catalysis B: Environmental. 2012;125:439-48.

[146] Gallon HJ. Dry reforming of methane using non-thermal plasma-catalysis [PhD]. Manchester: The University of Manchester; 2010.

[147] Mei D, Zhu X, He Y-L, Yan JD, Tu X. Plasma-assisted conversion of CO_2 in a dielectric barrier discharge reactor: understanding the effect of packing materials. Plasma Sources Science and Technology. 2015;24:015011.

[148] Fridman A, Nester S, Kennedy LA, Saveliev A, Mutaf-Yardimci O. Gliding arc gas discharge. Progress in Energy and Combustion Science. 1999;25:211-31.

[149] Tu X, Whitehead JC. Plasma dry reforming of methane in an atmospheric pressure AC gliding arc discharge: Co-generation of syngas and carbon nanomaterials. International Journal of Hydrogen Energy. 2014;39:9658-69.

[150] Tippayawong N, Inthasan P. Investigation of light tar cracking in a gliding arc plasma system. International Journal of Chemical Reactor Engineering. 2010;8: A50.

[151] Swierczynski D, Courson C, Kiennemann A. Study of steam reforming of toluene used as model compound of tar produced by biomass gasification. Chemical Engineering and Processing. 2008;47:508-13.

[152] Van Durme J, Dewulf J, Sysmans W, Leys C, Van Langenhove H. Abatement and degradation pathways of toluene in indoor air by positive corona discharge. Chemosphere. 2007;68:1821-9.

[153] Manion JA, Huie RE, Levin RD, Burgess Jr. DR, Orkin VL, Tsang W. NIST Chemical Kinetics Database, NIST Standard Reference Database 17. 2015.12 ed. Gaithersburg, Maryland, 2015.

[154] Zhang H, Zhu F, Li X, Cen K, Du C, Tu X. Rotating gliding arc assisted water splitting in atmospheric nitrogen. Plasma Chemistry & Plasma Processing. 2016;36:813-34.

[155] Lim M.S, Chun Y.N. Light tar decomposition of product pyrolysis gas from sewage sludge in a gliding arc plasma reformer. Environmental Engineering Research. 2012;17:89-94.

[156] Trushkin AN, Kochetov IV. Simulation of toluene decomposition in a pulse-periodic discharge operating in a mixture of molecular nitrogen and oxygen. Plasma Physics Reports. 2012;38:407-31.

[157] Nunnally T, Tsangaris A, Rabinovich A, Nirenberg G, Chernets I, Fridman A. Gliding arc plasma oxidative steam reforming of a simulated syngas containing naphthalene and toluene. International Journal of Hydrogen Energy. 2014;39:11976-89.

[158] Ge H, Hu DX, Li XG, Tian Y, Chen ZB, Zhu YM. Removal of low-concentration benzene in indoor air with plasma-MnO2 catalysis system. Journal of Electrostatics. 2015;76:216-21.

[159] Zhang HR, Eddings EG, Sarofim AF. Modeling benzene and naphthalene formation in a premixed propylene flame. Fall Technical Meeting of the Western States Section of the Combustion Institute 2005. United States, Stanford: Western States Section/Combustion Institute; 2005. p 657-75.

[160] Kohno H, Berezin AA, Jen-Shih C, Tamura M, Yamamoto T, Shibuya A, et al. Destruction of volatile organic compounds used in a semiconductor industry by a capillary tube discharge reactor. IEEE Transactions on Industrial Applications. 1998; 34:953-66.

[161] Yu L, Li X, Tu X, Wang Y, Lu S, Yan J. Decomposition of naphthalene by dc gliding arc gas discharge. Journal of Physical Chemistry A. 2010;114:360-8.

[162] Huang H, Ye D, Leung DYC, Feng F, Guan X. Byproducts and pathways of toluene destruction via plasma-catalysis. Journal of Molecular Catalysis A: Chemical. 2011;336:87-93.

[163] Du CM, Yan JH, Cheron B. Decomposition of toluene in a gliding arc discharge plasma reactor. Plasma Sources Science & Technology. 2007;16:791-7.

[164] Blin-Simiand N, Jorand F, Magne L, Pasquiers S, Postel C, Vacher JR. Plasma reactivity and plasma-surface interactions during treatment of toluene by a dielectric barrier discharge. Plasma Chemistry and Plasma Processing. 2008;28:429-66.

[165] Abdelaziz AA, Seto T, Abdel-Salam M, Otani Y. Influence of N_2/O_2 mixtures on decomposition of naphthalene in surface dielectric barrier discharge based reactor. Plasma Chemistry and Plasma Processing. 2014;34:1371-85.

[166] Aerts R, Tu X, De Bie C, Whitehead JC, Bogaerts A. An investigation into the dominant reactions for ehylene destruction in non-thermal atmospheric plasmas. Plasma Processes and Polymers. 2012;9:994-1000.

[167] Zhu X, Gao X, Qin R, Zeng Y, Qu R, Zheng C, et al. Plasma-catalytic removal of formaldehyde over Cu-Ce catalysts in a dielectric barrier discharge reactor. Applied Catalysis B: Environmental. 2015;170:293-300.

[168] Trushkin AN, Grushin ME, Kochetov IV, Trushkin NI, Akishev YS. Decomposition of toluene in a steady-state atmospheric-pressure glow discharge. Plasma Physics Reports. 2013;39:167-82.

[169] Bartolotti LJ, Edney EO. Density functional theory derived intermediates from the OH initiated atmospheric oxidation of toluene. Chemical Physics Letters. 1995; 245: 119-22.

[170] Lu SY, Sun XM, Li XD, Yan JH, Du CM. Decomposition of toluene in a rotating glidarc discharge reactor. IEEE Transactions on Industrial Applications. 2012;40:2151-6.

[171] Liu S, Mei D, Wang L, Tu X. Steam reforming of toluene as biomass tar model compound in a gliding arc discharge reactor. Chemical Engineering Journal. 2017;307:793-802.

[172] Kong M, Yang Q, Fei J, Zheng X. Experimental study of Ni/MgO catalyst in carbon dioxide reforming of toluene, a model compound of tar from biomass gasification. International Journal of Hydrogen Energy. 2012;37:13355-64.

[173] Chen T, Liu H, Shi P, Chen D, Song L, He H, et al. CO_2 reforming of toluene as model compound of biomass tar on Ni/Palygorskite. Fuel. 2013;107:699-705.

[174] Lindon MA, Scime EE. CO_2 dissociation using the Versatile atmospheric dielectric barrier discharge experiment (VADER). Frontiers in Physics. 2014;2.

[175] Bityurin VA, Filimonova EA, Naidis GV. Simulation of naphthalene conversion in biogas initiated by pulsed corona discharges. IEEE Transactions on Plasma Science. 2009;37:911-9.

[176] Machala Z, Morvová M, Marode E, Morva I. Removal of cyclohexanone in transition electric discharges at atmospheric pressure. Journal of Physics D: Applied Physics. 2000;33:3198-213.

[177] Xiao Z, Xu D, Hao C, Qiu J, Liu K. High concentration xylene decomposition and diagnostic analysis by non-thermal plasma in a DBD reactor. Plasma Science and Technology. 2017;19:064009.

[178] Yu L, Tu X, Li X, Wang Y, Chi Y, Yan J. Destruction of acenaphthene, fluorene, anthracene and pyrene by a dc gliding arc plasma reactor. Journal of Hazardous Materials. 2010;180:449-55.

[179] Bao X, Kong M, Lu W, Fei J, Zheng X. Performance of Co/MgO catalyst for CO_2 reforming of toluene as a model compound of tar derived from biomass gasification. Journal of Energy Chemistry. 2014;23:795-800.

[180] Zhu X, Gao X, Zheng C, Wang Z, Ni M, Tu X. Plasma-catalytic removal of a low concentration of acetone in humid conditions. RSC Advances. 2014;4:37796.

[181] Abdelaziz AA, Seto T, Abdel-Salam M, Otani Y. Influence of nitrogen excited species on the destruction of naphthalene in nitrogen and air using surface dielectric barrier discharge. Journal of Hazardous Materials. 2013;246-247:26-33.

[182] Lee S, Liu S-J. OES and GC/MS study of RF plasma of xylenes. Plasma Chemistry and Plasma Processing. 2016;37:149-58.

[183] Bityurin VA, Filimonova EA, Naidis GV. Mechanisms of conversion of heavy hydrocarbons in biogas initiated by pulsed corona discharges. 2008:135-42.

[184] Abdelaziz AA, Seto T, Abdel-Salam M, Otani Y. Performance of a surface dielectric barrier discharge based reactor for destruction of naphthalene in an air stream. Journal of Physics D: Applied Physics. 2012;45:115201.

[185] Sleiman M, Conchon P, Ferronato C, Chovelon J-M. Photocatalytic oxidation of toluene at indoor air levels (ppbv): Towards a better assessment of conversion, reaction intermediates and mineralization. Applied Catalysis B: Environmental. 2009;86:159-65.

[186] Liang W, Li J, Li J, Jin Y. Abatement of toluene from gas streams via ferro-electric packed bed dielectric barrier discharge plasma. Journal of Hazardous Materials. 2009;170:633-8.

[187] Norinaga K, Yang H, Tanaka R, Appari S, Iwanaga K, Takashima Y, et al. A mechanistic study on the reaction pathways leading to benzene and naphthalene in cellulose vapor phase cracking. Biomass and Bioenergy. 2014;69:144-54.

[188] Lee HM. Abatement of gas-phase p-xylene via dielectric barrier discharges. Plasma Chem Plasma P. 2003;23:541-58.

[189] Zhu X, Gao X, Qin R, Zeng Y, Qu R, Zheng C, et al. Plasma-catalytic removal of formaldehyde over Cu–Ce catalysts in a dielectric barrier discharge reactor. Applied Catalysis B: Environmental. 2015;170-171:293-300.

[190] Mei D, Ashford B, He Y-L, Tu X. Plasma-catalytic reforming of biogas over supported Ni catalysts in a dielectric barrier discharge reactor: Effect of catalyst supports. Plasma Processes and Polymers. 2017;14:e1600076.

[191] Eliott RM, Nogueira MFM, Silva Sobrinho AS, Couto BAP, Maciel HS, Lacava PT. Tar reforming under a microwave plasma torch. Energ Fuel. 2013;27:1174-81.

[192] Istadi, Amin N. Co-generation of synthesis gas and C$_2$+ hydrocarbons from methane and carbon dioxide in a hybrid catalytic-plasma reactor: A review. Fuel. 2006;85:577-92.

[193] Aziznia A, Bozorgzadeh HR, Seyed-Matin N, Baghalha M, Mohamadalizadeh A. Comparison of dry reforming of methane in low temperature hybrid plasma-catalytic corona with thermal catalytic reactor over Ni/γ-Al$_2$O$_3$. Journal of Natural Gas Chemistry. 2012;21:466-75.

[194] Wang D. Study of Ni/Char catalyst for biomass gasification in an updraft gasifier: influence of catalyst granular size on catalytic performance. Bioresources. 2013;8:3479-89.

[195] Aziz MAA, Jalil AA, Triwahyono S, Saad MWA. CO$_2$ methanation over Ni-promoted mesostructured silica nanoparticles: Influence of Ni loading and water vapor on activity and response surface methodology studies. Chemical Engineering Journal. 2015;260:757-64.

[196] Srivastava N, Wang CJ. Effects of water addition on OH radical generation and plasma properties in an atmospheric argon microwave plasma jet. Journal of Applied Physics. 2011;110:053304.

[197] Guo Y.F, Ye D Q, Chen K.F, He J.C. Toluene removal by a DBD-type plasma combined with metal oxides catalysts supported by nickel foam. Catalysis Today. 2007;126:328-37.

[198] Morgan. LXCat database. 2016.

[199] Taghvaei H, Jahanmiri A, Rahimpour MR, Shirazi MM, Hooshmand N. Hydrogen production through plasma cracking of hydrocarbons: Effect of carrier gas and hydrocarbon type. Chemical Engineering Journal. 2013;226:384-92.

[200] Nozaki T, Tsukijihara H, Fukui W, Okazaki K. Kinetic analysis of the catalyst and nonthermal plasma hybrid reaction for methane steam reforming. Energy Fuel. 2007;21:2525-30.

[201] Artetxe M, Nahil MA, Olazar M, Williams PT. Steam reforming of phenol as biomass tar model compound over Ni/Al$_2$O$_3$ catalyst. Fuel. 2016;184:629-36.

[202] Quitete CPB, Bittencourt RCP, Souza M. Steam reforming of tar model compounds over nickel catalysts supported on barium hexaaluminate. Catalysis Letters. 2015;145:541-8.

[203] Artetxe M, Alvarez J, Nahil MA, Olazar M, Williams PT. Steam reforming of different biomass tar model compounds over Ni/Al$_2$O$_3$ catalysts. Energy Conversion and Management. 2017;136:119-26.

[204] Liu SY, Mei DH, Nahil MA, Gadkari S, Gu S, Williams PT, et al. Hybrid plasma-catalytic steam reforming of toluene as a biomass tar model compound over Ni/Al$_2$O$_3$ catalysts. Fuel Processing Technology. 2017;166:269-75.

[205] Qian KZ, Kumar A. Catalytic reforming of toluene and naphthalene (model tar) by char supported nickel catalyst. Fuel. 2017;187:128-36.

[206] Zhang H, Li X, Zhu F, Bo Z, Cen K, Tu X. Non-oxidative decomposition of methanol into hydrogen in a rotating gliding arc plasma reactor. International Journal of Hydrogen Energy. 2015;40:15901-12.

[207] Akashi-Ronquest M, Amaudruz PA, Batygov M, Beltran B, Bodmer M, Boulay MG, et al. Improving photoelectron counting and particle identification in scintillation detectors with Bayesian techniques. Astroparticle Physics. 2015;65:40-54.

[208] Zipf EC, McLaughlin RW. On the dissociation of nitrogen by electron impact and by E.U.V. photo-absorption. Planetary and Space Science. 1978;26:449-62.

[209] Rehman F, Lozano-Parada JH, Zimmerman WB. A kinetic model for H_2 production by plasmolysis of water vapours at atmospheric pressure in a dielectric barrier discharge microchannel reactor. Int J Hydrogen Energ. 2012;37:17678-90.

[210] Zhang H, Du CM, Wu AJ, Bo Z, Yan JH, Li XD. Rotating gliding arc assisted methane decomposition in nitrogen for hydrogen production. International Journal of Hydrogen Energy. 2014;39:12620-35.

[211] Bruggeman P, Schram D, González MÁ, Rego R, Kong MG, Leys C. Characterization of a direct dc-excited discharge in water by optical emission spectroscopy. Plasma Sources Science and Technology. 2009;18:025017.

[212] Czernichowski A, Nassar H, Ranaivosoloarimanana A, Fridman AA, Simek M, Musiol K, et al. Spectral and electrical diagnostics of gliding arc. Acta Physica Polonica A. 1996;89:595-603.

[213] Xiang G, Xu S, Wu Z, Zhongyang L, Mingjiang N, Kefa C. The mechanism of naphthalene decomposition in corona radical shower system by DC discharge. 2009:713-7.

[214] Brosset C, Allouche A. Plasma-wall interactions in tokamaks, a scope between physics and chemistry. Actual Chimique. 2005:5-13.

[215] Marinov NM, Pitz WJ, Westbrook CK, Vincitore AM, Castaldi MJ, Senkan SM, et al. Aromatic and polycyclic aromatic hydrocarbon formation in a laminar premixed n-butane fame. Combustion and Flame. 1998;114:192-213.

[216] Garcia XA, Hüttinger KJ. Steam gasification of naphthalene as a model reaction of homogeneous gas/gas reactions during coal gasification. Fuel. 1989;68:1300-10.

[217] Devi L, Ptasinski KJ, Janssen FJJG. Decomposition of naphthalene as a biomass tar over pretreated olivine: Effect of gas composition, kinetic approach, and reaction scheme. Industrial Engineering & Chemistry Research. 2005;44:9096-104.

[218] Croiset E, Rice SF, Hanush RG. Hydrogen peroxide decomposition in supercritical water. Aiche Journal. 1997;43:2343-52.

[219] Larson RA, Ju H-L, Snoeyink VL, Recktenwalt MA, Dowd PA. Some intermediates in the wet air oxidation of phenanthrene adsorbed on powdered activated carbon. Water Research. 1988;22:337-42.

[220] Ray K, Sengupta S, Deo G. Reforming and cracking of CH_4 over Al_2O_3 supported Ni, Ni-Fe and Ni-Co catalysts. Fuel Process Technol. 2017;156:195-203.

[221] Zhang H, Zhu F, Bo Z, Cen K, Li X. Hydrogen production from methanol decomposition in a gliding arc discharge plasma with high processing capacity. Chemistry Letters. 2015;44:1315-7.

[222] Zhou L, Li L, Wei N, Li J, Basset J-M. Effect of $NiAl_2O_4$ formation on Ni/Al_2O_3 atability during dry reforming of methane. ChemCatChem. 2015;7:2508-16.

[223] Wang C-B, Tang C-W, Tsai H-C, Chien S-H. Characterization and catalytic oxidation of carbon monoxide over supported cobalt catalysts. Catalysis Letters. 2006;107:223-30.

[224] Liao X, Gerdts R, Parker SF, Chi LN, Zhao YX, Hill M, et al. An in-depth understanding of the bimetallic effects and coked carbon species on an active bimetallic $Ni(Co)/Al_2O_3$ dry reforming catalyst. Physical Chemistry Chemical Physics. 2016; 18: 17311-9.

[225] Zhao XX, Lu GX. Modulating and controlling active species dispersion over Ni-Co bimetallic catalysts for enhancement of hydrogen production of ethanol steam reforming. International Journal of Hydrogen Energy. 2016;41:3349-62.

[226] You XJ, Wang X, Ma YH, Liu JJ, Liu WM, Xu XL, et al. Ni-Co/Al_2O_3 Bimetallic catalysts for CH_4 steam reforming: Elucidating the role of Co for improving coke resistance. Chemcatchem. 2014;6:3377-86.

[227] Sengupta S, Ray K, Deo G. Effects of modifying Ni/Al_2O_3 catalyst with cobalt on the reforming of CH_4 with CO_2 and cracking of CH4 reactions. International Journal of Hydrogen Energy. 2014;39:11462-72.

[228] Gonzalez-delaCruz VM, Pereniguez R, Ternero F, Holgado JP, Caballero A. In situ XAS study of synergic effects on Ni-Co/ZrO_2 methane reforming catalysts. Journal of Physical Chemistry C. 2012;116:2919-26.

[229] Xu JK, Zhou W, Li ZJ, Wang JH, Ma JX. Biogas reforming for hydrogen production over nickel and cobalt bimetallic catalysts. International Journal of Hydrogen Energy. 2009;34:6646-54.

[230] Mei D, Ashford B, He Y-L, Tu X. Plasma-catalytic reforming of biogas over supported Ni catalysts in a dielectric barrier discharge reactor: Effect of catalyst supports. Plasma Processes and Polymers. 2017;14:1600076.

[231] Andonova S, de Ávila CN, Arishtirova K, Bueno JMC, Damyanova S. Structure and redox properties of Co promoted Ni/Al_2O_3 catalysts for oxidative steam reforming of ethanol. Applied Catalysis B: Environmental. 2011;105:346-60.

[232] Xiao ZR, Li L, Wu C, Li GZ, Liu GZ, Wang L. Ceria-promoted Ni-Co/Al_2O_3 catalysts for n-dodecane steam reforming. Catalysis Letters. 2016;146:1780-91.

[233] Nabgan W, Abdullah TAT, Mat R, Nabgan B, Jalil AA, Firmansyah L, et al. Production of hydrogen via steam reforming of acetic acid over Ni and Co supported on La_2O_3 catalyst. International Journal of Hydrogen Energy. 2017;42:8975-85.

[234] Huang X, Jia CC, Wang CZ, Xiao FK, Zhao N, Sun NN, et al. Ordered mesoporous CoO-NiO-Al_2O_3 bimetallic catalysts with dual confinement effects for CO_2 reforming of CH_4. Catalysis Today. 2017;281:241-9.

[235] Hu X, Lu GX. Investigation of steam reforming of acetic acid to hydrogen over Ni-Co metal catalyst. Journal of Molecular Catalysis A: Chemical. 2007;261:43-8.

[236] van Heesch BEJM, Pemen GAJM, Yan KP, van Paasen SVB, Ptasinski KJ, Huijbrechts PAHJ. Pulsed corona tar cracker. IEEE Transactions on Plasma Science. 2000;28:1571-5.

[237] Abdelaziz AA, Seto T, Abdel-Salam M, Ishijima T, Otani Y. Influence of applied voltage waveforms on the performance of surface dielectric barrier discharge reactor for decomposition of naphthalene. Journal of Physics D: Applied Physics. 2015;48:195201.

[238] Nair SA, Yan K, Pemen AJM, van Heesch EJM, Ptasinski KJ, Drinkenburg AAH. Tar removal from biomass derived fuel gas by pulsed corona discharges: Chemical kinetic study II. Industrial Engineering & Chemistry Research. 2005;44:1734-41.

[239] Martens T, Bogaerts A, van Dijk J. Pulse shape influence on the atmospheric barrier discharge. Applied Physics Letters. 2010;96:131503.

[240] Wu Z, Wang J, Han J, Yao S, Xu S, Martin P. Naphthalene decomposition by dielectric barrier discharges at atmospheric pressure. IEEE Transactions on Plasma Science. 2017;45:154-61.

[241] Van Heesch BEJM, Pemen GUAJM, Keping Y, Van Paasen SVB, Ptasinski KJ, Huijbrechts PAHJ. Pulsed corona tar cracker. IEEE Transactions on Plasma Science. 2000;28:1571-5.

[242] Mista W, Kacprzyk R. Decomposition of toluene using non-thermal plasma reactor at room temperature. Catalysis Today. 2008;137:345-9.

[243] Liu L, Wang Q, Song J, Ahmad S, Yang X, Sun Y. Plasma-assisted catalytic reforming of toluene to hydrogen rich syngas. Catalysis Science & Technology. 2017;7:4216-31.

[244] Zhu T, Li J, Liang W, Jin Y. Synergistic effect of catalyst for oxidation removal of toluene. Journal of Hazardous Materials. 2009;165:1258-60.

[245] Liu L, Wang Q, Ahmad S, Yang X, Ji M, Sun Y. Steam reforming of toluene as model biomass tar to H 2 -rich syngas in a DBD plasma-catalytic system. Journal of the Energy Institute. 2017.

List of Academic Publications and Awards

- **Peer-reviewed journal papers**

[1] <u>**Shiyun Liu**</u>, Danhua Mei, Li Wang, Xin Tu. Steam reforming of toluene as biomass tar model compound in a gliding arc discharge reactor. *Chemical Engineering Journal*. 2017; 307: 793-802. **(IF: 6.216)**

[2] <u>**Shiyun Liu,**</u> Danhua Mei, S. Gadkari, Sai Gu, Mohamad A. Nahil, Paul Williams, Xin Tu. Hybrid plasma-catalytic steam reforming of toluene as biomass tar model compound over Ni/Al_2O_3 catalyst. *Fuel Processing Technology*. 2017; 166: 269-275. **(IF: 3.752)**

[3] <u>**Shiyun Liu**</u>, Danhua Mei, Ze Shen, Xin Tu. Nonoxidative conversion of methane in a dielectric barrier discharge reactor: prediction of reaction performance based on neural network model. *Journal of Physical Chemistry C*. 2014; 118: 10686-10693. **(IF: 4.536)**

[4] Li Wang*, <u>**Shiyun Liu***</u>, Chao Xu, Xin Tu. Direct conversion of methanol to $n-C_4H_{10}$ and H_2 in a dielectric barrier discharge reactor. *Green Chemistry*. 2016; 18: 5658-5666. **(IF: 9.125**; * **Equal contribution)**

[5] Xinbo Zhu*, <u>**Shiyun Liu***</u>, Yuxiang Cai, Xiang Gao, Jinsong Zhou, Chenghang Zheng, Xin Tu. Post-Plasma catalytic removal of methanol over Me-Ce catalysts in an atmospheric dielectric barrier discharge. *Applied Catalysis B: Environmental*. 2016; 183:124-132. **(IF:9.446**; * **Equal contribution)**

[6] Danhua Mei, <u>**Shiyun Liu**</u>, Xin Tu. CO_2 reforming with methane for syngas production using a dielectric barrier discharge plasma coupled with $Ni/\gamma-Al_2O_3$ catalysts: process optimization through response surface methodology. *Journal of CO_2 Utilization*, 2017; 21:314-326. **(IF: 4.292)**

[7] Danhua Mei, Ya-Ling He, <u>**Shiyun Liu**</u>, Joseph D. Yan, Xin Tu. Optimization of CO_2 conversion in a cylindrical dielectric barrier discharge reactor using Design of Experiments. *Plasma Processes and Polymers*. 2016; 13: 544-556. **(IF: 2.846)**

- **Conference contributions**

[8] **<u>Shiyun Liu,</u>** Danhua Mei, S. Gadkari, Sai Gu, Mohamad A. Nahil, Paul Williams, Xin Tu. Steam reforming of toluene as a model compound of biomass tar in a coaxial dielectric barrier discharge reactor over Ni-based catalysts. *23rd International Symposium on Plasma Chemistry (ISPC 2017)*, Canada, July 2017**(Poster).**

[9] **<u>Shiyun Liu</u>**, Danhua Mei, Xin Tu, Plasma gas cleaning process for the conversion of biomass tar model compounds into syngas. *International Conference on Plasma Science (IEEE ICOPS 2017),* USA, May 2017 **(Oral presentation)**.

[10] **<u>Shiyun Liu</u>**, Danhua Mei, Li Wang, Chunfei Wu, Xin Tu. Plasma gas cleaning process for the conversion of model tar from biomass gasification. *2017 International Bioenergy Conference*, Manchester, UK, March 2017 **(Poster).**

[11] **<u>Shiyun Liu</u>**, Danhua Mei, Xin Tu, Plasma-catalytic reforming of toluene for syngas prouction. *The 23rd Joint Annual Conference of the Chinese Society of Chemical Science and Technology in the UK and Society of Chemical Industry's Chinese UK Regional Group (CSCST-SCI)*, Nottingham, UK ,September 2016 **(Oral presentation).**

[12] **<u>Shiyun Liu</u>**, Danhua Mei, Xin Tu. Steam reforming of model tar compound from biomass gasification over Ni-based catalyst in a dielectric barrier discharge reactor. *The 23rd Joint Annual Conference of the Chinese Society of Chemical Science and Technology in the UK and Society of Chemical Industry's Chinese UK Regional Group (CSCST-SCI)*, Nottingham, UK, September 3, 2016 **(Poster)**.

[13] **<u>Shiyun Liu</u>**, Danhua Mei, Li Wang, Xin Tu. Plasma reforming of toluene as biomass tar model compound in a gliding arc discharge reactor. *International Workshop on Plasma for Energy and Environmental Applications (IWPEEA)*, Liverpool, UK, August 21-24, 2016 **(Poster).**

[14] **<u>Shiyun Liu</u>**, Danhua Mei, Xin Tu. Plasma reforming of toluene as biomass tar model compound in a gliding arc discharge reactor. *International Workshop for Plasmas for Energy and Environmental Applications (IWPEEA-2016)*, Liverpool, UK, August 21-24, 2016 **(Poster)**.

[15] **<u>Shiyun Liu</u>**, Danhua Mei, Xin Tu. Conversion of methane into hydrogen and C_2 hydrocarbons in a dielectric barrier discharge reactor. *The 42nd International Conference on Plasma Science (IEEE ICOPS 2015)*, Antalya, Turkey, May 24-28, 2015 **(Oral presentation)**.

[16] Mohamad A Nahil, **<u>Shiyun Liu,</u>** Danhua Mei, Chunfei Wu, Xin Tu, Paul Williams. Low temperature plasma treated catalysts for steam reforming of tars from biomass gasification. *UK Catalysis Conference 2016*, Belfast, UK, January 6-8, 2016 **(Poster)**.

[17] Danhua Mei, **<u>Shiyun Liu</u>**, Joseph D. Yan, Xin Tu, Plasma-catalysis for the conversion of CO_2 into value-added chemicals, *International Symposium on Plasmas for Catalyses and Energy Materials (ISPCEM-2014)*, Tianjin, China, September 13-16 2014 **(Oral presentation)**.

[18] Danhua Mei, Yuxuan Zeng, **<u>Shiyun Liu</u>**, Xin Tu. Plasma-catalysis for energy and environmental applications. *International Symposium on Non-Thermal/Thermal Plasma Pollution Control Technology and Sustainable Energy (ISNTP-10)*, Florianopolis, SC, Brazil, August 1-5, 2016 **(Oral presentation)**.

[19] Danhua Mei, Yuxuan Zeng, **<u>Shiyun Liu</u>**, Xin Tu. Plasma-catalysis for energy and environmental applications. *1st Sino-German Symposium on Atmospheric Pressure Gas Discharges and Plasma Applications*, Beijing, China, October 11-17, 2015 **(Oral presentation)**.

- **Awards**

[1] *Chinese Government Award for Outstanding Self-Financed Students Abroad*, March 2018, Chinese government.

[2] *Best Poster Award*, International Workshop on Plasma for Energy and Environmental Applications (IWPEEA), August 2016, Liverpool, UK.